

METHOD FOR THE DETERMINATION OF
URANIUM ISOTOPE RATIOS AND ITS
APPLICATION AS A NOVEL GEOCHEMICAL
TRACER

Leja Rován

Doctoral Dissertation
Jožef Stefan International Postgraduate School
Ljubljana, Slovenia

Supervisor: Assist. Prof. Dr. Marko Štrok, Jožef Stefan Institute, Ljubljana, Slovenia

Evaluation Board:

Prof. Dr. Sonja Lojen, Chair, Jožef Stefan Institute, Ljubljana, Slovenia

Assist. Prof. Dr. Tea Zuliani, Member, Jožef Stefan Institute, Ljubljana, Slovenia

Prof. Dr. Dagmara Struminska-Parulska, Member, Faculty of Chemistry, University of Gdańsk, Poland

MEDNARODNA PODIPLomsKA ŠOLA JOŽEFA STEFANA
JOŽEF STEFAN INTERNATIONAL POSTGRADUATE SCHOOL



Leja Rovan

METHOD FOR THE DETERMINATION OF URANIUM
ISOTOPE RATIOS AND ITS APPLICATION AS A
NOVEL GEOCHEMICAL TRACER

Doctoral Dissertation

METODA ZA DOLOČANJE URANOVIIH IZOTOPSKIIH
RAZMERIJ IN NJENA UPORABA KOT NOVO
GEOKEMIJSKO SLEDILO

Doktorska disertacija

Supervisor: Assist. Prof. Dr. Marko Štrok

Ljubljana, Slovenia, October 2021

“It always seems impossible until it's done.”

Nelson Mandela

Acknowledgments

Firstly, I would like to express my appreciation to my supervisor Assist. Prof. Dr. Marko Štrok, who encouraged me, supported my work during the past four years, advising me on many topics, and broadened my knowledge by teaching me how to solve scientific questions. Thanks are also addressed to the members of the committee for the evaluation of the doctoral dissertation, Prof. Dr. Sonja Lojen, Assist. Prof. Dr. Tea Zuliani and Prof. Dr. Dagmara Struminska-Parulska for their valuable comments and suggestions that improved this dissertation.

I would also like to express my special gratitude to Prof. Dr. Ljudmila Benedik, who introduced me to the world of radiochemistry, shared her wide-ranging knowledge with me, taught me everything she knows, advised me on many topics, and encouraged me through the years to become a better scientist. Milka, thank you for all the help.

I sincerely appreciate all the help and support from current and past colleagues at the Radiochemistry Laboratory and from other fellow students and colleagues at the Department of Environmental Sciences. Thank you for taking the time to teach me new techniques, procedures, new knowledge and having patience with me when stuff at the beginning was not so clear. Special thanks to Dr. Marta Jagodic Hudobivnik for her support, and willingness to help me whenever I needed some advice or assistance.

The experimental part related to this doctoral dissertation was mostly performed at the Department of Environmental Sciences, Jožef Stefan Institute (IJS, Ljubljana, Slovenia). First year sampling was performed with the help of the Karst Research Institute, Slovenian Academy of Sciences and Arts (Postojna, Slovenia) and the Faculty of Civil and Geodetic Engineering Institute, University of Ljubljana (Ljubljana, Slovenia). Thanks to Prof. Dr. Metka Petrič, Assist. Prof. Dr. Simon Rusjan and Klaudija Lebar for the help with the Ljubljanica River sampling. I would also like to thank the Research Station Martinska, Ruđer Bošković Institute (Croatia), for the help with the fieldwork and the sample preparation for the Krka River in Croatia. Additional thanks also go to Dr. Barbara Horvat from the Slovenian National Building and Civil Engineering Institute (Ljubljana, Slovenia) for her help with the sample preparation of rock samples and all the colleagues from the Department of Environmental Sciences for assisting with the field work.

This work has been financially supported by the Slovenian Research Agency through research program P2-0075, project J1-9179, and the Young Researcher's program.

This work would not have been possible without the endorsement from my family and friends. Thank you for all the support given during my PhD studies and for being there for me at the time when I needed it the most.

Abstract

U and Th isotopic composition have been proven to be a valuable tool in environmental science, oceanography, hydrology, geology, nuclear forensics, and science-based archaeology. These applications require simultaneous detection of both minor and major isotopes at high accuracy. Often, the amount of sample or concentration of U and Th are low and therefore require high measurement sensitivity. The use of multicollector inductively coupled plasma mass spectrometry (MC-ICP-MS) can yield improved precision for low-abundance isotopes and mass-limited samples by the high absolute sensitivity, simultaneous detection of ions with the multicollector detector block, and higher sample throughput. This can be achieved only with proper optimization of measurement protocol. Measurements with MC-ICP-MS require sample pre-processing in order to reduce matrix interferences and pre-concentrate samples with too low concentrations for direct measurements. These procedures can themselves induce isotope fractionations and consequently yield biased results. Several different protocols have been reported so far, but none with a clear indication of its performance with respect to the mass bias. Therefore, different protocols had been compared in this dissertation and the best one was further optimized in order to ensure reliable, high-quality data on U and Th isotope ratios. The combination of coprecipitation with $\text{Ca}_3(\text{PO}_4)_2$ as the preconcentration technique and extraction chromatography with UTEVA resin precleaned in 6 M HNO_3 as the separation technique was chosen as an optimal analytical protocol with the highest accuracy. Other techniques had higher column matrix effects, owing to the direct contribution of the organic material stripped from the resin, which was shown to be the biggest influence on precise and accurate U results. The optimal protocol was then used to introduce U and Th as novel environmental tracers to study hydrogeochemical processes in karstic systems with predominantly carbonate lithology. In a dynamic karst river system with the heterogeneous geologic framework, classical hydrogeological approaches are sometimes not enough to properly investigate these complex karstic processes. The combined use of geochemical and physicochemical parameters with U and Th isotopic composition significantly improved the understanding of karst hydrodynamics. The Ljubljana River catchment and the Krka River in Croatia were the first case studies where U and Th isotope disequilibrium have been used to provide a new perspective to already known data. The $^{234}\text{U}/^{238}\text{U}$ activity ratio of dissolved U was found to be a trusted tracer of groundwater and river water sources, reflecting the variability of discharge and lithology of the catchment, and mixing water from different sources. Isotopically lighter U was co-precipitated with carbonate in flowstone and tufa without fractionation, therefore U isotope ratios in terrestrial carbonate formations could reflect the storage of CO_2 as authigenic carbonate in tufa. Th and U concentrations and their isotope ratios in carbonate materials were also shown to be a good indicator of carbonate detrital contaminations.

Povzetek

Uporaba U in Th izotopske sestave se je izkazala kot pomembno orodje v znanosti o okolju, oceanografiji, hidrologiji, geologiji, jedrski forenziki in arheologiji. Te aplikacije zahtevajo hkratno zaznavanje izotopov z manjšo in večjo vsebnostjo z visoko natančnostjo. Količina U in Th v vzorcu ali njuna koncentracija je pogosto majhna, zato je potrebna visoka merilna občutljivost. Uporaba multikolektorskega masnega spektrometra s sklopljeno induktivno plazmo (MC-ICP-MS) lahko z visoko absolutno občutljivostjo, hkratnim zaznavanjem ionov z večkolektorskim detektorskim blokom in možnostjo analize več vzorcev v krajšem časovnem obdobju doseže izboljšano natančnost. To lahko dosežemo le s pravilno optimizacijo merilnega protokola. Meritve z MC-ICP-MS zahtevajo predhodno obdelavo vzorca, da se zmanjšajo interference v matriki in predhodno koncentriranje vzorca z nizko koncentracijo za neposredne meritve. Ti procesi lahko sami od sebe povzročijo izotopsko frakcionacijo in posledično dajejo pristranske rezultate. Zaenkrat so poročali o več različnih protokolih, vendar nobenem z jasnimi navedbami glede njegove učinkovitosti na masno odstopanje. Zato so bili v tej disertaciji primerjani različni protokoli, najboljši pa je bil nadalje optimiziran, da je zagotovil zanesljive in visokokakovostne podatke o U in Th izotopskih razmerjih. Kombinacija soobarjanja s $\text{Ca}_3(\text{PO}_4)_2$ kot tehnika predhodnega koncentriranja in ekstrakcijska kromatografija z UTEVA smolo, predhodno očiščeno v 6 M HNO_3 kot separacijska tehnika, je bila izbrana kot optimalni protokol z najvišjo natančnostjo. Ostale tehnike so imele večji vpliv matrike na koloni zaradi neposrednega prispevka organskega materiala, odstranjenega iz kolone, kar se je izkazalo za največji vpliv na natančnost U rezultatov. Optimalni protokol je bil nato uporabljen za uvedbo U in Th kot nova okoljska sledila za preučevanje hidrogeokemičnih procesov v kraškem svetu s pretežno karbonatno podlago. V dinamičnem kraškem rečnem sistemu s heterogeno geološko podlago klasični hidrogeološki pristopi včasih niso dovolj za pravilno raziskovanje teh zapletenih kraških procesov. Skupna uporaba geokemičnih in fizikalno-kemijskih parametrov z U in Th izotopsko sestavo je znatno izboljšala razumevanje kraške hidrodinamike. Povodje reke Ljubljanice in reka Krka na Hrvaškem sta bili prvi dve študiji, pri katerih se je U in Th izotopsko neravnovesje uporabilo kot novo perspektivo k že obstoječim podatkom. Ugotovljeno je bilo, da je razmerje aktivnosti $^{234}\text{U}/^{238}\text{U}$ raztopljenega U zanesljiv sledilec podzemnih in rečnih vodnih virov, kar odraža spremenljivost pretoka in litologije povodja ter mešanja vod iz različnih virov. Izotopsko lažji U se je soobarjal brez frakcionacije s karbonatom v sigi in lehnjaku, zato U izotopska razmerja v kopenski karbonatni formaciji lahko odražajo shranjevanje CO_2 kot avtigenega karbonata v lehnjaku. Koncentracije Th in U ter njuna izotopska razmerja v karbonatnih materialih so se prav tako pokazale kot dober pokazatelj onesnaženosti s karbonatno devtritičnostjo.

Contents

List of Figures	xv
List of Tables	xvii
Abbreviations	xix
Symbols	xxi
1 Introduction	1
1.1 Natural Radioactivity in Environment	5
1.1.1 Basics of radioactive decay	5
1.1.2 Radioactive decay series	5
1.2 U and Th Geochemical Properties	7
1.2.1 U occurrence and properties	8
1.2.2 Th occurrence and properties	9
1.3 U and Th Isotopes	10
1.3.1 U isotopes	10
1.3.2 Th isotopes	15
1.4 Behavior of U and Th Isotopes in Karst Environment	17
1.5 U and Th Isotopic Analysis	18
1.5.1 Sampling and sample pretreatment	19
1.5.2 Sample preparation and separation	20
1.5.3 Instrumental methods	23
1.5.4 Uncertainty	30
1.5.5 Data reporting	31
2 Aims and Hypotheses	35
3 Scientific Publications	37
3.1 Optimization of the Sample Preparation and Measurement Protocol for the Analysis of Uranium Isotopes by MC-ICP-MS without Spike Addition	39
3.2 Comparison of Uranium Isotopes and Classical Geochemical Tracers in Karst Aquifer of Ljubljana River catchment (Slovenia)	57
3.3 Uranium Isotopes as a Possible Tracer of Terrestrial Authigenic Carbonate	97
4 Conclusions	115
Appendix A Permissions for Reproduction of Included Publications	119
A.1 Permission for Reproduction of Publications 3.1	119
A.2 Permission for Reproduction of Publications 3.2	119
A.3 Permission for Reproduction of Publications 3.3	120

References	121
Bibliography	141
Biography	143

List of Figures

Figure 1.1: ^{238}U , ^{235}U and ^{232}Th radioactive decay series.	6
Figure 1.2: Three cases of possible radionuclides equilibriums: secular equilibrium (left), transient equilibrium (right), and no equilibrium (bottom).	7
Figure 1.3: Distribution of U (left) and Th (right) complexes as a function of pH in the presence of ligands in water.	9
Figure 1.4: A model of the oxidation-based U fractionation.	12
Figure 1.5: Components affecting accurate determination of isotope ratios.	19
Figure 1.6: Schematic of the MC-ICP-MS instrument.	25

List of Tables

Table 1.1: Characteristic of studied members of U and Th decay chains from this thesis.	11
Table 1.2: Overview of sample preparation procedures for U and Th isotopic analysis....	23

Abbreviations

AMS	... Accelerator Mass Spectrometry
CITAC	... Cooperation on International Traceability in Analytical Chemistry
e.g.	... For example
HDPE	... High-density Polyethylene
ICP-MS	... Inductively Coupled Plasma Mass Spectrometry
ICP-QMS	... Inductive Coupled Plasma with Quadruple Mass Spectrometry
IRMM	... Institute of Reference Materials and Measurements
ISO	... International Organization for Standardization
LA-MC-ICP-MS	... Laser Ablation Multicollector Inductive Coupled Plasma Mass Spectrometry
MC-ICP-MS	... Multicollector Inductively Coupled Plasma Mass Spectrometry
MS	... Mass Spectrometry
NIST	... National Institute of Standards and Technology
SD-ICP-MS	... Single Detector Inductive Coupled Plasma Mass Spectrometry
SI unit	... International System of Units
SIMS	... Secondary Ion Mass Spectrometry
TBP	... Tri-n-butyl Phosphate
TEVA	... Tetravalent Actinide
Th-series	... Thorium-series
TIMS	... Thermal Ionization Mass Spectrometry
TRU	... Trans Uranium elements
U-series	... Uranium-series
UTEVA	... Uranium and Tetravalent Actinide

Symbols

m_i	...	Atomic mass of isotope of interest
Bq	...	Becquerel
Ca	...	Calcium
$Ca_3(PO_4)_2$...	Calcium phosphate
Co	...	Cobalt
cps	...	Counts per second
Cu	...	Copper
λ	...	Decay constant
δ	...	Delta notation
γ	...	Gamma-ray
$t_{1/2}$...	Half-life
HCl	...	Hydrochloric acid
HF	...	Hydrofluoric acid
H_2O_2	...	Hydrogen peroxide
N_0	...	Initial number of atoms
Fe	...	Iron
$Fe(OH)_3$...	Iron(III) hydroxide
Pb	...	Lead
Mg	...	Magnesium
Mn	...	Manganese
MnO_2	...	Manganese dioxide
f	...	Mass bias correction factor
R_T	...	Mass bias corrected ratio
R_m	...	Measured ratio
Hg	...	Mercury
n	...	Neutron
HNO_3	...	Nitric acid
N	...	Number of atoms
N_t	...	Number of atoms at time t
pCO_2	...	Partial pressure of carbon dioxide
‰	...	Parts per-mil
$\%$...	Percent
$HClO_4$...	Perchloric acid
$PtAr^+$...	Platinum argid
Pu	...	Plutonium
t	...	Time
ThH^+	...	Thorium hydride
UH^+	...	Uranium hydride
UO^+	...	Uranium oxide
Zn	...	Zinc

Chapter 1

Introduction

Accurate and precise determination of Uranium-series (U-series) and Thorium-series (Th-series) isotope ratios have many important applications in environmental science, oceanography, hydrology, and science-based archaeology. Understanding of past climate changes, the carbon cycle, ocean chemistry and paleoclimate, determining volcanic and igneous histories, dating cave painting and bones, and understanding processes of neotectonics and land formation relies upon the determination of U- and Th-series isotope ratio data. Isotopic compositions can also be used for studying redox conditions, chemical weathering and for continental weathering or mixing processes in hydrologic and marine systems (Andersen, Stirling, & Weyer, 2017; Bourdon, Henderson, Lundstrom, & Turner, 2003).

The most commonly studied elements of U- and Th-series are uranium (U) and thorium (Th) and they can be fractionated in a broad range of geological and hydrological systems. In environment, U and Th fractionations are an efficient process because of U and Th different solubility in different oxidation states and their diverse mobility during changing environmental conditions (Chabaux, Riotte, & Dequincey, 2003). Additionally, U and Th isotopes of interest are long-lived radionuclides which decay to another radionuclide (Loveland, Morrissey, & Seaborg, 2017). These U and Th characteristics can be exploited in the form of an isotopic ratio ($^{234}\text{U}/^{238}\text{U}$, $^{238}\text{U}/^{235}\text{U}$, $^{230}\text{Th}/^{232}\text{Th}$, $^{234}\text{U}/^{232}\text{Th}$, and $^{238}\text{U}/^{232}\text{Th}$) to study environmental interactions and water sources in hydrogeological studies and to understand the time of an element fractionation process in dating applications (Bischoff & Fitzpatrick, 1991; X. Chen, Romaniello, Herrmann, Wasylenko, & Anbar, 2016; Garnett, Gilmour, Rowe, Andrews, & Preece, 2004; Kopylova, Guseva, Shestakova, Khvaschevskaya, & Arakchaa, 2015). U isotope ratios were also recognized as an important indicator to differentiate types of environmental nuclear contamination, where measurements of anthropogenic U isotopic ratios ($^{235}\text{U}/^{238}\text{U}$, $^{233}\text{U}/^{238}\text{U}$, $^{236}\text{U}/^{238}\text{U}$, and $^{233}\text{U}/^{236}\text{U}$) are of importance in the environmental monitoring of contaminated territories to study impact of nuclear weapon explosions, nuclear power generation, reprocessing of spent nuclear fuel, and nuclear reactor accidents (Boulyga et al., 2002; Donohue, 1998; Sakaguchi et al., 2009; Steier et al., 2008).

Many such applications involve a limited amount of sample and/or contain a small amount of measured analyte with a prerequisite for high precision isotopic composition measurements. Currently, the most suitable technique for isotopic analyses in environmental samples is MC-ICP-MS, with high absolute sensitivity and simultaneous detection of ions with multicollector detector block (Baxter, Rodushkin, & Engström, 2012; Becker, 2005; Yang, 2009). The use of this equipment has also created considerable misperception in inconsistencies regarding how to obtain accurate isotope amount ratios. To fully understand the instrument, proper optimization is required to reach high

sensitivity for the detection of the smallest amounts of minor isotopes and high accuracy to differentiate between small fractions in natural samples. MC-ICP-MS complexity brings errors to measured isotope ratios, such as spectral interferences arising from isobaric interferences, instrumental mass bias, sample matrix effects as a result of the presence of other elements in the sample matrix, or the instrumental mass bias from changing daily plasma conditions (Albarède et al., 2004; Baxter et al., 2012; Becker, 2005; Wieser & Schwieters, 2005; Yang et al., 2018). To avoid such undesirable matrix and instrumental error effects, careful optimization of the measurement protocol of the measured analyte is needed.

Although several techniques for the determination of U and Th isotopic composition exist (Andersen et al., 2017; Goldstein, 2003; van Calsteren & Thomas, 2006), there is no report, which would compare their performance and allow for an evidence-based decision on the best one. Studies in the literature use many different protocols for the improvement of the precision of determining U and Th isotopes with mass bias correction during sample preparation and measurement steps due to sample requirements (Boulyga, Konegger-Kappel, Richter, & Sangély, 2015; Sakaguchi et al., 2009; Wieser & Schwieters, 2005) or instrument abilities (Andersen, Stirling, Potter, & Halliday, 2004; Goldstein, 2003; Park & Jeong, 2018). Therefore, available analytical techniques for sample pre-treatment and separation of U and Th were compared in the dissertation in terms of precision and accuracy of U-series isotope ratio determination with MC-ICP-MS (Section 3.1). The best protocol was optimized to reduce reagent blank contribution and to define optimum measurement conditions. In order to ensure reliable, high-quality data on U and Th isotope ratios and the most suitable performance for low-level samples by MC-ICP-MS, controlling factors, such as finding the proper aliquot concentration, cup configuration or establishing the long-term analytical performance of the instrument are necessary. The results of both fractionation during sample preparation and optimization of mass spectrometric measurement methods provide means for choosing the methodology which enables accurate determination of U isotope ratios for samples with low concentrations (Rovan & Štok, 2019).

The developed methodology enables different applications of U and Th isotope ratios in the environmental studies. In hydrology, U and Th isotope ratios can be investigated as an environmental tracer for studying different physicochemical processes in estuarine water (Swarzenski, 2003), seawater (Tissot & Dauphas, 2015; Weyer et al., 2008), and continental surface water and groundwater (Chabaux et al., 2003; Q. Chen et al., 2020; Cho & Choo, 2019; Siebert et al., 2019). In this dissertation, the developed U and Th methodology was applied to the samples from environments where freshwater draining areas with a predominantly carbonate lithology are the most frequent. For these hydrogeological settings not much is known, compared to the presence and behavior of natural U and Th isotopes in ancient and recent marine environments, which were widely studied (Andersen et al., 2016; Stirling, Andersen, Potter, & Halliday, 2007; Tissot & Dauphas, 2015; Weyer et al., 2008). In such environments, U is also found in much lower concentrations (Q. Chen et al., 2020; Cho & Choo, 2019; Palmer & Edmond, 1993), which represent an analytical challenge. Analyses of U and Th isotopes' disequilibrium and concentration in surface water in a karstic environment are used to provide a signature of a particular groundwater or river water type that can be related to its area of origin, to identify the mixing of waters of different origins, and to provide information about through-flow speeds and directions (Bourdon, Bureau, Andersen, Pili, & Hubert, 2009; Chabaux, Bourdon, & Riotte, 2008; Chabaux et al., 2003; Huckle et al., 2016). They are also proven to be a useful tool for identifying young carbonates and for quantifying the amount of U bound to detrital material (Bourdon et al., 2009; Garnett et al., 2004; Nyachoti, Jin, Tweedie, & Ma, 2019).

To improve the understanding of such complex karstic systems, a baseline for U and Th isotopes in different karst areas needs to be provided. Usage of classical hydrogeological approaches is sometimes not enough to properly investigate sensitive karstic processes and the combined use of classical geochemical and physicochemical parameters with U and Th concentrations and their isotopic compositions are recommended. Case studies, where the precise determination of U and Th isotope ratios was performed, were the karst aquifer of the Ljubljana River catchment (Rovan et al., 2020) and the Krka River in Croatia (Rovan et al., 2021).

The Ljubljana River catchment in Slovenia has numerous springs and sinks, and represents an interesting and challenging study environment for quantifications of hydrological and geochemical processes during different hydrological conditions (Section 3.2). The carbonate dissolution precipitation processes from the groundwater within karstic conduits are important for quantification of carbon fixation or loss during groundwater movement through the carbonate massif and to get information about the groundwater quality (Hartmann, Goldscheider, Wagener, Lange, & Weiler, 2014). To investigate these groundwater hydrodynamics, environmental tracers are usually used to investigate the recharge, groundwater flow, and water-rock interactions (Sappa, Vitale, & Ferranti, 2018). To study temporal and spatial variations in the Ljubljana catchment, the potential of using U concentrations and isotope compositions in springs and streams was explored. U and Th values were employed as alternative tracers to classical geochemical ones, such as elemental ratios, physicochemical parameters, and alkalinity, to analyze the sources of water and water mixing under different flow regimes in the groundwater system. Additional information on water sources that cannot be determined only by using classical geochemical approaches was carried out by analyzing U and Th concentrations and U isotope ratios in bedrock from different lithological units (Rovan et al., 2020).

The Krka River in Croatia (Section 3.3) is a specific groundwater-fed karstic river, characterized by complex hydrology and seasonally variable diffuse subsurface recharge. It represents a unique model system, where tufa is precipitating in a turbulent stream at morphologic discontinuities and in lotic environments. Tufa is especially attracting attention as a potential environmental archive that can provide insight into water-rock interactions, hydraulic connections, recharge, and terrestrial CO₂ cycling in terms of storage, evasion, and transfer to the ocean (Arenas et al., 2014; J. Chen, Zhang, Wang, Xiao, & Huang, 2004; Dabkowski et al., 2012). In a dynamic karst river system with alternating lentic and turbulent lotic sections, the carbonate precipitation rarely occurs in isotopic equilibrium for either C or O isotopes (Andrews, 2006; Brasier, Andrews, Marca-Bell, & Dennis, 2010; Lojen et al., 2004). The use of traditional isotopes and geochemical parameters in combination with U isotopic composition was thereby adopted to gain new knowledge on this interesting and extensively studied karstic system and to help with the identification and quantification of authigenic carbonate precipitated in the Krka River (Rovan et al., 2021).

Overall, U and Th can be used as an additional environmental tracer to gain more knowledge and understanding of complex systems with predominantly carbonate lithology. The developed methodology enables relatively easy measurement of isotope ratios at high levels of precision and accuracy, which is important for U and Th isotope measurements in environments where their concentrations in samples are low. This dissertation is organized in four chapters. In the introduction chapter, the subject of the dissertation is introduced, with the focus on reviewing basic chemical and radioactive properties of U and Th isotopes in the natural environment and explanation of possible measurement factors that can contribute to the precision and accuracy of U and Th isotope ratio results. In the aims and hypothesis, the purpose of the dissertation is presented. This is followed by the presentation of methodology, results and discussion of the dissertation in the form of three

published peer-reviewed publications in Sections 3.1-3.3. The method optimization and validation for reliable determination of U and Th isotopic composition is shown in Section 3.1 and the application of U and Th isotopes as a tracer of geochemical processes in two different studied karst aquifers is presented in Sections 3.2 and 3.3. The major findings, together with hypothesis testing, are summed up in the Conclusions.

1.1 Natural Radioactivity in Environment

Nuclides that are present in the environment are either stable or unstable. The stability of nuclides is determined by the number of neutrons and protons in its structure. Therefore, radioactive nuclides or radionuclides are unstable nuclides with the out of balance number of neutrons in their nuclei and excess energy, which they lose by the decay process. Energy is released sooner or later by the emission of gamma-rays or by subatomic particles (i.e. radiation) (Jeřkovský et al., 2019).

1.1.1 Basics of radioactive decay

Radioactivity is an important property of radionuclides. The law of radioactivity states that the number of atoms disintegrating per time is proportional to the number of atoms N . The basic equation of radioactive decay is:

$$-\frac{dN}{dt} = N\lambda \quad (1.1)$$

In Eq. (1.1), N is the number of atoms of the radionuclide and λ is its decay constant. It is defined as the probability that a given atom would decay in some time dt . The decay constant is related to the half-life:

$$\lambda = \frac{\ln 2}{t_{1/2}} \quad (1.2)$$

Half-life, $t_{1/2}$ from Eq. (1.2) is a valuable characteristic of radionuclide. It is defined as the amount of time taken for the number of nuclei of specific nuclide present in a sample at a given time to exactly halve. It ranges from less than 10^{-6} s to 10^{10} years for different radionuclides and can be measured for all the commonly used radionuclides.

When the initial number of atoms of specific radionuclide is N_0 at time $t = 0$, the number of atoms that do not undergo radioactive decay during time t (N_t) is:

$$N_t = N_0 e^{-\lambda t} \quad (1.3)$$

All above equations describe the kinetics of the radioactive decay law: the number of radioactive nuclei in a radioactive sample that disintegrate during a given time interval decreases exponentially with time (Kónya & Nagy, 2018b; L'Annunziata, 2012; Loveland et al., 2017).

In a radioactivity process, unstable nuclides decay into another nuclide in a unit of time, which results in the emission of particles (alpha and beta) or electromagnetic radiation (gamma-rays). Radioactive decay occurs spontaneously, irreversibly and randomly. The SI unit for activity is the *Becquerel* (Bq) and the activity is given in reciprocal seconds (Kónya & Nagy, 2018b).

1.1.2 Radioactive decay series

Natural radionuclides have been present since the formation of the Earth and are continuously produced by nuclear reactions of cosmic rays with atoms in the atmosphere (Kónya & Nagy, 2018a). In nature, radionuclides can be divided into primordial, cosmogenic, and anthropogenic radionuclides. Primordial radionuclides are the ones, which

exist from the time the elements were formed and have half-lives greater than 10^9 years. There are three naturally occurring radioactive decay series of primordial radionuclides; ^{238}U decay series, ^{235}U decay series, and ^{232}Th decay series (Figure 1.1) (Sen & Peucker-Ehrenbrink, 2012). Each starts with an actinide nuclide (^{238}U , ^{235}U , and ^{232}Th), having a long half-life and ends with a stable isotope of lead (^{206}Pb , ^{207}Pb , and ^{208}Pb , respectively). In between is a series of radionuclides, which have half-life ranging from microseconds to thousands of years. These decay series have an important characteristic that the parent nuclides (which are at the beginning of the decay chain) are radioactive and have a very long half-life compared to others in decay series. Therefore, the relatively long half-life make these radionuclides suited to investigate geological processes that occur over time scales similar to their decay period (Bourdon, 2003; L'Annunziata, 2012; Loveland et al., 2017).

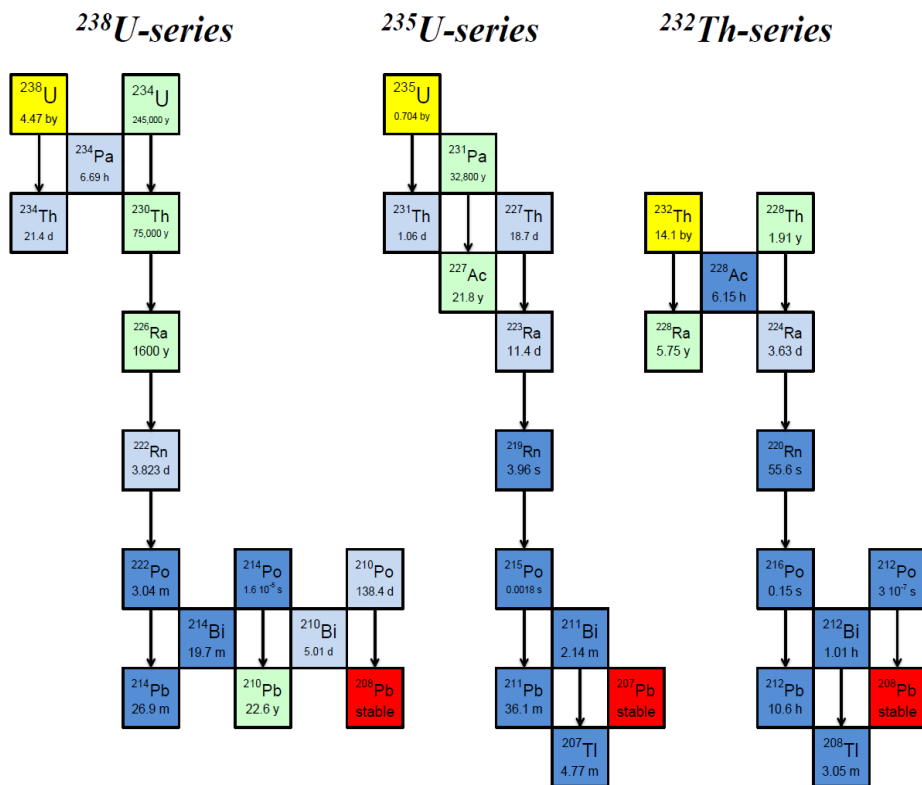


Figure 1.1: ^{238}U , ^{235}U and ^{232}Th radioactive decay series (Sen & Peucker-Ehrenbrink, 2012).

Properties of the radioactive decay series depend on the ratio of the decay constants of the nuclides in a series. There are three cases depending upon if the parent nuclide half-life is greater or less than the daughter nuclide half-life and they are presented in Figure 1.2.

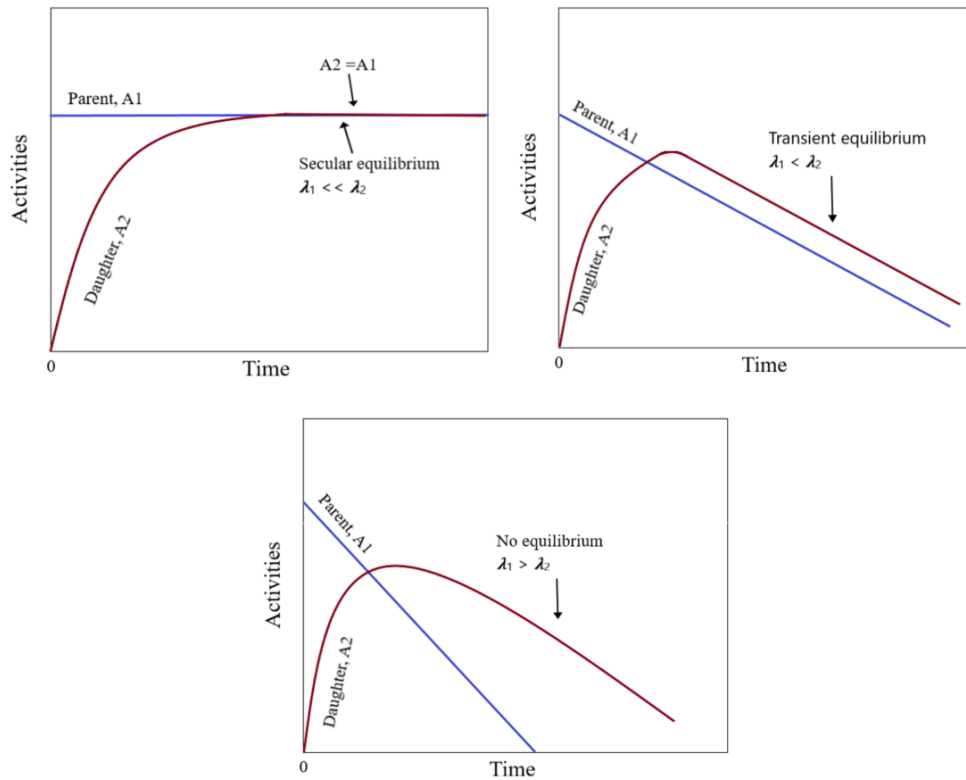


Figure 1.2: Three cases of possible radionuclides equilibria: secular equilibrium (left), transient equilibrium (right), and no equilibrium (bottom) (adopted by L'Annunziata, 2012).

In the first case, the parent radionuclide decays much more slowly than the daughter radionuclide ($\lambda_1 \ll \lambda_2$), the half-life of the parent radionuclide is much longer compared to the daughter's half-life. After approximately 10 half-lives, secular radioactive equilibrium is established and the activity of daughter and parent are the same if the system was closed for that period of time (Kónya & Nagy, 2018b; L'Annunziata, 2012; Loveland et al., 2017). Another case of the radioactive equilibria is when parent radionuclide decays more slowly than the daughter radionuclide ($\lambda_1 < \lambda_2$). After 10 half-lives of the daughter radionuclides, transient radioactive equilibrium is established after which the daughter isotope decays with the half-life of the parent isotope. The third case is when the parent isotope half-life is less than the daughter isotope half-life ($\lambda_1 > \lambda_2$). Parent isotope will decay, leaving behind the daughter isotope alone and no equilibrium will be established (Gilmore, 2008; Kónya & Nagy, 2018b). If the U or Th radioactive decay series remains undisturbed for more than 6 half-lives of the longest half-lived intermediate radionuclide, all radionuclides will have approximately equal activities and we can consider that secular radioactive equilibrium is established.

1.2 U and Th Geochemical Properties

Knowledge of the chemical properties of the U and Th isotopes is essential to better understand isotope's behavior in the environment, especially during the possible natural disturbance that will cause their fractionations.

1.2.1 U occurrence and properties

U was formed over the lifetime of the galaxy and injected into the solar system and Earth more than 4.5 billion years ago. Therefore, U constitutes one of the principal long-lived radioactive elements (Dicke, 1969).

U is the heaviest naturally occurring element on Earth (Stirling et al., 2007). In aqueous solutions, U exists in four oxidation states, U(III), U(IV), U(V), and U(VI), but commonly occurs only in states U(IV) and U(VI) (Langmuir, 1978). U(III) and U(V) are generally assumed to be unstable and easily change their oxidation state further. Therefore, U(III) and U(V) are short-lived and uncommon in nature (Grenthe, Fuger, Lemire, Muller, & Nguyen-Trung Cregu, C. Wanner, 1992). Under oxidizing conditions, U exists in the U(VI) state, mainly as uranyl ion UO_2^{2+} , and it is highly soluble and mobile. Under reducing conditions, U exists in the U(IV) state, mainly as insoluble complexes with hydroxides, and it is highly immobile (Ivanovich & Harmon, 1992).

The average U concentration in Earth's crust is around 2.2 $\mu\text{g/g}$, but different types of rocks show different concentration ranges. The continental crust contains approximately 30% of the U on Earth (Hu & Gao, 2008). In continental rocks, U concentrations range from 2 $\mu\text{g/g}$ in sedimentary rocks to (4–10) $\mu\text{g/g}$ in granites, while in other rocks the U content is much lower. U concentration of (30–200) $\mu\text{g/g}$ can be found in phosphate rocks, where U can be substituted with calcium in the apatite crystal structure (Liesch, Hinrichsen, & Goldscheider, 2015). U is incompatible with many rocks that form minerals and it is generally incorporated into various minor phases, or it can be found on grain boundaries (Porcelli, 2003). Naturally occurring U minerals are composed of oxides (uraninite and pitchblende), silicates (zircon, coffinite), phosphate (monazite, autunite), and vanadates (carnonite). In soils, there is generally less U than in the source rock, but it depends on soil type and maturity (Liesch et al., 2015). U can also be found in river water at concentrations around 0.3 $\mu\text{g/L}$ as a result of weathered and eroded continental crust. All U that is dissolved in river waters reaches the open sea and commonly does not precipitate during river-seawater mixing. U is homogeneously distributed in the ocean, owing to the long U ocean residence time ($5 \cdot 10^5$ years) compared to the ocean mixing time ($1.6 \cdot 10^3$ years) (Colodner, Edmond, & Boyle, 1995). In the open ocean, U concentration in seawater is found around 3.3 $\mu\text{g/L}$. In the estuarine zones, water-soluble U behaves conservatively and U concentration correlates linearly to water salinity (Ku, Mathieu, & Knauss, 1977; Saari, Schmidt, Huguet, & Lanoux, 2008). However, the concentration of U in aqueous solutions mostly depends on temperature, pressure, pH, redox potential, ionic strength, the occurrence of complex-forming ligands, on kinetics of mineral dissolution and sorption processes (Chabaux et al., 2003; Liu, Shi, & Zachara, 2009; Palmer & Edmond, 1993).

As was mentioned above, U is insoluble under reducing conditions and tends to precipitate as insoluble uraninite UO_2 . But the solubility can increase at low pH by the formation of uranous fluoride complexes and above pH 7 by complexation with hydroxyl ions (Chabaux et al., 2003). At the Earth's surface, U can be highly mobile, because of its affinity to form stable complexes, as uranyl ion in a wide range of pH values. The mobility can be additionally increased by the formation of stable complexes with inorganic (carbonate, phosphate) and organic (humic and fulvic acids) ligands. In an environment near pH 7, complexes with carbonate and phosphate are dominant. At lower pH and in saline groundwater, chloride, sulphate, and fluoride complexes become important (Figure 1.3, left) (Chabaux et al., 2003; Porcelli, 2003). U concentration and its mobility is also controlled by adsorption. The elemental adsorption onto adsorbents depends on physical parameters such as temperature, cationic exchange capacity, specific surface, and the chemical characteristics of the solution. U mobility is mostly limited by strong adsorption

on a mineral surface in soils and sediments at specific pH and in the presence or absence of strong complexing agents (Liesch et al., 2015; Porcelli, 2003). The presence of carbonate in solution restrains U retention onto minerals at pH above 7. On the other hand, humic acids significantly increase U sorption onto clay minerals at acidic pH (Chabaux et al., 2003). A special case of U adsorption is the adsorption to colloids, which can rather increase mobility. How colloids can carry a large fraction of U depends on the composition, structure, and size distribution of colloids. Examples of the U colloids are amorphous Fe-, Mn- and Al-oxyhydroxides and humic and fulvic acids along with microorganisms (Porcelli, 2003). Another important example of U mobility is a biological and microbiological activity in soils and waters. There are numerous pathways in which U(VI) can be reduced to U(IV), including direct biotic transformation mediated by metabolically different microorganisms such as sulfate-reducing, iron-reducing, and fermenting bacteria. Moreover, the reduction can also proceed as abiotic reduction by redox-active minerals and solutes such as Fe(II)- or sulfide-bearing minerals, aqueous Fe(II), sulfide species, and organic compounds (Chabaux et al., 2003; Stylo et al., 2015; Wall & Krumholz, 2006). Some of these mechanisms can decrease or increase U mobility in water.

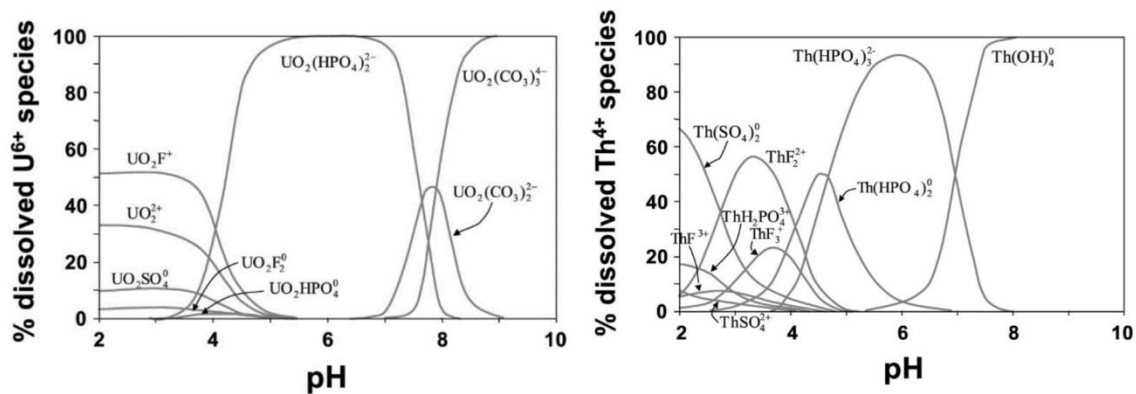


Figure 1.3: Distribution of U (left) and Th (right) complexes as a function of pH in the presence of ligands in water (Langmuir, 1978; Langmuir & Herman, 1980).

1.2.2 Th occurrence and properties

Thorium is a naturally occurring radioactive metallic element (Wickleder, Fourest, & Dorhout, 2008). The most stable oxidation state for Th on the Earth surface is Th(IV), both in minerals and when dissolved in solutions. It is relatively immobile under most circumstances. Th in general has a larger ionic radius than U, but U has a larger atomic number. This causes the heavier nuclide U to be more easily accommodated in minerals than the lighter nuclide Th at a given oxidation state. This is a phenomenon known as the actinide contraction (Blundy, 2003). Therefore, Th diffusion in solid is generally very slow because of its large size and charge (Van Orman, Grove, & Shimizu, 1998). The most common Th compound is thorium dioxide ThO₂, which has very low solubility at low temperatures and in aqueous solutions, and it tends to be enriched in the oxidized zones (Wickleder et al., 2008). However, the chemistry of Th in aqueous solutions is dependent on the ability to form complexes with other ions in solution. The mobility of Th is controlled by its ability to form complexes both with inorganic and organic ligands. The solubility is limited by the formation of the hydroxide form (e.g. Th(OH)₄), but it can increase with weakly decreased pH (Langmuir & Herman, 1980). In surface and

groundwaters Th complexes mainly with sulfate, fluoride, phosphate, and hydroxide and can also form strong organic complexes with humic and fulvic acids (Figure 1.3, right).

Th is found in small amounts in most rocks and soil and it is about three times more abundant than U. Especially, it can be located in ore deposits that were formed during fractional crystallization of peralkaline magmas (Cuney, 2009). In the Earth's crust, the Th concentration is 10.5 $\mu\text{g/g}$ in the upper crust and 1.2 $\mu\text{g/g}$ in the lower crust (Hu & Gao, 2008). In the primitive mantle, the concentration of Th is estimated to vary from 29.8 ng/g (in chondritic) to 83.4 ng/g (Palme & O'Neill, 2007). The geochemistry of Th shows its preference for acidic rocks, where its concentrations reach several tens of $\mu\text{g/g}$, mostly in granites. In nature, Th does not occur in its metallic form, it occurs only as oxides (thorianite), silicates (thorite), and phosphate. The most common source of Th is a rare earth phosphate mineral, monazite. Monazite contains up to 12 % of Th phosphate and it is found in igneous rocks. The highest concentrations of Th and U are found in igneous rocks of granite composition and some shales and phosphate rocks. Under certain geological circumstances, Th is not incorporated in common rock-forming minerals and may be enriched in specific minerals to such concentrations that it can be extracted (Choppin, Liljenzin, & Rydberg, 2002; International Atomic Energy Agency, 2019). In water, Th exists at very low concentrations, of the order of tens of pg/L (Rutgers van der Loeff & Geibert, 2008; Swarzenski, 2003). A small amount of Th is also supplied to the ocean from land via rivers and terrigenous particles (Rutgers van der Loeff & Geibert, 2008). The primary anthropogenic sources of Th release in the air, soil, and water are U and Th mining, milling and processing, tin processing, phosphate rock processing, and phosphate fertilizer production, coal-fired utilities, and industrial boilers (Jia et al., 2008).

In natural waters, Th is considered to be a highly particle reactive radionuclide. For that reason, it is efficiently removed from the dissolved phase onto colloids and particulates during its residence time in aqueous systems. Th exhibits this affinity for particle surfaces in both fresh and marine waters. Because of its reactivity, Th can be easily adsorbed onto the mineral surface. Even at pH as low as 2, Th can be strongly adsorbed onto Fe-hydroxides. Th has also a strong affinity for organic matter as a ligand and it can be only released from aquifer minerals by weathering (Chabaux et al., 2003).

1.3 U and Th Isotopes

1.3.1 U isotopes

Natural U is composed of three isotopes: ^{238}U , ^{235}U , and ^{234}U . They are all radioactive and decaying with alpha decay. ^{238}U and ^{235}U are primordial radionuclides, where ^{238}U has the highest abundance of 99.27% and the longest half-life of $t_{1/2} = 4.47$ billion years. ^{235}U has an abundance of 0.72% and a half-life of $t_{1/2} = 704$ million years. ^{234}U occurs as a decay product of ^{238}U and has an abundance of 0.0054% and a half-life of $t_{1/2} = 0.245$ million years (Kónya & Nagy, 2018b). U characteristics are summarized in Table 1.1. With the help of ^{238}U and ^{235}U long half-lives, it is possible to elucidate the earliest history of the solar system, to have information on the formation of Earth's atmosphere and hydrosphere, and on subsequent terrestrial processing via ongoing tectonic, magmatic, metamorphic, and glacial events throughout geological time. Parent-daughter pair ^{238}U with shorter half-life of ^{234}U has been utilized as chronometers and tracers in the environmental, archaeological and geochemical sciences, with respect to paleoclimate and magmatic time-scale research spanning the last half million years of the late Quaternary (Andersen et al., 2017; Bourdon et al., 2003). A small additional contribution to the abundance of ^{235}U may come from the decay of extinct ^{247}Cm and has been used in cosmochemistry to constrain the evolution of

the early solar system (Stirling, Halliday, & Porcelli, 2005). In addition to the aforementioned U isotopes, a small abundance of ^{236}U can also occur naturally on Earth from neutron-capture processes within U ores ($^{236}\text{U}/^{238}\text{U} < 10^{-9}$) (Bu et al., 2017; Murphy, Froehlich, Fifield, Turner, & Schaefer, 2015).

Table 1.1: Characteristic of studied members of U and Th decay chains from this thesis.

Characteristic	^{238}U	^{235}U	^{234}U	^{232}Th	^{230}Th
Half-life (years)	4.47×10^9	7.04×10^8	2.45×10^5	1.41×10^{10}	7.54×10^4
Natural abundance (%)	99.27	0.72	0.0054	99.82	0.02
Type of decay	Alpha	Alpha	Alpha	Alpha	Alpha

U isotope fractionation

An undisturbed isotopic system can be considered as closed when the activity of the parent radioactive isotope is similar to that of its intermediate or final decay product. Closed system behavior is characteristic for radionuclides, where there is no exchange of parent or daughter isotopes with the surrounding environment, and radionuclides inside the system are in radioactive equilibrium (Figure 1.2) provided that the system is closed for approximately 10 half-lives of the longest lived decay product. Changes in parent-daughter isotope ratios are controlled only by the radioactive decay laws. In the case when decay product is not in radioactive equilibrium at the event when the system becomes closed, the age of this event can be calculated with the decay Eq. (1.3), where t is the time since the fractionation process of parent-daughter separation started. Once the parent radionuclide or its intermediate enter or depart from the system during a period comparable to the daughter radionuclide half-life period and at a comparable size of the system distance, the radioactive equilibrium will be disturbed. In the U- and Th-series, several natural processes are capable of disrupting closed system behavior.

In the natural environment, U isotopes have a small difference in mass, although several percent (%) to a few per-mil (‰) levels of isotopic fractionations can be observed (Andersen et al., 2017; Bourdon et al., 2003). Isotopic fractionation is usually described as physico-chemical processes that result in a change in abundance between light and heavy isotopes (Vanhaecke & Kyser, 2012). The causes of the fractionation are usually related to geochemical processes that cause preferential mobilization of one of the isotopes. In general, radioactive isotopes can become fractionated during processes that discriminate physico-chemical behavior, such as crystallization, dissolution, phase change, partial melting, adsorption, degassing, oxidation/reduction, complexation, or by the recoil effect (Bourdon, 2003). The main mechanisms controlling the U isotopic fractionation can be expressed in association with many different chemical transformations, which are most often happening during low-temperature processes. The most common processes are different solubility of U isotopes, present in different redox state, microbial mediated reduction, adsorption, and the alpha recoil process (Fleischer, 1982; Suksi, Rasilainen, & Pitkänen, 2006; Uvarova, Kyser, Geagea, & Chipley, 2014; Weyer et al., 2008).

The $^{234}\text{U}/^{238}\text{U}$ ratio Percent variations in $^{234}\text{U}/^{238}\text{U}$ activity ratios have been reported in natural terrestrial environments, especially in low-temperature terrestrial environments (Andersen, Erel, & Bourdon, 2009; Andersen et al., 2007; Stirling et al., 2007; Uvarova et al., 2014). Natural waters are generally enriched in ^{234}U , and the $^{234}\text{U}/^{238}\text{U}$ activity ratios can deviate from the secular radioactive equilibrium by more than 10% (Chabaux et al., 2003; Riotte & Chabaux, 1999). A mechanism that creates such a disequilibrium between ^{234}U and ^{238}U is the alpha recoil process. Here the radioactive daughter isotope is mobilized from its initial position by the energy of alpha decay. This causes displacement of the recoil atom and induces changes in the physico-chemical properties of the recoil atom and damages the host mineral (Chabaux et al., 2003). The preferential dissolution of ^{234}U is mainly caused by a direct release of ^{234}U daughter isotope into the aqueous phase through the emission of one alpha particle and two beta particles, owing to the radioactive decay of ^{238}U to ^{234}U (Kigoshi, 1971). Other processes that account for ^{234}U enrichment may be enhanced oxidation of ^{234}U (Suksi et al., 2006), decay-induced damage of the mineral matrix near the ^{234}U decay product, chemical differences between U and the intermediate daughter radioactive isotopes in the decay chain, or a combination of all (Andersen et al., 2009; Fleischer, 1982; Suksi et al., 2006). A more detailed explanation of oxidation-based ^{234}U fractionation is shown in a conceptual model in Figure 1.4, which was first presented by Ordonez-Regil et al. (Ordonez-Regil, Schleiffer, Adloff, & Roessler, 1989). According to the model, the decay product of ^{238}U (e.g. ^{234}Th) is pushed by alpha recoil into areas in the rock matrix where oxygen atoms accumulate around the ^{234}Th . Because ^{234}Th atom accumulates smaller oxygen atoms around it, the oxidation potential of ^{234}U increases at the end of the recoil trajectory, where ^{234}U is produced as the decay product of short-lived ^{234}Pa in the more mobile U(VI) state. This creates a difference in the valence of ^{234}U and ^{238}U . To obtain notable $^{234}\text{U}/^{238}\text{U}$ fractionation due to valence differences, ^{238}U must have been present in the U(IV) state for a long time (Ordonez-Regil et al., 1989; Suksi et al., 2006). As such, $^{234}\text{U}/^{238}\text{U}$ ratio is sensitive to the recoil effect process and can depart from secular radioactive equilibrium in a solid mineral or water.

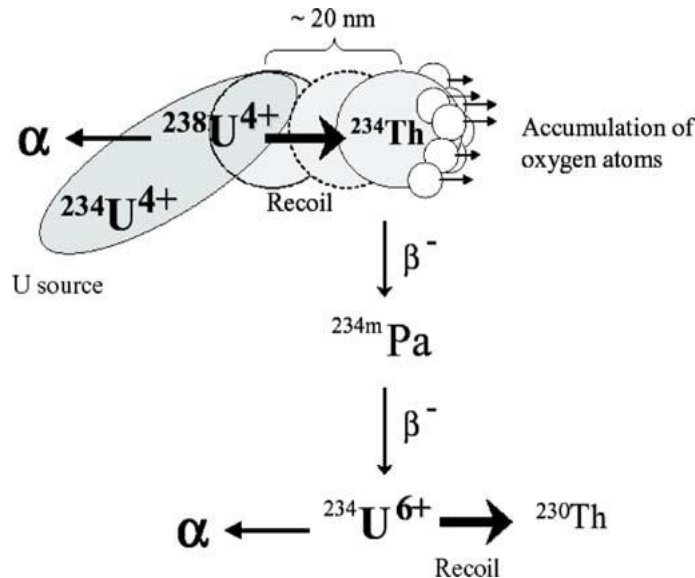


Figure 1.4: A model of the oxidation-based U fractionation (Suksi et al., 2006).

Typically, the $^{234}\text{U}/^{238}\text{U}$ ratios of the dissolved U will depend on the importance of ^{234}U alpha-induced effects in relation to the ordinary mobilization of U. This can be affected by a broad range of factors, such as redox conditions, residence time, historical weathering

and precipitation (Andersen et al., 2009). Therefore, the $^{234}\text{U}/^{238}\text{U}$ ratio can have information about the environment, where U was mobilized. For example, if the weathering in the environment is low, the $^{234}\text{U}/^{238}\text{U}$ ratio will be higher, owing to the more pronounced alpha effect. Additionally, a higher U ratio was associated with low discharge, increased contribution from groundwater (Durand, Chabaux, Rihs, Düringer, & Elsass, 2005; Lidman, Peralta-Tapia, Vesterlund, & Laudon, 2016; Riotte & Chabaux, 1999; Riotte et al., 2003), the long residence time of groundwater (Lidman et al., 2016; Schaffhauser et al., 2014), differences in mineralogy (Durand et al., 2005), and drier climate (Robinson, Belshaw, & Henderson, 2004). It was also observed that $^{234}\text{U}/^{238}\text{U}$ of U(IV) is always lower than that of in U(VI). The assumption is that the 30% of the ^{238}U is oxidized during its decay to ^{234}U , which results in its mobilization. There the recoil products were displaced, stripped of some electrons, and thus became more susceptible to oxidation into the soluble and more leachable U(VI) form (Kolodny, Torfstein, Weiss-Sarusi, Zakon, & Halicz, 2017). Terrestrial waters reflect ^{234}U loss from the solid and display excess in ^{234}U , yielding $^{234}\text{U}/^{238}\text{U}$ activity ratios higher than the secular equilibrium value of 1.00, but in fine-grained residual sediments in soils and suspended particulate loads in the river, the U activity ratio is lower than 1.00. Seawater, for instance, presents a $^{234}\text{U}/^{238}\text{U}$ activity ratio of 1.147 ± 0.001 (Andersen et al., 2007; Robinson et al., 2004), while river water and groundwater usually demonstrate larger ^{234}U excesses (Chabaux et al., 2008, 2003). The observed ^{234}U - ^{238}U disequilibrium in continental surface waters can be used as a proxy for the degree of continental weathering or mixing processes in the hydrologic and marine systems (Andersen et al., 2007; Robinson et al., 2004). The difference between ^{234}U and ^{238}U in seawater presents information about weathering history and environmental changes in the past (Henderson, 2002; Robinson et al., 2004). Additionally, non-detrital matter such as carbonates, iron oxides, and organic matter and clay mineral are usually characterized by $^{234}\text{U}/^{238}\text{U}$ activity ratios significantly higher than 1, because of the ^{234}U mobilization from detrital matter and causing the ^{234}U enrichment in surrounding pore fluids and freshwaters (Paces, Nichols, Neymark, & Rajaram, 2013; Plater, Ivanovich, & Dugdale, 1992). In soils, the $^{234}\text{U}/^{238}\text{U}$ activity ratio can also increase above 1.00, when the U precipitation from a previously ^{234}U enriched soil water was observed (Andersen, Vance, Keech, Rickli, & Hudson, 2013; Chabaux et al., 2008).

The $^{238}\text{U}/^{235}\text{U}$ ratio Not so long ago it was assumed that the current $^{238}\text{U}/^{235}\text{U}$ ratio was a constant value (e.g. 137.88) in our solar system (Steiger & Jäger, 1977), just because U was thought to be too heavy to undergo significant isotope fractionation and was used indiscriminately for the purpose of U-series and U-Pb geochronology and cosmochronology. In recent years, the discovery of a significant measurable $^{238}\text{U}/^{235}\text{U}$ variability in the terrestrial and extraterrestrial environment changed this assumption, and variations of $^{238}\text{U}/^{235}\text{U}$ ratios in the permil-level range (‰) have been widely documented (Brennecka, Borg, Hutcheon, Sharp, & Anbar, 2010; Goldmann, Brennecka, Noordmann, Weyer, & Wadhwa, 2015; Stirling et al., 2007; Tissot & Dauphas, 2015; Weyer et al., 2008). The natural variability of more than 0.03‰ in the $^{238}\text{U}/^{235}\text{U}$ ratio for a range of natural materials has been primarily associated with the variable solubility of U in different redox states, adsorption, or leaching and is due to thermodynamic or nuclear field shift effects (Fujii, Higuchi, Haruno, Nomura, & Suzuki, 2006; Nomura, Higuchi, & Fujii, 1996; Schauble, 2007). The nuclear field shift effect results in isotope fractionation because of variable nuclear volumes and electron density distributions for different isotopes. The most strong effect was predicted on heavy masses with large nuclei, especially when changes occur in the oxidation state (Schauble, 2007). One example of such nuclei is also U. The ^{238}U nucleus is more likely to lose electrons when it goes under reduction, owing to its larger volume than the ^{235}U nucleus. In other words, for U, the nuclear field shift effect in the zero-point

vibrational frequencies involves electron exchange in the s configuration. These are electrons with a significant probability of being near the nucleus or shielding f - p configurations. The effect on isotope fractionation is governed by how variable neutron numbers influence the nuclear binding energy. When U(VI) is reduced to U(IV), the f electrons are usually exchanged and heavier U in the lower oxidation state is favored. Despite the small mass difference between ^{235}U and ^{238}U and their strong bonding to the crystal lattice, it has been shown that during reduction at equilibrium, this effect is to be three times as large as compared to more common (for other stable isotopes) mass-dependent vibrational effect (Bigeleisen, 1996; Schauble, 2007).

Driven in part by nuclear field shift effects, U isotopic fractionation between U(IV) and U(VI) and its abundance in sediments makes U isotopes potential tracers of paleo-redox conditions to reconstruct the redox evolution of the oceans and atmosphere, especially in low-temperature aqueous geochemistry (Andersen et al., 2014; Dahl et al., 2014; Kendall, Brennecka, Weyer, & Anbar, 2013; Noordmann, Weyer, Georg, Jöns, & Sharma, 2016). More than 1‰ of U isotopic variation was found in terrestrial near-surface samples (Stirling et al., 2007; Weyer et al., 2008). This was stimulated by the finding of significant fractionation of U isotopes, in particular during U reduction and incorporation into anoxic shales, compared to the relatively insignificant fractionation of the $^{238}\text{U}/^{235}\text{U}$ observed in other oceanic environments (Weyer et al., 2008). Reconstruction of environmental changes in the past on a local or global scale and understanding the present isotopic budget of the marine U cycle is also an important example for the use of the $^{238}\text{U}/^{235}\text{U}$ ratio. Based on the fluxes of the individual rivers, the mean value of $^{238}\text{U}/^{235}\text{U}$ ratio of -0.34‰ was estimated in rivers and the mean value of -0.39‰ was suggested for seawaters. The global seawater value is a little lower than the mean value of river waters, indicating that the integrated U sink from the oceans predominantly fractionates U isotopes towards higher $^{238}\text{U}/^{235}\text{U}$ ratio values (Andersen et al., 2015, 2016; Noordmann et al., 2016; Tissot & Dauphas, 2015). The ^{238}U - ^{235}U disequilibrium is also a promising tool to monitor redox conditions in U bioremediation and mineral exploration studies (Bopp, Lundstrom, Johnson, & Glessner, 2009; Brennecka, Borg, et al., 2010). In co-magnetic U-bearing minerals, more than 5.4‰ difference between ^{238}U and ^{235}U was observed (Hiess, Condon, McLean, & Noble, 2012). Excess ^{235}U has also been detected in carbonaceous chondrites and their calcium- and aluminum-rich inclusions in extraterrestrial materials (Brennecka, Weyer, et al., 2010; Stirling et al., 2005). Additionally, it is also necessary for cosmochronology studies to coupled $^{238}\text{U}/^{235}\text{U}$ and $^{207}\text{Pb}/^{206}\text{Pb}$ data sets to determine more accurate dates for U-Pb and Pb-Pb geochronology (Brennecka, Borg, et al., 2010; Goldmann et al., 2015; Hiess et al., 2012; Stirling et al., 2005; Weyer et al., 2008). An extinct short-lived radioactive isotope ^{247}Cm ($t_{1/2} = 15.6$ million years) that decays with alpha decay into ^{235}U is important in cosmochemistry for understanding how r-process nuclides were synthesized in stars and for understanding the astrophysical context of solar system formation (Blake & Schramm, 1973).

Anthropogenic U isotopic composition An issue for measuring natural U isotope variability is the potential contamination with anthropogenic U. Pollution of natural samples from the nuclear industry and weapons or use of commercially available U concentration standards made from depleted U can be problematic. Anthropogenic ^{235}U can come from nuclear fission fuel, where ^{235}U is enriched or can occur as depleted ^{235}U , from the U residual product, which may be used in penetrating weapons (Grenthe et al., 2010). Anthropogenic U is therefore widespread across the globe, and it has a significant effect in areas that have been exposed to depleted U, such as in sediment near nuclear fuel production plants or in soils from war zones and tests sites (Lloyd, Chenery, & Parrish, 2009; Oliver, Graham, MacKenzie, Ellam, & Farmer, 2007).

Additionally, the ultra-trace amount of ^{236}U is found in environmental and biological samples and has mainly been introduced by nuclear weapon explosions, nuclear power generation, reprocessing of its spent fuel, and nuclear reactor accidents (Sakaguchi et al., 2009; Steier et al., 2008). Therefore, U isotope ratios are not only important characteristics for environmental monitoring, but also for nuclear safeguards and nuclear forensic studies (Boulyga et al., 2015; Kristo et al., 2016). ^{236}U determination was recognized as an important indicator to differentiate types of environmental nuclear contamination (Donohue, 1998; Sakaguchi et al., 2009). It is produced by the neutron capture reaction $^{235}\text{U} (n, \gamma) ^{236}\text{U}$ with thermal neutrons and by the alpha decay of ^{240}Pu (Ghiorso, Brittain, Manning, & Seaborg, 1951). Measurements of $^{236}\text{U}/^{238}\text{U}$ isotopic ratios are of importance in the environmental monitoring of contaminated territories as a tracer for the source identification of anthropogenic U present in the environment (Boulyga et al., 2002; Steier et al., 2008). $^{236}\text{U}/^{238}\text{U}$ ratios in a spent fuel rod are on the order of a few permil (Steier et al., 2008), while in naturally occurring ores ratios are below 10^{-9} (Murphy et al., 2015). Also, nuclear safeguard programs seek to determine the U isotope abundances of micron size particles, where anomalous amounts of ^{233}U and ^{236}U may indicate artificial isotope enrichment or depletion processes (Boulyga et al., 2015; Wieser & Schwieters, 2005). Recently, when ^{233}U was detected in environmental samples, the $^{233}\text{U}/^{236}\text{U}$ ratio can be established as a tracer for discriminating between different radioactive emissions, where the ratio was found between $(0.1\text{--}3.7) \cdot 10^{-2}$ (Hain et al., 2020).

1.3.2 Th isotopes

In a natural environment, there are six Th isotopes, ^{227}Th , ^{228}Th , ^{230}Th , ^{231}Th , ^{232}Th , and ^{234}Th . The most common isotope is alpha-emitting ^{232}Th , a primordial radioactive isotope from the ^{232}Th decay series, with a natural abundance of 99.98% and a half-life of $t_{1/2} = 14.05$ billion years. Another important Th isotope is alpha-emitting ^{230}Th , a radioactive decay product from the ^{238}U decay series, with a natural abundance of 0.02% and a half-life of $t_{1/2} = 75,400$ years. Other Th isotopes occur only in trace amounts (Kónya & Nagy, 2018b). ^{230}Th and ^{232}Th are the most commonly studied Th members, owing to their relatively long half-life, high natural abundance, and alpha-particle radiation. Their characteristics are summarized in Table 1.1. These radioactive isotopes are suited to investigate many geological processes that occur over time scales similar to their decay period and have been used to track the origins of particle and sediment in a marine environment, because of their different sources in the ocean (Jia et al., 2008; Rutgers van der Loeff & Geibert, 2008). In an estuarine environment, Th is of interest mainly as a tracer of sediment mixing and as a proxy for other particle-reactive species (Swarzenski, 2003). In sediment, Th has been used as a source for other radioactive isotopes that can be mobilized to the water column and are of interest as tracers (Rutgers van der Loeff & Geibert, 2008). Th isotopes have also been used to trace the seasonal deposition and continental dust (Church & Sarin, 2008), to determine particle removal rates, settling velocity of particles, export of particulate organic carbon and nitrogen, and the rate constants and turnover times for the coagulation and disaggregation of colloids (Bacon & Anderson, 1982; Baskaran, Santschi, Benoit, & Honeyman, 1992; Somayajulu & Goldberg, 1966).

Th isotopic composition

In natural waters, ^{232}Th is normally included within siliciclastic detrital material such as clay minerals and remains adsorbed onto particulates or grains of soil, owing to its high insolubility in solutions; therefore, it is carried in the particulate form in river waters

(Bischoff & Fitzpatrick, 1991; Garnett et al., 2004). ^{230}Th inside carbonate rocks or minerals are usually from the carbonate precipitation of U from the water, where ^{230}Th ingrow within the material from the radioactive decay of ^{234}U at a predictable rate. Regardless of the different solubility of U and Th, carbonate precipitated from water may also contain detrital ^{232}Th trapped in the calcite matrix (Chabaux et al., 2008, 2003). As it is not possible to remove all detrital ^{232}Th physically, various analytical techniques and mathematical methods have been developed to correct for detrital Th in the impure carbonate materials (Kaufman, 1993). As a result, it has been generally accepted that when the $^{230}\text{Th}/^{232}\text{Th}$ activity ratio is lower than 20, there is a possibility of an increase of detrital contamination in carbonate rock samples (Ball, Sims, & Schwieters, 2008; Garnett et al., 2004). This is relevant in U-series dating applications, which usually involves calculating ages from radioactive decay and ingrowth relationships between ^{238}U , ^{234}U , and ^{230}Th . The difference in U and Th isotopes in rocks are used for correcting the age for the effects of detrital contamination, normally in carbonate materials (Bischoff & Fitzpatrick, 1991; Garnett et al., 2004). Correction for such impure carbonates is generally performed using an assumed initial $^{230}\text{Th}/^{232}\text{Th}$ ratio. For continental carbonates, a typical crustal Th ratio is used (Ludwig & Paces, 2002), but for marine carbonates, correction of initial ^{230}Th is corrected with an assessment of the $^{230}\text{Th}/^{232}\text{Th}$ ratio in the local seawater (Robinson et al., 2004).

Th isotope ratio also plays an important role as an additional tool for U isotope ratio in characterizing a broad spectrum of natural processes, including the timing and mechanisms of climate and environmental changes, the calibration of the radiocarbon timescale, human evolution, oceanographic processes, tectonic and seismic processes, and magmatic processes (Bourdon et al., 2003; Ivanovich & Harmon, 1992). ^{238}U - ^{230}Th disequilibrium can provide an important geochemical tool for investigating recent volcanologic processes (Ball et al., 2008). Th isotopes can also be exploited to study water–rock interactions and sources of water mineralization in hydrogeological studies (X. Chen et al., 2016; Kopylova et al., 2015). Isotope distribution among the different phases of water is generally assumed to mostly depend on the behavior of their respective parent radioactive isotope, especially on their sorption or solubility properties. The dissolved load in a river is expected to have a $^{230}\text{Th}/^{234}\text{U}$ ratio lower than 1, for example in river waters, soil pore water, and groundwaters, due to the preferential leaching of U during weathering. Conversely, the suspended load is expected to have a $^{230}\text{Th}/^{234}\text{U}$ ratio greater than 1, like in river sediments, soil, and weathered rocks. This is often seen in U-rich and ^{232}Th -poor peatlands, trapped in authigenic particles. However, some sediments also have a $^{230}\text{Th}/^{234}\text{U}$ ratio lower than 1, which has been attributed to the role of organic matter in complexing and mobilizing Th (Dosseto, Bourdon, & Turner, 2008). There was also an observation that the $^{230}\text{Th}/^{232}\text{Th}$ ratio in the dissolved load of rivers depends on the watershed lithology. Rivers draining carbonates appear to have a higher $^{230}\text{Th}/^{232}\text{Th}$ ratio than those draining silicates and this was explained by a high U/Th ratio of carbonate rocks (Dosseto, Bourdon, Gaillardet, Allègre, & Filizola, 2006; Dosseto, Turner, & Douglas, 2006). In groundwaters, weathering is a dominant flux of ^{230}Th into groundwater and the $^{230}\text{Th}/^{232}\text{Th}$ ratio will be similar to bulk aquifer rocks if Th-bearing and U-bearing phases weather at similar rates (Porcelli, 2003, 2008). The $^{230}\text{Th}/^{232}\text{Th}$ activity ratio in groundwaters was estimated from 1.0 to 1.9 (Ivanovich, Tellam, Longworth, & Monaghan, 1992), where the average crust has 0.83 (S. Luo, Ku, Roback, Murrell, & McLing, 2000). However, the ratio will mostly depend on the type of the examined aquifer.

1.4 Behavior of U and Th Isotopes in Karst Environment

Karstic carbonate rocks cover 13-14% of the Earth's land surface and around 10% of the world's population relies on karstic aquifers as an important freshwater resource (Ford & Williams, 2007). Karst environment provides a valuable insight into the carbon dynamics since carbonate weathering in the watersheds affects the development of karst landforms and epikarst structures (Z. Chen et al., 2017). Carbonate saturated water circulates in a myriad of micropore, fissure, and fracture matrices of epikarst, conduits, caves, and sinkholes and is controlled by rock and groundwater characteristics (Hartmann et al., 2014). Karst aquifers are critically dependent upon hydrological conditions and climate change because they show spatially variable rapid infiltration, and their water flow is controlled by heterogeneous permeability (Ravbar, Petrič, & Kogovšek, 2010; White, 2002). Karst systems are challenging environments due to the heterogeneous geologic framework. The precipitation of calcium carbonate in supersaturated rivers can create myriad formations that can have different influences on the karstic environment. In such a complex setting, tufa can also precipitate under special conditions, which can have information on the regional climate, water temperature and chemistry, discharge, microbiological characteristics of the river water and the substrate, lithology of the catchment area, land use, but also the microenvironment at the locus of precipitation. Its authigenic and detrital components can be used as paleoenvironmental archives (Capezzuoli, Gandin, & Pedley, 2014; Pedley, 1990).

The potential sources of U in karst waters include atmospheric deposition of dust particles, limestone host rock and soil. However, soil and limestone host rock have always been considered as the primary sources for U and Th in karst waters (Q. Chen et al., 2020). U is a water-soluble element and is susceptible to dissolution in surface water, therefore its concentration can record the composition of the fluid from which the carbonate was precipitated. In contrast, Th generally exhibits much higher abundance in impure carbonates, owing to its low solubility in water (Zhao & Zheng, 2014). In aerated systems, dissolved U exists in the form of uranyl and uranyl carbonate ions, as a U(VI), while in anoxic sediments, U can be taken up by carbonate in the form of U(IV) (Ivanovich & Harmon, 1992). In a karstic environment, U solubility and affinity at higher pH (around 8) can be increased in soils and facilitates adsorption of U to carbonate surface and co-precipitation with calcite (X. Chen et al., 2016; Kelly, Rasbury, Chattopadhyay, Kropf, & Kemner, 2006). Th can also be captured in tufa carbonates. Due to being highly particle reactive and insoluble in surface water, Th will not co-precipitate as U, but it is possible that Th from siliciclastic detrital material such as clay minerals will be trapped in the calcite matrix (Chabaux et al., 2003; Rován et al., 2020, 2021; Zhang, Guan, Jian, Feng, & Zou, 2014). In karstic water, the dissolved $^{234}\text{U}/^{238}\text{U}$ activity ratio is higher than the secular equilibrium of the U isotopes because of the alpha recoil effect. U isotopes have been used as a tracer of groundwater and river water for studying spatial changes in host rock composition and hydraulic connections in karstic aquifers. The disequilibrium can reflect different sources of water mixing, bedrock lithology variability and changing of water discharge (Bourdon et al., 2009; Chabaux et al., 2008; Riotte et al., 2003; Rován et al., 2020, 2021; Zbracki et al., 2017). U has also been proven to be a useful tool for identifying young carbonates (Teichert et al., 2003; Zhao, Zheng, & Zhao, 2016). In saturated carbonate waters, U isotope ratio is without any apparent fractionation transferred into carbonate precipitation of authigenic carbonates and is distinguished from the marine carbonate formed in geological history by its higher $^{234}\text{U}/^{238}\text{U}$ activity ratio (Andersen, Stirling, Zimmermann, & Halliday, 2010; Malov & Zykov, 2020; Wang & You, 2013). However, the presence of detrital carbonate can result in deviations from the

$^{234}\text{U}/^{238}\text{U}$ activity ratio of dissolved U (Rovan et al., 2021). The $^{238}\text{U}/^{235}\text{U}$ isotope fractionation during precipitation of carbonate from aquatic solutions shows no resolvable fractionation at pH range of karst water (7.5 to 8.5) and the carbonate $\delta^{238}\text{U}$ should be the same as the water from where the carbonate is formed (X. Chen et al., 2016). However, it is possible that the $^{238}\text{U}/^{235}\text{U}$ isotope fractionation in authigenic carbonates will depend upon the changing pH, ionic strength, pCO_2 , Mg^{2+} and Ca^{2+} concentrations or adsorption on mineral surfaces (Brennecke, Wasylenki, Bargar, Weyer, & Anbar, 2011; X. Chen, Romaniello, & Anbar, 2017; Rován et al., 2021; Stirling et al., 2007).

1.5 U and Th Isotopic Analysis

Measurement of U and Th isotopic compositions in environmental samples requires high accuracy to differentiate between small fractionations and high sensitivity to detect the smallest amounts of minor isotopes in natural samples (Boulyga, Koepf, Konegger-Kappel, Macsik, & Stadelmann, 2016). In recent years, MC-ICP-MS becomes the preferred tool for precise measurements of U and Th isotopic ratios for low-abundance isotopes and mass-limited samples, owing to the high absolute sensitivity and simultaneous detection of ions with the multicollector detector block compared to quadrupole-based ICP-MS, and higher sample throughput compared to thermal ionization mass spectrometry (TIMS) (Albarède et al., 2004; Becker, 2005; Wieser & Schwieters, 2005).

On the other hand, MC-ICP-MS is a very complex instrument and to achieve accurate and precise isotope ratio data, proper optimization is required to exploit its full potential. When measuring isotope ratios using MC-ICP-MS, their performance can be affected by counting-statistic errors, spectral interferences arising from isobaric interferences, instrumental mass bias, or sample matrix effects as a result of the presence of other elements in the sample matrix (Albarède et al., 2004; Baxter et al., 2012; Becker, 2005; Wieser & Schwieters, 2005). The instrument itself could also, to some extent, discriminate various isotopes of the same element in a manner that resembles isotope fractionation in nature, owing to the different daily plasma conditions and can cause a significant deviation of isotope amount ratio from the true value (Yang et al., 2018).

A key issue here is to accurately determine U and Th isotope ratios that undergo a rather small isotopic fractionation effect in the environment and to know and understand most of isotopic biases effects from the analytical procedure that contribute to the inaccurate result, either during sample preparation or measurement. Normally, a wrong interpretation makes good isotopic data meaningless. It is essential to join methodological knowledge about chemical analysis and the quality of data because sources of uncertainty can arise from the whole measurement process (Rovan & Štok, 2019). Profound analytical work and careful method development with design of metrologically sound measurement protocol are very important in order to guarantee a validated measurement method. Therefore, in Figure 1.5 key factors are presented that have to be taken into consideration during sample pretreatment, sample preparation and separation, measurement, and data processing, including the calculation of the uncertainty for the best qualitative and quantitative U and Th isotope ratio determination.

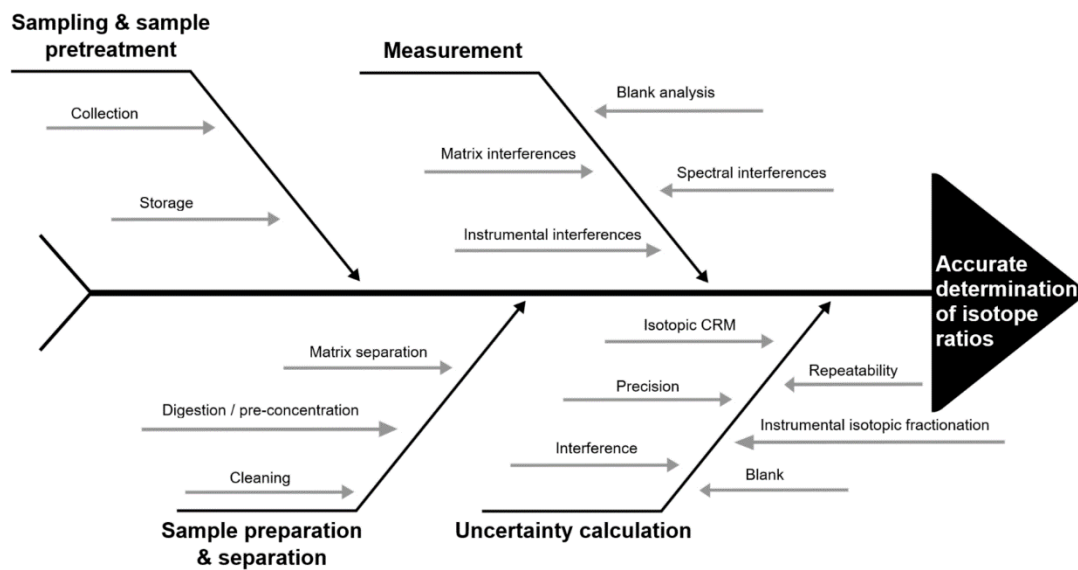


Figure 1.5: Components affecting accurate determination of isotope ratios (adopted by Irrgeher et al., 2016).

1.5.1 Sampling and sample pretreatment

The sampling design of the analytical procedure starts with the analytical problem that wants to be addressed. More demands are put on the quality of the analytical results, bigger the analytical problem becomes and more thought has to be given to the sampling design. The same also applies for elemental and isotopic analysis at low-level concentrations where high precision results are desired. Depending on the sampling matrix, the analyte of interest, and techniques that will be used, an effort has to be put into the preparation of contamination-free sampling containers. The correct choice of suitable materials for the containers, consumables, and lab clothing has to be used for a validated procedure for contamination-free sample (P. Hoffmann, 2008).

The size of the single sample which needs to be collected depends upon the expected concentration of the measuring element in the material and used analytical method. For U-series isotopic analysis, experiences show that 1 L samples, which are stored in prewashed high-density polyethylene (HDPE) bottles, represent an optimal choice for the determination of U isotopes in water samples (Andersen et al., 2016; Ljudmila Benedik, Rován, Klemenčič, Gantar, & Prosen, 2015; Grzymko, Marcantonio, McKee, & Mike Stewart, 2007; Kraemer & Brabets, 2012; Skwarzec, Strumińska, & Borylo, 2001). Water samples that are not processed immediately after sampling must be long-term protected against contamination, losses, or other changes. Samples for U isotopes analyses are filtered through 0.45- μm pore size filters and acidified to pH 2 to prevent adsorption of U isotopes to the particulate matter and to the walls of the container, and to reduce any bacterial activity in water (ISO, 2006b). The required size of the solid sample is determined by the grain size of the material, the homogeneity of distribution of the measuring element and used analytical method. Collected rock samples are usually oven-dried, crushed in a brass mortar to a smaller size, and further crushed with a gyratory crusher and sieved below 1 mm (ISO, 2006a). For the U and Th isotopic analysis, an aliquot of no more than 1 g of samples of solid matter is normally used. If the sample mass is higher than 1 g, possible problems with the sample matrix are observed (Bourdon et al., 2009; Huckle et al., 2016; Jia et al., 2008; Rodríguez, Tomé, & Lozano, 2001; Weyer et al., 2008).

1.5.2 Sample preparation and separation

Prior to mass spectrometric isotopic analysis, the transformation of any kind of sample into a measurable state is necessary. For this purpose, analyte must be in diluted nitric acid solution. Mass spectrometry, which uses plasma ionization, usually requires matrix removal and purification of samples. Especially for MC-ICP-MS analysis, transformation involves pre-concentration for water samples and matrix digestion or extraction for solid samples, in order to end up with the sample in a liquid form and the analyte of interest dissolved in a solution that can be directly introduced into the instrument (Irrgeher & Prohaska, 2016). As a result, a careful sample preparation procedure is needed to separate U and Th isotopes from the sample matrix and other possible interferences and also to improve the detection limit, increase the sensitivity and enhance the accuracy of the result, especially for samples with low-level U and Th concentrations (Andersen et al., 2017; Bourdon et al., 2003).

Environmental water samples rarely contain U and Th concentrations above $\mu\text{g/g}$ level; thereby, chemical methods are required for purifying, and concentrating sufficient quantities of the analyte of interest. A series of U concentration methods for water samples already exist and usually involve evaporation or co-precipitation with either iron(III) hydroxide ($\text{Fe}(\text{OH})_3$), calcium phosphate ($\text{Ca}_3(\text{PO}_4)_2$), or manganese dioxide (MnO_2) (Horwitz et al., 1992; Jia et al., 2008; Rodríguez et al., 2001; Skwarzec et al., 2001; Thakkar, 2001; Vera Tomé, Jurado Vargas, & Martín Sánchez, 1994).

In the case of solid samples, a quantity sufficient to be representative of solid material is ground to a fine powder and aliquot is dissolved in mineral acids. Then the solution can be separated from undissolved solid residue by centrifugation or filtration. Sample digestion is generally required for all solid sample matrices. Solid samples, which contain U and Th, are usually dissolved and digested in mineral acid mixtures (nitric acid (HNO_3), perchloric acid (HClO_4), hydrochloric acid (HCl) and hydrofluoric acid (HF)) (Carrasco Lourtau & Rubio Montero, 2016; Inn et al., 2016; Jurečič et al., 2014; Selvig, Inn, Outola, Kurosaki, & Lee, 2005; Trdin, Nečemer, & Benedik, 2017). Digestion is facilitated by heating or microwave digestion. The sample can also be dissolved and digested with alkaline fusion, or fusion with lithium borates (Carrasco Lourtau & Rubio Montero, 2016; Inn et al., 2016; Jurečič et al., 2014; Trdin et al., 2017). To extract a particular component within a specific soil or sediment sample, instead of total dissolution, a leaching procedure can be used. Leaching represents the removal of a geochemical component of solid-phase natural-matrix materials (e.g. carbonate minerals, oxides of Fe and Mn) combined with the release of an analyte of interest during the dissolution or desorption from the solids. Results present indirect evidence for probable geochemical associations of the element in question with these geochemical components and provide information regarding the conditions under which the element may be released to the environment. Leaching analysis can be done in a short time and without the use of time-consuming procedures and aggressive reagents, as is sometimes with total dissolution (L. Benedik, Pintar, & Byrne, 1999; International Atomic Energy Agency, 1991; Schultz, Burnett, & Inn, 1998). However, leaching can also provide some difficulties, such as readsorption, non-selectivity of extraction reagents, and incomplete dissolution of target phases (Schultz et al., 1998); therefore these problems need to be recognized and avoided to the extent possible. To extract mainly the carbonate-associated U and Th fractions from the sample, soft leaching procedures are normally used, (1 M Na-acetate in 25% acetic acid, 3 M HNO_3 , 7 M HNO_3 , 0.1 M HCl , 2% HCl , and warm H_2O_2) (Bourdon et al., 2009; Garnett et al., 2004; Nyachoti et al., 2019; Robinson et al., 2004; Štok & Smodiš, 2010; Wang & You, 2013; Watanabe & Nakai, 2006; Weyer et al., 2008). Meaningful U and Th isotope ratios can also be obtained from environmental solid material using a laser ablation system coupled to MC-ICP-MS, with minimal sample pre-

treatment because of the instrument's high sensitivity. The sample usually requires preparation of thin sections and some polishing to enhance any surface texture and to promote stable ion beams. Uncertainty with using a small sample size is higher than can be achieved with using larger sample sizes, but information can be related directly to a micrometer-sized area of the sample (Goldstein, 2003; Spooner, Chen, Robinson, & Coath, 2016; van Calsteren & Thomas, 2006; Varga et al., 2018). An overview of sample preparation procedures for U and Th isotopic analysis is presented in Table 1.2.

Chemical separation

After the pre-concentration or digestion step, it is important to separate U and Th isotopes from the matrix elements and interferences. This is mainly to ensure interference-free measurements and the best possible matching between the sample and the standards used for the calibration. Matrix separation procedure, following either single stage or multiple stage protocols, eliminates major molecular interferences, such as isobaric and polyatomic interferences. Molecular interferences in U analysis are the result of the combination of impurity elements present in the sample (Pb-oxides, Pb-nitrides, Pb-nitrogen-oxygen, Hg-chlorides, and $^{232}\text{ThH}^+$) and can affect high precision measurements with increased and unwanted signal intensities (Boulyga et al., 2016; Pollington, Kinman, Hanson, & Steiner, 2016; Wieser & Schwieters, 2005). Similar interferences can occur also in Th analysis. Nowadays, many different standard separation procedures exist for U and Th isotopic analysis (Andersen et al., 2017; Goldstein, 2003). Separation methods involving anion or cation exchange chromatography, extraction chromatography, solvent extraction, phase separation, and co-precipitation can be found and are based on different retention behavior of the analyte and the interfering components. An overview of possible U and Th chemical separation techniques is shown in Table 1.2. Additionally, automated separation systems have also been developed, which further increase the quality of sample preparation (Romaniello et al., 2015; Wefing et al., 2017).

One of the separation methods for U and Th analysis is extraction chromatography. Chromatographic resins were developed specifically for actinides and many different commercially available resins, such as uranium and tetravalent actinide (UTEVA), tetravalent actinide (TEVA), and trans uranium elements (TRU) are now widely used for U and Th purification for isotopic analysis (Boulyga et al., 2016; Eikenberg et al., 2001; Goldstein, Rodriguez, & Lujan, 1997; Layne & Sim, 2000; Pietruszka, Carlson, & Hauri, 2002; Stirling et al., 2005; Tissot & Dauphas, 2015; Weyer et al., 2008). These chromatographic materials are characterized by high distribution coefficients for U in HNO_3 and for Th in HCl. Ion exchange chromatography is also a valuable method for the determination of U and Th isotopes at ultra-trace levels. Typically, ion exchange resin such as Dowex AG-1x8 has been used to separate U from matrix elements (Adriaens, Fassett, Kelly, Simons, & Adams, 1992; J. H. Chen & Wasserburg, 1981; Lawrence Edwards, Chen, & Wasserburg, 1987). Using only ion exchange resin, U or Th cannot be completely separated from the matrix. Fe^{3+} ions and other metal ions (Co^{2+} , Cu^{2+} , and Zn^{2+}) can form stable chloride complexes, obstructing sufficient separation of U and Th from the matrix (Adriaens et al., 1992). Therefore, in some high precision measurement cases, more than one separation step is needed, and usually, Th fractions are passed through a second ion exchange or extraction column (Cheng et al., 2013; Yokoyama, Makishima, & Nakamura, 1999).

Each separation method requires strict control of method blanks and good recoveries, because of possible effects of on-column isotope fractionation (Adriaens et al., 1992; J. H. Chen & Wasserburg, 1981; Oi, Kawada, Hosoe, & Kakihana, 1991). It was observed that residual extractant materials in the eluent can negatively influence U or Th isotopic

behavior during measurements (Pietruszka et al., 2002; Rován & Štok, 2019). The presence of organics is especially evident in the case of U separation with solvent extraction (tri-n-butyl phosphate (TBP)), which is based on using organic solutions (Horwitz, Dietz, Nelson, LaRosa, & Fairman, 1990). To reduce the organic interferences from the residual resin, precleaning of resin using a significant concentration of HNO_3 can be practiced before purification of U or Th fractions. Concentrated HNO_3 and hydrogen peroxide (H_2O_2) can be employed at the end of separation for the destruction of remaining organic residue. Significantly increasing washout times between sample analysis can also lower the U and Th isotopic biases (Goldstein, 2003). Alternatively, use of matrix-matched isotope certified reference materials could also be applied.

Tracer addition

Sample preparation for isotopic analysis is extensive and chemical recoveries can vary considerably from sample to sample. Precise elemental concentrations and isotopic compositions for mass spectrometric methods are usually determined by isotope dilution methods (Faure, 1977). The isotope dilution method is based on the determination of the isotopic composition of an element in a mixture of a known quantity of a tracer with an unknown quantity of the normal element. The tracer is a solution, containing a known concentration or isotope ratios of a particular element or elements for which isotopic composition has been changed by enrichment of one or more of its isotopes. The nature of the added tracer depends on the measurement technique and it is important that the tracer must be of high-purity (Goldstein, 2003).

For U and Th isotopic composition measurements with mass-spectrometric methods, long-lived radioactive tracers, such as ^{233}U , ^{236}U , ^{229}Th can be used (Frank, Kober, & Mangini, 2006; Pietruszka et al., 2002; Robinson et al., 2004; Seth, Thirlwall, Houghton, & Craig, 2003), whereas, for isotopic measurements with radiometric methods, short-lived tracers (^{232}U and ^{229}Th) are normally practiced (Ljudmila Benedik et al., 2015; Eikenberg et al., 2001; Štok & Smodiš, 2010) (Table 1.2). To improve dating precision and to determine the relative abundances of U and Th isotopes more precisely, mixed tracer spikes, such as ^{233}U - ^{229}Th , ^{236}U - ^{229}Th , or ^{233}U - ^{236}U - ^{229}Th can also be applied (Cheng et al., 2013; Garnett et al., 2004; Henderson, Slowey, & Fleisher, 2001; Pietruszka et al., 2002; Shen et al., 2002; Stirling, Lee, Christensen, & Halliday, 2000). Alternatively, for precise U and Th isotopic ratio measurements, one can use natural and known isotopic ratio of $^{238}\text{U}/^{235}\text{U}$ or a double spike ratio (^{233}U - ^{236}U) that is composed of two synthetically produced isotopes and does not naturally occur in the sample. With that, also reliable internal correction of instrumental mass discrimination of the measured isotopes during sample measurement is performed (Andersen et al., 2004; Condon, McLean, Noble, & Bowering, 2010; Goldmann et al., 2015; Lawrence Edwards et al., 1987; Tissot & Dauphas, 2015; Weyer et al., 2008). However, in some cases, the double spike method is not recommended for the analytical use (Boulyga et al., 2015; Sakaguchi et al., 2009; Wieser & Schwieters, 2005). It is possible that the instrument cup configuration does not allow for the simultaneous measurement of ^{234}U using ion counters and ^{233}U and ^{236}U using Faraday detectors or the measurements of ^{233}U or ^{236}U ions are required. In these cases, instead of the double spike method, the use of the standard-sample bracketing method is applied (Andersen et al., 2004; Boulyga et al., 2016).

Tracers are normally standardized by mixing them with either a gravimetric standard or a well-characterized secular radioactive equilibrium standard for which U and Th isotope abundances are well known (Ludwig et al., 1992). Preparation of U or Th tracer isotopes generally involve nuclear reactions, followed by chemical separations to purify U or Th isotopes. ^{233}U and ^{236}U can be prepared by neutron and alpha activation of ^{232}Th ,

respectively, whereas ^{229}Th is commonly prepared by milking a ^{233}U supply (Goldstein, 2003). After the tracer is added to the sample, proper tracer-sample equilibrium must be obtained for accurate isotopic analyses. Generally, HNO_3 is added to the tracer-sample mixture and left to dry-down, for which tracer and sample are converted to the same chemical form (Pietruszka et al., 2002; Stirling et al., 2000).

Table 1.2: Overview of sample preparation procedures for U and Th isotopic analysis.

<p>Pre-concentration techniques (for water samples)</p>	<ul style="list-style-type: none"> • Evaporation • Co-precipitation with $\text{Fe}(\text{OH})_3$ • Co-precipitation with $\text{Ca}_3(\text{PO}_4)_2$ • Co-precipitation with MnO_2
<p>Digestion techniques (for solid samples)</p>	<ul style="list-style-type: none"> • Mineral acids (HNO_3, HClO_4, HF) • Microwave digestion (closed or open) • Alkaline fusion • Fusion with lithium borate • Leaching • Laser ablation
<p>Separation techniques</p>	<ul style="list-style-type: none"> • Extraction chromatography • Ion-exchange chromatography • Extraction chromatography & Ion-exchange chromatography • Solvent extraction
<p>Tracer addition</p>	<ul style="list-style-type: none"> • Long-lived tracers (^{233}U, ^{236}U, ^{229}Th) • Mixed spike tracers (^{233}U-^{229}Th, ^{236}U-^{229}Th, ^{233}U-^{236}U-^{229}Th) • Natural U isotopic ratio ($^{238}\text{U}/^{235}\text{U}$) • Double spike (^{233}U-^{236}U)

1.5.3 Instrumental methods

The analytical methods used for determination of U or Th isotope ratios depend mainly on what isotopes are of interest, their half-lives, decay mode, and risk of interferences in the various techniques. In order to quantify U and Th concentrations and isotope ratios, there are two principal measurement methods, alpha spectrometry and mass spectrometry (Goldstein, 2003; Ivanovich & Harmon, 1992). Alpha spectrometry is based on the detection of alpha particles formed during radioactive decay of alpha nuclides and utilizes charged particle detectors that give information on the detected energy and the intensity, which can be used for quantification. Alpha emitters with short half-life have large specific activity, which is activity per unit of mass of radionuclide and are therefore more suitable for alpha spectrometry (Vajda, Martin, & Kim, 2012). In mass spectrometry (MS), for determining U and Th isotope ratios, the most common techniques in use are thermal

ionization (TIMS), secondary ion (SIMS), accelerator (AMS), and plasma ionization (ICP-MS). In ICP-MS different setups can be found, such as with a quadrupole mass filter (ICP-QMS), a magnet sector with a single detector system (SD-ICP-MS), a multicollector system (MC-ICP-MS) and by using laser ablation (LA-(MC)-ICP-MS). In all instruments, measured elements or isotopes are ionized, separated according to mass, and detected using Faraday collectors or ion-counters (Prohaska, Irrgeher, Zitek, & Jakubowski, 2014).

Choosing the optimal method for the determination of U and Th isotope ratios is not an easy task. Alpha spectrometry is a traditional radiometric method for measuring radionuclides emitting alpha particles and still provides one of the most cost-effective, simple and reliable methods for U and Th analysis. It is very suitable for analysis where higher detection limits and lower precision are acceptable. Nevertheless, alpha spectrometry requires long counting times (from days up to weeks) and a limited precision for the analysis in low-level concentrations, due to the counting statistics (Hou & Roos, 2008; Vajda et al., 2012). Mass spectrometric methods represent the standard accepted methods for U and Th isotopes determination with long half-lives, in terms of sample size requirements, detection limit, analytical precision, and time of analysis. Traditionally, the technique of choice for achieving the highest accuracy and precision of isotope ratios has been TIMS. The instrument improved analytical precision, time of analysis, and sample size requirement in U and Th isotope applications, compared with decay counting techniques (J. H. Chen & Wasserburg, 1981; Hou & Roos, 2008; Platzner, 1997). In recent years, MC-ICP-MS had emerged as an alternative to TIMS, because of TIMS extensive sample preparation and limited number of samples to be placed in sample changer, which needs to be kept under vacuum during measurements. MC-ICP-MS has brought a simple and robust sample introduction, high sample throughput, high mass resolution, and lower detection limits (Goldstein, 2003; Hou & Roos, 2008; Wieser & Schwieters, 2005). The flat-topped peaks in MC-ICP-MS generated by double-focusing configuration provide an accurate and precise determination of isotope ratios, with precision reaching to 0.001 % (Albarède et al., 2004).

Inductively coupled plasma mass spectrometry

Inductively coupled plasma mass spectrometry is based on the formation of charged atomic ions in an inductively coupled argon plasma at its temperature 10000 K. The chemically separated analyte of interest is aspirated into the plasma source as an aerosol at ambient pressure, where the sample is immediately dissociated and ionized. To reduce polyatomic oxide and hydride interferences that are produced at conventional aspiration with wet plasma, the sample can be aspirated with dry plasma, with a desolvating nebulizer system (Vanhaecke, van Holderbeke, Moens, & Dams, 1996). Formed ions are transferred via a set of nickel cones into an expansion chamber, held in a vacuum, and enabling ions to undergo supersonic expansion. Most of the sample is lost there. Behind the cones, ions are optically focused by a series of ion lenses onto the entrance slit and into the mass analyzer. The mass separator (often quadrupole or magnetic sector field) operates at a high vacuum, where ions are separated according to their mass/charge ratio. In most MC-ICP-MS instruments, ions are focused on a Nier-Johnson double-focusing geometry, which incorporates an electrostatic analyzer, followed by a magnetic analyzer. Ions that are passing through the mass spectrometer entrance slit are energy- then direction-focused. The double focusing configuration provides the flat-topped peak shapes that are required for high precision isotope measurements. Ions are then detected using a secondary electron multiplier or/and a Faraday cup. There are two options how the instrument is set up. Normally, ICP-MS is a single-collector instrument, which is equipped with one detector. Ions are detected sequentially and the instrument is operated under dynamic (e.g. scanning) conditions. Another option is that ICP-MS is set as a multicollector instrument, which has

a set of parallel detectors, allowing simultaneous detection of ions at different mass-to-charge ratios. This instrument is usually operated under static (e.g. fixed magnet field) conditions (Jakubowski, Horsky, Roos, Vanhaecke, & Prohaska, 2014). MC-ICP-MS instruments (Figure 1.6) are usually equipped with multiple Faraday and ion-counting collectors, enabling the simultaneous measurement of up to twenty-one ion beams (Goldstein, 2003; Wieser & Schwieters, 2005). Additionally, to allow direct analysis, different sample introduction systems can be coupled to the instrument, such as laser ablation, gas chromatography, or liquid chromatography (Günther-Leopold, Wernli, Kopajtic, & Günther, 2004; Krupp & Donard, 2005; Stirling et al., 2000). MC-ICP-MS has been developed into a dedicated tool for isotopic analysis and displays high isotope ratio precision.

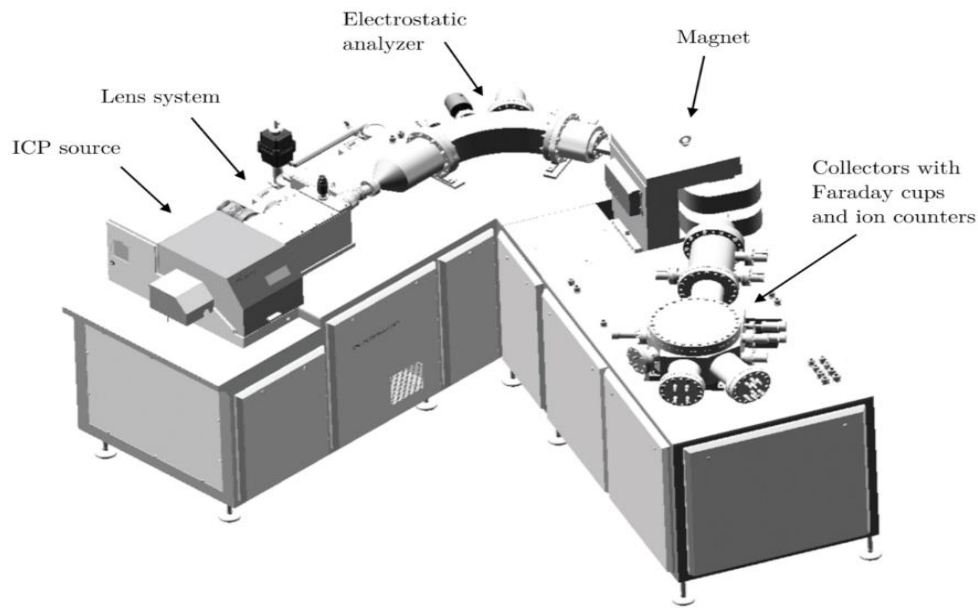


Figure 1.6: Schematic of the MC-ICP-MS instrument (Nu Instruments Ltd., 2014).

For U and Th isotope analysis, a solution of dilute HNO_3 is used for sample introduction into plasma source. It is also desirable to add a small amount of concentrated HF, just to minimize sample memory effects. Additionally, to reduce the sample memory effect, the tube has to be flushed between sample runs with the same dilute acid as used for the sample (Goldstein, 2003). A great feature in U and Th MC-ICP-MS analysis is that the ionization efficiency is almost 100 % (Turner, Calsteren, Vigier, & Thomas, 2001). Many different protocols exist for U and Th isotopic analysis by MC-ICP-MS (Ball et al., 2008; Pietruszka et al., 2002; Rubin, 2001; Seth et al., 2003; Stirling et al., 2000; Watanabe & Nakai, 2006). In a typical protocol, U isotopes are monitored by aligning Faraday collector for masses ^{238}U and ^{235}U , while low intensity ^{234}U ion beam is measured simultaneously in the ion-counting collector (Andersen et al., 2004; Boulyga et al., 2016; Stirling et al., 2007). This protocol can also be performed in two sequences, where the first sequence stays the same as before. In the second sequence, a mass of the ^{235}U is moved to the ion-counting channel where ^{234}U ion beam is being measured and ^{238}U is measured at the Faraday collector. When ^{235}U is determined on two different types of detectors, this provides an estimation of the drift in the relative gain between the ion-counter and Faraday cup and the ^{234}U ion beam intensity could be corrected at the end of each of the two-sequence cycle (Pietruszka et al., 2002; Seth et al., 2003; Stirling et al., 2000). Typical runs for U or Th isotopic measurements involve around 60 to 100 cycles with different integration times for

samples and instrumental background. The total duration of data acquisition takes from 15 min and up to 1 hour for each sample, which includes background measurement and peak centering. Sample sizes of total U or Th vary from 1 ng to 1000 ng (Boulyga et al., 2016; Robinson et al., 2004; Stirling et al., 2000; Weyer et al., 2008). MC-ICP-MS measurement protocol for Th involves the simultaneous measurement of ^{230}Th and ^{232}Th , where ^{230}Th is measured on ion-counter and ^{232}Th on Faraday collector (Ball et al., 2008; Rubin, 2001; Seth et al., 2003; Watanabe & Nakai, 2006). For a combined U-Th analysis, it is better to measure Th simultaneously with U in one sequence (Robinson et al., 2004; Stirling et al., 2000). In that way, analytical precision is comparable and more accurate. In a two-sequence routine, first Th isotopic composition is measured, and then U isotopes are monitored. Two-sequence routine provides the mass fractionation correction and Faraday-ion counter gain corrections.

Measurement related factors

With respect to U and Th isotopic analysis, MC-ICP-MS has two major drawbacks, which are not present in other instruments and these are high plasma-generated ion source instability (Shen et al., 2002) and poor abundance sensitivity of some MC-ICP-MS instruments that allows the estimation of the magnitude of the tail contribution (Thirlwall, 2001). Because of these disadvantages and the complexity of the instrument, careful characterization of different measurement-related factors is necessary to ensure the accuracy and precision of the results.

Blank analysis It is very important to monitor the background levels of the analyte of interest for isotopic analysis. It is necessary to perform a procedure blank, where the entire method is followed in the same manner as the sample itself, but in the absence of the analyte. Sources of contamination can originate from sampling, digestions, extractions, chemical separation, or come from the measurement itself. Therefore, it is very important to monitor each preparatory step separately, in order to identify sources of contamination and to monitor the detection limit for the single steps in the sample preparation procedure and during the measurement itself (Irrgeher & Prohaska, 2016). For the detection of extremely low abundant isotopes, thorough control of sample preparation procedure and low instrumental background levels are required. This is especially important for environmental samples with minor U or Th isotopic differences in natural samples (Andersen et al., 2007; Seth et al., 2003; Stirling et al., 2007; Tissot & Dauphas, 2015; Weyer et al., 2008) and for samples, where the sample amount of anthropogenic components from the natural U background have to be determined (Boulyga et al., 2016).

During measurement by MC-ICP-MS, different options of monitoring instrumental background are possible. Depending on the isotopic system of interest, there are three different ways to measure the zero value. The most common way is using zero ESA (electrostatic analyzer) deflection. Instrumental background obtains the electronic background noise level, with no beam passing through the flight tube. As a result, no peak will be measured and the zero measurement can be obtained. The second option is zero at half mass, where the half-mass position would be used. This zero measurement is applied for large abundance tail corrections. The third option is on-peak zero using a blank solution, where a blank is recorded prior to the measurement of the sample (Nu Instruments Ltd., 2014). For U and Th isotope analysis, background measurements are typically monitored at half mass on either side of the peak (Robinson et al., 2004; Seth et al., 2003; Stirling et al., 2000).

Matrix effect In MC-ICP-MS, several types of matrix effects have been characterized. Spectral matrix effects occur when an element or molecule overlaps in mass with the isotope of interest. Non-spectral matrix effects include changes in instrumental sensitivity and mass bias, due to the presence of matrix elements in the analyte inherited from the natural sample, differences in the concentration and in the oxidation state of the element in the sample and the standard, and the presence of organic material from the natural sample. To have an accurate result, efficient matrix separation and purification from the analyte is crucial to prevent matrix-based interferences (Albarède et al., 2004; Becker, 2005; Pietruszka & Reznik, 2008; Thirlwall, 2002; Wieser, Buhl, Bouman, & Schwieters, 2004). It is especially important to have matrix-matching between the calibration standard and the samples because a variable matrix can induce a systematic bias (Horsky, Irrgeher, & Prohaska, 2016). Therefore, to overcome many matrix-based interferences, the appropriate selection of sample preparation or an adequate introduction system for the separation of the matrix and the analyte of interest need to be selected (Prohaska, 2014). In the case of the U and Th isotope ratio analyses using ICP-MS, various chromatographic protocols were developed for high precision analysis (Table 1.2) (Andersen et al., 2017; Bourdon et al., 2003). Additionally, automated separation systems, based on chromatographic methods, have also been developed, which further increase the quality of sample preparation and decrease matrix effects (Romaniello et al., 2015; Stirling et al., 2000; Varga et al., 2018; Wefing et al., 2017).

Spectral interference The occurrence of spectral interference mainly results from stray ions resulting in a signal at the time of measurement, ions of different kinetic energy, and single- or multiple-charged mono- or polyatomic ions of the same ratio as the analyte of interest but deriving from other than the analyte ion. Stray ions and ions of different kinetic energy can be sufficiently reduced with the double-focusing mass analyzer, which MC-ICP-MS has. Spectroscopic interferences of the source that are attributed to the presence of isobaric atomic ions multiply charged ions, and polyatomic ions of various origins can be reduced with more difficulty. Isobaric interferences exist when the signals of isotopes of different elements coincide at the same nominal mass. Multiple charged monoatomic ions are usually doubly charged ions and are found at half of their nominal mass. Polyatomic interferences are less predictable and mostly depend on the sample composition and the operational parameters of the instrument. They are introduced by the sample itself and from the discharge gas, contaminants, and reagent and solvent used. These interferences are usually resolved by applying higher mass resolution, by reducing the width of the entrance slit to shift interference away from the analyte, mathematical correction procedure, or chemical separation and purification system (Prohaska, 2014).

Spectral interferences in U and Th isotopic analyses by MC-ICP-MS have to be identified and subsequently controlled. Polyatomic molecular species (e.g. oxides, hydrides, and argides) are often the cause for low precision isotopic analysis and they result from the combination of impure elements present in the sample with matrix elements (hydrogen, oxygen) or the plasma gas (argon). Typical U isobaric interferences are mostly the result of the combination of impurity elements present in the sample (Pb-oxides, Pb-nitrides, Pb-nitrogen-oxygen, Hg-chlorides, and $^{232}\text{ThH}^+$) or the plasma gas (PtAr^+) (Boulyga et al., 2016; Pollington et al., 2016; Seth et al., 2003; Wieser & Schwieters, 2005). During mass spectrometric analysis, additional UH^+ and UO^+ may be formed and the rate of these interferences production is variable and dependent on operational conditions and the type of sample introduction system (Tissot & Dauphas, 2015; Weyer et al., 2008). Most often, various chromatographic protocols are considered to provide the necessary purification levels to avoid spectral interferences for U isotope analyses by MC-ICP-MS in low mass resolution (Hiess et al., 2012; Stirling et al., 2005; Tissot & Dauphas, 2015; Weyer et al.,

2008). Some studies have measured in high mass resolution to avoid potential unidentified polyatomic interferences across the U mass range (Connelly et al., 2012). Peak tailing of higher abundant isotopes ($^{238}\text{U}^+$ ions) into the low-energy ion $^{236}\text{U}^+$ can also significantly contribute to the unwanted signal intensities (Boulyga et al., 2016; Cheng et al., 2013; Hiess et al., 2012). Peak tailing interference can be physically reduced by applying retardation potentials to the ion of interest before they enter a secondary electron multiplier. The remaining peak tailing contribution is then determined by measuring standard, if possible with certified reference materials (Boulyga et al., 2016; Cheng et al., 2013; Seth et al., 2003).

Instrumental interference The source of instrumental interferences is the result of the system electronics or stray electrons in the system or the detection unit. Scattering electrons can be observed when Faraday detectors are used. However, an electron suppressor or a small magnet ensure that no secondary electrons are released from the detector. Additionally, the Faraday cup design minimizes the secondary electrons escape angle by increasing the Faraday cup length (Prohaska, 2014).

Mass bias correction

Mass bias is an isotopic fractionation that can happen during measurement in MC-ICP-MS and can be produced by variable transmission of the ion beam in a mass spectrometer, as intensity bias related to multiplier dead time, or as an offset from the true ratio associated with beam intensity differences between isotopes. Instrumental mass bias is also not constant and may drift with time (Shen et al., 2002). Therefore, correction methods are required and the most commonly used mass bias correction models are the double spike technique, internal standardization, and external standard-sample-standard bracketing technique.

Double spike technique The double spike technique for mass bias correction is based on two mass spectrometer runs, for an unspiked sample and for a spiked sample in which two enriched isotopes are added to the test sample. Together these define the mass bias corrected isotopic composition of an analyte element which must have four or more isotopes. It is important that spike composition is known (Yang, 2009). There are some disadvantages to this method, such as the availability of enriched double spikes, which are sometimes difficult to obtain due to regulations of export of radioactive materials; the cost of high-purity enriched double spikes; the effort required to calibrate the isotopic composition of the spike; the need for at least four interference-free isotopes of the analyte and the need to avoid cross-contamination between two runs (Yang et al., 2018). It is also possible that the precision of the technique will suffer since all measurement errors propagate into the final result. A major advantage is that the mass bias correction factor can be directly determined for each sample, thus providing accurate isotope ratio data (Yang, 2009).

To accurately correct mass-dependent fractionation during U or Th analyses, a ^{233}U - ^{236}U double spike (IRMM-3636), prepared at the Institute of Reference Materials and Measurements (IRMM), Belgium, can be used (Richter et al., 2008). U double spike was derived from high-purity isotopes, its ratio and uncertainty were determined by gravimetric principles, therefore can be traced to the SI system of units. Measurements with a ^{233}U - ^{236}U double spike can be performed separately, or combined with the U isotopic composition run (Goldstein, 2003). Spike tracers are normally measured on Faraday collectors, simultaneously with ^{238}U and ^{235}U , during the first sequence (Brennecke, Borg, et al., 2010; Stirling et al., 2007; Tissot & Dauphas, 2015; Weyer et al., 2008). This shortens the analysis

routine and consumes less sample. The ^{233}U - ^{236}U double spike can also be used to correct Th mass fractionation, because no possible differential fractionation of U and Th isotopes during chemical separation was revealed (Cheng et al., 2013).

Internal standardization technique With the internal standardization technique for mass bias correction, the correction factor is determined in the sample solution by using a pair of isotopes of the analyte element that are believed to be invariant in nature, or by the use of one or more isotope ratios of one or more reference elements added to the sample. There are three possibilities of internal standardization technique that can be used for mass bias correction, using a pair of analyte isotopes, using a pair of isotopes of another element, the value of which is calculated against the analyte ratio in a certified reference material, and an alternative method, regression internal standardization with the use of isotopes of another element as an internal standard (Yang, 2009).

The internal standardization technique is largely used for many different isotopes, however for U and Th isotopes it is not so popular due to lack of non-radiogenic isotopes of an analyte adequate to use for mass bias correction and expansion of other correction techniques for high U and Th accuracy and precision (double spike method and standard-sample-standard bracketing method).

External standard-sample-standard bracketing technique The standard-sample-standard bracketing is an external standardization procedure and in this technique isotope ratio in the sample is measured interspersed with analyses of reference material of known isotope ratio. The composition of the reference material must be known so that the instrumental mass bias can be quantified and transferred to measured isotope ratio and it is essential that analytical concentrations in the sample and the standard have to be matched (Condon, Schoene, McLean, Bowring, & Parrish, 2015; Stirling et al., 2000; Yang, 2009).

The sample-standard bracketing technique has been widely used for U and Th mass bias correction due to its simplicity. It has been performed to cancel out the drift in the Faraday to ion-counter gain and for other instrumental fractionations (Andersen et al., 2004; Boulyga et al., 2016; Robinson et al., 2004; Stirling et al., 2000). By analyzing the standard before and after the sample, the drift from the Faraday to ion-counter gain can be canceled out by linear interpolation. The main two advantages to this protocol are that data acquisition times are shorter than those that are for multi-static protocols and less sample is consumed, therefore ion beam intensities are not restricted by the necessity to keep ^{235}U ion counts below 1,000,000 cps when ^{235}U has to be measured on the ion-counter detector. The main disadvantages are no correction for short-term non-linear perturbations in the Faraday to ion counter gain, which may limit the accuracy of the measurements, and possible matrix differences between the sample and standard, which may compromise the reliability of the mass bias correction (Goldstein, 2003). For that reason, analyte concentrations in the sample and the standard have to be matched carefully and perfect separation of sample matrix is required. In addition, a longer warm-up time for the instrument is necessary to ensure its stability, shorten the measurement time, and to minimize any temporal drifts in mass bias (Yang et al., 2018). External standardization for Th isotopic measurements can determine Faraday-ion counter gain and mass fractionation correction with a standard solution of natural Th (Layne & Sim, 2000; Rubin, 2001; Turner et al., 2001) or of natural U (Mason & Henderson, 2010; Nakai, Fukuda, & Nakada, 2001). The advantage of external standardization with natural U is that Th isotopic composition can be acquired on small samples as a single static measurement. However, instrumental mass fractionation can vary between solution runs as a function of time and solvent loading; thereby it is preferable to use matrix-matched Th standards

instead. External standard-sample-standard bracketing technique can be sometimes the only possible method to use for U and Th correction of mass bias. In some cases, other methods are not recommended due to ^{233}U and ^{236}U presence in the sample; such as in the process of nuclear fission, the global fallout from nuclear atomic bombs, and nuclear reactor accidents (Sakaguchi et al., 2009). Also in the nuclear safeguard programs, where the U isotopes are determined in the micron size particle and anomalous amounts of ^{233}U and ^{236}U may indicate artificial isotope enrichment or depletion processes (Boulyga et al., 2015; Wieser & Schwieters, 2005). To analyze environmental samples at sub-nanogram levels and when only a small amount of sample is available, it is also preferable to measure the ion signals from minor U isotopes (e.g. ^{234}U) using ion counters and ^{233}U and ^{236}U using Faraday detectors because of more efficient mass bias corrections (Andersen et al., 2004; Goldstein, 2003; Park & Jeong, 2018). However, this can be problematic when the instrument cup configuration does not allow for the simultaneous measurement of ^{234}U using ion counters and ^{233}U and ^{236}U using Faraday detectors (Andersen et al., 2004; Boulyga et al., 2016). In this case, instead of the double spike method, the use of the standard-sample bracketing method needs to be applied.

1.5.4 Uncertainty

The fundamental importance to produce an accurate value for an analyte of interest is to account for all possible sources of uncertainty arising from a measurement procedure. Many factors contribute to the uncertainty of isotope ratios and significant differences in the isotopic composition between samples can be assured if all possible sources of uncertainty are considered. To make a meaningful comparison of isotope ratio results obtained in many different studies, especially when small isotopic effects are being looked at, the combined standard uncertainty associated with the methodology used should be calculated and assigned to isotope data (Irrgeher & Prohaska, 2014). Therefore, it is important to avoid reported isotope ratio data with only the standard deviation or standard error of the measurement. The major sources of uncertainty of the measurement itself include blank correction, instrumental isotopic fractionation correction, potential interference corrections, uncertainties of standard reference materials used, used atomic weights constants and isotope abundances from tables constants, repeatability (within-run-precision), and reproducibility (between-run-precision) (Albarède et al., 2004; Horsky et al., 2016; Irrgeher & Prohaska, 2016; Williams, 2010). Calculation procedures for individual parameters should be undertaken in accordance with guidelines of International Organization for Standardization (ISO) guide (ISO, 2008), which outlines a general procedure for evaluating and expressing uncertainty, and Measurement Uncertainty Working (EURACHEM/CITAC) guide (Ellison & Williams, 2012), which specifies an approach for the quantification of uncertainty in analytical chemistry.

For U and Th isotope analysis by MC-ICP-MS, the following sources of uncertainties are usually assessed: mass bias and the certified value of the standard used for mass bias correction, measurement repeatability of the mass bias standard and the sample, possible molecular interferences, peak tailing, Faraday cup amplifier gain and baseline (Boulyga, Klötzli, & Prohaska, 2006; Boulyga et al., 2016; Cheng et al., 2013; Shen et al., 2002; Stirling et al., 2000; Weyer et al., 2008). The U and Th instrumental performance can also be affected by the instability of the ion beam, dark noise and non-linearity of the ion-counter, error in measuring the efficiency of the ion-counter detector, amplifier noise on larger peaks via Faraday cups, and relative Faraday cup yield and its non-linearity (Bürger et al., 2012; Bürger, Essex, Mathew, Richter, & Thomas, 2010; Ludwig, 2003). The uncertainty of mass bias correction is usually estimated by calculating the combined standard uncertainty for the external standard-sample bracketing technique or the double

spike mass bias correction method and is normally quoted at the 95% confidence level (Yang, 2009). Measurement repeatability is most often derived from the pooled estimate of standard deviation, which is estimated from suitably matched quality control standards (Boulyga et al., 2016). Possible molecular interferences are usually monitored with certified reference standards or by measurement with the certified double spike standard (Weyer et al., 2008). For minor isotopes, peak-tailing effects can be a big addition to the source of uncertainty, whereas for major isotopes the peak-tailing effects are often insignificant (Cheng et al., 2013). Other possible uncertainties in the U and Th isotope ratio analyses are mostly comparatively small and can be insignificant or unimportant when profound analytical work is performed. Therefore, they are sometimes not included in the uncertainty budget. The major source of uncertainty is typically the uncertainty of the certified value of the certified standard used for mass bias correction (Boulyga et al., 2016; Bürger et al., 2012, 2010; Condon et al., 2010; D. L. Hoffmann et al., 2007; Richter & Goldberg, 2003). Sometimes, a completely different uncertainty budget in the U isotopic measurement by MC-ICP-MS can be estimated. The dominant component in the combined standard uncertainty can be in some cases the measurement repeatability, owing to the plasma flickering (Pereira de Oliveira et al., 2010), the contribution of the blank correction (Pereira de Oliveira et al., 2010; Robinson et al., 2004) or the variation of the ion-counter yield (Kappel, Boulyga, & Prohaska, 2012). Therefore, situations might change during continuous measurements and other uncertainty contributions can increase the combined standard uncertainty. In order to timely recognize changes in the analytical procedure that might potentially introduce a negative effect on the quality of the results, it is important to routinely monitor and control all possible factors that can contribute to the overall assessment of the uncertainty budget.

1.5.5 Data reporting

Isotopic data can be reported in absolute and/or relative values. Absolute isotope ratios are sometimes not recommended, because different laboratories performed different data correction procedures, for blank and mass bias, and it is difficult to establish international comparability. With the use of certified reference materials, this task is easier to perform, but there are not enough available isotope certified reference materials and those that exist are provided with high uncertainties assigned to the certified values (Irrgeher & Prohaska, 2016). For many applications, it is generally of more interest to know the relative differences in isotopic ratios between samples. Isotopic composition is often reported as a delta (δ) value to a common standard solution (Eq. (1.4)). Delta value is suggested as the ratio of an unknown sample to a preferably internationally accepted standard and is expressed in parts per mill (‰):

$$\delta(R^{i/j}) = \left[\left(R_T^{i/j \text{ sample}} / R_T^{i/j \text{ std}} \right) - 1 \right] \times 1000 \quad (1.4)$$

where $R_T^{i/j \text{ sample}}$ and $R_T^{i/j \text{ std}}$ are mass bias corrected ratios in the sample and standard, respectively (Coplen, 2011; Irrgeher, Vogl, Santner, & Prohaska, 2014; Yang, 2009). Very small variations in the isotopic composition can also be expressed in at parts per ten thousand (Coplen, 2011). The delta notation provides a means to circumvent the use of the stated uncertainties of certified reference materials and it allows small differences in number ratios to be expressed without precisely knowing the absolute isotopic abundance of an element. It is still important to use the delta values with isotopic reference materials as a common reference, because of the easier comparison of measurement results on an international level and with the literature (Irrgeher et al., 2014). For isotope ratios

demonstrated as delta values, no further model for mass bias correction has to be applied, compared to isotope ratios that are displayed as absolute values. All sources of mass discrimination are expected to be similar for the used reference material and the unknown sample, without knowing the absolute isotopic abundances of an element. With absolute isotope ratio measurements, several sources of uncertainty need to be taken into consideration, and correction approaches, calibration processes, or used reference values have to be applied. When absolute values are reported, the reference value of the reference standard must be clearly stated (Irrgeher & Prohaska, 2016).

Although, delta values can significantly reduce the impact of using different strategies for mass bias corrections and the uncertainties on reference materials, for precise and accurate isotopic results it is still recommended to use mass bias corrections on absolute ratios before applying delta values. Many different mass bias correction models have been reported, such as linear law, power law, exponential law, first-order, and second-order mass bias correction (Albarède et al., 2004; Irrgeher et al., 2014). The most widely applied correction model in MC-ICP-MS measurements remains the exponential law (Eq. (1.5)):

$$R_T^{i/j} = R_m^{i/j} (m_i/m_j)^f \quad (1.5)$$

where $R_T^{i/j}$ is the mass bias corrected ratio or true value, $R_m^{i/j}$ is the measured ratio, m_i and m_j are absolute atomic masses of isotopes of interest, and f is the mass bias correction factor (Albarède et al., 2004).

Currently, there is still no accepted convention on how to report variability between U or Th isotopes and either absolute ratios, delta values or epsilon notations have been used (Andersen et al., 2004; Boulyga et al., 2016; Cheng et al., 2013; Stirling et al., 2007; Weyer et al., 2008). Absolute values are most often applied in nuclear safeguard and nuclear forensic, where U isotope ratios are reported as $^{234}\text{U}/^{238}\text{U}$, $^{235}\text{U}/^{238}\text{U}$, and $^{236}\text{U}/^{238}\text{U}$ (Boulyga et al., 2016, 2002; Bürger et al., 2012; Kappel et al., 2012), and in geochronology where $^{234}\text{U}/^{238}\text{U}$ and $^{238}\text{U}/^{235}\text{U}$ are stated (Hiess et al., 2012). For studies focusing on isotopic fractionation processes, delta notation (Eq. (1.4)) is the common way to report $^{238}\text{U}/^{235}\text{U}$ variability, because it eliminates changes in the $^{238}\text{U}/^{235}\text{U}$ ratio over time through radioactive decay and uncertainties arising from the determination of absolute ratios (Cheng et al., 2013; Tissot & Dauphas, 2015; Weyer et al., 2008). There is no generally accepted standard to be used to calculate relative $^{238}\text{U}/^{235}\text{U}$ ratios. Several isotopically pure U standards from the IRMM and the National Institute of Standards and Technology (NIST) have been used (Bopp et al., 2009; Brennecke, Borg, et al., 2010; Condon et al., 2010; Richter et al., 2010; Stirling et al., 2007; Weyer et al., 2008). However, intercomparison of $^{238}\text{U}/^{235}\text{U}$ between many standards has been performed and it was recommended that the use of CRM-112a standard (or CRM-145 standard, which is a solution made of CRM-112 metal) would be the most standardized way to report relative $^{238}\text{U}/^{235}\text{U}$ variability. A large proportion of studies have used this reference standard, which is widely available and commonly used (Andersen et al., 2014, 2016; Cheng et al., 2013; Hiess et al., 2012; Stirling et al., 2007; Tissot & Dauphas, 2015; Weyer et al., 2008).

For $^{234}\text{U}/^{238}\text{U}$ variability, both absolute ratios and delta notation are used (Andersen et al., 2009, 2004; Cheng et al., 2013; Seth et al., 2003; Stirling et al., 2007), however, absolute values as the activity ratio (Eq. (1.6)) are more frequently to be reported (Andersen et al., 2009; Durand et al., 2005; Grzymko et al., 2007; Riotte & Chabaux, 1999; Seth et al., 2003). The activity ratio is calculated from the mass bias corrected $^{234}\text{U}/^{238}\text{U}$ isotope ratios ($R_T^{i/j}$, Eq. (1.5)) and by using the decay constants of ^{234}U and ^{238}U (λ_{234} and λ_{238}) (Cheng et al., 2013).

$${}^{234}\text{U}/{}^{238}\text{U activity ratio} = \lambda_{234}/\lambda_{238} \times U_{\text{T}}^{234/238} \quad (1.6)$$

For Th isotopes, only absolute ratios as the ${}^{230}\text{Th}/{}^{232}\text{Th}$ activity ratio are used to discern any significant differences in the environment (Ball et al., 2008; X. Luo, Rehkämper, Lee, & Halliday, 1997; Robinson et al., 2004; Seth et al., 2003; Shen et al., 2002; Stirling et al., 2000; Turner et al., 2001). The activity ratio in Eq. (1.7) is calculated from the mass bias corrected ${}^{230}\text{Th}/{}^{232}\text{Th}$ isotope ratio ($R_{\text{T}}^{i/j}$, Eq. (1.5)) and by using the decay constants of ${}^{230}\text{Th}$ and ${}^{232}\text{Th}$ (λ_{230} and λ_{232}) (Cheng et al., 2013).

$${}^{230}\text{Th}/{}^{232}\text{Th activity ratio} = \lambda_{230}/\lambda_{232} \times Th_{\text{T}}^{230/232} \quad (1.7)$$

Chapter 2

Aims and Hypotheses

The aim of the dissertation is to accurately determine U and Th isotope ratios with MC-ICP-MS for samples with low-level U and Th concentrations and to correctly interpret analytical data in the context of application in geochemistry. To achieve that, the optimization of the MC-ICP-MS protocol was necessary to obtain high precision and accuracy for U and Th isotope data needed for applications in geochemistry. After verification of the analytical performance of the MC-ICP-MS instrument, sample preparation approaches were tested to evaluate their possible influence on U isotopic composition for determining U isotope ratios using MC-ICP-MS. The most commonly used U preconcentration and separation techniques in water and solid samples were tested, and the analytical procedure was optimized in terms of the smallest procedural blanks, the highest recovery, and the smallest bias from the standard reference value. The results of both optimization of MS measurement methods and U isotope behavior during sample preparation provide means for establishing the methodology, which enables accurate determination of U and Th isotope ratios in samples with low-level U and Th concentrations. The optimal protocol was then used to introduce U and Th as novel environmental tracers to study hydrogeochemical processes in karstic systems with predominantly carbonate lithology. The Ljubljana River catchment and the Krka River in Croatia were the first two case studies where developed methodology was applied. It is expected that the combined use of geochemical and physicochemical parameters with U and Th isotopic composition would show significantly improved understanding of karst hydrodynamics and provide a new perspective to already known data.

Hypotheses

Within the dissertation, the following hypotheses were tested:

1. Different sample pre-treatment and U separation protocols induce different levels of undesired biases between U and Th isotopes, which needs to be quantified in order to be able to select appropriate ones.
2. Optimization of U pre-treatment, separation and measurement protocols will result in methodology with lowest procedural blanks and undesired biases, which will be sufficiently good to be applicable in karst aquifer geochemistry.
3. U and Th isotopes will prove to be a useful tracer of geochemical processes in different studied karst aquifers.

Chapter 3

Scientific Publications

The dissertation consists of three publications. Publications presented in this dissertation are listed in such a manner that their consecutive appearances follow the general hypotheses of the dissertation. The first two hypotheses are covered by the first manuscript dealing with the optimization of the sample preparation and measurement protocol for the U isotope analysis (3.1). The last hypothesis is covered by the last two manuscripts ((3.2) and (3.3), where developed methodology was applied on the samples from the environment with predominantly carbonate lithology. The candidate's contributions to the individual scientific articles are described before each article. In the dissertation, publications appear in the following order:

Rovan, Leja, Štrok, Marko. Optimization of the sample preparation and measurement protocol for the analysis of uranium isotopes by MC-ICP-MS without spike addition. *Journal of analytical atomic spectrometry*. 2019, vol. 34, no. 9, str. 1882-1891. ISSN 0267-9477. DOI: 10.1039/C9JA00144A.

Rovan, Leja, Lojen, Sonja, Zuliani, Tea, Kanduč, Tjaša, Petrič, Metka, Horvat, Barbara, Rusjan, Simon, Štrok, Marko. Comparison of uranium isotopes and classical geochemical tracers in Karst aquifer of Ljubljana River catchment (Slovenia). *Water*. 2020, vol. 12, no. 7, str. 2064-1-2064-29. ISSN 2073-4441. DOI: 10.3390/w12072064.

Rovan, Leja, Zuliani, Tea, Horvat, Barbara, Kanduč, Tjaša, Vreča, Polona, Jamil, Qasim, Čermelj, Branko, Bura Nakić, Elvira, Cukrov, Neven, Štrok, Marko, Lojen, Sonja. Uranium isotopes as a possible tracer of terrestrial authigenic carbonate. *Science of the Total Environment*. 2021, vol. 797, str. 149103. DOI: 10.1016/j.scitotenv.2021.149103

3.1 Optimization of the Sample Preparation and Measurement Protocol for the Analysis of Uranium Isotopes by MC-ICP-MS without Spike Addition

Rovan, L., Štrok, M., Journal of analytical atomic spectrometry. 2019, vol. 34, no. 9, str. 1882-1891. DOI: 10.1039/C9JA00144A.

In this publication, the optimization of MC-ICP-MS measurement protocol is established to obtain high precision and accuracy for U isotope ratios ($^{235}\text{U}/^{238}\text{U}$ and $^{234}\text{U}/^{238}\text{U}$). Additionally, the possible influence on U isotopic composition is tested with different aqueous sample preparation and separation techniques using MC-ICP-MS measurements. The analytical method with the smallest U biases from the reference values was selected as the optimal procedure for application to real samples. The obtained results show that different sample preparation and separation methods influence U isotopic composition and consequently the final results of unknown samples. With the optimization of MC-ICP-MS measurements by controlling and correcting the factors, which can occur during measurements as instrumental mass bias, the accurate and precise analysis of U isotope ratios was achieved. The optimal analytical procedure with the highest achievable precision and accuracy for U isotopes was the combination of coprecipitation with $\text{Ca}_3(\text{PO}_4)_2$ as the preconcentration technique and extraction chromatography with UTEVA resin precleaned in 6 M HNO_3 as the separation technique. The combination of coprecipitation with $\text{Fe}(\text{OH})_3$ and ion exchange chromatography (DOWEX resins) provided the worst achievable accuracy for U isotopes. The experiment results reveal the extent of U biases during different physicochemical processing of samples in the range of -254–2.60‰ for $^{235}\text{U}/^{238}\text{U}$ and -299–8.90‰ for $^{234}\text{U}/^{238}\text{U}$. Obtained results show that the column matrix effects directly lead to the organic material stripped from the resin and can significantly influence the accurate determination of U isotope ratio with MC-ICP-MS measurements. By reducing impurity effects and other potential contaminations, the combination of sample preparation and measurement protocol optimization can be applied to real samples where the influence of matrix effect is significant and extremely small isotopic variations need to be detected with high accuracy and precision. It is also important for various applications requiring extensive sample pre-treatment procedures where using the $^{233}\text{U}/^{236}\text{U}$ double spike method for correcting for mass bias during sample preparation and separation steps is not feasible.

The candidate's contribution to this publication consisted of the optimization of the instrument performance for low-level U sample concentrations and to find the most suitable analytical procedure with the smallest bias from the standard reference material, with testing the most commonly used pre-concentration and separation techniques for U analyses. After assessing possible uncertainty contributions from the instrument and analytical procedure, she established the extent of deviation of U isotope ratios from the U isotopic standard in the evaluated methods. The candidate prepared figures and tables and drafted the manuscript.

JAAS



PAPER

View Article Online
View Journal | View IssueCite this: *J. Anal. At. Spectrom.*, 2019, **34**, 1882

Optimization of the sample preparation and measurement protocol for the analysis of uranium isotopes by MC-ICP-MS without spike addition†

Leja Rovani^{ab} and Marko Štrok^{*ab}

This study quantifies the behaviour of uranium isotope ratios ($^{235}\text{U}/^{238}\text{U}$ and $^{234}\text{U}/^{238}\text{U}$) with different aqueous sample preparation and separation techniques using multi-collector inductively coupled plasma mass spectrometry (MC-ICP-MS) measurements and optimization of the MC-ICP-MS measurement protocol to obtain high precision and accuracy for uranium isotope ratios. The obtained results were compared with reference values, and they show that different sample preparation and separation methods influence the uranium isotopic composition and consequently the final results of unknown samples. The analytical procedure with the highest achievable precision and accuracy for uranium isotopes was the combination of coprecipitation with $\text{Ca}_3(\text{PO}_4)_2$ and extraction chromatography with precleaned UTEVA resins. The combination of coprecipitation with $\text{Fe}(\text{OH})_3$ and ion exchange chromatography (DOWEX resins) provided the lowest achievable accuracy for uranium isotopes. The results reveal the extent of uranium biases during different physicochemical processing of samples in the range of -254 to 2.60% for $^{235}\text{U}/^{238}\text{U}$ and -299 to 8.90% for $^{234}\text{U}/^{238}\text{U}$. A combination of sample preparation and measurement protocol optimization is of importance for various applications requiring extensive sample pre-treatment procedures where the $^{235}\text{U}/^{236}\text{U}$ double spike method for correcting for mass bias during sample preparation and separation steps is not feasible and to establish a methodology which enables the accurate determination of uranium isotope ratios in low-level concentration samples.

Received 18th April 2019
Accepted 16th July 2019

DOI: 10.1039/c9ja00144a

rsc.li/jaas

Introduction

Uranium (U) is the heaviest naturally occurring element on Earth.¹ It commonly occurs in two oxidation states, U(IV) and U(VI). Under oxidizing conditions, uranium exists in the U(VI) state, mainly as uranyl ion UO_2^{2+} , and it is highly soluble and mobile. Under reducing conditions, uranium exists in the U(IV) state, mainly as insoluble complexes with hydroxides, and it is highly immobile.^{2–4}

Uranium has three naturally occurring radioisotopes, ^{238}U ($t_{1/2} = 4.5$ billion years), ^{234}U ($t_{1/2} = 245$ 000 years), and ^{235}U ($t_{1/2} = 0.7$ billion years).⁵ Furthermore, small amounts of ^{236}U can also occur naturally on Earth from neutron-capture processes within uranium ores ($^{236}\text{U}/^{238}\text{U} < 10^{-9}$).^{6,7} Uranium isotopic data are an essential dating and tracing tool for a broad spectrum of geological and hydrological processes.^{5,8} A significant natural variability of more than 0.03% in the $^{235}\text{U}/^{238}\text{U}$ ratio for a range of natural materials has been reported. This is due to the

variable solubility of uranium in different redox states and nuclear field shift effects.^{1,5,9,10} For $^{234}\text{U}/^{238}\text{U}$, large natural variations in the environment (>10%) can be observed mainly because of the effect of alpha recoil.^{10–13} Uranium isotope ratios are also an important characteristic for nuclear safeguards and nuclear forensic studies.¹⁴ ^{236}U determination was recognized as an important indicator to differentiate types of environmental nuclear contaminations.^{15,16} Measurements of $^{236}\text{U}/^{238}\text{U}$ isotope ratios are of importance in the environmental monitoring of contaminated territories to study nuclear weapon explosions, nuclear power generation and reprocessing of its fuel, and nuclear reactor accidents.^{17,18} Recently, when ^{233}U was detected in environmental samples, the $^{233}\text{U}/^{236}\text{U}$ ratio can be established as a tracer for discriminating between two different contamination sources.¹⁹

Measurement of the uranium isotopic composition in environmental samples requires high sensitivity to detect the smallest amounts of minor isotopes and high accuracy to differentiate between small fractionations in natural uranium samples.²⁰ In recent years, the use of multi-collector inductively coupled plasma mass spectrometry (MC-ICP-MS) afforded improved precision owing to the high absolute sensitivity and simultaneous detection of ions with a multi-collector detector block compared to quadrupole-based ICP-MS, and higher sample throughput compared to thermal ionisation mass

^aDepartment of Environmental Sciences, Jožef Stefan Institute, Jamova 39, SI-1000 Ljubljana, Slovenia. E-mail: marko.strok@ijs.si; Tel: +38615885243

^bJožef Stefan International Postgraduate School, Jamova 39, SI-1000 Ljubljana, Slovenia

† Electronic supplementary information (ESI) available. See DOI: 10.1039/c9ja00144a

spectrometry (TIMS). Therefore, MC-ICP-MS is the preferred tool for precise measurements of uranium isotope ratios for low-abundance isotopes and mass-limited samples.^{21–23}

An MC-ICP-MS is a very complex instrument used to achieve accurate isotope ratio data, and proper optimization is required to exploit its full potential. When measuring isotope ratios using MC-ICP-MS, counting-statistical errors contribute only a part of the total variance of isotope ratio measurements. MC-ICP-MS performance can be affected by spectral interferences arising from isobaric interferences, instrumental mass bias, or sample matrix effects as a result of the presence of other elements in the sample matrix.^{22–25} Molecular interferences in uranium analysis, which are the result of the combination of impurity elements present in the sample (Pb-oxides, Pb-nitrides, Pb-nitrogen-oxygen, Hg-chlorides, and ²³²ThH⁺) or the plasma gas (PtAr⁺), can affect high precision measurements with increased and unwanted signal intensities.^{20,22,26} Therefore, analyte separation from the sample matrix is necessary to avoid these undesirable effects. However, if the separation recovery is incomplete, this can introduce serious isotope biases, and thus, 100% quantitative recovery of the analyte should be targeted. In addition, the instrumental mass bias in MC-ICP-MS can also cause a significant deviation of the isotope amount ratio from the true value. It was suggested that an instrument itself could also, to some extent, discriminate various isotopes of the same element in a manner that resembles mass-independent fractionation in nature. The most common reason for this can be found in plasma conditions, which are changing during different measurement sessions.²⁷ However, the exact cause for this phenomenon is still unknown and it is still not clear if these biases potentially influence the accuracy of uranium isotope ratio data. Anyhow, careful optimization of the measurement protocol is required to minimize any possible instrumental mass bias arising from MC-ICP-MS.

Several protocols have been reported to obtain uranium isotope ratios using MC-ICP-MS;^{5,21,28} however, considerable challenges still exist in accurately determining uranium isotope ratios with dynamic ranges of 10^{−6} or higher. Therefore, a ²³³U/²³⁶U double spike can be added to a sample to improve the precision of determining uranium isotopes with mass bias correction during sample preparation and measurement steps. However, in some cases, where the measurements of ²³³U or ²³⁶U ions are required, the double spike method is not recommended for use in uranium isotope analysis. The main disadvantages of this method are the availability of enriched double spikes, which are sometimes difficult to obtain due to regulations of export of radioactive materials; the effort required to calibrate the isotopic composition of the spike; and the need to avoid cross-contamination between two runs.²⁷ ²³³U and ²³⁶U can also be present in the sample. Ultra-trace amounts of ²³⁶U exist in various materials found in the environment, due to the process of nuclear fission, the global fallout from nuclear atomic bombs, and nuclear reactor accidents.¹⁵ Also, nuclear safeguard programs seek to determine the uranium isotope abundance of micron size particles, where anomalous amounts of ²³³U and ²³⁶U may indicate artificial isotope enrichment or depletion processes.^{14,22} In addition, to analyse environmental

samples at sub-nanogram levels and when only a small amount of the sample is available, it is preferable to measure the ion signals from minor uranium isotopes such as ²³⁴U using ion counters and ²³³U and ²³⁶U using Faraday detectors because of more efficient mass bias correction.^{21,29,30} However, this can be problematic when the instrument cup configuration does not allow for the simultaneous measurement of ²³⁴U using ion counters and ²³³U and ²³⁶U using Faraday detectors. In this case, instead of the double spike method, samples are usually spiked with only one isotope, ²³³U or ²³⁶U,^{31–33} or the use of a standard-sample bracketing method is applied for mass bias correction.^{20,29} For standard-sample bracketing, it is essential to ensure that the analyte concentration in the sample and the standard is matched carefully and for that, perfect separation of the sample matrix is required. In addition, it is possible that temporal drift in mass bias between bracketing standards can occur and therefore careful and precise optimization of the MC-ICP-MS instrument is also needed.^{27,34}

This study is divided into two parts. The first part presents the optimization of the MC-ICP-MS protocol, to obtain high precision and accuracy for uranium isotope data. We examine several methodological possibilities to establish the most appropriate concentration of the purified uranium aliquot, to find the most appropriate cup configurations of uranium isotope measurements, and to verify the analytical performance of the MC-ICP-MS instrument. The second part of the study aims to test different sample preparation approaches to evaluate their possible influence on uranium isotopic composition for determining uranium isotope ratios (²³⁵U/²³⁸U and ²³⁴U/²³⁸U) using MC-ICP-MS. We try to find the analytical procedure that will provide the smallest procedural blanks and the most accurate purified uranium fraction results with the lowest amount of impurities and the smallest bias from the standard reference value. This is especially important for the cases when the double spike method is unsuitable for use as a procedural mass bias correction method. The most commonly used preconcentration and separation techniques for determining uranium in any sample were tested. The results of both optimization of MS measurement methods and uranium isotope behaviour during sample preparation provide means for establishing the methodology, which enables accurate determination of uranium isotope ratios in low-level sample concentrations.

Experimental

Reagents, standards, and samples

All chemical procedures and measurements were performed under clean room conditions. Chemical reagents and acids were prepared with deionized water (>18 MΩ cm, Millipore Milli-Q-Plus) and with clean laboratory equipment. The uranium isotopic standard IRMM-184 (European Commission – JRC, Institute of Reference Materials and Measurements, Belgium) was used for correcting the mass bias and testing the possible influence of various uranium sample preparation approaches. Depleted and enriched uranium isotopic standards IRMM-183 and IRMM-185 were used as quality control and

quality assurance (QA & QC) samples. The uranium standard reference material SRM-3164 (National Institute of Standards & Technology, USA) was used for calibration and interference correction of single-collector mass spectrometry, MC-ICP-MS optimization, and daily performance checks.

Instrumentation

Uranium isotope ratios were measured using a Nu plasma II (Nu Instruments Ltd., UK) MC-ICP-MS with a high-efficiency Aridus II™ (Cetac Technologies, NE, USA) sample introduction system. The mass spectrometer is equipped with 16 Faraday and five ion-counting detectors.

Before uranium isotope ratio measurements, uranium concentrations in the samples were determined using an Agilent 8800 triple quadrupole ICP-MS (ICP-QQQ) (Agilent Technologies, Tokyo, Japan).

Uranium isotope ratio measurements using MC-ICP-MS

Before uranium isotope ratio measurements, routine optimization of MC-ICP-MS was performed. The instrument system was tuned by adjusting the torch position, instrumental gas flows, ion lens positions, and high-tension (HT) voltages. This resulted in the most optimal and stable beam intensity for the ^{238}U beam collected in a Faraday detector and reduced background noise. Table 1 lists typical instrument parameters for uranium analysis. During tuning and before the analysis sequence, peak centering was performed manually for $m/z = 238$ on Faraday cups L2 or L3. Before the analytical session, Faraday cup preamplifier gain was performed. The instrumental background was measured using zero electrostatic analyser (ESA) deflection.

Table 1 Operating conditions for uranium analysis on a Nu plasma II MC-ICP-MS

Plasma conditions	
RF power (W)	1300
Ar cooling gas (L min^{-1})	13.0
Ar auxiliary gas (L min^{-1})	0.8
Nebulizer gas pressure (Psi)	39.7–40.1
Sample introduction (Aridus II™)	
Ar sweep gas (L min^{-1})	5.8–6.3
Sample uptake rate ($\mu\text{L min}^{-1}$)	115
Spray chamber ($^{\circ}\text{C}$)/membrane ($^{\circ}\text{C}$)	110/160
Method settings	
Cup configuration	$^{238}\text{U}(\text{L}2)\text{--}^{235}\text{U}(\text{L}5)\text{--}^{234}\text{U}(\text{IC}0)$ or $^{238}\text{U}(\text{L}3)\text{--}^{235}\text{U}(\text{IC}0)\text{--}^{234}\text{U}(\text{IC}1)$
Cycles/blocks	10 cycles/6 blocks
Integration time (s)	30 (zero-ESA); 4 (sample)
Magnet delay time (s)	2
Transfer time (s)	150
Wash time–2% HNO_3 (s)	120
Analytical concentration (ng mL^{-1})	5
Sensitivity (V)	~2–4 for 5 ng mL^{-1}
Total analysis time	14 min per sample

Two cup configurations were used during optimization for uranium isotopic measurements. The typical protocol used for measuring uranium isotope ratios using MC-ICP-MS was the combination of ^{238}U and ^{235}U ions on the Faraday detectors (L2 and L5 cups, respectively) and ^{234}U ions on the ion counter detector (IC0 cup). In the second method, measurement of ^{238}U ions on the Faraday detector (L3 cup) and ^{235}U and ^{234}U ions on the ion counter detectors (IC0 and IC1 cups, respectively) was performed. With the two different cup configurations, the drift in the relative gain between the ion counter and Faraday detector was estimated and the stability of uranium isotope signals at low concentrations was studied.

The standards and samples were diluted with 2% HNO_3 to obtain a constant uranium concentration for isotopic measurements. The measured isotope ratios ($^{235}\text{U}/^{238}\text{U}$ and $^{234}\text{U}/^{238}\text{U}$) were calibrated against the corresponding isotope ratios in IRMM-184 standard, which had been measured before and after the sample measurement. The external standard-sample bracketing approach was used for instrumental mass bias correction.

The protocol for uranium isotopic measurement involved 60 cycles (10 cycles/6 blocks) with an integration time of 4 s for samples and 30 s for instrumental background. The sample introduction rate was $115 \mu\text{L min}^{-1}$ and uranium consumption for each analysis was ~6.6 ng of uranium for a solution containing 5 ng mL^{-1} uranium. The sample uptake time before data acquisition was 150 s. The rinse time was 120 s using 2% HNO_3 between measurements and memory effects were negligible (~0.02% of the ^{238}U signal intensity). The total duration of data acquisition was ~14 min for a single sample. The typical sensitivity for ^{238}U from a 5 ng mL^{-1} solution was 2–4 V (Table 1). $^{235}\text{U}/^{238}\text{U}$ and $^{234}\text{U}/^{238}\text{U}$ isotope ratios were calculated as the mean ratios of 60 replicates with an outlier test that was implemented in Nu plasma II instrument software (Nu Instruments Calculation Editor – NICE). The values that deviate from the mean by more than two sigma were considered as outliers. An Excel spreadsheet was used for assembling data outputs and performing further corrections (standard-sample bracketing).

The obtained atomic ratios of uranium isotopes were corrected with the exponential law mass bias correction model:

$$R_m^{ij} = R_T^{ij} \left(\frac{m_i}{m_j} \right)^f$$

where R_m^{ij} is the measured ratio, R_T^{ij} is the mass bias corrected ratio or true value, m_i and m_j are the absolute atomic masses of the isotopes of interest, and f is the mass bias correction factor.²⁴ The correction factors for each isotope ratio were calculated as an average value of two isotope ratios measured in a certified standard divided by the certified value. Comparable corrections were applied to the respective isotope ratios in samples. Uncertainty estimation was performed according to EURACHEM-CITAC recommendations.³⁵ For uranium isotope analysis, the following sources of uncertainties were assessed: mass bias and the certified value of the standard used for mass bias correction, measurement repeatability of the mass bias standard and the sample, possible molecular interferences,

peak tailing, and Faraday cup amplifier gain and baseline.^{24,36} The uncertainty of mass bias correction was estimated by calculating the combined standard uncertainty for the external standard-sample bracketing technique and was quoted at a 95% confidence level.³⁴ Measurement repeatability was derived from the pooled estimate of standard deviation, which was estimated from suitably matched quality control standards.²⁰ Molecular interferences, peak tailing effect, Faraday cup amplifier gain, and baseline associated uncertainties were comparatively small in our case and were not included in the uncertainty budget. After the overall assessment for uranium isotope ratio analysis, the major source of uncertainty is the uncertainty of the certified value of the certified standard used for mass bias correction.

Sample preparation

To evaluate the possible uranium biases in water samples, the most commonly used uranium preconcentration and separation techniques were tested. The most optimal technique with the highest achievable precision and accuracy for uranium isotopes was identified. Such techniques have been reported previously^{37–42} and are briefly described below.

Uranium preconcentration techniques. Different methods used in this study were applied to purified deionized water spiked with natural uranium standards with known uranium isotopic composition.

Four different uranium preconcentration techniques for water samples were tested: coprecipitation with either $\text{Fe}(\text{OH})_3$, $\text{Ca}_3(\text{PO}_4)_2$, or MnO_2 and evaporation. In the first procedure, 1 mL of FeCl_3 solution (5 mg mL^{-1}) was added to 400 mL of water and the pH was adjusted to 9 with concentrated ammonia solution to coprecipitate uranium with $\text{Fe}(\text{OH})_3$. In the second procedure, 0.5 mL of 1.25 M $\text{Ca}(\text{NO}_3)_2$ was added to the sample and left until the water solution was boiling. A uranium $\text{Ca}_3(\text{PO}_4)_2$ precipitate was formed by adding 0.2 mL of 3.2 M $(\text{NH}_4)_2\text{HPO}_4$ and enough concentrated ammonia solution to form a precipitate. In these two procedures, the precipitate was separated by centrifugation and washed with deionized water to neutral pH. The precipitate was then dissolved according to the specific separation technique discussed below. In the third procedure, coprecipitation with MnO_2 was achieved by adding 0.2 M KMnO_4 solution (1 mL per 1 L) to a sample acidified with HCl and the pH was adjusted to 9 using concentrated ammonia solution and by adding 0.3 M MnCl_2 solution (2 mL per 1 L). The precipitate was then dissolved with a mixture of concentrated HCl and H_2O_2 . After evaporation to dryness, the residue was dissolved according to the specific separation technique discussed below. For the preconcentration of uranium with evaporation, the water sample was evaporated on a hot plate to dryness and the residue was then dissolved according to the specific separation technique discussed below.

Uranium separation techniques. After the preconcentration step, it is important to separate uranium isotopes from the matrix elements and interferences. This was accomplished by various combinations of separation procedures, such as

extraction chromatography, ion exchange chromatography, and solvent extraction. Each of the procedures used has been previously optimized either by resin producers or by other authors to give the maximum uranium recovery.

The first uranium separation procedure was based on using a uranium and tetravalent actinide (UTEVA) extraction chromatographic resin prepared in deionized water. The second procedure also used a UTEVA extraction chromatographic resin; however, it was precleaned by soaking overnight in 6 M HNO_3 and then washed several times with deionized water. In both procedures, the samples were dissolved in 5 mL of 3 M HNO_3 after uranium preconcentration and transferred into a pre-conditioned UTEVA column. This was prepared by adding 2 mL of UTEVA resin to the column and washing with 10 mL of deionized water, 5 mL of 1 M HNO_3 , and 10 mL of 3 M HNO_3 . After the sample was loaded, the column was washed with 20 mL of 3 M HNO_3 , 5 mL of 9 M HCl, and 25 mL of 5 M HCl with 0.5 M oxalate. Uranium isotopes were eluted with 15 mL of 1 M HCl in a clean beaker, and the eluate was evaporated to dryness. To destroy any organic residue in the resin, the dry residue was digested three times with a mixture of HNO_3 and H_2O_2 before measurements.

For the third separation procedure, ion exchange chromatography with extraction chromatography was used. First, preconcentrated uranium samples were dissolved in 5 mL of 8 M HNO_3 and transferred onto an anion-exchange resin (1×8 , 100–200 mesh, chloride form) prepared in 8 M HNO_3 . To pre-condition the column in 8 M HNO_3 , 5 mL of the resin prepared in deionized water was added to the column and washed with 50 mL of deionized water, 30 mL of 1 M HNO_3 , and 30 mL of 5 M HNO_3 . The column was preconditioned with 50 mL of 8 M HNO_3 . After the sample was loaded onto the column, uranium isotopes were eluted with 60 mL of 8 M HNO_3 , evaporated to dryness, dissolved in 5 mL of 3 M HNO_3 , and transferred to the pre-cleaned UTEVA column. The samples were then treated in the same way as in the UTEVA extraction chromatography procedure.

Uranium isotopes were also separated using an anion-exchange resin (1×8 , 100–200 mesh, chloride form) prepared in 9 M HCl. After preconditioning the column using 5 mL of the resin prepared in deionized water and washing with 50 mL of deionized water, 30 mL of 1 M HCl, 30 mL of 5 M HCl, and 50 mL of 9 M HCl, the sample was dissolved with 5 mL of 9 M HCl and loaded onto the column. The column was then washed with 60 mL of 9 M HCl and uranium isotopes were eluted from the anion-exchange resin with 60 mL of 0.1 M HCl. The uranium sample was then evaporated to dryness and cleaned three times with a mixture of HNO_3 and H_2O_2 .

Separation with solvent extraction, in which uranium isotopes were separated from 5 M HNO_3 with a TBP solution in toluene, was also tested. A uranium sample in 10 mL of 5 M HNO_3 was extracted by shaking with 5 mL of 50% TBP solution in toluene. The organic phase was washed two times with 5 mL of 5 M HNO_3 containing 2 mL L^{-1} of concentrated HF. Uranium isotopes were stripped with 10 mL of deionized water containing one drop of concentrated HNO_3 . The last step was repeated two times.

Results and discussion

Optimization of the measurements of uranium isotope ratios using MC-ICP-MS

To achieve a suitable performance for low-level concentration uranium samples, it is important to optimize the uranium concentration introduced into the MC-ICP-MS. Therefore, an examination of several methodological possibilities was carried out. First, the most appropriate concentration of the aliquot of a purified natural uranium fraction was established. The results in Fig. S1 (ESI†) indicate that the most optimal uranium concentration for measurements is 5 ng mL^{-1} . This concentration was selected as the lowest concentration with the smallest difference of $^{235}\text{U}/^{238}\text{U}$ and $^{234}\text{U}/^{238}\text{U}$ isotope ratios from the certified value. Then the most appropriate cup configurations of uranium isotope measurements were determined, to find the protocol with which the uranium isotope signal is the most stable if sample concentrations require measurements at concentrations lower than 5 ng mL^{-1} . The results in Fig. S2 (ESI†) show that for samples with uranium concentrations lower than 0.5 ng mL^{-1} , it is better to use a cup configuration in which ^{238}U ions are measured on a Faraday detector (L3 cup) and ^{235}U and ^{234}U ions are measured on ion counter detectors (IC0 and IC1 cups, respectively). Finally, the long-term analytical performance of the MC-ICP-MS instrument was assessed, to test the instrument accuracy and precision for uranium isotope ratio measurements. Fig. S3 (ESI†) shows that the analytical performance of MC-ICP-MS for the measured isotope ratios of the uranium standard is in good agreement with the certified value. The analytical precision of the

instrument was further assessed by analysing two uranium isotopic standards: depleted uranium standard (IRMM-183) and enriched uranium standard (IRMM-185) (Table S1 in the ESI†) and the experimental values are in good agreement with the corresponding certified values.

These results are presented and discussed in more detail in the ESI.†

Bias of uranium isotopes during different sample preparation and separation techniques

Prior to mass spectrometry analysis, a careful sample preparation procedure is needed to separate uranium isotopes from the sample matrix and other possible interferences and also to improve the detection limit, increase the sensitivity and enhance the accuracy of the result, especially for uranium samples with low-level concentrations.^{3,21} A series of methods already exist for the determination of uranium in different kinds of samples; however, there is little information on the extent of uranium isotope ratio biases introduced by different methods. Therefore, it is important to quantify this and find the analytical technique which will give us the most precise and accurate result for uranium isotope ratios.

To identify the optimal analytical technique for determining uranium isotope ratios using MC-ICP-MS, different sample preparation approaches for water samples were tested (Fig. 1 and 2). Following each preconcentration technique (coprecipitation with $\text{Fe}(\text{OH})_3$: Fe-precipitation, $\text{Ca}_3(\text{PO}_4)_2$: Ca-precipitation, MnO_2 : Mn-precipitation, and evaporation), uranium was separated using one of the four most common uranium separation techniques (extraction chromatography

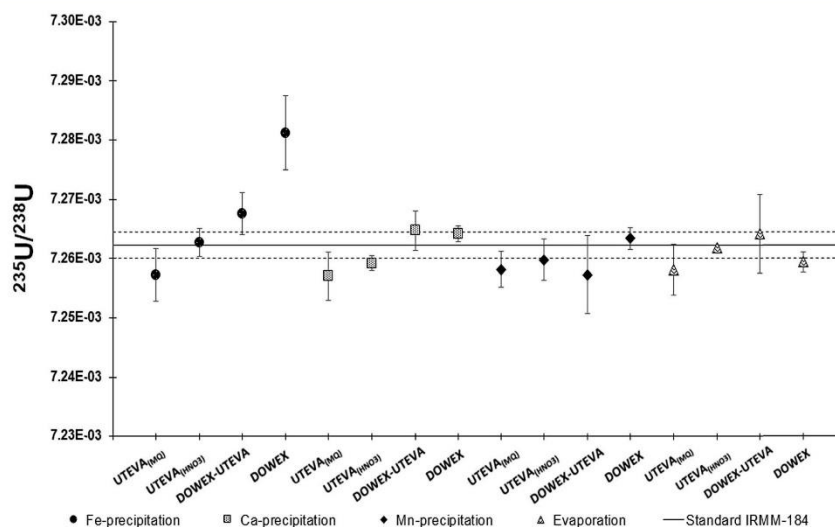


Fig. 1 Deviation of $^{235}\text{U}/^{238}\text{U}$ isotope ratios from the certified value (solid line) for various tested uranium preconcentration and separation techniques (mean values, $n = 3$). Uncertainties are shown as $2s$, where s is the standard deviation.

with UTEVA resin prepared in deionized water: UTEVA_(MO), extraction chromatography with UTEVA resin pre-cleaned in 6 M HNO₃; UTEVA_(HNO₃), combination of ion exchange chromatography and extraction chromatography: DOWEX-UTEVA, and ion exchange chromatography: DOWEX). Uranium separation with solvent extraction (TBP) was also tested. Table S1† lists the numerical results (ESI†). For each combination, three replicates were performed. The certified value of the uranium isotopic standard (IRMM-184) with expanded measurement uncertainty ($k = 2$) is included and compared with the measured uranium isotope ratios obtained using different sample preparation approaches.

Some of the evaluated methods show deviations from the uranium isotopic standard, especially the combination of coprecipitation with Fe(OH)₃ and separation with ion exchange chromatography (DOWEX), where the ²³⁵U/²³⁸U and ²³⁴U/²³⁸U ratios differ significantly from the uranium isotopic standard (2.60‰ and -56.30‰, respectively). This may be caused by the insufficient separation of uranium isotopes from Fe³⁺ by ion exchange chromatography. Ion exchange chromatography is a valuable method for the determination of uranium isotopes at ultra-trace levels. Uranium as UO₂²⁺ can form complexes with many common anions (chlorides, nitrates or sulphates) and it can use strongly basic anion exchange resins for separation from the sample matrix.⁴³ Uranium forms stable chloride complexes with a high distribution coefficient in 9 M HCl, so purification is usually done in HCl. However, Adriaens *et al.* reported that iron could not be completely separated from uranium using only ion exchange resins. Fe³⁺ ions and other metal ions (Co²⁺, Cu²⁺, and Zn²⁺) can form stable chloride complexes, similar to those of uranium. As a result, uranium and other metal complexes are simultaneously adsorbed on the resins, making it difficult to efficiently separate uranium.⁴⁴ This can explain the larger deviations from the isotopic standard for the combination of coprecipitation with Fe(OH)₃ and separation with ion exchange chromatography (DOWEX), where some Fe particles were still seen in the sample solution (orange-brown solution). In addition, other combinations of preconcentration techniques with ion exchange chromatography (DOWEX) show no significant deviations of uranium isotopes from the uranium isotopic standard and this indicates that the preconcentration technique can contribute to accurate results in uranium isotope analysis.

Purification of uranium isotopes by ion exchange chromatography can be also carried out in HNO₃. The distribution coefficient of uranium in 8 M HNO₃ in such a resin is very different from that of thorium, which can be present in the sample matrix. This enables the effective isolation of uranium from thorium in HNO₃. However, the distribution coefficient for other major elements in 8 M HNO₃ is much closer to that of uranium, and therefore an additional purification step is often required. An additional step is usually done with extraction chromatography.⁴⁵ Our results however demonstrate deviations of the ²³⁵U/²³⁸U and ²³⁴U/²³⁸U ratios from the uranium isotopic standard for the combination of ion exchange chromatography and extraction chromatography in almost every preconcentration technique (-0.69 to 0.74‰ for ²³⁵U/²³⁸U and -5.60 to 2.59‰ ²³⁴U/²³⁸U). This can be explained with the low recoveries, which

were obtained from the separation technique. If the recovery is incomplete, this can introduce mass bias for uranium isotope ratios. Uranium isotope ratios also show greater uncertainties for the combination of separation techniques compared to other approaches used in the study. This suggests that the combination of ion exchange chromatography and extraction chromatography is not the most reliable and repeatable separation technique for the use of low-level uranium samples.

Extraction chromatography is another very common method for the separation of uranium from a sample matrix. Especially UTEVA resins in HNO₃ are highly selective for the separation of uranium isotopes in the U(VI) state. Extraction chromatography has a higher selectivity toward uranium isotopes at lower concentrations of HNO₃ and HCl compared to ion exchange chromatography. As a result, the use of UTEVA resins avoids the problem of interference from coexisting anions.³⁸ Adriaens *et al.* also applied the UTEVA resin in their study and reported more efficient isolation of uranium isotopes compared to ion exchange separation. This was due to more effective separation of iron and lead from uranium. However, they found some problems with insufficient purification of uranium from thorium, which can indicate the difficulty in the effective separation of uranium in low-level samples.⁴⁴ This finding can be also applied to our results. Fig. 1 and 2 show the deviations of uranium isotopes from the uranium isotopic standard with extraction chromatography (-0.73 to 0.052‰ for ²³⁵U/²³⁸U and 1.90-8.90‰ ²³⁴U/²³⁸U). It is possible that uranium was not completely purified from the interferences. For this reason, it is important to give a lot of attention to the step of washing the column to remove interfering elements to get the purified uranium fraction.

Furthermore, Fig. 1 and 2 show that uranium separation with UTEVA resins prepared in deionized water also has some negative side effects for the accurate determination of uranium isotopes (-0.73 to 0.57‰ for ²³⁵U/²³⁸U and 1.90-6.04‰ ²³⁴U/²³⁸U). Organic interferences from the residual resin may affect uranium isotope mass bias.³² In this case, precleaning the resins using HNO₃ can reduce the organic interference of purified uranium fractions during sample preparation.

Uranium separation with solvent extraction (TBP) shows that large biases occurred during measurements of the uranium isotopic composition using MC-ICP-MS, as evidenced by extensive deviations for the ²³⁵U/²³⁸U and ²³⁴U/²³⁸U ratios (-254‰ and -299‰, respectively) (Table S1†). In addition, chemical recoveries for solvent extraction were the lowest compared to those for other separation techniques (~40%) and the remaining organic residue in the last step of uranium sample preparation was difficult to destroy. Therefore, uranium separation with solvent extraction is not recommended for determining uranium isotopes using MC-ICP-MS in low-level concentration samples.

The clear deviation from the uranium isotopic standard for some analytical methods could also be explained by different speciation and oxidation states during separation. Anbar *et al.* demonstrated such a possible bias for iron isotopes during ion exchange chromatography. They linked these biases to different iron speciation and oxidation states during different eluting steps.⁴⁶ To confirm that such biases can also occur for uranium

JAAS

View Article Online

Paper

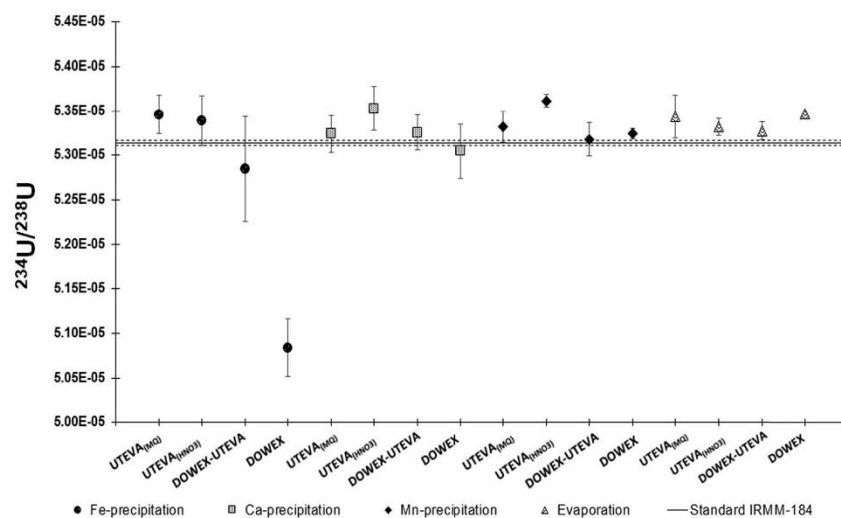


Fig. 2 Deviation of $^{234}\text{U}/^{238}\text{U}$ isotope ratios from the certified value (solid line) for various tested uranium preconcentration and separation techniques (mean values, $n = 3$). Uncertainties are shown as $2s$, where s is the standard deviation.

isotopes, further analyses of the elution profile of uranium for each chromatography separation are necessary.

The most plausible explanation for the observations presented in Fig. 1 and 2 can be that the column chemistry indirectly leads to a matrix effect in MC-ICP-MS. The most likely

Table 2 Recovery values and uranium contribution in procedural blanks for various analytical methods

Analytical method		Recovery values (%)	Uranium contribution in procedural blanks (ng)
Preconcentration	Separation		
Fe-precipitation	UTEVA _{MQ}	66–90	0.08
	UTEVA _{HNO₃}	70–75	0.08
	DOWEX-UTEVA	47–73	0.13
	DOWEX	57–94	0.19
Ca-precipitation	UTEVA _{MQ}	54–76	0.11
	UTEVA _{HNO₃}	73–80	0.08
	DOWEX-UTEVA	43–64	0.17
	DOWEX	44–123	0.18
Mn-precipitation	UTEVA _{MQ}	75–93	0.16
	UTEVA _{HNO₃}	86–94	0.15
	DOWEX-UTEVA	58–84	0.16
	DOWEX	51–109	0.19
Evaporation	UTEVA _{MQ}	73–96	0.13
	UTEVA _{HNO₃}	65–93	0.07
	DOWEX-UTEVA	58–86	0.16
	DOWEX	61–114	0.11

reason for this effect is organic materials being stripped from the resins during the collection of the uranium fraction. The presence of organics is especially observed in the case of uranium separation with solvent extraction (TBP), where results show extensive deviations for uranium isotope ratios from the uranium isotopic standard. There were still visible signs of organics in the sample solution before measurements on an MC-ICP-MS, regardless of trying to destroy any remaining visible residue. This effect is also observed when uranium separation was performed with extraction chromatography. Results from the UTEVA resin prepared in deionized water show negative side effects to the accurate uranium isotope ratios, compared to results from the UTEVA resin, previously cleaned in 6 M HNO₃, which show significantly smaller deviations of $^{235}\text{U}/^{238}\text{U}$ and $^{234}\text{U}/^{238}\text{U}$ ratios from the uranium isotopic standard. Here, we can conclude that the presence of organic interference can extensively contribute to the mass bias effect.

From the obtained results, the best coprecipitation procedure for determining uranium isotopes using MC-ICP-MS is coprecipitation with Ca₃(PO₄)₂ or coprecipitation with MnO₂, and the best separation technique is extraction chromatography with HNO₃ precleaned UTEVA resin and a combination of ion exchange chromatography and extraction chromatography (DOWEX-UTEVA). These procedures yield the smallest deviation from the uranium isotopic standard.

Table 2 lists the informative recovery values obtained for each procedure. Recoveries were calculated from the uranium concentration added to the water sample and the uranium concentration measured in the sample after preconcentration and separation using ICP-QQQ. Table 2 also lists the contribution of uranium from each procedural blank. The results show

that the highest chemical recoveries (65–94%) were obtained for extraction chromatography with pre-cleaned UTEVA resin irrespective of the preconcentration technique. The lowest recoveries (43–86%) were obtained for the combination of ion exchange chromatography and extraction chromatography irrespective of the preconcentration technique. This was expected because, in the combination of two separation techniques, some uranium is often lost during analysis. It is also the most time-consuming analytical separation technique. The smallest uranium procedural blank contribution was found for extraction chromatography with HNO₃ pre-cleaned UTEVA resin (~0.08 ng of ²³⁸U). The highest contribution of uranium from procedural blanks was with coprecipitation with MnO₂ (~0.17 ng of ²³⁸U) irrespective of the separation technique and for the combination of ion exchange chromatography and extraction chromatography (~0.16 ng of ²³⁸U).

Considering all these results, uranium analytical recoveries, uranium blank contribution, time of analysis, and uranium isotopic measurements, we found that the best outcome was obtained when the combination of coprecipitation with Ca₃(PO₄)₂ and pre-cleaned UTEVA resin was used as the separation technique.

Conclusions

In this study, different analytical methods were tested for determining uranium isotope ratios in water samples using MC-ICP-MS. The analytical method with the smallest uranium biases measured using MC-ICP-MS was selected as the optimal procedure for application to real samples. The study results indicate that the optimal analytical procedure was the combination of coprecipitation with Ca₃(PO₄)₂ as the preconcentration technique and extraction chromatography with UTEVA resin pre-cleaned in 6 M HNO₃ as the separation technique. In addition, the accurate and precise analysis of uranium isotope ratios was achieved with the optimization of MC-ICP-MS measurements by controlling and correcting the factors, which can occur during measurements as instrumental mass bias.

This experiment was designed to find any significant bias of uranium during sample preparation that may increase the possible risk of contamination of the analyte during sample preparation and when the double spike method is unsuitable for use for these corrections. We found that the column matrix effects directly lead to the organic material being stripped from the resin and can significantly influence the accurate determination of the uranium isotope ratio with MC-ICP-MS measurements. By reducing impurity effects and other potential contaminations, the most optimal procedure can be applied to real samples where the influence of the matrix effect is significant and extremely small isotopic variations need to be detected with high accuracy and precision.

Conflicts of interest

There are no conflicts to declare.

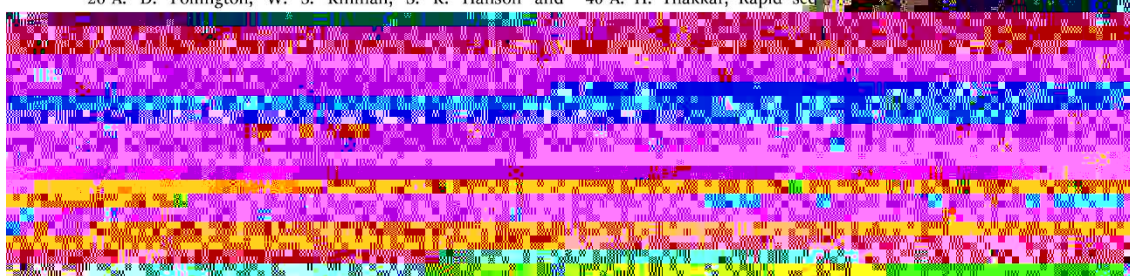
Acknowledgements

This work was supported by the Slovenian Research Agency (Programme group P2-0075, Project J1-9179) and the Young Researcher's program. We thank Ljudmila Benedik and Marta Jagodic for their help with the laboratory analysis.

References

- 1 C. H. Stirling, M. B. Andersen, E.-K. Potter and A. N. Halliday, Low-temperature isotopic fractionation of uranium, *Earth Planet. Sci. Lett.*, 2007, **264**, 208–225.
- 2 S. Weyer, A. D. Anbar, A. Gerdes, G. W. Gordon, T. J. Algeo and E. A. Boyle, Natural fractionation of ²³⁸U/²³⁵U, *Geochim. Cosmochim. Acta*, 2008, **72**, 345–359.
- 3 C. H. Stirling, M. B. Andersen, R. Warthmann and A. N. Halliday, Isotope fractionation of ²³⁸U and ²³⁵U during biologically-mediated uranium reduction, *Geochim. Cosmochim. Acta*, 2015, **163**, 200–218.
- 4 D. Langmuir, Uranium solution-mineral equilibria at low temperatures with applications to sedimentary ore deposits, *Geochim. Cosmochim. Acta*, 1978, **42**, 547–569.
- 5 M. B. Andersen, C. H. Stirling and S. Weyer, Uranium Isotope Fractionation, *Rev. Mineral. Geochem.*, 2017, **82**, 799–850.
- 6 W. Bu, J. Zheng, M. E. Ketterer, S. Hu, S. Uchida and X. Wang, Development and application of mass spectrometric techniques for ultra-trace determination of ²³⁶U in environmental samples—a review, *Anal. Chim. Acta*, 2017, **995**, 1–20.
- 7 M. J. Murphy, M. B. Froehlich, L. K. Fifield, S. P. Turner and B. F. Schaefer, *In situ* production of natural ²³⁶U in groundwaters and ores in high-grade uranium deposits, *Chem. Geol.*, 2015, **410**, 213–222.
- 8 B. Bourdon, S. Turner, G. M. Henderson and C. C. Lundstrom, Introduction to U-series Geochemistry, *Rev. Mineral. Geochem.*, 2003, **52**, 1–24.
- 9 E. A. Schauble, Role of nuclear volume in driving equilibrium stable isotope fractionation of mercury, thallium, and other very heavy elements, *Geochim. Cosmochim. Acta*, 2007, **71**, 2170–2189.
- 10 Y. A. Uvarova, T. K. Kyser, M. L. Geagea and D. Chipley, Variations in the uranium isotopic compositions of uranium ores from different types of uranium deposits, *Geochim. Cosmochim. Acta*, 2014, **146**, 1–17.
- 11 J. Suksi, K. Rasilainen and P. Pitkänen, Variations in ²³⁴U/²³⁸U activity ratios in groundwater—A key to flow system characterisation?, *Phys. Chem. Earth, Parts A/B/C*, 2006, **31**, 556–571.
- 12 H. Cheng, R. Lawrence Edwards, C.-C. Shen, V. J. Polyak, Y. Asmerom, J. Woodhead, J. Hellstrom, Y. Wang, X. Kong, C. Spötl, X. Wang and E. Calvin Alexander, Improvements in ²³⁰Th dating, ²³⁰Th and ²³⁴U half-life values, and U–Th isotopic measurements by multi-collector inductively coupled plasma mass spectrometry, *Earth Planet. Sci. Lett.*, 2013, **371–372**, 82–91.
- 13 M. B. Andersen, Y. Erel and B. Bourdon, Experimental evidence for ²³⁴U–²³⁸U fractionation during granite

- weathering with implications for $^{234}\text{U}/^{238}\text{U}$ in natural waters, *Geochim. Cosmochim. Acta*, 2009, **73**, 4124–4141.
- 14 S. Boulyga, S. Konegger-Kappel, S. Richter and L. Sangély, Mass spectrometric analysis for nuclear safeguards, *J. Anal. At. Spectrom.*, 2015, **30**, 1469–1489.
 - 15 A. Sakaguchi, K. Kawai, P. Steier, F. Quinto, K. Mino, J. Tomita, M. Hoshi, N. Whitehead and M. Yamamoto, First results on ^{236}U levels in global fallout, *Sci. Total Environ.*, 2009, **407**, 4238–4242.
 - 16 D. L. Donohue, Strengthening IAEA safeguards through environmental sampling and analysis, *J. Alloys Compd.*, 1998, **271–273**, 11–18.
 - 17 S. F. Boulyga, J. L. Matusevich, V. P. Mironov, V. P. Kudrjashov, L. Halicz, I. Segal, J. A. McLean, A. Montaser and J. Sabine Becker, Determination of $^{236}\text{U}/^{238}\text{U}$ isotope ratio in contaminated environmental samples using different ICP-MS instruments, *J. Anal. At. Spectrom.*, 2002, **17**, 958–964.
 - 18 P. Steier, M. Bichler, L. Keith Fifield, R. Golser, W. Kutschera, A. Priller, F. Quinto, S. Richter, M. Srncik, P. Terrasi, L. Wacker, A. Wallner, G. Wallner, K. M. Wilcken and E. Maria Wild, Natural and anthropogenic ^{236}U in environmental samples, *Nucl. Instrum. Methods Phys. Res., Sect. B*, 2008, **266**, 2246–2250.
 - 19 S. J. Tumey, T. A. Brown, B. A. Buchholz, T. F. Hamilton, I. D. Hutcheon and R. W. Williams, Ultra-sensitive measurements of ^{233}U by accelerator mass spectrometry for national security applications, *J. Radioanal. Nucl. Chem.*, 2009, **282**, 721–724.
 - 20 S. F. Boulyga, A. Koepf, S. Konegger-Kappel, Z. Mocsik and G. Stadelmann, Uranium isotope analysis by MC-ICP-MS in sub-ng sized samples, *J. Anal. At. Spectrom.*, 2016, **31**, 2272–2284.
 - 21 S. J. Goldstein and C. H. Stirling, Techniques for Measuring Uranium-series Nuclides: 1992–2002, *Rev. Mineral. Geochem.*, 2003, **52**, 23–57.
 - 22 M. E. Wieser and J. B. Schwieters, The development of multiple collector mass spectrometry for isotope ratio measurements, *Int. J. Mass Spectrom.*, 2005, **242**, 97–115.
 - 23 J. S. Becker, Recent developments in isotope analysis by advanced mass spectrometric techniques: Plenary lecture, *J. Anal. At. Spectrom.*, 2005, **20**, 1173.
 - 24 F. Albarède, P. Telouk, J. Blichert-Toft, M. Boyet, A. Agranier and B. Nelson, Precise and accurate isotopic measurements using multiple-collector ICPMS, *Geochim. Cosmochim. Acta*, 2004, **68**, 2725–2744.
 - 25 D. C. Baxter, I. Rodushkin and E. Engström, Isotope abundance ratio measurements by inductively coupled plasma-sector field mass spectrometry, *J. Anal. At. Spectrom.*, 2012, **27**, 1355.
 - 26 A. D. Pollington, W. S. Kinman, S. K. Hanson and for accurate isotope amount ratio measurements by MC-ICP-MS, *J. Anal. At. Spectrom.*, 2018, **33**, 1849–1861.
 - 28 P. van Calsteren and L. Thomas, Uranium-series dating applications in natural environmental science, *Earth-Sci. Rev.*, 2006, **75**, 155–175.
 - 29 M. B. Andersen, C. H. Stirling, E.-K. Potter and A. N. Halliday, Toward epsilon levels of measurement precision on $^{234}\text{U}/^{238}\text{U}$ by using MC-ICPMS, *Int. J. Mass Spectrom.*, 2004, **237**, 107–118.
 - 30 J.-H. Park and K. Jeong, Experimental evaluation of the detection methods of thermal ionization mass spectrometry for isotopic analysis of ultra-trace level uranium, *Microchem. J.*, 2018, **137**, 334–341.
 - 31 B. Seth, M. F. Thirlwall, S. L. Houghton and C.-A. Craig, Accurate measurements of Th–U isotope ratios for carbonate geochronology using MC-ICP-MS, *J. Anal. At. Spectrom.*, 2003, **18**, 1323–1330.
 - 32 A. J. Pietruszka, R. W. Carlson and E. H. Hauri, Precise and accurate measurement of ^{226}Ra – ^{230}Th – ^{238}U disequilibria in volcanic rocks using plasma ionization multicollector mass spectrometry, *Chem. Geol.*, 2002, **188**, 171–191.
 - 33 L. F. Robinson, N. S. Belshaw and G. M. Henderson, U and Th concentrations and isotope ratios in modern carbonates and waters from the Bahamas, *Geochim. Cosmochim. Acta*, 2004, **68**, 1777–1789.
 - 34 L. Yang, Accurate and precise determination of isotopic ratios by MC-ICP-MS: a review, *Mass Spectrom. Rev.*, 2009, **28**, 990–1011.
 - 35 S. L. R. Ellison and A. Williams, *Eurachem/CITAC Guide: Quantifying Uncertainty in Analytical Measurement*, 3rd edn, 2012.
 - 36 M. Horsky, J. Irrgeher and T. Prohaska, Evaluation strategies and uncertainty calculation of isotope amount ratios measured by MC ICP-MS on the example of Sr, *Anal. Bioanal. Chem.*, 2016, **408**, 351–367.
 - 37 G. Jia, G. Torri, R. Ocone, A. Di Lullo, A. De Angelis and R. Boschetto, Determination of thorium isotopes in mineral and environmental water and soil samples by α -spectrometry and the fate of thorium in water, *Appl. Radiat. Isot.*, 2008, **66**, 1478–1487.
 - 38 E. P. Horwitz, M. L. Dietz, R. Chiarizia, H. Diamond, A. M. Essling and D. Graczyk, Separation and preconcentration of uranium from acidic media by extraction chromatography, *Anal. Chim. Acta*, 1992, **266**, 25–37.
 - 39 F. Vera Tomé, M. Jurado Vargas and A. Martín Sánchez, Yields and losses at each step in preparing uranium and thorium samples for alpha spectrometry, *Appl. Radiat. Isot.*, 1994, **45**, 449–452.
 - 40 A. H. Thakkar, Rapid sequential separation of actinides



The Ljubljana River catchment mainly consists of karstified Mesozoic limestone and dolomite (Figure 2, [40,41]), and poljes are covered with Quaternary alluvial sediments. In the western and north-western part of the aquifer at Pivka basin (site 6), north of Planinsko polje (site 9), and in the sub-catchments of the Hotenjka and Logašičica rivers (sites 10 and 11), some shales, marls, and quartz sandstone can be found. The depth of the unsaturated zone can reach up to several hundred meters, and the carbonate rocks are more than 1000 m thick [42]. The neo-tectonic strike-slip Idrija fault zone stretches across the study area in the Dinaric direction (north-west to south-east). Along the fault system, a chain of four poljes with several short sinking streams has developed.

The two poljes investigated in the study are the Cerknjsko polje at an altitude of ~550 m a.s.l. and the Planinsko polje at an altitude of ~450 m a.s.l. (Figures 1–3 and Table 1) Cerknjsko polje, the larger of the two, represents the first (highest) level of the studied system and is bordered on the north by Upper Triassic dolomite (“Hauptdolomite”) and Jurassic limestone and on the south mainly by Cretaceous limestone with some dolomite (Figure 2). The south-eastern part of Cerknjsko polje is regularly covered by an intermittent lake, which is at least partly present during most of the year. The two main sinking streams here are Stržen (sampling site 1), which mainly drains the Cretaceous limestone area with some dolomite of the Javorniki plateau south of the Cerknjsko polje, and Cerknjsčica (site 2), which mainly drains the late Triassic and Jurassic dolomite with some limestone at the north and north-eastern sides of the Cerknjsko polje. The groundwater flows from the Cerknjsko polje partly toward the north-west to the Rak stream and Planinsko polje (second and third level of the study area, respectively). It also flows partly to the north through a mixed limestone and dolomite massif with some minor occurrences of siliciclastic sediments in the western part toward the main Ljubljana springs (sites 12 and 13) and the spring of the short tributary of Ljubljana River (Bistra, site 14) at the southern edge of Ljubljana Basin at an altitude of ~300 m a.s.l.

At the second level (Figure 3), at ~510–520 m a.s.l., the Rak stream with its two main springs Mali most (site 3) and Kotliči (site 4) collects water from the Cerknjsko polje and Javorniki plateau (Figures 1 and 2) and sinks at Veliki most (site 5). At a similar altitude, ~6.8 km west-northwest from the sink at site 5, the Pivka River sinks into the Postojna cave (site 6). The river Pivka and its tributaries drain the Eocene flysch area in the west and Cretaceous limestone south-west and south of the polje and flow for a few kilometers across the Pivško basin that is covered with alluvial stream sediments.

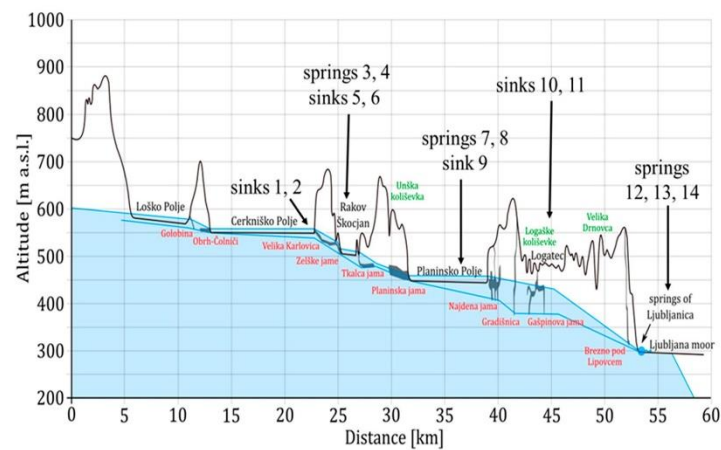


Figure 3. Schematic altitude profile of the sampled area; the blue lines represent water levels at high and low water. Adapted from [38].

Planinsko polje at ~450 m a.s.l. represents the third level of the study area. The sinking river Unica has two main springs: The Unica Spring (site 7), which emerges from the large Planina cave system that is connected to the Postojna cave and Malenščica (site 8) ~800 m east-northeast from site 7. The water of the Malenščica spring emerges from one main and some smaller intermittent orifices at elevations between 448 and 470 m a.s.l. The Unica River (site 9) was sampled ~300 m downstream of the confluence with Malenščica stream. The total discharge of the Unica River is 1–100 m³ s⁻¹, with an average of 21 m³ s⁻¹ [43].

The sinking rivers Hotenjka (site 10, 545 m a.s.l.) and Logaščica (site 11, 475 m a.s.l.) drain the area with mixed lithology, which is dominated by Triassic dolomite with some limestone and some marls, shales, and quartz sandstone in the western part of the Ljubljana catchment (Figure 2).

The main springs of the Ljubljana River emerge along the contact of non-carbonate and carbonate rocks at the southwestern border of the Ljubljana Basin (Ljubljana Marshes [42,44]) at ~300 m a.s.l. The two main springs are Močilnik (site 12) and Retovje (site 13). In this area, the Bistra karst spring (site 14), a tributary of Ljubljana River, was also sampled.

The underground connections and hydrogeology of the Ljubljana aquifer have been studied extensively [42,45–48]; however, they are difficult to describe because the flow directions change with the groundwater level and discharge [47]. Rusjan et al. [37] estimated the mean transit time (MTT) and the fraction of young water in the Ljubljana aquifer for the 2016–2017 period based on the isotopic composition of karst water and precipitation. The MTT ranged from ~4 months at sites 3 and 6 up to 9 months at site 8. Further, the mean fraction of young water for the entire catchment was 0.28; in other words, ~28% of the water in the catchment was younger than 2.3 months.

Table 1. Coordinate locations (obtained using Google Earth Pro), dominant bedrock lithology, elevations, and discharge (obtained from hydrological services of the Slovenian Environment Agency) of karst springs and sinks.

Location	Name of Spring/Stream	Coordinates (Google Earth)	Type	Dominant Bedrock Lithology	Elevation (m.a.s.l.)	Discharge (m ³ /s) Min./Max./Mean
1	Stržen	45°46'14.64" N, 14°20'10.69" E	sinking stream	alluvial sediments	550	NA ¹
2	Cerkniščica	45°47'04.20" N, 14°20'20.64" E	sinking stream	alluvial sediments	550	0.1/37.3/1.1
3	Rak-Mali most	45°47'26.28" N, 14°18'11.81" E	karst spring	limestone + dolomite	500	0.003/35.5/4.2
4	Rak-Kotlič	45°47'21.00" N, 14°17'42.10" E	karst spring	limestone + dolomite	500	0.005/29.9/10.3
5	Rak-Yeliki most	45°47'44.44" N, 14°17'19.49" E	sinking stream	limestone + dolomite	500	0.01/45.3/15.7
6	Pivka	45°46'55.10" N, 14°12'13.42" E	sinking stream	flysch	500	0.1/43.3/4.3
7	Unica-Planina cave	45°49'11.48" N, 14°14'44.72" E	karst spring	limestone + dolomite	450	0.3/88.9/15.6
8	Malenščica	45°49'21.00" N, 14°15'19.21" E	karst spring	limestone + dolomite	450	1.1/11.2/6.6
9	Unica-Hasberg	45°49'43.45" N, 14°15'19.21" E	sinking stream	alluvial sediments	450	0.9/90.2/22.2
10	Hotenjška	45°55'48.69" N, 14°8'23.83" E	sinking stream	alluvial sediments	545	NA ¹
11	Logaščica	45°54'48.12" N, 14°13'43.02" E	sinking stream	alluvial sediments	475	0.1/17.2/0.5
12	Ljubljanska-Močimik	45°57'19.52" N, 14°17'32.95" E	karst spring	limestone	300	2.6/81.0/31.3
13	Ljubljanska-Retovje	45°57'15.50" N, 14°17'57.36" E	karst spring	limestone	300	2.6/81.0/31.3
14	Ljubljanska-Bistra	45°56'48.96" N, 14°56'48.96" E	karst spring	dolomite	300	0.9/20.5/7.5

¹ NA—data not available.

2.2. Sampling and Sample Preparation

Water samples were collected at 14 sites: seven main springs and seven sinking streams or sinks (where accessible). All main springs and tributaries were analyzed (Figures 1 and 2).

Sampling was performed in five campaigns: in October 2017 at nearly average water level (discharge), in December 2017 and March 2018 at high discharge, and in May and August 2018 at low discharge. Figure 4 shows the daily precipitation in the sampling period at Postojna, a regular monitoring station of the hydrometeorological network of the Slovenian Environment Agency. The station is located ~2 km north of the sampling site 6.

Water samples at three sites were collected only four times: sites 1 and 2 were flooded in October 2017 because of the intermittent character of Cerknica Lake and because the Logaščica stream (site 5) dried out in August 2018.

The water temperature (T) and pH were measured in the field using the Hydrolab MS5 probe. The conductivity and redox potential were measured using the Ultrameter II 6 PFC (Myron Company). Discharge data were obtained from the Slovenian Environment Agency’s regular hydrological monitoring program.

The water samples were stored in prewashed high-density polyethylene (HDPE) bottles. Samples for analyzing the alkalinity (two 60-mL aliquots) were filtered on-site through 0.2-µm membrane filters (Sartorius Minisart 16534K) and stored in 30-mL HDPE bottles. Samples for metal analyses were filtered on-site too, through 0.45-µm pore size filters (Minisart 16555K) and acidified with concentrated supra-pure HNO₃ (Merck). All water samples were stored in the refrigerator at 4 °C until analysis. Another 1 L sample was collected at each sampling site for the analysis of U isotopes. These samples were vacuum-filtered through 0.45-µm pore size Millipore filters and acidified with concentrated supra-pure HNO₃ to pH 2 in the laboratory within 12 h after sampling.

Bedrock samples were manually obtained at randomly selected outcrops of prevailing rock types in the catchment areas of respective streams near sampling sites 1, 3, 4, 5, 6, 7, 8, 12, and 14. The samples were oven-dried (60 °C), crushed in brass mortar to a rock size below ~5 cm, further crushed with a gyratory crusher (Retsch BB50) and sieved below 1 mm, and finally milled in a vibrating disk mill (Siebtechnik) and sieved below 125 µm for X-ray fluorescence (XRF) and X-ray diffraction (XRD) analyses.

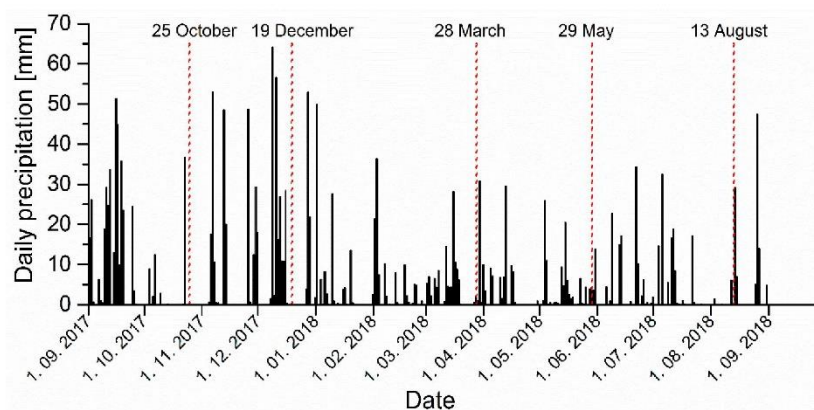


Figure 4. Daily precipitation data during the sampling period for the Postojna meteorological station (2 km south of sampling site 6) with sampling dates (red dotted line). (Source: Slovenian Environment Agency, www.meteo.si).

2.3. Physiochemical and Chemical Sample Analyses

2.3.1. Rock Samples

Elemental analysis of rock samples was performed on melted disks by XRF (Thermo Scientific ARL Perform'X Sequential XRF, 60 kV, 40 mA) with OXAS software. The disks were prepared by mixing ignited pulverized sample and Fluxana powder (FX-X50-2, Lithium tetraborate 50%/Lithium metaborate 50%) in 1:10 ratio to decrease the melting temperature. The mixture was melted in the furnace (Claisse, The Bee Electric Fusion). To avoid gluing the melt in the platinum vessel, a few drops of LiBr were added to the sample-Fluxana mixture. UniQuant 5 software was used for raw data treatment. The calculated analytical errors were <0.1% for Ca; <6% for Mg, Al, and Si; and <15% for Na and K.

Mineralogical analysis was performed on pulverized samples with X-ray diffraction (XRD; Empyrean PANalytical X-Ray Diffractometer, Cu X-Ray source) in 0.013° steps from angles of 4°–70° under clean room conditions. Mineral and standard-less Rietveld refinement analysis were performed using X'Pert Highscore plus 4.1 software on XRD data.

The share of the (non)carbonate fraction was determined by calcimetry (OFITE calcimeter, OFI Testing Equipment Inc., USA) with an analytical error of <5%.

2.3.2. Water Samples and Thermodynamic Modelling

The total alkalinity was measured by Gran titration [49] with a precision of ±1% within 24 h after sample collection.

Major elements (Ca, Mg, K, Na, Si, and Al) were determined by an Agilent 7900x ICP-MS (Agilent Technologies, Tokyo, Japan). For the calibration, single standard solutions of 1000 mg/L obtained from Merck (Darmstadt, Germany) were used. Rh (Merck) was used as an internal standard. For the accuracy check, two surface water reference materials, SLRS-5 (National Research Council Canada, Ottawa, ON, Canada) and SPS-SW1 (Spectrapure Standards, Manglerud, Norway), were analyzed multiple times during the measurements. The recoveries of all elements varied between 97% to 102%, and the repeatability was better than 5%.

Thermodynamic computations (PHREEQC) were used to calculate the HCO_3^- concentration and saturation indices of calcite ($\text{SI}_{\text{calcite}}$) from the pH, total alkalinity, and temperature as inputs [50]. The Pearson correlation coefficients between measured parameters were calculated using the Origin 9 Pro program.

2.4. U and Th Sample Analysis

All chemical procedures and measurements were performed under clean room conditions. Chemical reagents and acids were prepared with deionized water (>18 MΩ cm, Millipore Milli-Q-Plus) and with clean laboratory equipment which was soaked overnight in 10% HNO_3 . The analytical procedures used for U and Th isotopes in water and solid samples have been reported previously [51–53] and are briefly described below.

In carbonate rock samples, the determination of U and Th isotopes was performed. After the samples were ground to a fine powder, an aliquot of 1 g of carbonate powder was precisely weighed. To extract mainly the carbonate-associated U and Th fractions from the residual phase, a soft leaching procedure was applied [51]. Dissolution was performed in a centrifuge tube where 15 mL of 1 M NaAc in 25% HAc (pH 4) was added. The samples were then shaken for 2 h at room temperature. After shaking, the samples were centrifuged and filtered through 0.45-μm pore size Millipore filters and washed two times with an additional 5 mL of deionized water. The dissolved residue was then dried down on a hotplate and re-dissolved in 5 mL of 3 M HNO_3 to be prepared for column chromatography.

To test the removal of non-carbonate fraction contamination in carbonate leach samples, the total dissolution of the samples was performed [52]. The samples were digested with two dissolution techniques, by mineral acids and by lithium borate fusion, owing to the difficulties faced in achieving good recovery for Th with acid digestion. For sample digestion by mineral acids, 1 g of carbonate

powder and 10 mL of HNO_3 were added in a Teflon beaker. The mixture was then placed on a hot plate at 110 °C. After the HNO_3 evaporated, a mixture of 10 mL of HNO_3 , 10 mL of HF, and 10 mL of HClO_4 was added at 200 °C to dissolve the sample. The last step was repeated at least two times to ensure complete dissolution. The dissolved residue was dissolved in 5 mL of 3 M HNO_3 to be prepared for U column chromatography. For sample digestion with lithium borate fusion, 1 g of precisely weighed carbonate samples and ~4 g of lithium borates were added in a platinum crucible. Fusion was performed in a Claisse LeoNeo furnace at 1050 °C for 23 min. After fusion, the glass was poured in 80 mL of stirred deionized water in a Teflon beaker. The content was then transferred to a glass beaker and washed with the additional 20 mL of deionized water. The glass beaker with the fused sample was stirred and heated to 125 °C, and 10 mL of concentrated HNO_3 was added to dissolve the lithium borate glass. After the glass was dissolved, the beaker was left on the hot plate with continuous stirring until the solution volume was reduced to 50 mL. This resulted in a 2–3 M HNO_3 solution. Then, the solution was cooled to 90 °C and 1 mL of 0.2 M polyethylene glycol solution (PEG) was added dropwise to remove silicates. Stirring was continued for another 1 h, after which the beaker was covered and left overnight to allow the precipitate to form and settle. The remaining solution was filtered before loading to the column for Th separation.

U and Th were separated by the combination of two extraction chromatographic resins, uranium and tetravalent actinide (UTEVA) and tetravalent actinide (TEVA) resin, both of which were precleaned by soaking overnight in 6 M HNO_3 and then washed several times with deionized water. Columns were preconditioned by adding 2 mL of UTEVA resin to the column and by washing with 10 mL of deionized water, 5 mL of 1 M HNO_3 , and 10 mL of 3 M HNO_3 . Leached samples prepared in 3 M HNO_3 were transferred onto an arranged tandem setup, where the preconditioned TEVA column was at the top and the preconditioned UTEVA column was at the bottom. Th was retained on the TEVA separation column and U was retained on the UTEVA separation column. The columns were then washed with 30 mL of 3 M HNO_3 . After washing, the columns were separated and treated independently. U separation on the UTEVA resin was performed in the same way as was done for the water samples described below. Th was eluted from the TEVA resin to a clean glass beaker with the consecutive addition of 20 mL of 9 M HCl and 5 mL of 6 M HCl. The eluate was evaporated to dryness and cleaned three times with a mixture of HNO_3 and H_2O_2 . U and Th in the total digestion samples were separated independently, with U on the UTEVA column and Th on the TEVA column, by the same procedure as that described above.

For the determination of U isotopes in water samples, U was coprecipitated with $\text{Fe}(\text{OH})_3$ [53]. In an aliquot containing 350 mL of water, 1 mL of FeCl_3 solution (5 mg/mL) was added and the pH was increased to 9 by adding a concentrated ammonia solution. The precipitate was separated by centrifugation and washed with deionized water to neutral pH. The U separation procedure was based on using UTEVA extraction chromatographic resin, which was precleaned by soaking overnight in 6 M HNO_3 and then washed several times with deionized water. The samples were dissolved in 5 mL of 3 M HNO_3 after U preconcentration and transferred onto a preconditioned UTEVA column. This was prepared by adding 2 mL of UTEVA resin to the column and washing with 10 mL of deionized water, 5 mL of 1 M HNO_3 , and 10 mL of 3 M HNO_3 . After the sample was loaded, the column was washed with 20 mL of 3 M HNO_3 , 5 mL of 9 M HCl, and 25 mL of 5 M HCl with 0.5 M oxalate. U isotopes were eluted with 15 mL of 1 M HCl in a clean beaker, and the eluate was evaporated to dryness. To destroy any possible organic residue that might co-elute from the resin, the dry residue was digested three times with a mixture of HNO_3 and H_2O_2 before measurements.

2.4.1. U and Th Concentration Measurements

U and Th concentrations were measured to determine the concentration of selected elements in unknown samples and to assess the concentration in diluted sample fractions for selecting appropriate dilution factors for the MC-ICP-MS measurements of isotope ratios. We also measured the concentration to assess impurity levels in blank samples, which were treated the same way as samples.

The exact U concentrations in water samples were determined by triple-quadrupole inductively coupled plasma mass spectrometry (ICP-QQQ). Aliquots of 5 mL U water samples were measured in 2% HNO₃ using an Agilent 8800 Triple Quadrupole ICP-MS (Agilent Technologies, CA, USA) by following a measurement protocol that differed slightly from that described elsewhere [54]. U standard solutions and samples were introduced into the ICP under wet plasma conditions and in no-gas mode. Interference correction and external calibration were performed using the U standard reference material SRM-3164 (National Institute of Standards & Technology, Gaithersburg, MD, USA).

After the dissolution of carbonate rock samples, U and Th concentrations were measured by using ICP-QQQ.

2.4.2. U Isotope Measurements

U isotope ratios were measured using a Nu plasma II (Nu Instruments Ltd., Wrexham, UK) MC-ICP-MS with the high-efficiency Aridus IITM (Cetac Technologies, Omaha, NE, USA) sample introduction system. The instrument setup is described in greater detail in Rován et al. [55]. The instrument mass bias was corrected with an external standard-sample bracketing method. The measured U isotope ratios were calibrated against the corresponding U isotopic standard IRMM-184 (European Commission - JRC, Institute of Reference Materials and Measurements, Belgium) that had been measured before and after the sample measurement. The standards and samples were diluted with 2% HNO₃ to obtain a constant concentration for isotopic measurements. The measurements were corrected for instrumental biases and chemical blanks, where the uncertainty was estimated by following the procedure described in Rován et al. [55]. The total process blanks for U isotope ratios ranged from 0.08 ng to 0.28 ng. The procedural blanks were negligible compared to the amount of U analyzed in samples. U isotope ratios are determined relative to the IRMM-184 standard and are presented in the delta notation (Equation (1)):

$$\delta^{238}\text{U in } \text{‰} = \left[\frac{({}^{238}\text{U}/{}^{235}\text{U})_{\text{sample}}}{({}^{238}\text{U}/{}^{235}\text{U})_{\text{standard}}} - 1 \right] \times 1000, \quad (1)$$

and recalculated to the $\delta^{238}\text{U}_{\text{CRM-112a}}$ values to assure comparability with previously published data [56].

U isotope ratios are also presented as ${}^{234}\text{U}/{}^{238}\text{U}$ activity ratios (Equation (2)), which are calculated from the corrected isotope ratios by using the decay constants (λ_{234} and λ_{238}) reported in Cheng et al. [57]:

$${}^{234}\text{U}/{}^{238}\text{U activity ratio} = \frac{\lambda_{234}}{\lambda_{238}} \times \left(\frac{{}^{234}\text{U}}{{}^{238}\text{U}} \right)_{\text{corrected}}. \quad (2)$$

The reported uncertainties are derived from the acquired data and are shown as $2s$, where s is the standard deviation.

The long-term analytical precision was assessed by measurements of the U isotopic standard (IRMM-184) at 5 ng/mL concentration over a period of 15 months. The mean values of ${}^{235}\text{U}/{}^{238}\text{U}$ and ${}^{234}\text{U}/{}^{238}\text{U}$ are $(7.2622 \pm 0.0049) \times 10^{-3}$ and $(5.314 \pm 0.017) \times 10^{-5}$, respectively. The measured values are in agreement with certified reference values [56]. The quality of the results was expressed in terms of the expanded uncertainty, where the main source of uncertainty is the uncertainty of the certified standard.

3. Results

3.1. Bedrock Composition of Ljubljana River Catchment

Table S1 shows the results of all chemical, mineralogical, and isotopic analyses of samples, and Table 2 lists essential data on the chemical and mineral compositions.

Table 2. Elemental and semi-quantitative mineral composition of carbonate fraction of bedrock samples.

Site	Mg mg g ⁻¹	Ca mg g ⁻¹	Mg/Ca at. ratio	Si mg g ⁻¹	Al mg g ⁻¹	Na mg g ⁻¹	K mg g ⁻¹	Non-Carbonate wt%	Calcite wt%	Dolomite wt%
1	4.48	387.89	0.02	1.30	27.24	1.47	6.18	3.91	100	0
3	3.11	386.26	0.01	2.66	9.40	1.43	1.05	4.50	99.7	0.3
4	4.98	386.54	0.02	0.66	24.35	2.47	4.27	3.16	100	0
5	3.49	388.76	0.01	0.39	24.35	2.03	4.27	4.18	100	0
6	3.45	389.49	0.01	0.77	14.09	1.78	1.20	2.93	100	0
7	6.03	380.27	0.03	2.80	14.09	2.72	1.20	4.84	99.6	0.4
8	5.63	381.73	0.02	4.60	2.07	1.90	BLD *	7.20	99	1
12	10.42	377.69	0.05	1.78	23.96	1.45	4.93	6.27	100	0
14	124.77	217.19	0.95	5.15	4.06	1.09	BLD *	0.95	6	94

* BLD = below the limit of detection.

Apart from the sample collected at site 14 (which contained dolomite with some calcite), all samples contained limestone with low-Mg calcite as the predominant mineral. The share of non-carbonate mineral fraction ranged from <1 wt% in dolomite (site 14) to 7.2 wt% for limestone collected at site 8 (Table 2). In all samples, traces of quartz and some unidentified clay minerals were detected.

The total U concentrations in the bedrock samples (Table S1, Figure 5) varied in the bulk samples from 1.02 to 4.88 μg g⁻¹, in the leached fraction (representing operationally defined carbonate fraction) from 0.74 to 3.42 μg g⁻¹, and in the residual fraction (non-carbonate, detrital phase) from 0.28 to 2.37 μg g⁻¹ of the total sample mass. The residual fraction was calculated as the difference between the bulk concentration and the leached fraction. The Th concentrations in rocks are much lower compared to the U concentrations; they range from 16.7 to 349 ng g⁻¹ in bulk samples, from 6.7 to 178 ng g⁻¹ in leached samples, and from 1.16 to 173 ng g⁻¹ of the total sample mass in residual fraction. The activity ratio of ²³⁴U/²³⁸U varied from 0.96 to 1.03 in bulk rocks, from 1.01 to 1.04 in carbonate fraction, and from 0.84 to 1.02 in non-carbonate residue. The δ²³⁸U values ranged between -0.59‰ and 0.15‰ in bulk samples, -0.99‰ and -0.51‰ in carbonate fraction, and -3.46‰ and 0.73‰ in non-carbonate fraction.

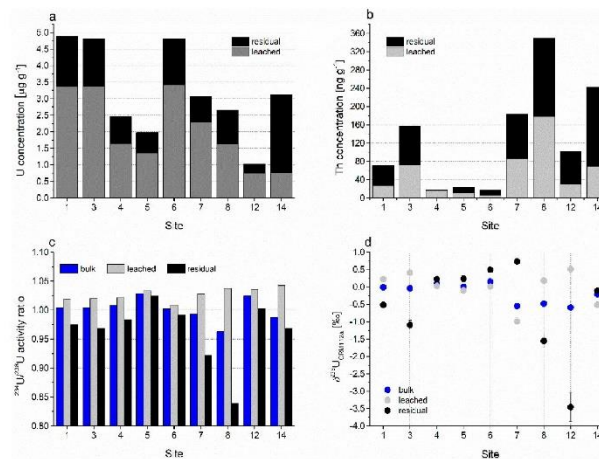


Figure 5. Concentrations of (a) U and (b) Th; (c) activity ratio of ²³⁴U/²³⁸U; and (d) δ²³⁸U value in bulk, leachable, and residual fraction of bedrock samples; Table S1 lists tabulated results and standard uncertainties.

3.2. Water Composition of Ljubljana River Catchment

Table 3 lists the means and ranges of the values of the measured physicochemical parameters and main ion concentrations in the sampled water for five seasonal sampling campaigns from October 2017 to August 2018, and Table S1 lists all measured values. Figures 6 and 7 show the seasonal variability of the measured physicochemical parameters and main ion concentrations in the sampled springs and sinking streams.

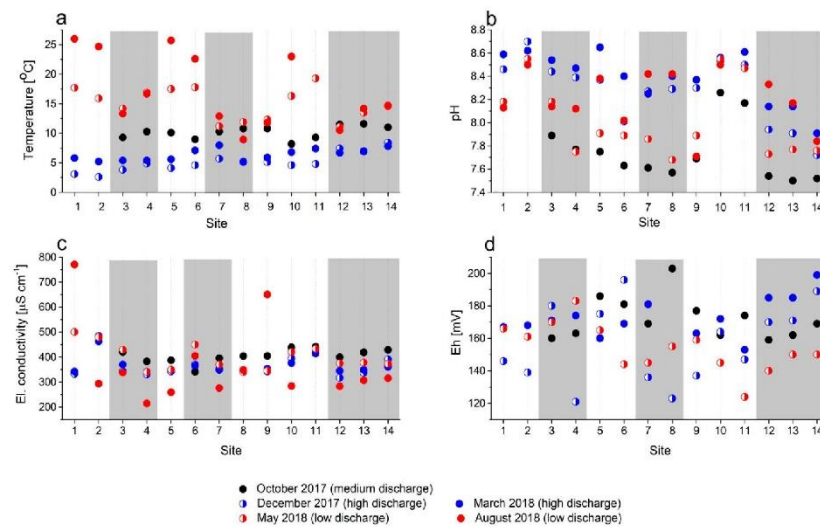


Figure 6. Seasonal variations of (a) temperature, (b) pH, (c) conductivity, and (d) redox potential in analyzed water samples; white areas represent sinking streams and grey bars represent karst springs.

The temperature variability at individual sampling sites during the entire sampling period ranged from 4.8 °C (site 12) to 10.4 °C (site 3) for springs and from 14.5 °C (site 11) to 22.9 °C (site 1) for sinking streams (Figure 6a). The water temperature gradually increased downstream with decreasing altitude at medium and high discharge (from October 2017 to March 2018); by contrast, surface streams warmed up rapidly and reached temperatures of up to 26 °C at low discharge and higher ambient temperature (sinks at sites 1 and 5, August 2018).

The average pH values of water (Figure 6b) generally decreased downstream; however, the differences between the seasons and at different discharges at each site were rather unsystematic, amounting to up to 0.9 units. At most sites, the lowest pH values were measured in the autumn at moderate discharge; however, no measurements were performed at that time at sites 1 and 2 because they were flooded. Consistently higher and seasonally much less variable values were measured in the sinking streams at sites 2, 10, and 11.

The electrical conductivity (Figure 6c) was relatively stable in most springs, except in August 2018, when some relatively low values were measured at very low water levels. By contrast, extremely high values were measured at the same time in sinking streams at sites 1 and 9.

The redox potential (Figure 6d) expressed in mV vs. Ag/AgCl 3.5 M KCl electrode varied rather randomly in a relatively narrow range of values and was always positive; specifically, oxidizing conditions prevailed in the water at all springs and sinks throughout the sampling period. No measurements were performed in August 2018 because the redox probe was malfunctioning.

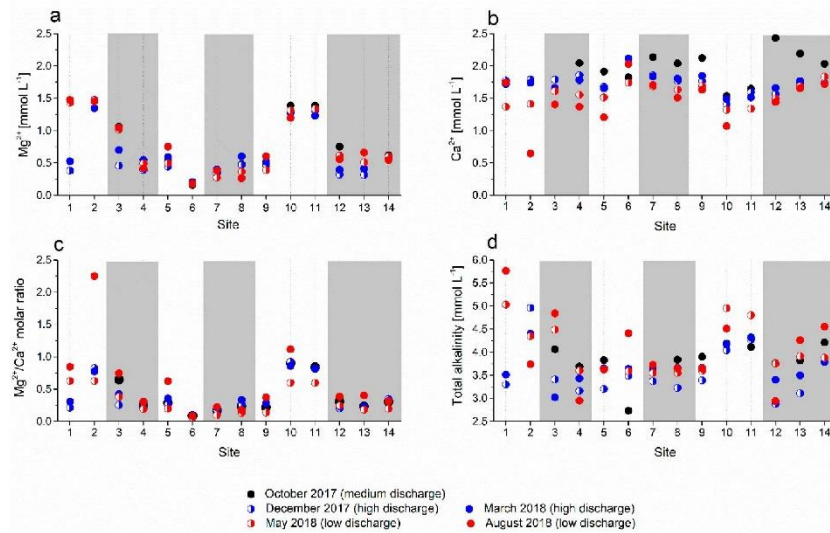


Figure 7. Concentrations of dissolved (a) Mg^{2+} , (b) Ca^{2+} , and (c) Mg^{2+}/Ca^{2+} molar ratio and (d) total alkalinity in analyzed water samples; white areas represent sinking streams and grey bars represent karst springs.

The Mg^{2+} concentration (Figure 7a) varied significantly among sites but did not change much seasonally and/or with varying discharge, except at site 1, where elevated Mg^{2+} concentrations were recorded in May 2018 and August 2018 at low discharge. The Mg^{2+} concentrations were conspicuously elevated in sinking streams at sites 2, 10, and 11. The Ca^{2+} concentrations (Figure 7b) were less variable; only in August 2018, an extremely low value was recorded in the sinking stream at site 2. The Mg^{2+}/Ca^{2+} ratios (Figure 7c) mainly followed the spatial variability of the Mg^{2+} content with higher values in sinking streams at sites 2, 10, and 11. In August 2018, the peak values coincided with low Ca^{2+} concentrations at respective sites.

The total alkalinity of water showed a spatial pattern resembling that of Mg^{2+} concentrations in the cool period at high discharge (Figure 7d, blue symbols). In the summer, at low discharge (August 2018), the alkalinities scattered and reached annual maximum values at some sites (sites 1, 6, 11, and 14) and annual minimum values at others (sites 2 and 4).

The sampled water was supersaturated with respect to calcite in all five sampling periods irrespective of the discharge ($SI_{calcite} > 0$, Table 3). The highest values of the calcite saturation index (defined as the log of the ratio between ion activity product and solubility product) were determined in August 2018 at the lowest discharge and highest temperature, and the lowest values were determined in October 2017 at moderate discharge. The most saturated water with respect to calcite was seen in the sinking streams at sites 1, 2, 10, and 11 (Table 3).

Table 3. Main mean values of hydrochemical parameters in sampled springs and sinking streams in five sampling campaigns (October 2017, December 2017, May 2018, March 2018, and August 2018); no data for redox potential is available for August 2018 because the ORP probe was malfunctioning in the field. In parentheses are shown the minimum and the maximum values.

Site	Temperature [°C]	pH	Conductivity [$\mu\text{S cm}^{-1}$]	Redox potential [mV]	Total alkalinity [mmol L ⁻¹]	Ca ²⁺ [mmol L ⁻¹]	Mg ²⁺ [mmol L ⁻¹]	Mg/Ca molar ratio	Na ⁺ [mmol L ⁻¹]	K ⁺ [mmol L ⁻¹]	Si _{calcite}
1	13.2	8.34	486	160	4.4	1.65	0.95	0.5	0.24	0.71	0.91
	(3.1–26.0)	(8.13–8.59)	(332–771)	(146–167)	(3.30–5.77)	(1.37–1.77)	(0.38–1.48)	(0.21–0.85)	(0.07–0.32)	(0.02–2.60)	(0.81–1.01)
2	12.1	8.59	431	156	4.36	1.4	1.44	1.12	0.23	0.18	0.79
	(2.6–24.7)	(8.50–8.70)	(294–485)	(139–168)	(3.74–4.96)	(0.64–1.79)	(1.35–1.48)	(0.63–2.25)	(0.16–0.33)	(0.03–0.33)	(0.18–1.09)
3	9.2	8.24	380	170	3.96	1.62	0.86	0.49	0.18	0.09	0.66
	(3.8–14.2)	(7.89–8.54)	(338–430)	(160–180)	(3.02–4.84)	(1.41–1.79)	(0.15–1.06)	(0.25–0.74)	(0.08–0.27)	(0.01–0.23)	(0.41–0.84)
4	10.8	8.1	322	160	3.37	1.72	0.47	0.25	0.09	0.07	0.59
	(4.9–16.9)	(7.75–8.47)	(215–383)	(121–183)	(2.95–3.69)	(1.37–2.05)	(0.39–0.55)	(0.19–0.31)	(0.07–0.14)	(0.02–0.17)	(0.33–0.89)
5	12.6	8.21	338	172	3.59	1.59	0.57	0.35	0.12	0.08	0.71
	(4.1–25.7)	(7.75–8.65)	(259–387)	(160–186)	(3.20–3.83)	(1.21–1.92)	(0.44–0.75)	(0.20–0.62)	(0.08–0.21)	(0.02–0.21)	(0.34–1.05)
6	12.2	8	386	173	3.57	1.97	0.18	0.08	0.48	0.35	0.58
	(4.6–22.6)	(7.63–8.40)	(341–450)	(144–196)	(2.73–4.41)	(1.74–2.12)	(0.16–0.21)	(0.06–0.10)	(0.28–0.81)	(0.04–0.66)	(0.05–0.94)
7	9.6	8.08	349	158	3.58	1.84	0.35	0.18	0.28	0.15	0.61
	(5.7–12.9)	(7.61–8.42)	(276–396)	(136–181)	(3.37–3.73)	(1.69–2.14)	(0.27–0.40)	(0.10–0.22)	(0.19–0.38)	(0.02–0.32)	(0.3–0.97)
8	8.4	8.07	356	159	3.59	1.75	0.44	0.23	0.25	0.09	0.56
	(5.1–11.9)	(7.57–8.42)	(340–404)	(123–203)	(3.23–3.84)	(1.51–2.04)	(0.26–0.60)	(0.13–0.33)	(0.08–0.88)	(0.03–0.21)	(0.20–0.86)
9	9.2	7.99	419	159	3.64	1.81	0.49	0.26	0.26	0.1	0.51
	(5.1–12.3)	(7.69–8.37)	(342–650)	(137–177)	(3.39–3.90)	(1.63–2.12)	(0.39–0.60)	(0.14–0.37)	(0.09–0.73)	(0.02–0.18)	(0.24–0.84)
10	11.8	8.48	383	161	4.37	1.36	1.29	0.88	0.07	0.04	0.95
	(4.6–23)	(8.26–8.56)	(284–439)	(145–172)	(4.04–4.95)	(1.07–1.54)	(1.20–1.39)	(0.60–1.12)	(0.03–0.14)	(0.03–0.09)	(0.73–1.15)
11	10.2	8.44	429	150	4.38	1.52	1.31	0.77	0.13	0.07	0.94
	(4.8–19.3)	(8.17–8.61)	(414–441)	(124–174)	(4.11–4.80)	(1.34–1.65)	(1.23–1.39)	(0.60–0.84)	(0.10–0.19)	(0.04–0.11)	(0.68–1.08)
12	9.4	7.94	344	164	3.35	1.72	0.53	0.28	0.36	0.11	0.4
	(6.7–11.5)	(7.54–8.33)	(283–400)	(140–186)	(2.88–3.76)	(1.44–2.43)	(0.32–0.75)	(0.20–0.39)	(0.17–1.00)	(0.02–0.28)	(0.22–0.68)
13	10.6	7.9	358	167	3.72	1.81	0.48	0.25	0.21	0.08	0.44
	(6.9–14.2)	(7.50–8.17)	(307–419)	(150–185)	(3.11–4.26)	(1.65–2.19)	(0.32–0.66)	(0.18–0.40)	(0.11–0.33)	(0.02–0.23)	(0.16–0.79)
14	11.3	7.75	374	177	4.06	1.83	0.59	0.3	0.18	0.05	0.35
	(7.8–14.7)	(7.52–7.91)	(315–429)	(150–199)	(3.79–4.55)	(1.72–2.03)	(0.54–0.32)	(0.20–0.35)	(0.10–0.23)	(0.02–0.11)	(0.18–0.52)

The Na^+ and K^+ concentrations in the analyzed water (Figure 8) had similar values at most sites of up to 0.5 mmol L^{-1} ; these two elements show a spatial pattern that differs from those of Mg^{2+} and Ca^{2+} , with higher concentrations in the headwaters at Cerknisko polje (sites 1 and 2), in the sinking stream at site 6, and in the hydraulically connected central spring at site 7 and the lowest concentrations in the sinking streams at sites 10 and 11. The concentrations were the highest at low discharge. The K^+ concentrations were low (or even below the limit of detection, Table 3) at most sites at medium and high discharge and higher but less scattered than those for Na^+ at low discharge in spring and summer 2018; the peak values were reached in the sinking stream at site 6, as in the case of Na^+ .

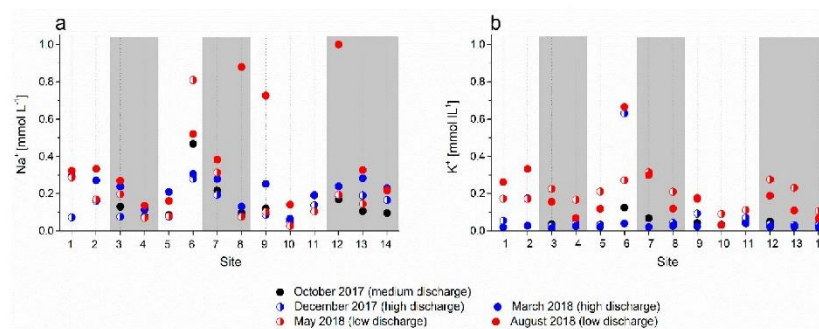


Figure 8. Concentrations of (a) Na^+ and (b) K^+ in analyzed water samples; white areas represent sinking streams and grey bars represent karst springs.

Concentration and Isotopic Composition of U in Water

The total U concentrations in water varied spatially and seasonally (Figure 9, Table S1). They ranged from 0.24 to 0.70 ng mL^{-1} (Figure 9a). In most cases, the concentrations were the lowest at the lowest discharge (August 2018), except at springs 3 and 12–14; by contrast, the concentrations were scattered (more so in sinking streams than in springs) during seasons with medium to high discharge.

The activity ratios of $^{234}\text{U}/^{238}\text{U}$ in water (Figure 9c) were consistently higher than the secular equilibrium value of 1.00 and varied seasonally, ranging from 1.17 to 1.38 in October 2017, 1.10 to 1.36 in December 2017, 1.10 to 1.42 in March 2018, 1.13 to 1.78 in May 2018, and 1.16 to 1.58 in August 2018. The mean and ranges of values decreased both spatially in the downstream direction and seasonally with increasing discharge.

The $\delta^{238}\text{U}$ values in water samples ranged from -0.86‰ to 3.46‰ in October 2017, 0.03‰ to 2.10‰ in December 2017, -0.293‰ to 2.74‰ in March 2018, -0.34‰ to 4.24‰ in May 2018, and -1.37‰ to 2.52‰ in August 2018. The activity ratios of $^{234}\text{U}/^{238}\text{U}$ in water samples show a general spatial pattern similar to that of the U concentrations. Except at sites 1, 4, and 7, the lowest $\delta^{238}\text{U}$ values were seen during periods of low discharge; at most sites, $\delta^{238}\text{U}$ values were scattered at moderate and high discharge, especially in the headwater and area section of the analyzed catchment.

Both $\delta^{238}\text{U}$ isotope ratios and $^{234}\text{U}/^{238}\text{U}$ activity ratios show a slightly similar pattern downstream; specifically, they show decreased seasonal variability and preferential enrichment of the lighter U isotope.

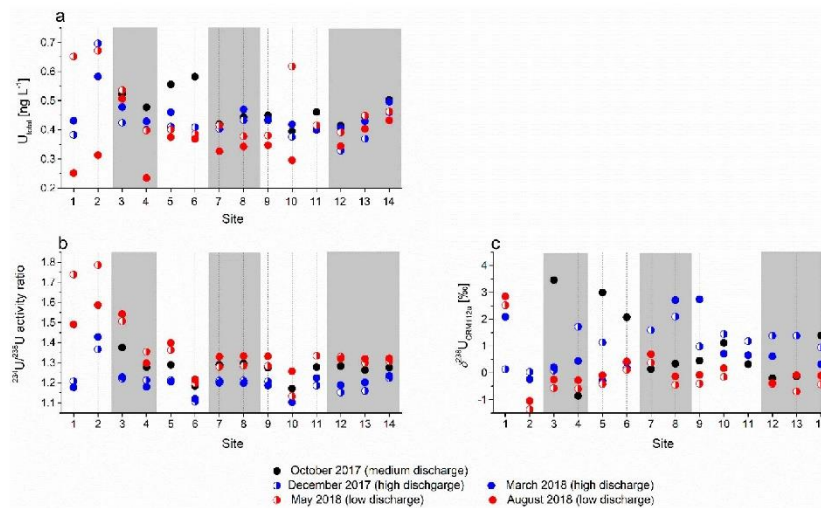
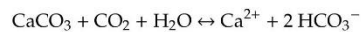


Figure 9. (a) U concentration, (b) $^{234}\text{U}/^{238}\text{U}$ activity ratio, and (c) $\delta^{238}\text{U}_{\text{CRM112a}}$ value in analyzed water samples; white areas represent sinking streams and grey bars represent karst springs.

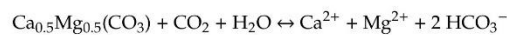
4. Discussion

4.1. Bedrock Weathering

The karst aquifer of the Ljubljana River is predominantly composed of limestone and dolomite; therefore, the dissolution of the carbonate bedrock can be considered as the governing influence on the groundwater chemistry. The carbonate dissolution in CO_2 -rich karst water proceeds as



for calcite and



for dolomite. Consequently, the sum concentration of dissolved Ca^{2+} and Mg^{2+} equals two times the HCO_3^- concentration assuming that all dissolved Ca and Mg are derived from carbonate dissolution. The ratio between the two elements depends upon the relative contributions of limestone (calcite) and dolomite weathering, and the deviation of the $(\text{Mg}^{2+} + \text{Ca}^{2+})$ concentration from $2 \times \text{HCO}_3^-$ concentration indicates the contribution of silicate weathering to the dissolved load of water. Both parameters are commonly used to reconstruct the source areas of groundwater in individual springs and streams.

Figure 10 shows the Mg^{2+} vs. Ca^{2+} plot of analyzed springs and streams in the Ljubljana River catchment and the correlation between the concentrations of $(\text{Mg}^{2+} + \text{Ca}^{2+})$ and HCO_3^- . The line $\text{Mg}^{2+}/\text{Ca}^{2+} = 1$ in Figure 10a represents the dissolution of pure dolomite, and the line $\text{Mg}^{2+}/\text{Ca}^{2+} = 0.33$ reflects the weathering of equal amounts of limestone and dolomite; dissolution of pure limestone produces the water solution that is plotted at or below the line $\text{Mg}^{2+}/\text{Ca}^{2+} = 0.1$ [58].

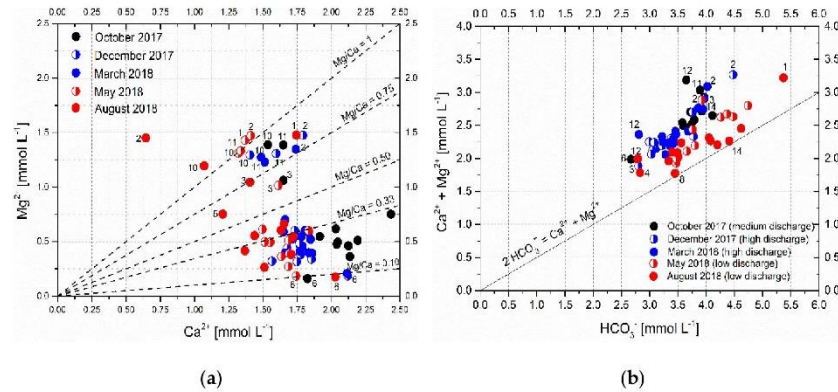


Figure 10. (a) Mg^{2+} vs. Ca^{2+} concentrations of the Ljubljana River catchment and (b) correlation between $(Mg^{2+} + Ca^{2+})$ and HCO_3^- concentration in springs and sinking streams of the Ljubljana River catchment.

Generally, most samples in Figure 10a are plotted between the lines $Mg^{2+}/Ca^{2+} = 0.1$ and 0.5 , indicating the dissolution of a mixture of limestone and dolomite; this corresponds to the dominant lithology of the Ljubljana River catchment. The sinking stream at site 6 (Pivka River) that is plotted at or below the line $Mg^{2+}/Ca^{2+} = 0.1$ drains an area with flysch and limestone bedrock.

Samples from sinking streams plotted above the line $Mg^{2+}/Ca^{2+} = 1$ (sites 2 and 10 in August 2018) contained more Mg^{2+} than could be supplied by the dissolution of pure dolomite, and samples at sites 1, 2, 10, and 11 in May 2018 were very close to, or at, the pure dolomite dissolution line. These streams drain areas composed predominantly of dolomite (Figure 2, [40,41]). Some Mg^{2+} can also be supplied by the weathering of silicate minerals accumulated in the flood sediments at Cerknjško polje (streams at sites 1 and 2) and in the sub-catchment of the Hotenjka (site 10) and Logaščica (site 11) streams, as shown in Figure 10b, where almost all samples are plotted above the carbonate dissolution line. Another plausible explanation of the increased Mg^{2+}/Ca^{2+} ratio in summer months is the precipitation of low-Mg calcite from supersaturated water, which preferentially removes Ca^{2+} from the solution and thus increases the Mg^{2+}/Ca^{2+} ratio in the residual water [59–61]. Considering the high supersaturation of these streams with respect to calcite (Table 3), calcite precipitation is possible, especially when the water temperature is high and both water evaporation from streams and enhanced degassing of CO_2 occur. Occasional occurrence of carbonate incrustations on leaves or rocks around the sinks in summer months supports this assumption. At increased discharge and lower temperature, the water samples from sites 2, 10, and 11 plotted between the $Mg^{2+}/Ca^{2+} = 0.75$ and 1 lines and the water sample from site 1 plotted between the $Mg^{2+}/Ca^{2+} = 0.2$ and 0.3 lines (Table S1). This indicates that with increasing discharge, these streams receive an increasing amount of water from the limestone-rich part of the aquifer. The stream at site 1 that crosses the southern part of Cerknjško polje predominantly receives water from the south from the limestone-dominated Javorniki plateau at medium and high discharge.

The spring of the Rak stream (site 3) plotted between the $Mg^{2+}/Ca^{2+} = 0.75$ and 0.5 lines at low and medium discharge and between the $Mg^{2+}/Ca^{2+} = 0.5$ and 0.33 lines at high discharge. It is hydraulically connected to the Cerknjško polje with sinking streams at sites 1 and 2 [42,47]; however, with increasing discharge, it also obtains an increasing fraction of water from Javorniki plateau (Figure 2). The Rak stream at site 5 is located close to its sink a few hundreds of meters downstream from the confluence with Kotlički spring (site 4, with Mg^{2+}/Ca^{2+} ratio of 0.21–0.31, Table S1); it had a Mg^{2+}/Ca^{2+} ratio of 0.62 in August 2018 and a ratio of 0.26–0.36 in other seasons. Therefore, it is closer to the Kotlički spring than to the Rak spring. Considering the extremely low discharge during the sampling campaign in August,

when water was sinking in numerous smaller pools, CaCO_3 precipitation owing to CO_2 degassing and evaporation is the most probable cause of this increase in the $\text{Mg}^{2+}/\text{Ca}^{2+}$ ratio at this site.

The springs of the Unica river in Planina cave (site 7, $\text{Mg}^{2+}/\text{Ca}^{2+} = 0.16\text{--}0.24$) and Malenščica (site 8, $\text{Mg}^{2+}/\text{Ca}^{2+} = 0.17\text{--}0.33$) at Planinsko polje in the central part of the Ljubljana river catchment have $\text{Mg}^{2+}/\text{Ca}^{2+}$ ratios that vary in a relatively narrow range of values. Despite their proximity, they obviously receive water from different sources, which also show other dissolved elements such as Na^+ or K^+ (Figure 8). The spring at site 7 is hydraulically connected with the Pivka river (sink at site 6, $\text{Mg}^{2+}/\text{Ca}^{2+} = 0.09\text{--}0.11$, [5,42,47]). However, in terms of the $\text{Mg}^{2+}/\text{Ca}^{2+}$ ratio, the water composition is closer to that of the water from the Rak stream and Javorniki plateau (sites 4 and 5), indicating that water from this direction prevails in these springs through most of the year.

At the northern edge of the Ljubljana aquifer, the main Ljubljana springs at sites 12 and 13 and the tributary at site 14 discharge well-homogenized water from the central part of the catchment [37]. However, the contribution of sinking streams at sites 10 and 11 can be detected occasionally in the springs at sites 12 and 13 ($\text{Mg}^{2+}/\text{Ca}^{2+} = 0.2\text{--}0.4$). By contrast, in the tributary at site 14, the $\text{Mg}^{2+}/\text{Ca}^{2+}$ ratio remains rather constant (0.30–0.33) and is representative of the integral composition of the aquifer with similar abundances of dolomite and limestone. The increased $\text{Mg}^{2+}/\text{Ca}^{2+}$ values in spring at site 14 agree with tracer experiments, which showed a hydraulic connection through dolomite-containing formations between sinks at Cerknjsko polje and this spring [62].

For all analyzed water samples, the sum of Mg^{2+} and Ca^{2+} concentrations was larger than $2 \times \text{HCO}_3^-$ concentration (Figure 10b), indicating that the weathering of silicates (e.g., clay minerals, feldspars) also contributes some solutes to the groundwater in the Ljubljana aquifer throughout the year. This contribution was the smallest in the summer (August 2018) and increased with increasing discharge. The largest contribution was found in samples taken from October 2017 to March 2018, which is consistent with the fact that in areas with thick soil and large bioproduction, such as the mainly forested karst catchments of central and southern Slovenia, silicate weathering rates and, consequently, mineralization of water increases in humid conditions owing to the higher weathering capacity of clastic rocks in comparison to that of carbonate rocks [63]. The sites with apparently the smallest contribution of silicate weathering at low discharge were the sinking stream at site 6 and springs at sites 7 and 8. At medium discharge, the least contribution of silicate weathering was observed at site 6 and in the spring at site 14; by contrast, at high discharge, the least silicate-derived mineralization was seen in the springs at sites 3 and 14. Interestingly, the sinking stream at site 6 (Pivka river) with abundant flysch in the headwater region and siliciclastic sediments in Pivka basin (Figure 2) seems to have the smallest dissolved load fraction originating from silicate weathering. Other water samples listed as those with a minor fraction of silicate-derived solutes were collected at springs draining carbonate rocks with no notable occurrences of siliciclastic rocks in their sub-catchments. By contrast, the largest contribution of silicate weathering was observed at high discharge in sinking streams at sites 1 and 2 at Cerknjsko polje and in the spring at site 12. While silicates are relatively abundant at Cerknjsko polje, where the sinks of the two streams are located, the spring at site 12 at the northern edge of Ljubljana aquifer emerges from the limestone area with no notable occurrences of silicate minerals in the immediate proximity. Some Upper Cretaceous marls (“Scalia”) occur in the catchment area between the sink of the Unica river (site 9) and the spring at site 12 [40], which could contribute to the silicate weathering affecting the mineralization of the spring water; however, this can only be speculated from the available data.

In principle, the discharge strongly influences the solute concentrations and physicochemical parameters of spring and river water. However, in the Ljubljana river catchment, most measured parameters seem to be only weakly correlated with the discharge, or the correlations change from positive to negative at certain points.

Table 4 shows the Pearson correlation coefficients calculated for each parameter at sites where discharge data were available based on water analyses from all five seasonal sampling campaigns. The conductivity, as a measure of total dissolved ions in water, showed no or only poor correlation

with the discharge, and the correlations, where they existed, were positive at some sites and negative at others. Ravbar et al. [64] showed that in complex karst aquifers, the electrical conductivity and, with it, the concentrations of individual solutes may show rather peculiar behavior at variable discharge, i.e., it may increase and decrease irrespective of the amount of water. This is explained by the fact that with an increasing water level, the catchment expands and incorporates groundwater from other parts of the aquifer with different lithologies and different hydraulic heads. Consequently, the origin, amount, and hydrochemical composition of water at the same spring may vary rather irregularly depending on the local hydrological conditions in the entire catchment area. This study used classical geochemical tracers (elemental concentrations, physicochemical parameters); therefore, we could only substantiate the existing knowledge about the Ljubljana aquifer's behavior [5,42,47].

Table 4. Pearson correlation coefficient (r) between discharge and measured parameters in water from the Ljubljana River catchment; statistically significant correlations ($r^2 > 0.6$) are highlighted.

Parameter/Site	2	3	4	5	6	7	8	9	11	12	13	14
Temperature	-0.96	-0.93	-0.89	-0.81	-0.93	-0.97	-0.64	-0.98	0.44	-0.87	-0.94	-0.85
pH	0.90	0.77	0.80	0.57	0.25	0.38	0.06	0.90	0.68	0.11	0.19	-0.18
Conductivity	0.64	-0.50	0.24	0.20	-0.74	0.15	0.04	-0.56	-0.28	-0.20	-0.21	0.57
Tot. alkalinity	0.77	-0.83	-0.24	-0.79	-0.63	-0.79	-0.39	-0.58	0.83	-0.47	-0.96	-0.69
Si _{calcit}	-0.33	0.65	0.82	0.33	-0.31	0.26	0.04	0.88	0.85	-0.10	-0.16	-0.66
Mg ²⁺	-0.50	-0.99	-0.23	-0.54	0.35	0.23	0.87	0.02	-0.34	-0.83	-0.91	0.57
Ca ²⁺	0.87	0.78	0.43	0.33	0.64	0.13	0.66	0.09	-0.78	-0.11	-0.07	-0.01
Na ⁺	-0.55	-0.54	-0.10	-0.09	-0.87	-0.61	-0.63	-0.25	0.01	-0.30	0.51	0.26
K ⁺	0.36	-0.52	0.50	-0.15	0.84	-0.65	0.91	0.76	-0.19	0.28	0.55	-0.10
Al _{tot}	-0.55	-0.23	-0.36	-0.02	-0.40	-0.35	0.72	0.70	0.01	0.07	-0.02	0.18
U _{tot}	0.54	-0.83	0.19	0.10	-0.48	0.21	0.27	0.18	-0.59	-0.82	-0.87	0.34
Mg ²⁺ /Ca ²⁺	-0.79	-0.98	-0.59	-0.49	-0.35	0.12	0.83	-0.07	0.58	-0.94	-0.75	0.60
δ ²³⁸ U	1.00	0.25	0.51	0.59	-0.41	0.50	0.87	0.59	0.18	0.60	0.59	0.75
²³⁴ U/ ²³⁸ U	-0.86	-0.90	-0.86	-0.87	-0.89	-0.49	-0.91	-0.93	0.13	-0.95	-0.95	-0.90

4.2. U and Th Isotopes in Bedrock

The analyzed rock samples from sites 1–5, 7, and 8 were Lower Cretaceous limestone. The sample from site 6 represented Upper Cretaceous limestone; that from site 12, Jurassic limestone; and that from site 14, Upper Triassic dolomite (“Hauptdolomit”) (Figure 2). Although samples from sites 1–5, 7, and 8 belonged to the same lithostratigraphic unit, their total U concentrations varied significantly from 1.99 to 4.88 μg g⁻¹ (Figure 5a). Jurassic limestone (site 12) had the lowest U concentration, whereas Triassic dolomite showed a similar range of values to Cretaceous limestone. Nevertheless, all measured U concentrations were within the typical range of values for carbonate rocks [65–67].

The U leached phase fraction was similar between sampling sites that belonged to the same lithostratigraphic unit (Figure 5a). The Cretaceous limestone samples had 61%–75% of the total U in the carbonate fraction and the Jurassic limestone sample, 72%. The dolomite sample (site 14) seemingly had the carbonate U fraction (24%). In our case, the carbonate fraction of the analyzed rock is defined as a leached fraction that is soluble in 1 M NaAc in 25% HAc, which was used as a soft leaching procedure to extract mainly the carbonate-associated U and Th fraction from a residual phase. The residual fraction of U in the analyzed rocks is the difference between the bulk sample and the leached fraction. In most samples, the non-carbonate U fraction was less than 30% of the total U. The exception was the dolomite sample (site 14), with virtually much higher non-carbonate U fraction, which is consistent with the fact that the weak acid preferentially extracted calcite whereas dolomite dissolution was incomplete; thus, the dolomite partly remained in the unleached fraction [68]. Therefore, the “carbonate fraction” of U in dolomite is most probably largely underestimated. In limestone samples, the residual fraction contained detrital minerals (traces of quartz, clay minerals) and only traces of dolomite. Considering the abundance of the detrital phase, which accounted for ~1–8 wt% (Table 2) of the total sample mass, the non-carbonate fraction of the bedrock is obviously strongly enriched in U.

The thorium (Th) concentrations in rock samples from the Ljubljana aquifer were generally lower than the U concentrations (Figure 5b). In addition, the Th concentrations in bulk samples were mostly higher than those in leached samples, and the difference, that is, enrichment of residual fraction in Th, was much more obvious than that for the U concentrations. Kelepertsis et al. [69] reported that Th in carbonate rocks is mainly associated with the non-detrital (i.e., carbonate) fraction, which is clearly not the case in our study area except for one Lower Cretaceous limestone (site 4). By contrast, Zhang et al. [70] associated Th in carbonate mostly with the clay fraction. The bulk Th concentration was very low in rock samples from sites 4, 5, and 6, which also have a relatively small fraction of the detrital phase (Figure 5b, Table 2). At other sites, the Th levels were much higher; this could be attributed to the increased content of detrital minerals and their enrichment in Th. A conspicuous case is the rock sample from the site 14, which had by far the lowest fraction of non-carbonate minerals (<1%, Table 2) but one of the highest Th concentrations. Obviously, as with the U content, the variability of Th levels in bedrock is high not only among different lithostratigraphic units but also within the same unit (i.e., samples of Upper Cretaceous limestone with variable U and Th contents).

The bulk samples of sedimentary carbonate rocks generally have $^{234}\text{U}/^{238}\text{U}$ activity ratios lower than 1 owing to alpha recoil effects. In a water–mineral system, ^{234}U is preferentially released from the solid phase to the water and the secular equilibrium of the $^{234}\text{U}/^{238}\text{U}$ activity ratio is disturbed. Consequently, the $^{234}\text{U}/^{238}\text{U}$ activity ratio is higher in water and lower in the mineral phases [23,25,27]. To confirm this, we calculated the $^{234}\text{U}/^{238}\text{U}$ activity ratio of the residual samples in the leaching experiment from the difference between the $^{234}\text{U}/^{238}\text{U}$ activity ratio for bulk and leached samples in consideration of the U mass balance. Here, we observed an even more conspicuous deviation in the $^{234}\text{U}/^{238}\text{U}$ activity ratios in residual samples than that reported for natural water [11,25,71]. The leached samples (Figure 5c) showed noticeably higher $^{234}\text{U}/^{238}\text{U}$ activity ratios than their corresponding bulk samples for most sampling sites, except at sites 5 (Lower Cretaceous) and 6 (Upper Cretaceous limestone), where the activity ratio for bulk and leached samples can be considered the same (difference was within measurement uncertainty). In addition, samples from sites 5 and 6 have one of the highest contributions of $^{234}\text{U}/^{238}\text{U}$ activity ratio for the U detrital phase. For the leached samples, where only the carbonate phase and some loosely bound U from clay minerals [69] were supposed to be present, the $^{234}\text{U}/^{238}\text{U}$ activity ratios for all samples were above 1 but lower than the activity ratio in river water or groundwater [11,24]. This was in agreement with the values specific to carbonate minerals [33,71,72]. Bulk samples with a $^{234}\text{U}/^{238}\text{U}$ activity ratio lower than 1 are considered to result from the loss of ^{234}U because of the weathering process [25,72]. For the residual fraction of rock samples, the $^{234}\text{U}/^{238}\text{U}$ activity ratio at sites 7 and 8 (Lower Cretaceous limestone) is significantly lower ($\ll 1$) than the leached (carbonate) fraction of samples. This agrees with the U concentrations at these locations, where the non-carbonate fraction is also among the lowest ones. The dolomite sample (site 14) cannot be distinguished from the limestone samples in terms of the bulk U and Th concentrations, and the apparently large residual (non-carbonate) fraction is most probably the result of incomplete dissolution of dolomite during the leaching process.

The $\delta^{238}\text{U}$ values (Figure 5d, Table S1) reflect $^{238}\text{U}/^{235}\text{U}$ variations relative to the U isotope ratios of the CRM-112a reference material. As mentioned before, carbonate rock samples from the Ljubljana River catchment have highly variable U isotope compositions. Our study found $\delta^{238}\text{U}$ values of -1.0‰ – 1.0‰ ; these are similar to those of previous studies of carbonate materials [15], [72] and references therein. The negative or near-zero $\delta^{238}\text{U}$ values of leached rock samples agree with the $\delta^{238}\text{U}$ values reported in [72], where various carbonate reference materials were tested. Stirling et al. [28] reported that the light U isotope composition may be the result of preferential leaching of isotopically light lattice-bound ^{235}U over ^{238}U from the minerals by percolating waters. In our study, carbonate rocks contained only minor fractions of siliciclastic materials. Therefore, the $\delta^{238}\text{U}$ values are in a similar range for bulk and leached samples. In addition, the variability of the $\delta^{238}\text{U}$ values of bulk, leached, and residual fractions was the smallest in samples from sites 4, 5, and 6; furthermore, these samples showed the lowest Th concentration, which is related to the smaller fraction of detrital Th-bearing

minerals. The exception is sampling site 12, where the $\delta^{238}\text{U}$ value of the residual phase was extremely low (-3.46‰). In this sample, the bulk U concentration as well as U concentrations in the leached and residual fraction were the lowest, and the contribution of the calculated detrital phase in the sample was small. Therefore, the $\delta^{238}\text{U}$ value differed greatly from the other results. Some studies further reported that carbonates can be isotopically enriched in ^{238}U , thereby yielding more positive $\delta^{238}\text{U}$ values (up to 1.0‰) [15] and references therein, [28], which is also in agreement with our results.

4.3. U Isotopes in Water

Because the karstic aquifer of Ljubljana is very complex, the U isotopic composition of ground and surface water can show many different behaviors in such a system. The total U concentration in water (Figure 9a) was similar or lower compared to some other carbonate aquifers [12,73] and was highly variable in the headwater part of the aquifer (Cerkniško polje—sites 1 and 2, sinking stream Rak (site 5) and river Pivka (site 6)) and in the tributary at site 10 from Logaško polje. In springs, the emerging water was obviously homogenized; therefore, less variability was recorded. The average U concentrations showed a decreasing trend downstream; however, this trend was not consistent for all sites and all seasons.

The $^{234}\text{U}/^{238}\text{U}$ isotopic composition is supposed to change during water–rock interactions and is mostly influenced by the alpha recoil effect [20,33,74]. Riotte et al. [74] and Riotte and Charbaux [75] reported that $^{234}\text{U}/^{238}\text{U}$ activity ratios close to 1 are characteristic of groundwater in crystalline aquifers, whereas higher activity ratios (up to 3.6 [73]) are associated with carbonate host rocks and karst areas. However, the $^{234}\text{U}/^{238}\text{U}$ activity ratios in all cases were reported to be negatively correlated with the discharge. This may happen because of the capacity of the bedrock to store water in aquifers connected with surface waters for prolonged periods of time (from days to tens of thousands of years); therefore, the $^{234}\text{U}/^{238}\text{U}$ ratios vary depending on the residence time of the groundwater recharging the streams [74–76].

The differences in the $^{234}\text{U}/^{238}\text{U}$ ratio between water and bedrock are reported to be mostly dependent upon the rock type and its permeability [11]. Therefore, the deviation in the $^{234}\text{U}/^{238}\text{U}$ activity ratios in surface waters might indicate U disequilibrium as a potential tracer of the lithology of the aquifer and the contribution of waters with long residence time to the spring or surface water. However, in the case of the Ljubljana river catchment, no apparent correlation was seen between the lithology and the $^{234}\text{U}/^{238}\text{U}$ ratio of groundwater.

The $^{234}\text{U}/^{238}\text{U}$ activity ratios in water varied by $\sim 6\%$ – 20% between low- and high-flow conditions (Figure 9b). In contrast to other parameters (alkali and earth alkali metals, alkalinity including total dissolved U concentration), the $^{234}\text{U}/^{238}\text{U}$ activity ratio was strongly negatively correlated with the discharge at most sampling sites (Table 4, Figure S1); therefore, it seems to be the best available geochemical tracer of sources of water in the analyzed catchment.

The difference between $^{234}\text{U}/^{238}\text{U}$ activity ratios at high and low discharge was the largest in the headwater area of Cerkniško polje in the sinking streams at sites 1 (1.21–1.73) and 2 (1.36–1.58), followed by the hydraulically connected spring of the Rak stream (site 3) (1.22–1.54); at other sampling sites, the seasonal variability was generally around or under 0.2. The highest $^{234}\text{U}/^{238}\text{U}$ activity ratios were recorded for the headwater streams at sites 1 and 2 at low discharge (May 2018, August 2018). At high discharge, the $^{234}\text{U}/^{238}\text{U}$ ratio in the sinking stream at site 1 was similar to that in the spring at site 4, and it was recharged mainly from the Javorniki plateau [47]; this connection was already established in tracing experiments. In the sinking stream at site 2, the $^{234}\text{U}/^{238}\text{U}$ values were the highest not only at a low water level but also during high discharge (Figure 9b); therefore, this tributary can be traced in downstream springs under any hydrological conditions. The stream at site 2 drains the area north of Cerkniško polje that is composed of Triassic dolomite; this is the same lithological formation that is also abundant in the sub-catchment of the spring at site 14, which shows elevated $^{234}\text{U}/^{238}\text{U}$ ratios under high-flow conditions compared to nearby springs (sites 12 and 13). Despite the proximity to the springs at sites 12 and 13, the spring at site 14 obviously received more water from the central part

of the aquifer that is dominated by limestone [62]. The laboratory leaching experiment with pulverized rock samples showed that the "Hauptdolomite" did not have higher $^{234}\text{U}/^{238}\text{U}$ ratios than other rock samples; however, the physical conditions in the field, such as grain size, porosity type, and rock permeability can significantly affect the leaching of U from the bedrock. Therefore, the $^{234}\text{U}/^{238}\text{U}$ activity ratio should be used with caution when interpreting the weathering processes [75].

In the Rak creek, at high and medium discharge, the $^{234}\text{U}/^{238}\text{U}$ activity ratio in the sinking stream at site 5 matched the discharge-weighted sum of $^{234}\text{U}/^{238}\text{U}$ ratios of the two springs (sites 3 and 4) contributing to the stream; the same applied to the springs at sites 7 and 8, yielding the sinking stream Unica (site 9). At low water level, when the discharge of the streams is also affected by the evaporation, the balance does not match, that is, the calculated $^{234}\text{U}/^{238}\text{U}$ activities ratios of the sinking streams deviate from the measured ones beyond the analytical uncertainty. In the springs of the central part of the aquifer, the mixing of groundwater representing the sinking stream at site 6 (Pivka river), Cerkniško polje, and Javorniki plateau (springs at sites 3 and 4 and sink at site 5) could also be traced to the springs of Unica (site 7) and Malenščica (site 8). However, the $^{234}\text{U}/^{238}\text{U}$ activity balance could not be estimated because the $^{234}\text{U}/^{238}\text{U}$ activity ratio of the drip water in the aquifer was not estimated. Therefore, one important contributing source cannot be considered in the calculation.

The tributary at site 10 had lower $^{234}\text{U}/^{238}\text{U}$ activity ratios compared to those at the Unica river and resembled those of the Pivka river (site 6). However, it cannot be traced to the main Ljubljana springs because of its generally small discharge that represents only a minor or almost negligible contribution to the discharge of these springs. The $^{234}\text{U}/^{238}\text{U}$ activity ratios of the tributary at site 11 cannot be distinguished from the water deriving from the Javorniki plateau and the Unica River. The $^{234}\text{U}/^{238}\text{U}$ ratio could thus be used as a tracer of the origin of water only in the first, second, and third levels of the catchment but not for the main springs at the edge of the Ljubljana basin.

Schaffhauser et al. [77] implied that with increasing water transit time through the aquifer, the ^{234}U enrichment of the water would be increased because of a longer flow path and/or longer contact of water with the aquifer. This is consistent with the negative correlation between $^{234}\text{U}/^{238}\text{U}$ activity and discharge (Figure S1). In the case of the karst aquifer of the Ljubljana River catchment, the ^{234}U enrichment decreased downstream (Figure 9b, Table S1). However, no correlation was found between the mean transit time (MTT) of water (as estimated by Rusjan et al. [37]) and the $^{234}\text{U}/^{238}\text{U}$ ratios or U concentration in water. The MTT was the longest at ~9 months in the central part of the aquifer for the flow section Rak creek (site 5)—Malenščica spring (site 8); however, the range of $^{234}\text{U}/^{238}\text{U}$ ratios in the water at these sites was rather small and the values were lower compared to those of the headwater tributaries. Along the entire downstream flow direction for sites (7, 8) → 9 → (12, 13, and 14), the range of $^{234}\text{U}/^{238}\text{U}$ ratios was rather similar whereas the MTT decreased from ~9 to 6–7 months. This also implies good homogenization of water, which was previously confirmed from the stable isotopes of water [37]. By contrast, the poor correlation between the transit time and the $^{234}\text{U}/^{238}\text{U}$ activity ratio can be explained by the fact that the recoil effect can be hampered because the redox condition was not reducing enough to allow the formation of reduced U(IV), which facilitates the emission of ^{234}U into the solution [74–76].

The river Pivka (site 6) had the shortest transit time (0.34 year) and a relatively large influence of surface discharge because of a relatively long surface flow path, and it exhibited the narrowest range of $^{234}\text{U}/^{238}\text{U}$ activity ratio values (1.1–1.2 for discharge varying across several orders of magnitude from 0.02 to 15.32 m³s⁻¹). In contrast to some other geochemical tracers (e.g., Na⁺, K⁺, Mg²⁺), its $^{234}\text{U}/^{238}\text{U}$ activity ratio could not be traced downstream toward the spring at site 7 at any time despite the short distance between sites 6 and 7 and the proven hydraulic connection, which is only occasionally interrupted [37,47]. The narrow range of $^{234}\text{U}/^{238}\text{U}$ values can be attributed to the different lithology of the Pivka sub-catchment, which consists of limestone, flysch, and stream deposits at the Pivka basin, in contrast to other sub-catchments, which are dominated by carbonate rocks. The mobilization of U from siliclastic rocks is reported to be much slower compared to the rapid dissolution of carbonate in CO₂-rich karst water and to be less dependent upon the discharge; therefore, the lower $^{234}\text{U}/^{238}\text{U}$

values in the stream at site 6 are not surprising [11,20,78,79]. This could also be explained as an effect of the partial oxidation of U(IV) bound to silicate or oxide minerals during weathering, where the alpha recoil effect cannot play such a role [11,20].

$\delta^{238}\text{U}$ in water varied greatly and far exceeded the range of published $\delta^{238}\text{U}$ values for river water (on average, -0.34‰ [9,31,80]). For the isotope composition of dissolved U in rivers, the authors hypothesized a smaller range of values than in the source rocks of the continental crust [9,10,28,31,80]. Weyer et al. [10] explained this by the relatively quantitative mobilization of ^{235}U and ^{238}U during weathering and the conservative behavior of U during transport in rivers [10]. U isotope fractionation of up to 1‰ has thus far been reported only for bacterial reduction processes or uptake by biota [15,81,82]. Therefore, the expected isotope fractionation of U during the dissolution of carbonate rocks should be small, and $\delta^{238}\text{U}$ values in spring and river water should resemble those of the bedrock.

Apart from the sinking stream at site 1, lower $\delta^{238}\text{U}$ values were associated with low discharge and higher ones, with large discharge; at medium discharge, the measured values scattered rather randomly. The spatial pattern is generally supposed to be consistent with that of the $^{234}\text{U}/^{238}\text{U}$ activity ratio; however, this was obviously not the case (Figure 9c). The relatively large variability of $\delta^{238}\text{U}$ values in the carbonate and non-carbonate fraction of bedrock (Figure 5d) suggests that the partial dissolution of different U pools in the bedrock and the partially variable hydraulic connections at low, medium, and high discharge could be a reason for this scattered $\delta^{238}\text{U}$ pattern in the spring and stream water in different seasons. Although the $\delta^{238}\text{U}$ values measured in different fractions of bedrock cannot be taken as respective end members for certain locations as the U budget in the water was accumulated before the water reached that site, their variability could explain differences in $\delta^{238}\text{U}$ values under different flow conditions generated by U isotope fractionation during incomplete dissolution and incongruent weathering of U [80]. Nevertheless, the inconsistency of the spatial and temporal patterns of $\delta^{238}\text{U}$ values shows that in such a complex karst aquifer, the $\delta^{238}\text{U}$ values of water may be influenced by various processes which mask the U fingerprint of the bedrock in the source area.

5. Conclusions

This study showed that classical geochemical tracers of the origin of water (physicochemical parameters, elemental ratios, and alkalinity) in the Ljubljana River catchment reflect the chemical composition of bedrock and provides some information about the groundwater flow and mixing of water in different parts of the aquifer. The variability of $\text{Mg}^{2+}/\text{Ca}^{2+}$ ratios, Na^+ and K^+ concentrations reflect the variable contributions of weathering of carbonate (limestone and dolomite) and silicate bedrock to the total dissolved loads in the spring and river water, and can explain the groundwater mixing in particular in the upper part of the aquifer. However, the complexity of the karst aquifer, which expands with the increasing water level, results in rather peculiar behavior of the physicochemical parameters and elemental composition of water, which show no straightforward relation to the discharge. Therefore, the interpretation of groundwater flow and mixing in the catchment based on classical geochemical tracers only remains rather uncertain.

U isotopes were used as a non-traditional isotope system to support traditional geochemical and isotopic tracers in an investigation of the origin and flow paths of groundwater. The variability of U concentrations and $^{234}\text{U}/^{238}\text{U}$ activity ratios in water was the largest in tributaries that drain areas containing siliciclastic rocks and where dolomite was equally or more abundant than limestone. The $^{234}\text{U}/^{238}\text{U}$ activity ratio of water was strongly correlated with the discharge, similar to the contribution of silicate weathering to the groundwater mineralization. The $^{234}\text{U}/^{238}\text{U}$ activity ratio was shown to be a useful tracer of groundwater flow and was complementary to general hydrochemical and isotopic parameters [37,42,47] mainly in the headwater region and central part of the studied aquifer. By contrast, in the lower area, the homogenization of the water made the identification of water sources impossible. Similar limitations for the interpretation of flow directions and mixing of water were also encountered previously when using other geochemical tracers. The $\delta^{238}\text{U}$ values varied in an unexpectedly large range, which cannot be explained within the scope of this study.

Uranium isotopes, in particular the $^{234}\text{U}/^{238}\text{U}$ activity ratio, showed considerable potential as a geochemical tracer of groundwater in karst aquifers, but in the present study, they could not outperform the combination of classical geochemical tracers or dyes used in previous studies. Not many studies have been performed so far, but the $^{234}\text{U}/^{238}\text{U}$ activity ratio showed by far the best correlation with the discharge of all analyzed tracers. Therefore, they shall remain in the focus as a potential tool in hydrogeological studies in spite of the relatively high costs of U isotope analyses.

The investigated catchment is evidently very complex. To better elucidate the origin of solutes, changing flow paths, and groundwater mixing under changing hydrological conditions, more detailed chemical and isotopic fingerprinting of the bedrock and observation of groundwater chemical and isotopic compositions under different flow conditions over a longer period remains necessary. Moreover, new non-traditional isotope tracers should be tested in the future.

Supplementary Materials: The following are available online at <http://www.mdpi.com/2073-4441/12/7/2064/s1>. Table S1: The physico-chemical parameters, major ion concentrations, and U isotopic compositions related to the sampled water and carbonate rocks for each sampling period, Figure S1: The $^{234}\text{U}/^{238}\text{U}$ activity ratio with water discharge for each individual location.

Author Contributions: Conceptualization, L.R., S.L., and M.P.; methodology and analyses, L.R., M.Š., T.Z., T.K., and B.H.; field work: T.K., L.R., M.P., S.R., and S.L.; writing—original draft preparation, L.R.; writing—review and editing, S.L., M.Š., T.K., T.Z., M.P., and S.R.; visualization, L.R., S.L., and M.P.; supervision, M.Š.; funding acquisition, S.L. and S.R. All authors have read and agreed to the published version of the manuscript.

Funding: This research was funded by the Slovenian Research Agency (Research programmes P1-0143 and P2-0075-2, Research projects J1-9179 and J2-7322, and the Young Researcher's program).

Acknowledgments: The authors thank Stojan Žigon for assisting with the laboratory and field work.

Conflicts of Interest: The authors declare no conflict of interest. The funders had no role in the design of the study; in the collection, analyses, or interpretation of data; in the writing of the manuscript, or in the decision to publish the results.

References

- Chen, Z.; Auler, A.S.; Bakalowicz, M.; Drew, D.; Griger, E.; Hartmann, J.; Jiang, G.; Moosdorf, N.; Richts, A.; Stevanovic, Z.; et al. The World Karst Aquifer Mapping project: Concept, mapping procedure and map of Europe. *Hydrogeol. J.* **2017**, *25*, 771–785. [[CrossRef](#)]
- Stevanović, Z. Global distribution and use of water from karst aquifers. *Geol. Soc. Lond. Spec. Publ.* **2018**, *466*, 217–236. [[CrossRef](#)]
- Hartmann, A.; Goldscheider, N.; Wagener, T.; Lange, J.; Weiler, M. Karst water resources in a changing world: Review of hydrological modeling approaches. *Rev. Geophys.* **2014**, *52*, 218–242. [[CrossRef](#)]
- White, W.B. Karst hydrology: Recent developments and open questions. *Eng. Geol.* **2002**, *65*, 85–105. [[CrossRef](#)]
- Ravbar, N.; Petrič, M.; Kogovšek, J. The characteristics of groundwater flow in karst aquifers during long lasting low flow conditions, example from SW Slovenia. In *Advances in Research in Karst Media. Environmental Earth Sciences*; Andreo, B., Carrasco, F., Durán, J., LaMoreaux, J., Eds.; Springer: Berlin/Heidelberg, Germany, 2010; pp. 131–136. [[CrossRef](#)]
- Sappa, G.; Vitale, S.; Ferranti, F. Identifying karst aquifer recharge areas using environmental isotopes: A case study in Central Italy. *Geosciences* **2018**, *8*, 351. [[CrossRef](#)]
- Calligaris, C.; Mezga, K.; Slejko, F.; Urbanc, J.; Zini, L. Groundwater characterization by means of conservative ($\delta^{18}\text{O}$ and $\delta^2\text{H}$) and non-conservative ($^{87}\text{Sr}/^{86}\text{Sr}$) isotopic values: The classical karst region aquifer case (Italy–Slovenia). *Geosciences* **2018**, *8*, 321. [[CrossRef](#)]
- Porcelli, D.; Swarzenski, P.W. The behavior of U- and Th-series nuclides in the estuarine environment. *Rev. Mineral. Geochem.* **2003**, *52*, 577–606. [[CrossRef](#)]
- Tissot, F.L.H.; Dauphas, N. Uranium isotopic compositions of the crust and ocean: Age corrections, U budget and global extent of modern anoxia. *Geochim. Cosmochim. Acta* **2015**, *167*, 113–143. [[CrossRef](#)]
- Weyer, S.; Anbar, A.D.; Gerdes, A.; Gordon, G.W.; Algeo, T.J.; Boyle, E.A. Natural fractionation of $^{238}\text{U}/^{235}\text{U}$. *Geochim. Cosmochim. Acta* **2008**, *72*, 345–359. [[CrossRef](#)]

11. Chabaux, F.; Riotte, J.; Dequincey, O. U-Th-Ra fractionation during weathering and river transport. *Rev. Mineral. Geochem.* **2003**, *52*, 533–576. [\[CrossRef\]](#)
12. Chen, Q.; Liu, S.; He, H.; Tang, J.; Zhao, J.; Feng, Y.; Yang, X.; Zhou, H. Seasonal variations of uranium in karst waters from Northeastern Sichuan, Central China and controlling mechanisms. *Geochem. Int.* **2020**, *58*, 103–112. [\[CrossRef\]](#)
13. Cho, B.W.; Choo, C.O. Geochemical behavior of uranium and radon in groundwater of Jurassic granite area, Icheon, Middle Korea. *Water* **2019**, *11*, 1278. [\[CrossRef\]](#)
14. Siebert, C.; Möller, P.; Magri, F.; Shalev, E.; Rosenthal, E.; Al-Raggad, M.; Rödiger, T. Applying rare earth elements, uranium, and $^{87}\text{Sr}/^{86}\text{Sr}$ to disentangle structurally forced confluence of regional groundwater resources: The case of the Lower Yarmouk Gorge. *Geofluids* **2019**, *2019*, 1–21. [\[CrossRef\]](#)
15. Andersen, M.B.; Stirling, C.H.; Weyer, S. Uranium isotope fractionation. *Rev. Mineral. Geochem.* **2017**, *82*, 799–850. [\[CrossRef\]](#)
16. Bourdon, B.; Turner, S.; Henderson, G.M.; Lundstrom, C.C. Introduction to U-series geochemistry. *Rev. Mineral. Geochem.* **2003**, *52*, 1–21. [\[CrossRef\]](#)
17. Liesch, T.; Hinrichsen, S.; Goldscheider, N. Uranium in groundwater — Fertilizers versus geogenic sources. *Sci. Total Environ.* **2015**, *536*, 981–995. [\[CrossRef\]](#)
18. Bischoff, J.L.; Fitzpatrick, J.A. U-series dating of impure carbonates: An isochron technique using total-sample dissolution. *Geochim. Cosmochim. Acta* **1991**, *55*, 543–554. [\[CrossRef\]](#)
19. Garnett, E.R.; Gilmour, M.A.; Rowe, P.J.; Andrews, J.E.; Preece, R.C. $^{230}\text{Th}/^{234}\text{U}$ dating of Holocene tufas: Possibilities and problems. *Quat. Sci. Rev.* **2004**, *23*, 947–958. [\[CrossRef\]](#)
20. Chabaux, F.; Bourdon, B.; Riotte, J. Chapter 3 U-Series geochemistry in weathering profiles, river waters and lakes. *Radioact. Environ.* **2008**, *13*, 49–104. [\[CrossRef\]](#)
21. Chen, X.; Romaniello, S.J.; Herrmann, A.D.; Wasylenki, L.E.; Anbar, A.D. Uranium isotope fractionation during coprecipitation with aragonite and calcite. *Geochim. Cosmochim. Acta* **2016**, *188*, 189–207. [\[CrossRef\]](#)
22. Kopylova, Y.; Guseva, N.; Shestakova, A.; Khvaschevskaya, A.; Arakchaa, K. Uranium and thorium behavior in groundwater of the natural spa area “Choygan mineral water” (East Tuva). *Iop Conf. Ser. Earth Environ. Sci.* **2015**, *27*, 012034. [\[CrossRef\]](#)
23. Fleischer, R.L. Alpha-recoil damage and solution effects in minerals: Uranium isotopic disequilibrium and radon release. *Geochim. Cosmochim. Acta* **1982**, *46*, 2191–2201. [\[CrossRef\]](#)
24. Andersen, M.B.; Stirling, C.H.; Porcelli, D.; Halliday, A.N.; Andersson, P.S.; Baskaran, M. The tracing of riverine U in Arctic seawater with very precise $^{234}\text{U}/^{238}\text{U}$ measurements. *Earth Planet. Sci. Lett.* **2007**, *259*, 171–185. [\[CrossRef\]](#)
25. Andersen, M.B.; Erel, Y.; Bourdon, B. Experimental evidence for ^{234}U – ^{238}U fractionation during granite weathering with implications for $^{234}\text{U}/^{238}\text{U}$ in natural waters. *Geochim. Cosmochim. Acta* **2009**, *73*, 4124–4141. [\[CrossRef\]](#)
26. Uvarova, Y.A.; Kyser, T.K.; Geagea, M.L.; Chipley, D. Variations in the uranium isotopic compositions of uranium ores from different types of uranium deposits. *Geochim. Cosmochim. Acta* **2014**, *146*, 1–17. [\[CrossRef\]](#)
27. Suksi, J.; Rasilainen, K.; Pitkänen, P. Variations in $^{234}\text{U}/^{238}\text{U}$ activity ratios in groundwater—A key to flow system characterisation? *Phys. Chem. Earthparts A/B/C* **2006**, *31*, 556–571. [\[CrossRef\]](#)
28. Stirling, C.H.; Andersen, M.B.; Potter, E.-K.; Halliday, A.N. Low-temperature isotopic fractionation of uranium. *Earth Planet. Sci. Lett.* **2007**, *264*, 208–225. [\[CrossRef\]](#)
29. Goldmann, A.; Brennecke, G.; Noordmann, J.; Weyer, S.; Wadhwa, M. The uranium isotopic composition of the Earth and the solar system. *Geochim. Cosmochim. Acta* **2015**, *148*, 145–158. [\[CrossRef\]](#)
30. Schauble, E.A. Role of nuclear volume in driving equilibrium stable isotope fractionation of mercury, thallium, and other very heavy elements. *Geochim. Cosmochim. Acta* **2007**, *71*, 2170–2189. [\[CrossRef\]](#)
31. Andersen, M.B.; Vance, D.; Morford, J.L.; Bura-Nakić, E.; Breitenbach, S.F.M.; Och, L. Closing in on the marine $^{238}\text{U}/^{235}\text{U}$ budget. *Chem. Geol.* **2016**, *420*, 11–22. [\[CrossRef\]](#)
32. Huckle, D.; Ma, L.; McIntosh, J.; Vázquez-Ortega, A.; Rasmussen, C.; Chorover, J. U-series isotopic signatures of soils and headwater streams in a semi-arid complex volcanic terrain. *Chem. Geol.* **2016**, *445*, 68–83. [\[CrossRef\]](#)
33. Bourdon, B.; Bureau, S.; Andersen, M.B.; Pili, E.; Hubert, A. Weathering rates from top to bottom in a carbonate environment. *Chem. Geol.* **2009**, *258*, 275–287. [\[CrossRef\]](#)

34. Palmer, M.R.; Edmond, J.M. Uranium in river water. *Geochim. Cosmochim. Acta* **1993**, *57*, 4947–4955. [[CrossRef](#)]
35. Goldstein, S.J.; Stirling, C.H. Techniques for measuring uranium-series nuclides: 1992–2002. *Rev. Mineral. Geochem.* **2003**, *52*, 23–57. [[CrossRef](#)]
36. Wieser, M.E.; Schwieters, J.B. The development of multiple collector mass spectrometry for isotope ratio measurements. *Int. J. Mass Spectrom.* **2005**, *242*, 97–115. [[CrossRef](#)]
37. Rusjan, S.; Sapač, K.; Petrič, M.; Lojen, S.; Bezak, N. Identifying the hydrological behavior of a complex karst system using stable isotopes. *J. Hydrol.* **2019**, *577*, 123956. [[CrossRef](#)]
38. Blatnik, M.; Gabrovšek, F.; Kogovšek, B.; Mayaud, C.; Petrič, M.; Ravbar, N. *Karst Hydrogeology—Research Trends and Applications: Abstracts & Guide Book*; Blatnik, M., Gabrovšek, F., Kogovšek, B., Mayaud, C., Petrič, M., Ravbar, N., Eds.; ZRC Publishing: Ljubljana, Slovenia, 2019.
39. Blatnik, M. Groundwater Distribution in the Recharge Area of Ljubljana Springs. PhD Thesis, University of Nova Gorica, Nova Gorica, Slovenia, 2019.
40. Pleničar, M. Postojna. In *Osnovna geološka karta SFRJ 1: 100.000, list Postojna*; (Basic geological map of SFR Yugoslavia 1:100 000, page Postojna); Federal Geological Survey: Belgrade, Serbia, 1970.
41. Pleničar, M. Tolmač lista Postojna L 33-77. In *Osnovna geološka karta SFRJ 1 : 100 000*; (Commentary to the page Postojna L 33-77, Basic geological map of SFR Yugoslavia 1:100 000); Federal Geological Survey: Belgrade, Serbia, 1967; Volume 62.
42. Ravbar, N.; Barberá, J.A.; Petrič, M.; Kogovšek, J.; Andro, B. The study of hydrodynamic behaviour of a complex karst system under low-flow conditions using natural and artificial tracers (the catchment of the Unica River, SW Slovenia). *Environ. Earth Sci.* **2012**, *65*, 2259–2272. [[CrossRef](#)]
43. Frantar, P. *Water Balance of Slovenia 1971–2000*; Frantar, P., Ed.; Ministry for Environment and Spatial Planning—Environmental Agency of the Republic of Slovenia: Ljubljana, Slovenia, 2008.
44. Petric, M. Case Study: Chapter 10.3—Case study: Characterization, exploitation, and protection of the Malenščica karst spring, Slovenia. In *Groundwater Hydrology of Springs*; Kresic, N., Stefanovic, Z., Eds.; Elsevier: Oxford, UK, 2010; pp. 428–441. [[CrossRef](#)]
45. Gabrovšek, F.; Turk, J. Observations of stage and temperature dynamics in the epiphreatic caves within the catchment area of the Ljubljana river (Slovenia). *Geol. Croat.* **2010**, *63*, 187–193. [[CrossRef](#)]
46. Sezen, C.; Bezak, N.; Šraj, M. Hydrological modelling of the karst Ljubljana River catchment using lumped conceptual model. *Acta Hydrotech.* **2018**, *87*–100. [[CrossRef](#)]
47. Kogovšek, J. Fizikalno-kemične značilnosti voda v zaledju Malenščice (Slovenija) (Physico-chemical properties of waters in the Malenščica recharge area (Slovenia), in Slovene with English abstract). *Acta Carsologica* **2004**, *33*, 143–158. [[CrossRef](#)]
48. Blatnik, M.; Mayaud, C.; Gabrovšek, F. Groundwater dynamics between Planinsko Polje and springs of the Ljubljana River, Slovenia. *Acta Carsologica* **2019**, *48*. [[CrossRef](#)]
49. Gieskes, J.M. The alkalinity-total carbon dioxide system in seawater. In *Marine Chemistry of The Sea*; Goldberg, E.D., Ed.; John Wiley and Sons: New York, NY, USA, 1974; Volume 5, pp. 123–151.
50. Parkhurst, D.L.; Appelo, C.A.J. User's guide to PHREEQC (version 2)—A computer 25 program for speciation, batch-reaction, one-dimensional transport, and inverse geochemical calculations. *Water-Resour. Investig. Rep.* **1999**. [[CrossRef](#)]
51. Štok, M.; Smodiš, B. Fractionation of natural radionuclides in soils from the vicinity of a former uranium mine Žirovski vrh, Slovenia. *J. Environ. Radioact.* **2010**, *101*, 22–28. [[CrossRef](#)]
52. Trdin, M.; Nečemer, M.; Benedik, L. Fast decomposition procedure of solid samples by lithium borates fusion employing salicylic acid. *Anal. Chem.* **2017**, *89*, 3169–3176. [[CrossRef](#)] [[PubMed](#)]
53. Benedik, L.; Rován, L.; Klemenčič, H.; Gantar, I.; Prosen, H. Natural radioactivity in tap waters from the private wells in the surroundings of the former Žirovski Vrh uranium mine and the age-dependent dose assessment. *Environ. Sci. Pollut. Res.* **2015**, *22*, 12062–12072. [[CrossRef](#)] [[PubMed](#)]
54. Tanimizu, M.; Sugiyama, N.; Ponzevera, E.; Bayon, G. Determination of ultra-low $^{236}\text{U}/^{238}\text{U}$ isotope ratios by tandem quadrupole ICP-MS/MS. *J. Anal. At. Spectrom.* **2013**, *28*, 1372. [[CrossRef](#)]
55. Rován, L.; Štok, M. Optimization of the sample preparation and measurement protocol for the analysis of uranium isotopes by MC-ICP-MS without spike addition. *J. Anal. At. Spectrom.* **2019**, *34*, 1882–1891. [[CrossRef](#)]

56. Standards for Nuclear Safety Security and Safeguards Unit. *Nuclear Certified Reference Materials 2019*; Directorate G – Nuclear Safety and Security, European Commission, Directorate General, Joint Research Centre Geel: Geel, Belgium, 2019; Volume 4.
57. Cheng, H.; Lawrence Edwards, R.; Shen, C.C.; Polyak, V.J.; Asmerom, Y.; Woodhead, J.; Hellstrom, J.; Wang, Y.; Kong, X.; Spötl, C.; et al. Improvements in ^{230}Th dating, ^{230}Th and ^{234}U half-life values, and U–Th isotopic measurements by multi-collector inductively coupled plasma mass spectrometry. *Earth Planet. Sci. Lett.* **2013**, *371–372*, 82–91. [[CrossRef](#)]
58. Szramek, K.; Walter, L.M.; Kanduč, T.; Ogrinc, N. Dolomite versus calcite weathering in hydrogeochemically diverse watersheds established on bedded carbonates (Sava and Soča Rivers, Slovenia). *Aquat. Geochem.* **2011**, *17*, 357–396. [[CrossRef](#)]
59. Fairchild, I.J.; Borsato, A.; Tooth, A.F.; Frisia, S.; Hawkesworth, C.J.; Huang, Y.; McDermott, F.; Spiro, B. Controls on trace element (Sr–Mg) compositions of carbonate cave waters: Implications for speleothem climatic records. *Chem. Geol.* **2000**, *166*, 255–269. [[CrossRef](#)]
60. Huang, Y.; Fairchild, I.J. Partitioning of Sr^{2+} and Mg^{2+} into calcite under karst-analogue experimental conditions. *Geochim. Cosmochim. Acta* **2001**, *65*, 47–62. [[CrossRef](#)]
61. Saunders, P.; Rogerson, M.; Wadhawan, J.D.; Greenway, G.; Pedley, H.M. Mg/Ca ratios in freshwater microbial carbonates: Thermodynamic, kinetic and vital effects. *Geochim. Cosmochim. Acta* **2014**, *147*, 107–118. [[CrossRef](#)]
62. Bauer, F.; Gospodarič, R.; Habič, P. *Underground Water Tracing: Investigations in Slovenia 1972–1975*; Institute for Karst Research SAZU: Postojna, Slovenia, 1976.
63. Kanduč, T.; Szramek, K.; Ogrinc, N.; Walter, L.M. Origin and cycling of riverine inorganic carbon in the Sava River watershed (Slovenia) inferred from major solutes and stable carbon isotopes. *Biogeochemistry* **2007**, *86*, 137–154. [[CrossRef](#)]
64. Ravbar, N.; Engelhardt, I.; Goldscheider, N. Anomalous behaviour of specific electrical conductivity at a karst spring induced by variable catchment boundaries: The case of the Podstenjšek spring, Slovenia. *Hydrol. Process.* **2011**, *25*, 2130–2140. [[CrossRef](#)]
65. Bell, K.G. *Uranium in Carbonate Rocks*; USGS, Geological Survey professional paper 474-A; U.S. Geological Survey: Washington, DC, USA, 1963; p. 29.
66. Romaniello, S.J.; Herrmann, A.D.; Anbar, A.D. Uranium concentrations and $^{238}\text{U}/^{235}\text{U}$ isotope ratios in modern carbonates from the Bahamas: Assessing a novel paleoredox proxy. *Chem. Geol.* **2013**, *362*, 305–316. [[CrossRef](#)]
67. Herrmann, A.D.; Gordon, G.W.; Anbar, A.D. Uranium isotope variations in a dolomitized Jurassic carbonate platform (Tithonian; Franconian Alb, Southern Germany). *Chem. Geol.* **2018**, *497*, 41–53. [[CrossRef](#)]
68. Lund, K.; Fogler, H.S.; McCune, C.C. Acidization—I. The dissolution of dolomite in hydrochloric acid. *Chem. Eng. Sci.* **1973**, *28*, 691–700. [[CrossRef](#)]
69. Kelepertsis, A.E. The geochemistry of uranium and thorium in some Lower Carboniferous sedimentary rocks (Great Britain). *Chem. Geol.* **1981**, *34*, 275–288. [[CrossRef](#)]
70. Zhang, W.; Guan, P.; Jian, X.; Feng, F.; Zou, C. *In situ* geochemistry of Lower Paleozoic dolomites in the northwestern Tarim basin: Implications for the nature, origin, and evolution of diagenetic fluids. *Geochem. Geophys. Geosyst.* **2014**, *15*, 2744–2764. [[CrossRef](#)]
71. Teichert, B.M.A.; Eisenhauer, A.; Bohrmann, G.; Haase-Schramm, A.; Bock, B.; Linke, P. U/Th systematics and ages of authigenic carbonates from Hydrate Ridge, Cascadia Margin: Recorders of fluid flow variations. *Geochim. Cosmochim. Acta* **2003**, *67*, 3845–3857. [[CrossRef](#)]
72. Wang, R.-M.; You, C.-F. Precise determination of U isotopic compositions in low concentration carbonate samples by MC-ICP-MS. *Talanta* **2013**, *107*, 67–73. [[CrossRef](#)]
73. Guerrero, J.L.; Vallejos, Á.; Cerón, J.C.; Sánchez-Martos, F.; Pulido-Bosch, A.; Bolívar, J.P. U-isotopes and ^{226}Ra as tracers of hydrogeochemical processes in carbonated karst aquifers from arid areas. *J. Environ. Radioact.* **2016**, *158–159*, 9–20. [[CrossRef](#)] [[PubMed](#)]
74. Riotte, J.; Chabaux, F.; Benedetti, M.; Dia, A.; Gérard, M.; Boulègue, J.; Etamé, J. Uranium colloidal transport and origin of the ^{234}U – ^{238}U fractionation in surface waters: New insights from Mount Cameroon. *Chem. Geol.* **2003**, *202*, 365–381. [[CrossRef](#)]
75. Riotte, J.; Chabaux, F. ($^{234}\text{U}/^{238}\text{U}$) activity ratios in freshwaters as tracers of hydrological processes: The Strengbach watershed (Vosges, France). *Geochim. Cosmochim. Acta* **1999**, *63*, 1263–1275. [[CrossRef](#)]

76. Durand, S.; Chabaux, F.; Rihs, S.; Düringer, P.; Elsass, P. U isotope ratios as tracers of groundwater inputs into surface waters: Example of the Upper Rhine hydrosystem. *Chem. Geol.* **2005**, *220*, 1–19. [[CrossRef](#)]
77. Schaffhauser, T.; Chabaux, F.; Ambroise, B.; Lucas, Y.; Stille, P.; Reuschlé, T.; Perrone, T.; Fritz, B. Geochemical and isotopic (U, Sr) tracing of water pathways in the granitic Ringelbach catchment (Vosges Mountains, France). *Chem. Geol.* **2014**, *374–375*, 117–127. [[CrossRef](#)]
78. Grzymko, T.J.; Marcantonio, F.; McKee, B.A.; Mike Stewart, C. Temporal variability of uranium concentrations and $^{234}\text{U}/^{238}\text{U}$ activity ratios in the Mississippi river and its tributaries. *Chem. Geol.* **2007**, *243*, 344–356. [[CrossRef](#)]
79. Amiotte Suchet, P.; Probst, J.-L.; Ludwig, W. Worldwide distribution of continental rock lithology: Implications for the atmospheric/soil CO_2 uptake by continental weathering and alkalinity river transport to the oceans. *Glob. Biogeochem. Cycles* **2003**, *17*, 1038. [[CrossRef](#)]
80. Noordmann, J.; Weyer, S.; Georg, R.B.; Jöns, S.; Sharma, M. $^{238}\text{U}/^{235}\text{U}$ isotope ratios of crustal material, rivers and products of hydrothermal alteration: New insights on the oceanic U isotope mass balance. *Isot. Environ. Health Stud.* **2016**, *52*, 141–163. [[CrossRef](#)]
81. Stylo, M.; Neubert, N.; Wang, Y.; Monga, N.; Romaniello, S.J.; Weyer, S.; Bernier-Latmani, R. Uranium isotopes fingerprint biotic reduction. *Proc. Natl. Acad. Sci. USA* **2015**, *112*, 5619–5624. [[CrossRef](#)]
82. Chen, X.; Zheng, W.; Anbar, A.D. Uranium isotope fractionation ($^{238}\text{U}/^{235}\text{U}$) during U(VI) uptake by freshwater plankton. *Environ. Sci. Technol.* **2020**, *54*, 2744–2752. [[CrossRef](#)] [[PubMed](#)]



© 2020 by the authors. Licensee MDPI, Basel, Switzerland. This article is an open access article distributed under the terms and conditions of the Creative Commons Attribution (CC BY) license (<http://creativecommons.org/licenses/by/4.0/>).



Supplementary Material

Comparison of Uranium Isotopes and Classical Geochemical Tracers in Karst Aquifer of Ljubljana River catchment (Slovenia)

Leja Rovan ^{1,2}, Sonja Lojen ^{1,3}, Tea Zuliani ^{1,2}, Tjaša Kanduč ¹, Metka Petrič ⁴, Barbara Horvat ⁵, Simon Rusjan ⁶ and Marko Štok ^{1,2,*}

¹ Department of Environmental Sciences, Jožef Stefan Institute, Jamova 39, SI-1000 Ljubljana, Slovenia; leja.rovan@ijs.si (L.R.); sonja.lojen@ijs.si (S.L.); tea.zuliani@ijs.si (T.Z.); tjasa.kanduc@ijs.si (T.K.)

² Jožef Stefan International Postgraduate School, Jamova 39, SI-1000 Ljubljana, Slovenia

³ School of Environmental Sciences, University of Nova Gorica, Glavni trg 8, SI-5271 Vipava, Slovenia

⁴ Karst Research Institute, Slovenian Academy of Sciences and Arts, Titov trg 2, SI-6230 Postojna, Slovenia; petric@zrc-sazu.si

⁵ Slovenian National Building and Civil Engineering Institute, Dimičeva 12, SI-1000 Ljubljana, Slovenia; barbara.horvat@zag.si

⁶ Faculty of Civil and Geodetic Engineering, University of Ljubljana, Jamova 2, SI-1000 Ljubljana, Slovenia; simon.rusjan@fgg.uni-lj.si

* Correspondence: marko.strok@ijs.si; Tel.: +0038615885243

Received: 17 June 2020; Accepted: 17 July 2020; Published: 21 July 2020



Table S1: The physico-chemical parameters, major ion concentrations, and U isotopic compositions related to the sampled water and carbonate rocks for each sampling period.

October 2017																				
Location	Name of the spring/stream	Discharge [m ³ /s]	T [°C]	pH	Conductivity [µS/cm]	Total alkalinity [mmol/L]	HCO ₃ ⁻ [mmol/L]**	U [ng/mL]	²³⁵ U/ ²³⁸ U absolute value (k=2)	²³⁵ U/ ²³⁸ U absolute value (k=2)	²³⁵ U/ ²³⁸ U activity ratio	$\delta^{235}\text{U}_{\text{VSMOW}}$ [‰]	$\delta^{235}\text{U}_{\text{CRM}}$ [‰]	Mg ²⁺ [mmol/L]	Cs ⁺ [mmol/L]	Mg/Ca	Na ⁺ [mmol/L]	K ⁺ [mmol/L]	Slcase ***	
*1	Stržen																			
*2	Cerfonska																			
3	Rak - Mali most	1.44	9.3	7.89	420	4.06	3.92	0.52	7.59E-05 ± 1.34E-07	1.3833 ± 0.13	1.38	4.57	3.46	1.06	1.65	0.64	0.13	0.04	0.41	
4	Rak - Kollč	2.92	10.3	7.77	383	3.69	3.58	0.48	7.13E-05 ± 1.26E-07	137.73 ± 0.67	1.30	0.24	-0.86	0.49	2.05	0.24	0.08	0.03	0.37	
5	Rak - Veliki most	4.36	10.1	7.75	387	3.83	3.72	0.56	7.11E-05 ± 1.19E-07	138.26 ± 0.28	1.29	4.10	2.99	0.53	1.92	0.29	0.08	0.03	0.34	
6	Pivka	1.95	9.0	7.63	341	2.73	2.67	0.38	6.49E-05 ± 9.64E-08	138.13 ± 0.05	1.18	3.18	2.07	0.16	1.82	0.09	0.47	0.13	0.05	
7	Unica - Flamina cave	12.12	10.3	7.61	396	3.68	3.59	0.42	6.73E-05 ± 1.42E-07	137.87 ± 0.14	1.22	1.24	0.14	0.36	2.14	0.17	0.22	0.07	0.23	
8	Malenska	6.71	10.8	7.57	404	3.84	3.74	0.44	7.11E-05 ± 1.50E-07	137.90 ± 0.08	1.29	1.44	0.34	0.48	2.04	0.23	0.10	0.03	0.20	
9	Unica - Hasberg	18.83	10.8	7.69	405	3.90	3.79	0.45	6.99E-05 ± 1.65E-07	137.91 ± 0.11	1.27	1.56	0.46	0.46	2.12	0.22	0.12	0.04	0.34	
10	Hotenika	**NA	8.2	8.26	439	4.19	3.97	0.39	6.42E-05 ± 1.33E-07	138.00 ± 0.18	1.17	2.22	1.12	1.39	1.54	0.90	0.06	0.03	0.73	
11	Logošica	0.11	9.3	8.17	441	4.11	3.89	0.46	7.01E-05 ± 1.67E-07	137.89 ± 0.24	1.27	1.43	0.33	1.39	1.65	0.84	0.10	0.05	0.75	
12	Ljubljanka - Mečnik	15.70	11.5	7.54	400	3.76	3.65	0.41	7.03E-05 ± 1.35E-07	137.82 ± 0.05	1.28	0.90	4.21	0.73	2.43	0.31	0.17	0.05	0.23	
13	Ljubljanka - Koroje	15.70	11.6	7.50	419	3.82	3.72	0.45	6.93E-05 ± 1.34E-07	137.83 ± 0.10	1.26	0.97	4.03	0.51	2.19	0.23	0.11	0.03	0.16	
14	Ljubljanka - Bistra	8.30	11.0	7.52	429	4.21	4.11	0.50	7.00E-05 ± 1.24E-07	138.04 ± 0.02	1.27	2.49	1.39	0.62	2.03	0.30	0.10	0.03	0.18	

* Sampling site flooded

**NA - data not available

*** calculated with PhreeQC



December 2017

Location	Name of the spring/stream	Discharge [m ³ /s]	T [°C]	pH	Conductivity [µS/cm]	Total alkalinity [mmol/L]	HCO ₃ ⁻ [mmol/L] ***	U [µg/mL]	²³⁵ U absolute value (kg) ±	²³⁸ U absolute value (kg) ±	²³⁵ U/ ²³⁸ U activity ratio	²³⁵ U/ ²³⁸ U δ ²³⁵ U _{CSM} ‰ [‰]	Mg ²⁺ [mmol/L]	Ca ²⁺ [mmol/L]	Mg/Ca	Na ⁺ [mmol/L]	K ⁺ [mmol/L]	SI _{calc} ***	
1	Stržen	**NA	3.1	8.46	332	3.30	3.12	0.38	6.02E-05 ± 5.95E-07	137.87 ± 0.45	1.21	1.24	0.38	1.77	0.21	0.07	0.06	0.83	
2	Cerkniška	2.10	2.6	8.70	485	4.96	4.48	0.70	7.89E-05 ± 4.19E-07	137.85 ± 0.07	1.36	1.14	0.03	1.48	1.79	0.82	0.16	0.17	0.18
3	Rak - Mali most	14.94	3.8	8.44	344	3.41	3.22	0.42	6.69E-05 ± 6.33E-07	137.86 ± 0.43	1.22	1.19	0.09	1.79	0.82	0.25	0.08	0.03	0.83
4	Rak - Količ	29.89	4.9	8.39	331	3.16	2.99	0.40	6.65E-05 ± 1.99E-07	138.09 ± 0.12	1.21	2.83	1.72	0.39	1.86	0.21	0.07	0.04	0.79
5	Rak - Veliki most	45.28	4.1	8.37	342	3.20	3.05	0.41	6.65E-05 ± 9.70E-08	138.01 ± 0.43	1.21	2.24	1.13	0.44	1.68	0.26	0.08	0.03	0.72
6	Pivka	15.32	4.6	8.01	370	3.49	3.38	0.41	6.07E-05 ± 2.65E-07	137.87 ± 0.23	1.10	1.28	0.18	1.19	2.12	0.09	0.28	0.63	0.51
7	Unča - Planina cave	79.02	5.7	8.27	353	3.37	3.22	0.40	6.98E-05 ± 1.00E-06	138.07 ± 0.09	1.16	2.69	1.59	0.34	1.85	0.18	0.19	0.02	0.71
8	Malesišča	9.38	5.1	8.29	342	3.23	3.08	0.43	6.64E-05 ± 3.98E-07	138.14 ± 0.37	1.21	3.20	2.10	0.47	1.77	0.27	0.08	0.04	0.69
9	Unča - Hasberg	88.40	5.1	8.30	342	3.39	3.23	0.43	6.62E-05 ± 3.90E-07	137.98 ± 0.23	1.20	2.09	0.98	0.49	1.77	0.28	0.09	0.09	0.71
10	Hotojška	**NA	4.6	8.53	395	4.04	3.76	0.38	6.05E-05 ± 3.64E-07	138.05 ± 0.44	1.10	2.55	1.44	1.30	1.40	0.92	0.05	0.03	0.88
11	Logišča	1.05	4.8	8.50	426	4.27	3.97	0.40	6.90E-05 ± 6.29E-07	138.01 ± 0.21	1.18	2.28	1.18	1.31	1.60	0.82	0.14	0.07	0.93
12	Ljubljana - Modlnik	80.95	7.4	7.94	317	2.88	2.80	0.33	6.32E-05 ± 4.69E-07	138.04 ± 0.13	1.15	2.48	1.38	0.32	1.57	0.20	0.19	0.04	0.29
13	Ljubljana - Rebojce	80.95	7.0	7.91	337	3.11	3.03	0.37	6.86E-05 ± 4.05E-07	138.04 ± 0.22	1.16	2.49	1.38	0.32	1.75	0.20	0.19	0.03	0.33
14	Ljubljana - Bistra	15.13	8.4	7.72	391	3.88	3.78	0.46	6.71E-05 ± 5.20E-07	137.98 ± 0.05	1.22	2.05	0.95	0.60	1.73	0.35	0.16	0.03	0.24

**NA - data not available
*** calculated with PhreeQC

March 2018

Location	Name of the spring/stream	Discharge [m ³ /s]	T [°C]	pH	Conductivity [µS/cm]	Total alkalinity [mmol/L]	HCO ₃ ⁻ [mmol/L] ***	U [µg/mL]	²³⁵ U absolute value (kg) ±	²³⁸ U absolute value (kg) ±	²³⁵ U/ ²³⁸ U activity ratio	²³⁵ U/ ²³⁸ U δ ²³⁵ U _{CSM} ‰ [‰]	Mg ²⁺ [mmol/L]	Ca ²⁺ [mmol/L]	Mg/Ca	Na ⁺ [mmol/L]	K ⁺ [mmol/L]	SI _{calc} ***	
1	Stržen	**NA	5.8	8.59	342	3.51	3.25	0.43	6.45E-05 ± 4.08E-07	138.14 ± 0.12	1.17	3.19	2.09	0.53	1.72	0.31	0.29	0.02	1.00
2	Cerkniška	2.20	5.2	8.62	463	4.40	4.02	0.58	7.83E-05 ± 4.67E-07	137.82 ± 0.09	1.42	0.86	-0.24	1.35	1.74	0.77	0.27	0.03	1.09
3	Rak - Mali most	9.03	5.4	8.54	370	3.02	2.81	0.48	6.73E-05 ± 3.28E-07	137.88 ± 0.14	1.23	1.31	0.21	0.70	1.66	0.42	0.24	0.01	0.84
4	Rak - Količ	18.32	5.4	8.47	341	3.43	3.22	0.43	6.47E-05 ± 4.72E-07	137.91 ± 0.15	1.18	1.54	0.44	0.55	1.78	0.31	0.11	0.02	0.89
5	Rak - Veliki most	27.35	5.6	8.65	380	3.65	3.35	0.46	6.61E-05 ± 4.98E-07	137.81 ± 0.22	1.20	0.81	-0.29	0.59	1.65	0.36	0.21	0.02	1.05
6	Pivka	7.53	7.1	8.40	365	3.64	3.43	0.37	6.14E-05 ± 4.38E-07	137.90 ± 0.22	1.12	1.49	0.39	0.21	2.11	0.10	0.31	0.04	0.94
7	Unča - Planina cave	55.02	8.0	8.25	349	3.59	3.43	0.42	6.36E-05 ± 4.55E-07	138.41 ± 0.17	1.16	5.18	4.08	0.40	1.83	0.22	0.28	0.02	0.75
8	Malesišča	8.28	5.2	8.40	343	3.66	3.46	0.47	6.57E-05 ± 4.05E-07	138.22 ± 0.15	1.20	3.82	2.71	0.60	1.81	0.33	0.13	0.03	0.85
9	Unča - Hasberg	63.30	5.9	8.37	353	3.66	3.47	0.44	6.51E-05 ± 3.11E-07	138.23 ± 0.09	1.18	3.85	2.74	0.52	1.85	0.28	0.25	0.02	0.84
10	Hotojška	**NA	6.8	8.56	376	4.17	3.86	0.42	6.05E-05 ± 1.32E-07	137.95 ± 0.06	1.10	1.82	0.72	1.27	1.49	0.86	0.06	0.03	0.97
11	Logišča	0.72	7.4	8.61	414	4.32	3.95	0.40	6.71E-05 ± 3.94E-07	137.94 ± 0.12	1.22	1.76	0.65	1.23	1.51	0.81	0.19	0.04	1.05
12	Ljubljana - Modlnik	52.00	6.7	8.14	345	3.40	3.28	0.41	6.99E-05 ± 9.99E-08	137.93 ± 0.10	1.19	1.72	0.61	1.66	0.24	0.24	0.02	0.56	
13	Ljubljana - Rebojce	52.00	6.9	8.14	349	3.50	3.37	0.43	6.59E-05 ± 1.76E-06	138.43 ± 0.12	1.20	5.34	4.24	0.41	1.77	0.23	0.28	0.02	0.60
14	Ljubljana - Bistra	10.02	7.8	7.91	361	3.79	3.68	0.50	6.77E-05 ± 9.57E-07	137.89 ± 0.14	1.23	1.42	0.32	0.58	1.83	0.32	0.23	0.02	0.43

**NA - data not available
*** calculated with PhreeQC



May 2018																				
Location	Name of the spring/stream	Discharge [m ³ /s]	T [°C]	pH	Conductivity [µS/cm]	Total alkalinity [mmol/L]	HCO ₃ ⁻ [mmol/L]	U [ng/mL]	²³⁸ U absolute value (k=2)	²³⁵ U absolute value (k=2)	²³⁸ U/ ²³⁵ U activity ratio	$\delta^{238}\text{U}_{\text{IRMM}} \delta^{238}\text{U}_{\text{CRM}}_{12a}$ [‰]	$\delta^{238}\text{U}_{\text{IRMM}} \delta^{238}\text{U}_{\text{CRM}}_{12a}$ [‰]	Ca ²⁺ [mmol/L]	Mg ²⁺ [mmol/L]	Mg/Ca	Na ⁺ [mmol/L]	K ⁺ [mmol/L]	SI _{calc} ***	
1	Stržan	**NA	17.7	8.18	500	5.03	4.74	0.65	9.53E-05 ± 1.29E-06	137.82 ± 0.06	1.73	0.86	-0.24	1.43	1.37	0.63	0.29	0.04	0.81	
2	Cerknišča	0.43	15.9	8.55	480	4.35	3.92	0.67	9.79E-05 ± 1.29E-06	137.83 ± 0.06	1.78	0.98	-0.12	1.47	1.41	0.63	0.17	0.03	1.08	
3	Rak - Mali most	0.42	14.2	8.18	430	4.49	4.26	0.54	8.26E-05 ± 9.72E-07	137.80 ± 0.05	1.50	0.77	-0.34	1.02	1.61	0.38	0.20	0.02	0.80	
4	Rak - Kofič	0.84	16.9	7.75	340	3.60	3.50	0.40	7.43E-05 ± 6.95E-07	137.88 ± 0.06	1.35	2.04	0.94	0.49	1.53	0.19	0.07	0.01	0.33	
5	Rak - Veliki most	1.27	17.5	7.91	350	3.62	3.50	0.40	7.47E-05 ± 9.15E-07	137.82 ± 0.05	1.36	0.88	0.22	0.50	1.51	0.20	0.08	0.01	0.49	
6	Pivka	0.85	17.8	7.89	450	3.59	3.47	0.38	6.57E-05 ± 7.26E-07	138.16 ± 0.19	3.38	2.28	1.19	3.38	2.28	1.74	0.06	0.81	0.08	0.33
7	Unica - Planina cave	3.80	11.2	7.86	370	3.55	3.45	0.42	6.51E-05 ± 6.61E-07	138.13 ± 0.17	1.19	3.16	2.05	0.27	1.69	0.10	0.31	0.03	0.39	
8	Malenšica	4.40	11.9	7.68	340	3.55	3.47	0.38	7.03E-05 ± 6.05E-07	137.98 ± 0.06	1.28	2.04	0.93	0.36	1.63	0.13	0.08	0.01	0.21	
9	Unica - Husberg	8.20	12.3	7.89	345	3.59	3.48	0.38	7.04E-05 ± 3.10E-07	137.97 ± 0.05	1.28	1.98	0.88	0.39	1.69	0.14	0.10	0.02	0.44	
10	Hotenka	**NA	16.3	8.55	420	4.95	4.48	0.62	6.22E-05 ± 5.26E-07	137.95 ± 0.09	1.13	1.87	0.76	1.31	1.32	0.60	0.03	0.01	1.12	
11	Legiščica	1.34	19.3	8.47	434	4.80	4.37	0.42	7.32E-05 ± 4.36E-07	137.89 ± 0.10	1.33	1.44	0.33	1.33	1.34	0.60	0.10	0.02	1.08	
12	Ljubljanska - Močnik	5.30	11.1	7.73	373	3.75	3.66	0.39	7.30E-05 ± 1.24E-06	138.05 ± 0.11	1.33	2.59	1.48	0.61	1.50	0.25	0.19	0.02	0.22	
13	Ljubljanska - Retovje	5.50	13.5	7.77	378	3.91	3.80	0.45	7.12E-05 ± 1.15E-06	138.04 ± 0.01	1.30	2.51	1.41	0.51	1.69	0.18	0.14	0.02	0.37	
14	Ljubljanska - Bištra	6.25	14.7	7.76	373	3.88	3.76	0.46	7.17E-05 ± 2.38E-07	137.91 ± 0.10	1.30	1.55	0.44	0.60	1.83	0.20	0.22	0.05	0.40	

**NA - data not available
*** calculated with PhreeQC

August 2018																				
Location	Name of the spring/stream	Discharge [m ³ /s]	T [°C]	pH	Conductivity [µS/cm]	Total alkalinity [mmol/L]	HCO ₃ ⁻ [mmol/L]	U [ng/mL]	²³⁸ U absolute value (k=2)	²³⁵ U absolute value (k=2)	²³⁸ U/ ²³⁵ U activity ratio	$\delta^{238}\text{U}_{\text{IRMM}} \delta^{238}\text{U}_{\text{CRM}}_{12a}$ [‰]	$\delta^{238}\text{U}_{\text{IRMM}} \delta^{238}\text{U}_{\text{CRM}}_{12a}$ [‰]	Ca ²⁺ [mmol/L]	Mg ²⁺ [mmol/L]	Mg/Ca	Na ⁺ [mmol/L]	K ⁺ [mmol/L]	SI _{calc} ***	
1	Stržan	**NA	26.0	8.13	771	5.77	5.37	0.25	8.18E-05 ± 1.26E-07	138.20 ± 0.38	1.49	3.63	2.52	1.48	1.74	0.85	0.44	0.59	1.03	
2	Cerknišča	0.10	24.7	8.50	294	3.74	3.40	0.31	8.70E-05 ± 5.62E-07	137.66 ± 0.31	1.58	-0.26	-1.37	1.45	0.64	2.25	0.56	0.07	0.78	
3	Rak - Mali most	0.063	13.3	8.14	338	4.84	4.62	0.51	8.46E-05 ± 5.69E-07	137.77 ± 0.02	1.54	0.53	-0.57	1.05	1.41	0.74	0.26	0.04	0.72	
4	Rak - Kofič	0.01	16.7	8.12	215	2.95	2.83	0.24	7.11E-05 ± 1.20E-07	137.77 ± 0.05	1.29	0.51	-0.60	0.42	1.37	0.30	0.12	0.04	0.56	
5	Rak - Veliki most	0.01	25.7	8.38	259	3.63	3.34	0.38	7.67E-05 ± 1.21E-07	137.79 ± 0.03	1.39	0.69	-0.42	0.73	1.21	0.62	0.20	0.05	0.95	
6	Pivka	0.02	22.6	8.02	405	4.41	4.20	0.37	6.67E-05 ± 1.10E-07	137.86 ± 0.18	1.21	1.20	0.10	0.18	2.03	0.09	1.13	0.09	0.86	
7	Unica - Planina cave	1.25	12.9	8.42	276	3.73	3.49	0.33	6.40E-05 ± 3.56E-07	137.90 ± 0.05	1.16	1.48	0.37	0.38	1.71	0.22	0.51	0.06	0.97	
8	Malenšica	1.80	9.0	8.42	349	3.65	3.45	0.34	7.31E-05 ± 3.73E-07	137.79 ± 0.04	1.33	0.65	-0.45	0.26	1.51	0.17	0.20	0.01	0.86	
9	Unica - Husberg	3.08	11.8	7.71	650	3.65	3.56	0.35	7.30E-05 ± 3.60E-07	137.79 ± 0.08	1.33	0.70	-0.40	0.60	1.63	0.37	0.30	0.02	0.24	
10	Hotenka	**NA	23.0	8.50	284	4.51	4.08	0.30	6.89E-05 ± 4.69E-07	137.83 ± 0.11	1.25	0.95	-0.15	1.20	1.07	1.12	0.05	0.02	1.04	
*11	Legiščica																			
12	Ljubljanska - Močnik	2.55	10.5	8.33	283	2.94	2.79	0.34	7.25E-05 ± 5.04E-07	137.79 ± 0.07	1.32	0.69	-0.41	0.55	1.44	0.32	0.32	0.01	0.68	
13	Ljubljanska - Retovje	2.55	14.2	8.17	307	4.26	4.05	0.40	7.24E-05 ± 4.57E-07	137.75 ± 0.23	1.32	0.41	-0.69	0.66	1.65	0.40	0.18	0.02	0.79	
14	Ljubljanska - Bištra	2.77	14.6	7.84	315	4.53	4.41	0.43	7.24E-05 ± 4.25E-07	137.79 ± 0.13	1.32	0.67	-0.43	0.54	1.72	0.39	0.11	0.02	0.52	

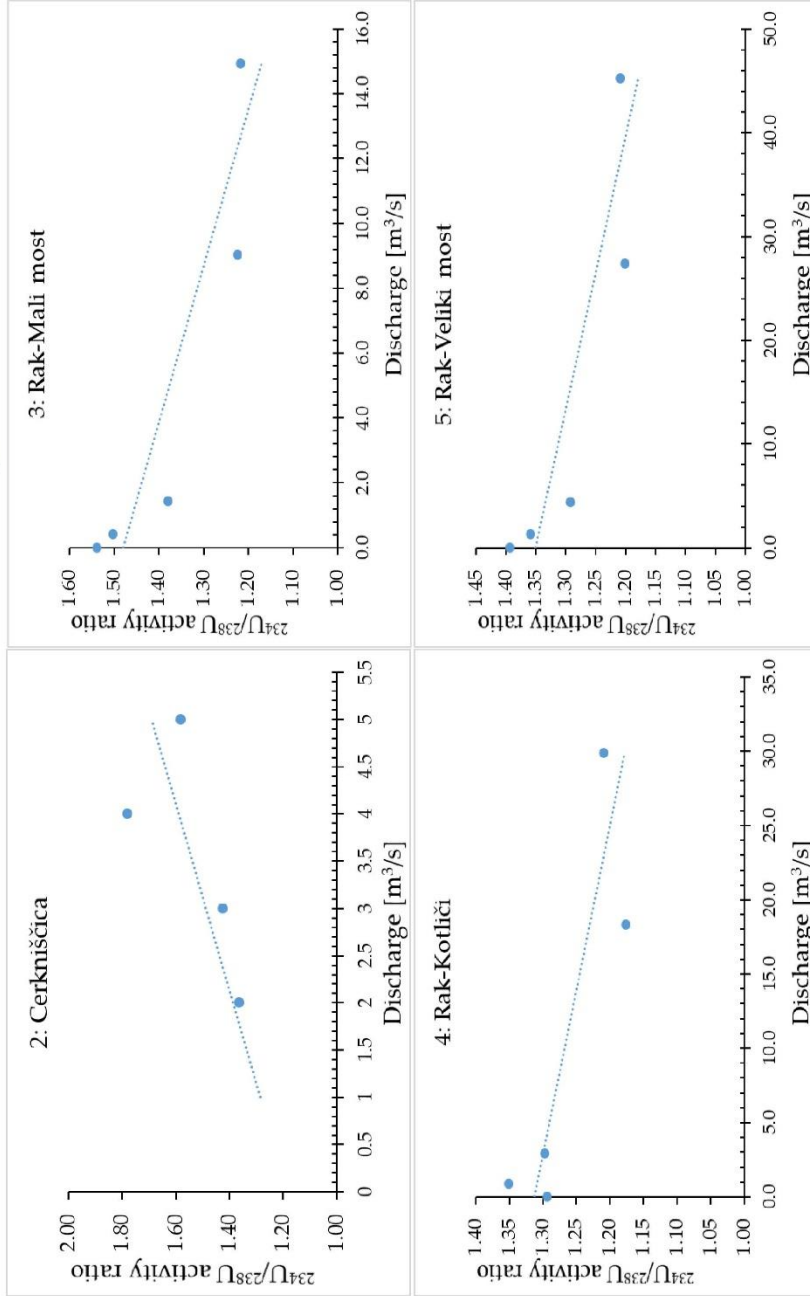
* Stream dried out
**NA - data not available

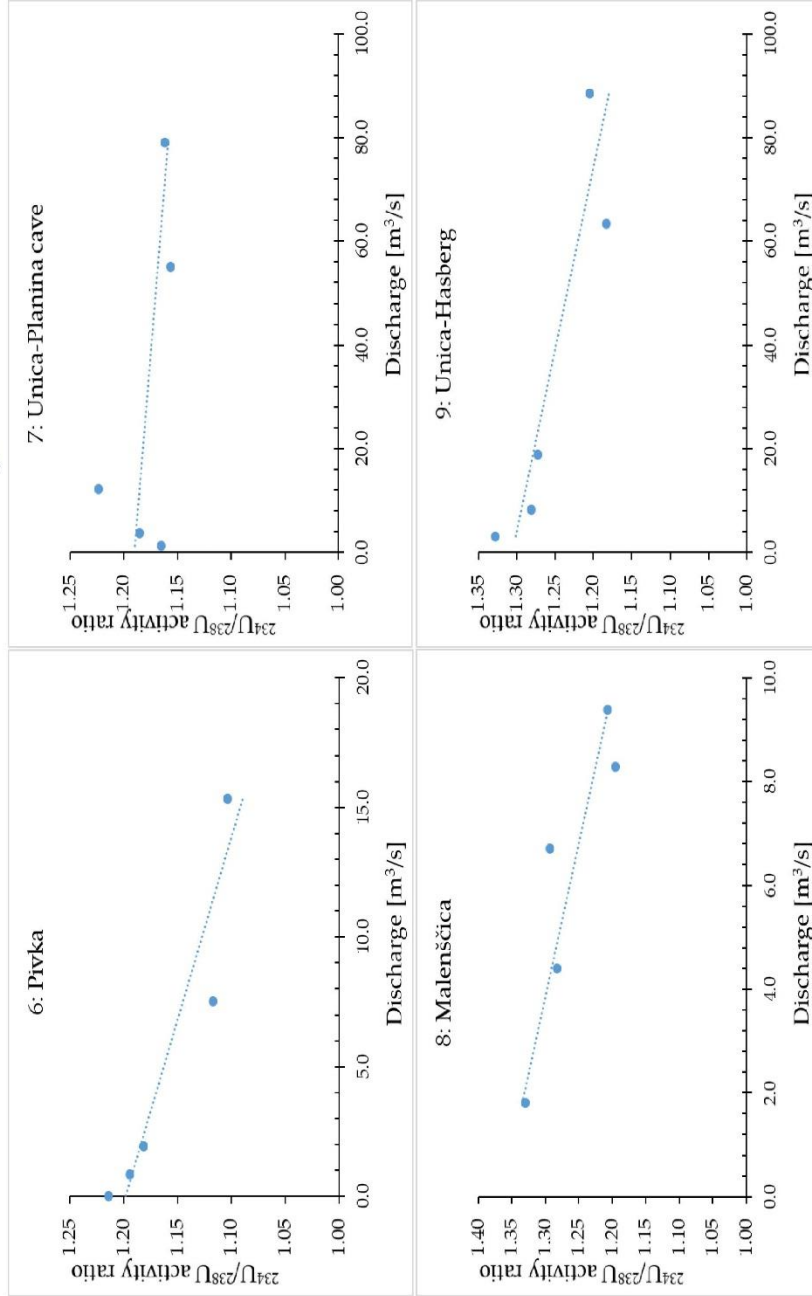


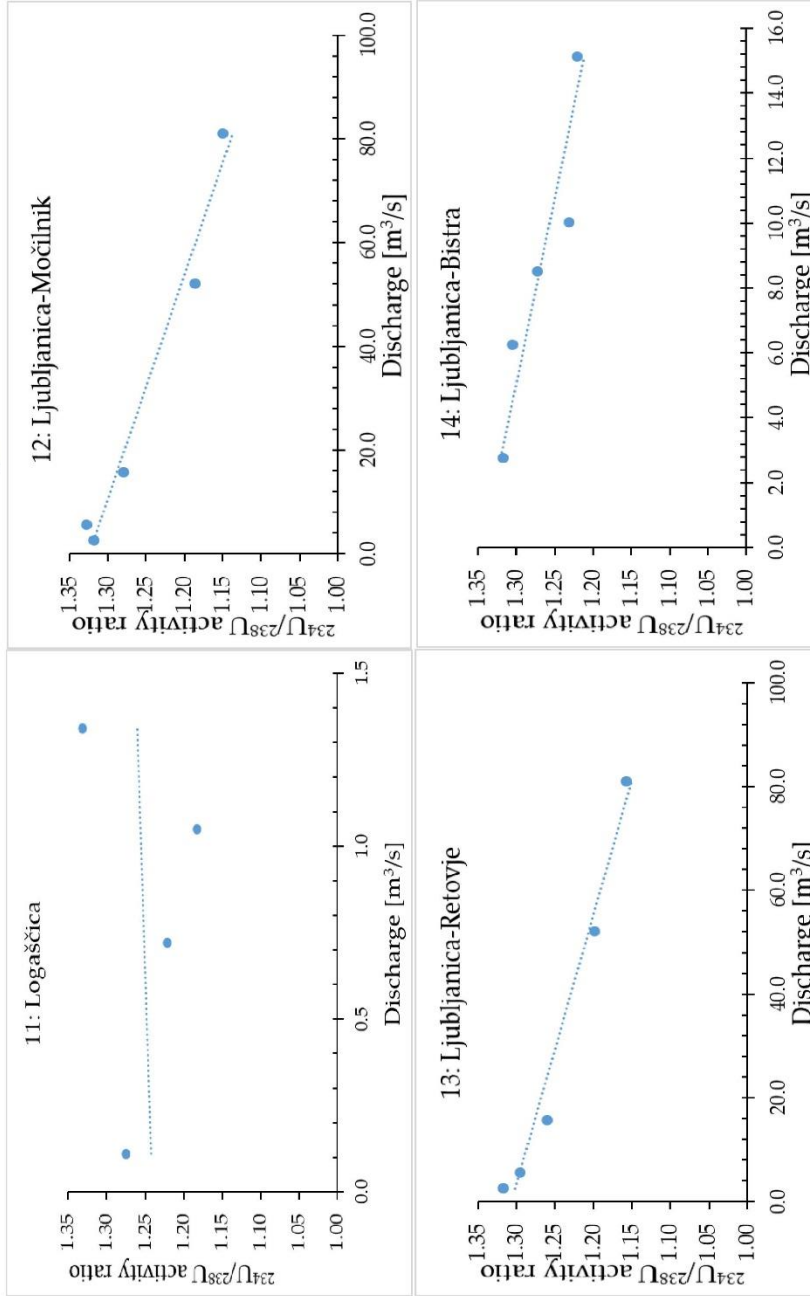
Location	Name of the spring/stream of rock sampling	Bulk rock sample						Leached rock sample							
		U [µg/g]	$^{234}\text{U}/^{238}\text{U}$ absolute value (k=2)	$^{238}\text{U}/^{235}\text{U}$ absolute value (k=2)	$^{234}\text{U}/^{238}\text{U}$ activity ratio	$\delta^{238}\text{U}_{\text{URMAN}}$ [‰]	$\delta^{238}\text{U}_{\text{CRM}}$ [‰]	Th [ng/g]	U [µg/g]	$^{234}\text{U}/^{238}\text{U}$ absolute value (k=2)	$^{238}\text{U}/^{235}\text{U}$ absolute value (k=2)	$^{234}\text{U}/^{238}\text{U}$ activity ratio	$\delta^{238}\text{U}_{\text{URMAN}}$ [‰]	$\delta^{238}\text{U}_{\text{CRM}}$ [‰]	Th [ng/g]
1	Stržen	4.88	5.52E-05 ± 1.08E-07	137.85 ± 0.05	1.004	1.10	-0.01	71.0	3.37	5.60E-05 ± 2.00E-07	137.88 ± 0.11	1.019	1.32	0.22	27.7
3	Rak - Mali most	4.82	5.52E-05 ± 1.06E-07	137.84 ± 0.05	1.004	1.07	-0.04	157.0	3.38	5.61E-05 ± 1.94E-07	137.91 ± 0.11	1.021	1.51	0.41	73.0
4	Rak - Količ	2.47	5.54E-05 ± 1.07E-07	137.86 ± 0.05	1.008	1.20	0.10	17.9	1.64	5.62E-05 ± 1.89E-07	137.85 ± 0.11	1.022	1.13	0.03	16.8
5	Rak - Veliki most	1.99	5.66E-05 ± 1.04E-07	137.85 ± 0.05	1.029	1.11	0.01	23.0	1.36	5.68E-05 ± 2.38E-07	137.84 ± 0.11	1.034	1.00	-0.10	11.3
6	Pivka	4.82	5.51E-05 ± 1.12E-07	137.87 ± 0.05	1.002	1.26	0.15	16.7	3.42	5.55E-05 ± 1.86E-07	137.85 ± 0.11	1.009	1.11	0.01	6.7
7	Unica - Planina cave	3.09	5.46E-05 ± 1.01E-07	137.77 ± 0.05	0.994	0.55	-0.55	184.0	2.29	5.65E-05 ± 1.96E-07	137.71 ± 0.12	1.027	0.11	-0.99	86.0
8	Malensčica	2.66	5.29E-05 ± 1.01E-07	137.78 ± 0.05	0.963	0.62	-0.48	349.0	1.64	5.71E-05 ± 1.96E-07	137.87 ± 0.11	1.038	1.29	0.18	178.0
12	Ljubljana - Mečnik	1.02	5.63E-05 ± 1.09E-07	137.77 ± 0.05	1.025	0.51	-0.59	103.0	0.74	5.69E-05 ± 2.05E-07	137.92 ± 0.11	1.035	1.61	0.51	30.4
14	Ljubljana - Bistra	3.12	5.43E-05 ± 1.10E-07	137.82 ± 0.05	0.987	0.89	-0.21	242.0	0.76	5.73E-05 ± 1.85E-07	137.78 ± 0.10	1.043	0.58	-0.52	69.1
Residual rock sample (calculated)															
Location	Name of the spring/stream of rock sampling	U [µg/g]	$^{234}\text{U}/^{238}\text{U}$ activity ratio	$\delta^{238}\text{U}_{\text{URMAN}}$ [‰]	$\delta^{238}\text{U}_{\text{CRM}}$ [‰]	Th [ng/g]	U [µg/g]	$^{234}\text{U}/^{238}\text{U}$ activity ratio	$\delta^{238}\text{U}_{\text{URMAN}}$ [‰]	$\delta^{238}\text{U}_{\text{CRM}}$ [‰]	Th [ng/g]				
1	Stržen	1.50	0.975	0.59	-0.52	43.5									
3	Rak - Mali most	1.44	0.969	0.01	-1.09	83.1									
4	Rak - Količ	0.82	0.984	1.34	0.23	1.2									
5	Rak - Veliki most	0.63	1.024	1.35	0.24	11.7									
6	Pivka	1.39	0.991	1.61	0.50	10.0									
7	Unica - Planina cave	0.78	0.922	1.87	0.73	98.5									
8	Malensčica	1.02	0.839	-0.45	-1.55	168.6									
12	Ljubljana - Mečnik	0.28	1.002	-2.35	-3.46	72.6									
14	Ljubljana - Bistra	2.37	0.969	0.99	-0.11	172.5									

Figure S1: The $^{234}\text{U}/^{238}\text{U}$ activity ratio with water discharge for each individual location

October 2017			December 2017			March 2018					
Location	Name of the spring/stream	Discharge [m ³ /s]	$^{234}\text{U}/^{238}\text{U}$ activity ratio	Location	Name of the spring/stream	Discharge [m ³ /s]	$^{234}\text{U}/^{238}\text{U}$ activity ratio	Location	Name of the spring/stream	Discharge [m ³ /s]	$^{234}\text{U}/^{238}\text{U}$ activity ratio
1	Stržen	¹ NA		1	Stržen	¹ NA		1	Stržen	¹ NA	
2	Cerknišča	¹ NA		2	Cerknišča	2.10	1.36	2	Cerknišča	2.20	1.42
3	Rak - Mali most	1.44	1.38	3	Rak - Mali most	14.94	1.22	3	Rak - Mali most	9.03	1.23
4	Rak - Kotlič	2.92	1.30	4	Rak - Kotlič	29.89	1.21	4	Rak - Kotlič	18.32	1.18
5	Rak - Veliki most	4.36	1.29	5	Rak - Veliki most	45.28	1.21	5	Rak - Veliki most	27.35	1.20
6	Pivka	1.95	1.18	6	Pivka	15.32	1.10	6	Pivka	7.53	1.12
7	Unica - Planina cave	12.12	1.22	7	Unica - Planina cave	79.02	1.16	7	Unica - Planina cave	55.02	1.16
8	Malensča	6.71	1.29	8	Malensča	9.38	1.21	8	Malensča	8.28	1.20
9	Unica - Hasberg	18.83	1.27	9	Unica - Hasberg	88.40	1.20	9	Unica - Hasberg	63.30	1.18
10	Hotenja	¹ NA		10	Hotenja	¹ NA		10	Hotenja	¹ NA	
11	Logašča	0.11	1.27	11	Logašča	1.05	1.18	11	Logašča	0.72	1.22
12	Ljubljaniica - Močlnik	15.70	1.28	12	Ljubljaniica - Močlnik	80.95	1.15	12	Ljubljaniica - Močlnik	52.00	1.19
13	Ljubljaniica - Retovje	15.70	1.26	13	Ljubljaniica - Retovje	80.95	1.16	13	Ljubljaniica - Retovje	52.00	1.20
14	Ljubljaniica - Bistra	8.50	1.27	14	Ljubljaniica - Bistra	15.13	1.22	14	Ljubljaniica - Bistra	10.02	1.23







3.3 Uranium Isotopes as a Possible Tracer of Terrestrial Authigenic Carbonate

Rovan, L., Zuliani, T., Horvat, B., Kanduč, T., Vreča, P., Jamil, Q., Čermelj, B., Bura Nakić, E., Cukrov, N., Štok, M., Lojen, S., Science of the Total Environment. 2021, vol. 797, str. 149103. DOI: 10.1016/j.scitotenv.2021.149103.

Tufa is attracting attention as a potential environmental archive in both authigenic and detrital components and can provide insight into water-rock interactions, hydraulic connections, recharge, and terrestrial CO₂ cycling in terms of storage, evasion, and transfer to the ocean. In a dynamic karst river system with alternating lentic and turbulent lotic sections, the carbonate precipitation rarely occurs in isotopic equilibrium for either C or O isotopes.

In this manuscript, the use of U concentration and isotopic composition ($\delta^{238}\text{U}$, $^{234}\text{U}/^{238}\text{U}$ activity ratio, measured by MC-ICP-MS) in combination with traditional isotopes ($\delta^{18}\text{O}$, $\delta^{13}\text{C}$) and geochemical parameters (U/Ca) in river water, tufa, bedrock, and soil was examined to explain the environmental influences on the formation of authigenic carbonate. With U isotopes, the estimation of the proportion of authigenic and detrital carbonate in tufa was explored and their performance with traditional isotopes and other geochemical parameters were compared in two connected rivers, the Krka and the Zrmanja River (Central Dalmatia, Croatia). Watershed of the Krka River is a specific groundwater-fed karstic river, characterized by complex hydrology and seasonally variable diffuse subsurface recharge. It represents a unique model system, where tufa is precipitating in a turbulent stream at morphologic discontinuities and in lotic environments. The U concentration and $^{234}\text{U}/^{238}\text{U}$ activity ratios in water in the tufa-precipitating sections decreased downstream in water and in precipitated carbonate because of active self-purification processes, i.e. adsorption of isotopically lighter U(VI) on mineral particles, sedimentation and co-precipitation with carbonate. U isotopic differences also reflect the changing bedrock lithology and the mixing of waters from different sources. The isotopic composition of carbonate in tufa mostly resembles the $^{234}\text{U}/^{238}\text{U}$ activity ratio and $\delta^{238}\text{U}$ values of dissolved U in water, but is also affected by the presence of detrital carbonate flushed into the river from soil and weathering of bedrock. This interpretation is confirmed by the $\delta^{18}\text{O}$ and $\delta^{13}\text{C}$ values of tufa, dissolved inorganic carbon, and in their isotopic signature, which showed the presence of lithic carbonate. U partitioning between water and carbonate can also be affected by complicated hydrology, variable temperature, and turbulence. The $\delta^{238}\text{U}$ has shown to be a much more sensitive tracer of bedrock composition than the $^{234}\text{U}/^{238}\text{U}$ activity ratio and large fluctuation of its values of water, carbonate-bound U and residual fraction cannot be fully explained with available data. In such a unique and complex watershed, geochemical parameters, traditional isotopes and U isotopic composition are affected by many different processes and a long-term systematic seasonal and event-based observation of isotopic composition of dissolved and suspended particulate U in water would be necessary to further elucidate the importance and contribution of such processes.

The candidate participated in samplings and she determined U isotopic composition and its concentration in the collected samples. Following the experimental part of the research, she performed U data analyses. The candidate prepared graphs, tables and drafted the manuscript in collaboration with other co-authors.



Contents lists available at ScienceDirect

Science of the Total Environment

journal homepage: www.elsevier.com/locate/scitotenv

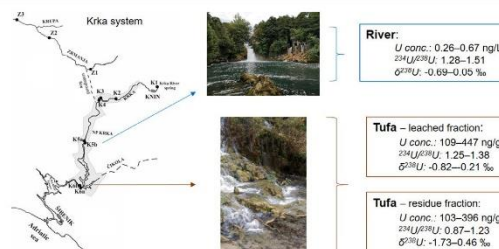
Uranium isotopes as a possible tracer of terrestrial authigenic carbonate

Leja Rovan^{a,b}, Tea Zuliani^{a,b}, Barbara Horvat^c, Tjaša Kanduč^a, Polona Vreča^a, Qasim Jamil^b, Branko Čermelj^d, Elvira Bura-Nakić^e, Neven Cukrov^e, Marko Štrok^{a,b,*}, Sonja Lojen^{a,f}^a Department of Environmental Sciences, Jožef Stefan Institute, Jamova cesta 39, 1000 Ljubljana, Slovenia^b Jožef Stefan International Postgraduate School, Jamova cesta 39, 1000 Ljubljana, Slovenia^c Slovenian National Building and Civil Engineering Institute, Dimičeva ulica 12, 1000 Ljubljana, Slovenia^d Marine Biology Station, National Institute of Biology, Fornače 40, 6330 Piran, Slovenia^e Division for Marine and Environmental Research, Ruder Bošković Institute, Bijenička cesta 54, 10000 Zagreb, Croatia^f School of Environmental Sciences, University of Nova Gorica, Glavni trg 8, 5271 Vipava, Slovenia

HIGHLIGHTS

- New insight of understanding possible environmental influences on tufa formation
- Combination use of traditional and U isotopes was evaluated in the karst aquifer.
- U isotopic composition was analysed with MC-ICP-MS.
- $\delta^{13}\text{C}$, $\delta^{18}\text{O}$ and U values confirmed carbonates authigenic origin.
- U isotopes are relevant for the construction of the CO_2 mass balance.

GRAPHICAL ABSTRACT



ARTICLE INFO

Article history:

Received 6 May 2021

Received in revised form 13 July 2021

Accepted 13 July 2021

Available online 17 July 2021

Editor: Filip M.G. Tack

Keywords:

Uranium isotopes

Karst aquifer

Authigenic carbonate

Tufa

Krka River

ABSTRACT

The concentration and isotopic composition of uranium ($\delta^{238}\text{U}$, $^{234}\text{U}/^{238}\text{U}$ activity ratio) in combination with traditional isotopes ($\delta^{18}\text{O}$, $\delta^{13}\text{C}$) were examined as potential tracers of authigenic carbonate formation in a karst aquifer. The U concentration and $^{234}\text{U}/^{238}\text{U}$ activity ratios in the tufa-precipitating sections of two connected karst rivers (Krka and Zrmanja, Croatia) decreased downstream in water and in precipitated carbonate due to active self-purification processes, i.e. adsorption of isotopically lighter U(VI) on mineral particles, sedimentation and co-precipitation with carbonate. The isotopic composition of carbonate in tufa mostly resembled the $^{234}\text{U}/^{238}\text{U}$ activity ratio and the $\delta^{238}\text{U}$ values of dissolved U in water but was also affected by the presence of detrital carbonate flushed into the river from soil and weathered bedrock. This interpretation was supported by the $\delta^{18}\text{O}$ and $\delta^{13}\text{C}$ values of tufa, which were shifted out of equilibrium with river water and dissolved in organic carbon and in their isotopic signature, which showed the presence of lithic carbonate. Large fluctuations of the $\delta^{238}\text{U}$ values of water, leachable U (eluted in acetic acid buffered with Na-acetate) and residual U fraction could not be fully explained by available data due to the overlapping U isotopic signatures of leachable (mainly carbonate) and residual fractions of soil, bedrock and tufa. Therefore, a long-term, systematic, seasonal and event-based observation of the isotopic composition of dissolved and suspended particulate U in water is necessary. Nevertheless, the U isotopes were found to have the potential to be used as identifiers of authigenic carbonate and the storage of CO_2 in terrestrial river sediments, to improve knowledge on fluxes within local and global biogeochemical carbon cycle.

© 2021 The Authors. Published by Elsevier B.V. This is an open access article under the CC BY-NC-ND license (<http://creativecommons.org/licenses/by-nc-nd/4.0/>).

* Corresponding author at: Department of Environmental Sciences, Jožef Stefan Institute, Jamova cesta 39, 1000 Ljubljana, Slovenia.

E-mail address: marko.strok@ijs.si (M. Štrok).

1. Introduction

The formation of authigenic carbonate has only recently been invoked as the third major global carbon sink (Zhao et al., 2016). Therefore, the identification of authigenic carbonate in marine and terrestrial settings is crucial for the estimation of the magnitude and locations of carbon fixation. The identification of authigenic terrestrial carbonates is usually based on their carbon and oxygen isotopic compositions (Leng et al., 2006). The terrestrial dissolved inorganic carbon (DIC) is usually depleted in ^{13}C compared to marine DIC, and the water from which the terrestrial carbonates are precipitated is usually significantly depleted in ^{18}O compared to the seawater (Gat and Gouffanti, 1981). In principle, both C ($\delta^{13}\text{C}$) and O ($\delta^{18}\text{O}$) isotopic compositions should be conspicuous enough to be used as identifiers of authigenic carbonate. However, in terrestrial environments, multiple sources of DIC with different or overlapping isotopic compositions do not allow for such appointment of a carbonate formation pathway. Spatially and temporally variable precipitation rates, cyclic episodes of deposition and erosion, mixing with detrital minerals, disequilibrium effects and diagenetic processes can affect the δ values of bulk terrestrial carbonate (Brasier et al., 2010; De Boever et al., 2017; Zavadlav et al., 2017; Yan et al., 2020), which can make the source appointment of carbonate uncertain.

Zhao et al. (2016) identified U concentrations in a cross-plot with the C isotope composition as the potential identifier of authigenic carbonate in limestone. The isotopes of U have already been proven in karst hydrogeology to be a useful tool for identifying young carbonates (Bourdon et al., 2009; Nyachoti et al., 2019), but a systematic analysis of U isotope fractionation in carbon cycle of a river has not been explored yet. In karst aquifers, U is released into the groundwater from bedrock and soil during weathering. Young karst groundwater is characterised by a dissolved $^{234}\text{U}/^{238}\text{U}$ activity ratio higher than the secular equilibrium of the U-series isotopes that is found in bedrock due to the so-called alpha recoil effect (Chen et al., 2020; Fleischer, 1982; Suksi et al., 2006). Therefore, the dissolved $^{234}\text{U}/^{238}\text{U}$ activity ratios are often used in hydrology as a tracer for studying spatial changes in bedrock lithology and the mixing of water from different sources (Chabaux et al., 2003; Chabaux et al., 2008; Bourdon et al., 2009). During precipitation, the dissolved $^{234}\text{U}/^{238}\text{U}$ activity ratio of water is transferred to the carbonate without any apparent fractionation. The authigenic carbonate should thus be distinguished from the marine carbonate formed in geological history by its elevated $^{234}\text{U}/^{238}\text{U}$ activity ratio (Teichert et al., 2003; Bourdon et al., 2009; Andersen et al., 2010; Wang and You, 2013; Andersen et al., 2017).

Natural variations in $^{238}\text{U}/^{235}\text{U}$, usually reported as $\delta^{238}\text{U}$ values, are in the permil range and can be primarily associated with the variable solubility of U in different redox states, adsorption or leaching, mostly due to thermodynamic or nuclear field shift effects (Stirling et al., 2007; Weyer et al., 2008; Brennecke et al., 2011). The co-precipitation of U in calcite from an aquatic solution is not associated with isotope fractionation. Therefore, similar to $^{234}\text{U}/^{238}\text{U}$ activity ratio, the $\delta^{238}\text{U}$ values of carbonate resemble those of the precipitating water (Chen et al., 2016) and depend mostly on the redox conditions in the basin (Andersen et al., 2017, and references therein).

Tufa is a terrestrial sediment most commonly composed of authigenic calcium carbonate precipitated at an ambient temperature from supersaturated water in rivers, springs or lakes (Ford and Pedley, 1996; Pedley, 2009) and represents an ideal material for investigation and testing of potential identifiers of terrestrial authigenic carbonate. It can contain variable amounts of mineral and organic detritus contributed by the surface runoff from soil and bedrock erosion or from autochthonous particulate organic matter. The precipitation of CaCO_3 in a supersaturated river follows the degassing of dissolved CO_2 at springs and at or close to the topographic discontinuities (e.g. rapids, waterfalls) along the watercourse. It is usually facilitated (or even induced) by the presence of biofilms and macrobiota, which influence the chemical and

isotopic characteristics of precipitates (Rogerson et al., 2008; Banks and Jones, 2012; Capezzuoli et al., 2014; Saunders et al., 2014). Tufa formation is thus an important process of the continental CO_2 cycle that accounts for the evasion of CO_2 from the river to the atmosphere as well as for the fixation of CO_2 in a carbonate sediment. Tufa as a CO_2 sink may indeed be rather small on a global scale, but it can play a considerable role in karst landscapes (González Martín and González Amuchastegui, 2014).

The aim of this study was to test the U isotopes as a potential identifier of authigenic carbonate in a specific terrestrial depositional setting of two hydraulically connected karst rivers (Krka and Zrmanja, Croatia). The spatial variability of geochemical (U/Ca) and isotopic ($\delta^{18}\text{O}$, $\delta^{13}\text{C}$, $\delta^{238}\text{U}$, and $^{234}\text{U}/^{238}\text{U}$ activity ratio) parameters were investigated in river water, in a series of tufa cascades and in the soil and bedrock, which are the two main sources of dissolved and detrital materials for tufa precipitation. The U isotope fractionation between river water and carbonate in tufa was estimated to provide complementary information to traditional (O, C) isotopes needed to differentiate between authigenic and detrital carbonate in tufa and to quantify the authigenic carbonate formation in karst rivers.

2. Study area

Krka River is a 75 km long karstic stream in Central Dalmatia, Croatia (Fig. 1), with an estimated drainage area of 2427 km² (Bonacci et al., 2006). The entire catchment is located at the Outer Dinaric carbonate platform composed mainly of Cretaceous limestone with some sporadic dolomite and Eocene limestone interchanged with clastic rocks (marl, conglomerate and flysch) (Mamudžić, 1971). In the wider area of Knin ~3 km downstream from the spring, small outcrops of the so-called Dinaride evaporitic mélange occur, which are composed of Permian to Triassic evaporites (gypsum, anhydrite and some sporadic dolomite) and associated sedimentary and igneous blocks, sometimes embedded within evaporites (Kulušić and Borojević Šostarić, 2014; Dedić et al., 2018). Two intermittent streams, Orašnica and Butišnica, drain these formations and discharge their weathering products into the Krka River near Knin.

The river is mainly groundwater-fed with some minor intermittent tributaries. The discharge at the spring varies between 1.5 and 10 m³ s⁻¹, while the discharge at the Skradinski buk waterfall at the head of the estuary is on average 51.3 m³ s⁻¹ (ranging from 5 to 476 m³ s⁻¹) (Bonacci et al., 2017). Previous studies have shown that a massive diffuse subsurface recharge from the northeast from the Zrmanja River takes place in the flow section between 18.8 and 22 km downstream from the spring, which contributes a considerable fraction of the water flow to the lower reaches of the stream (Bonacci, 1999; Lojen et al., 2004; Bonacci et al., 2006).

At present, tufa occurs along 50 km of the watercourse with a total fall of 242 m. The river is sectioned by nine larger barriers and numerous smaller cascades into a series of lentic and lotic environments (Cukrov et al., 2013). The recent measurements revealed highly variable annual tufa growth rates between <1 mm and 2 cm (Maric et al., 2020).

3. Materials and methods

3.1. Sampling

Samples of water, tufa, bedrock and soil were collected in September 2019 at the main cascades at Krka River (samples K1 to K6) and at Zrmanja River (samples Z1 to Z3, Fig. 1). The seasonal sink of the Zrmanja River occurs between sites Z1 and Z2.

The water samples for the analyses of the total alkalinity and isotope composition of DIC were filtered on-site through 0.2 μm pore-sized membrane filters (Sartorius Minisart 16534K) and stored in 100 mL high-density polyethylene (HDPE) bottles (for alkalinity) and 12 mL glass vials with septum caps without headspace (Labco Exetainer® for

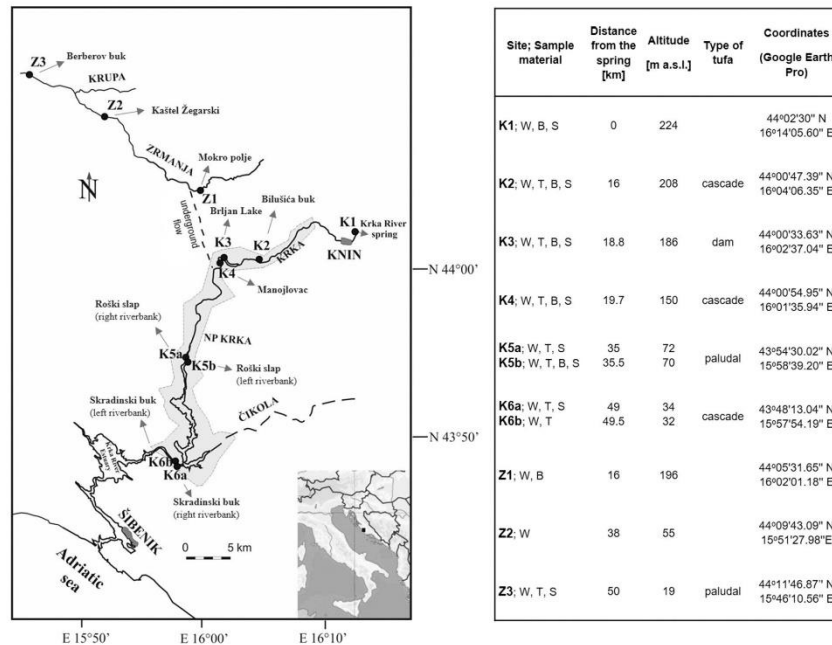


Fig. 1. Site map and sampling sites in the Krka-Zrmanja river system with a response legend of sampling locations and sampled material at Krka River (K) and Zrmanja River (Z); W = water, B = bedrock, S = soil, T = tufa.

$\delta^{13}\text{C}$ -DIC analysis). Samples for the water isotope analyses were kept unfiltered in 30 mL HDPE bottles without headspace. Samples for the major metal analyses were filtered through 0.45 μm pore-sized membrane filters (Sartorius Minisart 16555K) into pre-washed HDPE bottles and acidified on-site with supra pure HNO_3 (65%, Merck) to $\text{pH} \leq 1.5$. All samples were kept refrigerated at 4–8 °C until analysis. For the analysis of U isotopes, 1 L samples were kept in prewashed PE bottles in a cool box and transported to the laboratory, where they were vacuum filtered through a 0.45- μm pore-sized Millipore membrane filter. After filtration, the samples were acidified with concentrated supra-pure HNO_3 .

Three to five hand samples of recent tufa were collected from the riverbed at each site. Soil and rock samples were collected at outcrops adjacent to the tufa sampling sites.

3.2. Analyses

3.2.1. River water

Water temperature, pH, electrical conductivity and redox potential (Eh) were measured on-site with the multiprobe Ultrameter II 6 PFC (Myron Company, Carlsbad, CA, USA). The total alkalinity was determined by Gran titration (Gieskes, 1974) in approx. 50 mL samples using 0.05 M HCl with a precision of $\pm 1\%$ within 8 h after sample collection. Major element concentrations (Ca and Mg) were determined by an Agilent 7900x ICP-MS (Agilent Technologies, Tokyo, Japan).

The isotopic compositions of oxygen ($\delta^{18}\text{O}$) in the water were determined according to the modified IAEA Technical procedure note no. 43 (Tanweer et al., 2009) using the CO_2 - H_2O equilibration techniques (Epstein and Mayeda, 1953; Avak and Brand, 1995). Measurements were performed with a dual-inlet isotope ratio mass spectrometer Delta Plus (Finnigan MAT GmbH, Bremen, Germany) with a custom-

built automated CO_2 - H_2O equilibrator HDOeq 48 Equilibration Unit (M. Jaklitsch).

All measurements were performed together with laboratory reference materials (LRM) calibrated periodically against primary IAEA calibration standards to the VSMOW/SLAP scale. The defined isotope values and measurement uncertainty of LRMs used for the normalisation of data and independent quality control were calculated using the Kragten method (Carter and Barwick, 2011). The results were normalised to VSMOW/SLAP using the Laboratory Information Management System for Light Stable Isotopes (LIMS) programme and were expressed in the standard δ notation (in ‰):

$$\delta_{\text{sample}} [\text{‰}] = (R_{\text{sample}}/R_{\text{standard}} - 1) \times 1000 \quad (1)$$

where R_{sample} and R_{standard} represent heavy-to-light isotope ratios ($^{18}\text{O}/^{16}\text{O}$) in a sample and an international standard, respectively. For the normalisation of the results, two in-house working standards calibrated to the VSMOW/SLAP scale with defined $\delta^{18}\text{O}$ values and estimated measurement uncertainties $+0.36 \pm 0.04\%$ and $-19.73 \pm 0.02\%$ were used, respectively. As an independent quality control, the third laboratory working standard with $\delta^{18}\text{O} = -9.12 \pm 0.04\%$ and certified commercial reference materials USGS 45 and USGS 47 were used. The average sample repeatability was 0.03%.

For the determination of the isotopic composition of DIC, a volume of 100–200 μL of phosphoric acid was added to a septum-sealed vial (volume of 3.7 mL) and was then purged with pure He (6.0), 1 mL of the sample was then injected, and the headspace CO_2 was analysed (Miyajima et al., 1995; Spötl, 2005). The $\delta^{13}\text{C}_{\text{DIC}}$ values were determined using the mass spectrometer IsoPrime 100 coupled with the MultiflowBio equilibration module (Elementar Analysensysteme GmbH, Langensfeld, Germany).

Germany). To control the extraction procedure, a standard solution of Na_2CO_3 with a known $\delta^{13}\text{C}_{\text{DIC}}$ value of $-10.8 \pm 0.2\%$ was used. The average sample repeatability was 0.2%.

The concentration of particulate matter was determined using aliquots of 1 L river water filtered through pre-weighed glass fibre filters (Whatman GF/F) and dried until reaching a constant weight at 60 °C.

For the determination of U isotopes, the procedure reported by Rován and Štrok (2019) was used. U from the water sample was co-precipitated with $\text{Ca}_3(\text{PO}_4)_2$ and separated on the UTEVA column. U isotopes were eluted in a clean beaker with 15 mL of 1 M HCl. The eluate was evaporated to dryness, and the dry residue was digested three times with a mixture of HNO_3 and H_2O_2 before the measurements to destroy any possible organic residue that might co-elute from the resin.

The PHREEQC programme was used to calculate the concentration of dissolved inorganic carbon, the distribution of C species and the saturation indices of water with respect to calcite (SI_{calc}) (Parkhurst and Appelo, 1999).

The calcite precipitation rate (R) was calculated as described by Zavadlav et al. (2017) using the diffusion boundary layer (DBL) model by Buhmann and Dreybrodt (1985) as

$$R = \alpha \cdot \left([\text{Ca}^{2+}] - [\text{Ca}^{2+}]_{\text{eq}} \right) \quad (2)$$

where α is the reaction constant, and $[\text{Ca}^{2+}]$ and $[\text{Ca}^{2+}]_{\text{eq}}$ are the concentrations of dissolved Ca^{2+} in the solution and in the equilibrium with calcite at ambient conditions determined in the field. The α values considered the temperature range measured in the Krka River (between 15 and 23.6 °C). The DBL thickness was considered to be 100 μm given that the turbulent conditions in the river prevail, and for the available water layer thickness, a value of 10 cm was taken at all sampling sites (Liu et al., 1995; Liu and Dreybrodt, 1997).

3.2.2. Tufa, bedrock and soil

Samples of bedrock, soil and tufa were dried at 105 °C until reaching a constant weight and were crushed in bras mortar. After the removal of all visible plant remains, the samples were pulverised in a vibrating disk mill (Siebtechnik GmbH, Germany) and sieved below 90 μm .

For the elemental analysis, disks melted in the furnace (Claissie, Malvern Panalanalytical, Malvern, U.K.) were prepared with a mixture of Fluxana powder (FX-X50-2, 50% Li-tetraborate and 50% Li-metaborate) in the sample:Fluxana with a ratio of 1:10. A few drops of LiBr were added to avoid gluing the melt onto the platinum vessel. The measurement was performed using X-ray fluorescence spectroscopy (Thermo Scientific ARL Perform'X Sequential XRF, 60 kV, 40 mA, Thermo electron SA, Ecublens, Switzerland) with OXAS software. The XRF data were characterised using the software UniQuant 5. The calculated analytical errors were <0.1% for Ca, <6% for Mg, Al and Si and <15% for Na and K.

The non-carbonate fraction of rocks and soil was determined arbitrary as the sum of Al_2O_3 , SiO_2 , Fe_2O_3 , Na_2O and K_2O determined by the XRF.

A semiquantitative X-ray diffraction analysis was performed on dried pulverised samples in the range from 4° to 70° in steps of 0.013° under cleanroom conditions with an Empyrean PANalytical X-Ray Diffractometer (Thermo Scientific, Thermo electron SA, Ecublens, Switzerland). The mineral analysis along with standard-less Rietveld refinement was performed on XRD data using the X'Pert Highscore plus 4.1 software.

A stable isotope analysis of carbon and oxygen in carbonate was performed using the Europa 20-20 isotope ratio mass spectrometer upgraded with a Sercon HS source assembly and 20-22 electronic suite (Sercon Ltd., Crewe, U.K.). The pulverised samples were placed in Labco Exetainers®, dried overnight at 60 °C, sealed with septum caps and flushed with He (6.0). Then, 0.3 mL of hot 100% H_3PO_4 was injected into the vials. The acid was prepared following the instructions by Sharp (2017). The samples were digested for 72 h at 40 °C in a thermoblock fitted to the ANCA TG preparation unit for the trace gas analysis. All

samples were measured in triplicate, and the results were accepted if the standard deviation was equal or less than 0.1‰ for both $\delta^{13}\text{C}$ and $\delta^{18}\text{O}$. If the deviation was larger, the analysis was repeated until the required precision was achieved. The measurements were calibrated to the VPDB scale using NBS 19 and IAEA CO-9 certified reference materials. As controls, working standards IAEA-C2 with $\delta^{13}\text{C}_{\text{VPDB}}$ and $\delta^{18}\text{O}_{\text{VPDB}}$ values of -8.25 and -8.97% , respectively (Bernasconi et al., 2018), and KH2 with $\delta^{13}\text{C}_{\text{VPDB}}$ and $\delta^{18}\text{O}_{\text{VPDB}}$ values of 1.89 and -2.90% , respectively, were used.

Concentrations of Ca, Mg, U and U isotopes were analysed in bulk samples and in leachable fractions. A soft, less invasive leaching procedure was applied to extract carbonate-associated metals (Štrok and Smodiš, 2010); however, the procedure dissolved some easily soluble hydroxides and adsorbed metals in addition to calcite (Malov and Zykov, 2020). Therefore, it is hereafter referred to as a 'leachable' fraction, while the undissolved residue is referred to as a 'residual' fraction and was comprised of acid insoluble minerals (e.g. silicates, oxides). Theoretically, if dolomite were present in the sample, a minor portion of undissolved dolomite would also occur in the residual fraction (Rován et al., 2020).

For leaching, an aliquot of 1 g of tufa powder was precisely weighed in a centrifuge tube. 15 mL of 1 M sodium acetate (NaAc) in 25% acetic acid (HAc) were added, and the samples were then shaken for 2 h at room temperature. Next, the samples were centrifuged and filtered through 0.45 μm pore size Millipore filters and washed two times with 5 mL of deionized water. Small aliquots of the eluate were used for Mg and Ca analyses by ICP-MS, while the remainder was dried on a hotplate and re-dissolved in 5 mL of 3 M HNO_3 to be prepared for column chromatography.

The concentrations of total carbon (C), organic carbon (OC) and nitrogen (N) were determined in 5 to 7 mg of dried sediment ground in an agate mortar before analysis. Aliquots for total carbon and nitrogen were prepared in tin containers, while samples for organic carbon were weighed in silver containers. Prior to analysis, the aliquots for OC were acid-treated with 1 M, 2 M and 6 M HCl. This procedure was repeated until no visual effervescence was evident. The analysis was performed using a Vario Micro Cube elemental analyser (Elementar Langensfeld, Germany) with a combustion at 1150 °C. The samples were analysed in replicates, and the results were reported as the mean and standard deviation per sample.

The total dissolution of the samples (Trdin et al., 2017) was performed to test the separation of detrital fraction in the leached samples. Aliquots of 1 g of powdered samples were digested with lithium borates fusion. In a platinum crucible, approximately 4 g of lithium borates were added to the sample, and the fusion was performed in a Claissie LeoNeo furnace at 1050 °C for 23 min. The obtained glass was dissolved in glass beakers at 135 °C in 100 mL of deionized water with the addition of 10 mL of concentrated HNO_3 . After dissolution, the beakers were left on the hotplate with continuous stirring until the volume was reduced to 50 mL, which resulted in a 2–3 M HNO_3 solution. The solution was then cooled to 90 °C, and 1 mL of 0.2 M polyethylene glycol solution (PEG) was added to remove silicates. The stirring continued for 1 h. The precipitate was left to settle overnight, and the remaining solution was filtered and subjected to column chromatography.

U was separated from the matrix using UTEVA extraction chromatography in the same way as was described for the water samples.

The U concentration in the samples was determined using an Agilent 8800 Triple Quadrupole ICP-MS (Agilent Technologies, California, USA) following a measurement protocol that was described by Rován and Štrok (2019). Interference correction and external calibration were performed using the U standard reference material SRM-3164 (National Institute of Standards & Technology, Gaithersburg, MD, USA).

3.2.3. U isotope measurements

U isotope ratios were measured using a Nu plasma II (Nu Instruments Ltd., UK) MC-ICP-MS with the high-efficiency Aridus II™ (Cetac

Technologies, NE, USA) sample desolvation system as described by Rovani and Štrok (2019). The total process blanks for the U isotopic analysis ranged from 0.08 ng to 0.28 ng. The procedural blanks were negligible compared to the amount of U contained in the samples. U isotope ratios are expressed as delta notation (Eq. (1)) and as $^{234}\text{U}/^{238}\text{U}$ activity ratios (Eq. (3)).

$$\frac{^{234}\text{U}}{^{238}\text{U}} \text{ activity ratio} = \lambda_{234}/\lambda_{238} \times (^{234}\text{U}/^{238}\text{U})_{\text{corrected}} \quad (3)$$

The $\delta^{238}\text{U}$ values were determined relative to the IRMM-184 standard and were recalculated to the $\delta^{238}\text{U}_{\text{CRM-112a}}$ values to assure comparability with previously published data (Standards for Nuclear Safety Security and Safeguards Unit, 2019). The $^{234}\text{U}/^{238}\text{U}$ activity ratio was calculated from the mass bias corrected isotope ratios and by using the decay constants (λ_{234} and λ_{238}) reported by Cheng et al. (2013).

The long-term analytical precision was assessed using the measurements of the U isotopic standard (IRMM-184) at a 5 ng mL^{-1} concentration over a period of 15 months. The mean values of the $^{235}\text{U}/^{238}\text{U}$ and $^{234}\text{U}/^{238}\text{U}$ isotope ratios of U standards are $(7.2622 \pm 0.0049) \times 10^{-3}$, $(5.314 \pm 0.017) \times 10^{-5}$ and $(3.113 \pm 0.083) \times 10^{-6}$, respectively. The measured values are in agreement with certified reference values (Standards for Nuclear Safety Security and Safeguards Unit, 2019). The uncertainty on measured U isotopes was expressed in terms of the expanded uncertainty ($k = 2$) and was assessed from different sources of measurement uncertainty, which are described in more detail by Rovani and Štrok (2019). The reproducibility of replicate measurements was within 0.5% for the $^{234}\text{U}/^{238}\text{U}$ isotope ratios and 0.1% for the $\delta^{238}\text{U}$ values.

4. Results and discussion

Tabulated results of the elemental and isotopic analyses of water, tufa, bedrock, and soil samples are available in Supplementary materials.

4.1. Precipitation of tufa: insight from C and O stable isotopes

The prerequisite for the precipitation of tufa is a high supersaturation of water with respect to calcite. While the carbonate sheath impregnations in sluggish water were reported already at 1.6 to 2 times supersaturation (Merz-Preiß and Riding, 1999), the spontaneous carbonate precipitation at cascades and waterfalls occurs when supersaturation increases up to 4 to <10 times (Srdoc et al., 1985; Herman and Lorah, 1988). The precipitation of carbonate in rivers is triggered by the degassing of CO_2 , particularly (but not only) at topographic discontinuities (Pedley, 1990; Drysdale et al., 2002; Andrews and Brasier, 2005; Golubic et al., 2008; Capezzuoli et al., 2014). Major and trace elements, such as Mg, Sr, U etc., can co-precipitate with calcite, where the partitioning between water and carbonate results from the cumulative effects of the chemical composition of water, temperature, pH, speciation and adsorption on mineral surfaces, precipitation rate and microbial communities in the river (Rihs et al., 2000; Huang and Fairchild, 2001; Frank et al., 2006; Saunders et al., 2014; Chen et al., 2016; Ritter et al., 2018).

In the Krka River, a strong degassing of ^{13}C -depleted CO_2 without any notable CaCO_3 precipitation occurred between the spring (site K1) and Bilušića buk (K2), which is reflected by a decreased $p\text{CO}_2$ and concentration of DIC, an increased $\delta^{13}\text{C}$ value of DIC and an increased saturation index of calcite (Fig. 2a and b). In the tufa precipitating section of the river (sites K2–K6), the saturation index varied between 0.83 and 1.05, i.e. 6.8 to 11.1 times supersaturation. These values are very close to the SI_{calc} values reported for late summer in the period from 2001 to 2002 (0.87 to 1.17) (Lojen et al., 2004). The measured data on water in this study are only a snapshot of the physicochemical situation of the river, whereas the accumulation of tufa is a slow process, which

proceeds at a rate of <1 to about 19 mm year^{-1} (Maric et al., 2020). Individual hand samples of tufa analysed in this study were 5 to 10 cm thick, which means that their accumulation took several years to decades. Therefore, the isotopic composition of C and O in tufa shall be compared with the long-term ranges of historic data on the $\delta^{13}\text{C}$ values of DIC and the $\delta^{18}\text{O}$ values of water, which are presented in Fig. 2c and d (ranges of values taken from Lojen et al., 2004; Lojen et al., 2009; Cukrov et al., 2012). The $\delta^{13}\text{C}$ values of recent tufa were on average $-9.60 \pm 0.65\text{‰}$ and within the range of a $\pm 1\text{‰}$ deviation from the $\delta^{13}\text{C}$ values of DIC as predicted by Romanek et al. (1992) and Jimenez-Lopez et al. (2006). Although at the lowermost waterfall both analysed samples were strongly depleted in ^{13}C compared to the DIC analysed in this study, the $\delta^{13}\text{C}$ values of both tufa samples were within the long-term range of the $\delta^{13}\text{C}$ values of DIC. The O isotope composition of recent tufa analysed in this study were on average $-8.08 \pm 0.41\text{‰}$ and was almost identical to those determined 20 years earlier at the same locations (Lojen et al., 2004). The differences among the pairs of tufa samples from opposite riverbanks at sites K5 and K6 found in this study are surprisingly large because the differences in the $\delta^{18}\text{O}$ values of water measured at both riverbanks were small or within the analytical uncertainty.

Bonacci et al. (2017) analysed the hydrological situation at site K6 (Skradinski buk) in detail. The entire waterfall area consists of several unevenly distributed steps and dozens of small basins, where water flows relatively independently on the left and the right side during low flow conditions. The tributary Čikola that discharges into the Krka River from the left (eastern) side just above the waterfall regularly dries out during the summer, but the subsurface groundwater discharge continues through numerous submerged springs downstream into the estuary (Liu et al., 2019). Considering this, it is obvious that the hydrological conditions, hydrochemical composition and isotopic characteristics at the right and the left side of the river can be different. Unfortunately, no hydrological study of the analysed cascades of Roški slap area (K5) was done, but similar to Skradinski buk, the surface river flow splits into several channels and pools separated by small tufa islands with abundant vegetation at a lower discharge. Meanwhile, at a high water level, both riverbanks are flooded. On one hand, this can explain the larger fraction of detrital non-carbonate matter in tufa at site K5 compared to site K6 (5.3 and 6.3% at K5a and b compared to 1.5 and 1.7% at K6a and b) and the higher amount of organic carbon in tufa (0.6 and 1.1 wt% at K5a and b compared to 0.53% at both K6 sites, Table S2, Supplementary materials). The 2019 sampling campaign was conducted at a high water level when the left and right flows of the river were connected. At a low discharge, the differences could be larger, but no long-term monitoring data of $\delta^{18}\text{O}$ values of water at both river banks are available.

The carbonate precipitation in isotopic disequilibrium in rivers is not uncommon (Yan et al., 2020) and was observed even in controlled laboratory experiments for both C (Jimenez-Lopez et al., 2006) and O isotopes (Dietzel et al., 2009). Previous studies showed that in the Krka River, the carbonate precipitated close to the O isotope equilibrium only at the uppermost tufa barrier (K2). Further downstream, the discrepancy between the equilibrium $\delta^{18}\text{O}$ values of water and precipitate formed in the actual temperature range increased with an increasing annual average temperature and an increasing annual temperature variability of river water. In contrast to C isotopes, the O isotope fractionation between water and carbonate during the precipitation of calcite depends on the precipitation rate to a similar or even greater extent as on the temperature (Dietzel et al., 2009). The calculated calcite precipitation rates for the given conditions of temperature, pH and chemical composition of water at the time of sampling varied from $4.9 \cdot 10^{-9} \text{ g cm}^{-2} \text{ s}^{-1}$ at sites K2 and K6b to $5.6 \cdot 10^{-9} \text{ g cm}^{-2} \text{ s}^{-1}$ at site K4 (Table 1). Dietzel et al. (2009) found that with an increasing precipitation rate, the O isotope fractionation between water and calcite decreases, and this was confirmed by the study of tufa precipitation in a karstic river in Slovenia (Zavadlav et al., 2017). In the Krka River, the

L. Rován, T. Zulfiani, B. Horvat et al.

Science of the Total Environment 797 (2021) 149103

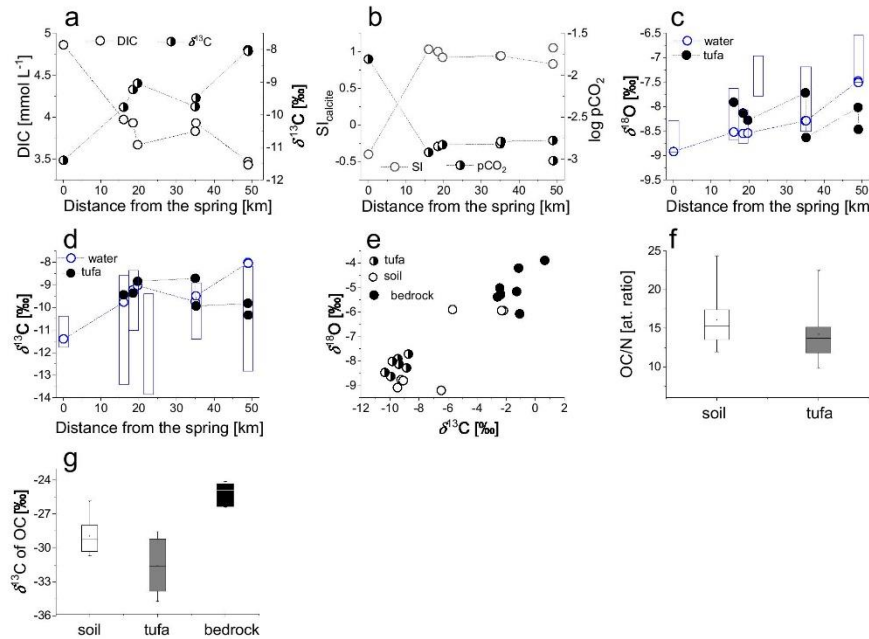


Fig. 2. Downstream variation of concentration and C stable isotope composition of dissolved inorganic carbon (a); saturation index of calcite and log pCO₂ (b); stable isotope composition of oxygen in the Krka River water and in tufa (c); stable isotope composition of dissolved inorganic C and carbonate in tufa (d); ranges of values of organic C to total N ratios in soil and tufa (f); and ranges of δ¹³C values of organic C in soil, tufa and bedrock (g). Hollow bars in (c, d) represent the range of values measured in the period 2000 to 2007 (Lojen et al., 2004; Lojen et al., 2009; Cukrov et al., 2012). The bar at 22 km represents the sampling site from 2001 to 2007 (Miljacka hydroelectric power plant), which was not accessible in 2019.

smallest O isotope fractionation between water and tufa was indeed observed at sites with the highest precipitation rates (K4, K5b), while a larger O isotope fractionation was found at sites with lower precipitation rates (K2 and K6). Still, the differences in the precipitation rate cannot account for the big differences observed between O isotope composition of carbonate from both riverbanks at sites K5 and K6.

The δ¹³C and δ¹⁸O values of tufa can be affected by the incorporation of suspended detrital carbonate washed out from soil, bedrock and eroded recent or old tufa. Fig. 2e shows the δ¹³C vs. δ¹⁸O plot of bedrock,

soil and tufa, and it is evident that tufa and bedrock carbonates form two separate groups, while the soil samples plot was in between the two groups with the whole range of values from typical of marine carbonate to typical of tufa. The lowest measured δ¹⁸O value in the soil (−9.48‰) was even lower than in any of the tufa samples. The presence of detrital carbonate from bedrock and soil can thus considerably alter the C and O isotope signatures of tufa and can be captured in tufa along with non-carbonate detritus. Hence, the relatively high δ¹³C values of tufa at sites K5a and K6a could be attributed to the washout of ¹³C-

Table 1

Measured physicochemical, elemental parameters, and isotopic analyses in river water from Krka River (K) and Zrmanja River (Z). Exact locations of sampling sites can be found in Fig. 1.

Site	Distance from the spring [km]	Temperature [°C]	pH	Conductivity [μS cm ⁻²]	Redox potential [mV]	Total alkalinity [mmol L ⁻¹]	Particulate matter [mg L ⁻¹]	Ca ²⁺ [mg L ⁻¹]	Mg ²⁺ [mg L ⁻¹]	R · 10 ⁻⁹ [g cm ⁻² s ⁻¹]
K1	0	9.9	7.11	426	111	4.03	4.2	56.8	14.3	ND
K2	16	15.0	8.21	726	96	4.01	2.0	119.7	19.7	4.9
K3	18.8	16.7	8.15	686	94	3.95	0.3	116.5	20.0	5.3
K4	19.7	17.2	8.10	688	98	3.68	<0.1	117.3	20.6	5.6
K5a	35	19.6	8.12	612	138	3.85	<0.1	104.1	17.1	5.4
K5b	35.5	19.7	8.10	617	111	3.94	1.6	105.3	17.3	5.5
K6a	49	23.1	8.07	481	163	3.48	6.5	83.7	12.8	5.2
K6b	49.5	23.6	8.31	469	113	3.54	13.5	80.8	12.0	4.9
Z1	16	NM	NM	NM	NM	3.41	1.3	52.6	11.0	ND
Z2	38	NM	NM	NM	NM	4.30	<0.1	70.7	6.2	ND
Z3	50	NM	NM	NM	NM	3.74	0.3	64.9	6.1	ND

NM: not measured; ND: not determined.

enriched soil and bedrock carbonate. This assumption is also supported by the C/N ratio of sedimentary organic matter in tufa (Fig. 2f), which is 14.6 ± 4.3 and is similar to that of the soil (16.1 ± 3.7). The same range of values was reported for riverine particulate organic matter, where fine particulates had an OC/N ratio between 10 and 16 and coarse ones between 14 and 25 (Hatten et al., 2012). C/N ratios above 20 are typical of terrestrial organic matter derived from vascular plants (Meyers, 1994), while the microbial (algal and bacterial) biomass has C/N ratios typically <10 (Kendall et al., 2001). The low $\delta^{13}\text{C}$ values of sedimentary organic C in tufa (average value of $-31.57 \pm 2.32\%$, Fig. 2g) reflect a mixture of soil organic matter and autochthonous riverine organic material derived from algae and highly ^{13}C -depleted vascular plants growing in the spray zone of the river (Marcenko et al., 1989).

The variability of the C and O isotopic signatures of Krka River tufa at consecutive barriers is therefore interpreted as a result of an annual fluctuation of the isotope composition of water, DIC, temperature, variable precipitation rates and variable fractions of lithic and soil carbonate incorporated into the tufa fabrics.

4.2. Uranium in water

The total dissolved U concentrations in the Krka and Zrmanja water fell within the typical range for rivers fed from carbonate aquifers (Alshamsi et al., 2013; Guerrero et al., 2016; Chen et al., 2020; Rován et al., 2020). In the tufa-precipitating river, the concentration of dissolved U decreased toward the estuary from 0.67 to 0.46 ng L^{-1} (Fig. 3a). A similar trend with maximum concentrations of dissolved load between sites K2 and K4 (16 to 20 km downstream from the spring) and decreasing values afterwards was observed for other metals in this (Table 1) and previous studies (Cukrov et al., 2008, 2013), which indicates that U, along with other dissolved metals, is subjected to active self-purification processes of adsorption, sedimentation and co-precipitation with carbonate. The main sedimentation basins are lakes Brljan between sites K2 and K3, the lake between sites K4 and K5 and lake Visovac between sites K5 and K6 with average sedimentation rates of 10, 8 and 7 mm per year, respectively (Cukrov et al., 2013). The Zrmanja River was depleted in U compared to the Krka River (Table S1, Supplementary materials), and the invasion of water masses from the Zrmanja sub-catchment between sites K3 and K5 could also contribute to the decrease in the dissolved U load in the Krka River. A conspicuous difference in the dissolved U concentration in the areas of cascades at sites K5 (Roški slap) and K6 (Skradinski buk) occurred between the right (K5a, K6a) and the left riverbanks (K5b, K6b). This difference is also reflected in the U content in bulk and leachable fraction of tufa at sites K5a and K5b; however, no such difference was noted in tufa at sites K6a and K6b (Fig. 3a). Because tufa integrates a long-term hydrochemical composition of water, it can be expected that at sites

K5a and b, the difference in the U concentration in the water at both riverbanks is likely systematic. Different environmental conditions at both riverbanks can obviously affect the dissolved U concentrations in the river at very short distances, which are then transferred to the river sediments.

The dissolved $^{234}\text{U}/^{238}\text{U}$ activity ratio has become a trusted tracer of groundwater and river water sources, reflecting the variability of the discharge and lithology of the catchment (Fleischer, 1982; Riotte and Chabaux, 1999; Chabaux et al., 2003; Riotte et al., 2003; Durand et al., 2005; Chabaux et al., 2008; Kraemer and Brabets, 2012; Guerrero et al., 2016; Zebracki et al., 2017; Navarro-Martinez et al., 2020; Rován et al., 2020). The enrichment of water in ^{234}U relative to bedrock depends on the rock type, permeability and groundwater transit time as well as on the weathering rate (Li et al., 2018). The interpretation of $^{234}\text{U}/^{238}\text{U}$ activity ratios in water is therefore never simple or straightforward.

The activity ratios of $^{234}\text{U}/^{238}\text{U}$ in the Krka River (Fig. 3b) generally decreased downstream from the spring, from 1.49 to 1.28, and is consistent with the findings of Suksi et al. (2006). In the reducing environment of the aquifer, due to the alpha recoil effect, ^{234}U is oxidised, while ^{238}U remains in the less soluble reduced form. Consequently, the solubility of ^{234}U is increased, and the $^{234}\text{U}/^{238}\text{U}$ activity ratio in groundwater at the orifice exceeds the equilibrium value of 1. In the aerated stream, the dissolution of U-containing particulates continues in the oxygenated environment, where ^{234}U and ^{238}U are released to the solution in equal proportions. Therefore, the $^{234}\text{U}/^{238}\text{U}$ activity ratio slowly decreases downstream. Another process that could decrease the dissolved $^{234}\text{U}/^{238}\text{U}$ activity ratio downstream is the dissolution of the finest suspended mineral particles. Thollon et al. (2020) analysed the river sediments of world largest rivers and found that the sediments in rivers draining catchment areas composed of sedimentary rocks generally had a clay fraction (that is transported as suspended load) enriched in ^{238}U compared to the coarser fraction. The dissolution of the finest suspended particles with a $^{234}\text{U}/^{238}\text{U}$ activity ratio around or below 1 would in fact push the $^{234}\text{U}/^{238}\text{U}$ activity ratio of water toward lower values.

The plateau of $^{234}\text{U}/^{238}\text{U}$ activity ratios of 1.38–1.39 occurred between sites K3 and K5, while at the lowermost waterfall, the $^{234}\text{U}/^{238}\text{U}$ activity dropped to 1.29. The Zrmanja River at site Z1 upstream from the temporary sink had a $^{234}\text{U}/^{238}\text{U}$ activity ratio of 1.51, so the inflow of ^{234}U -enriched groundwater from the Zrmanja River in the K3-K5 river sections could in part neutralise the general decreasing trend of the $^{234}\text{U}/^{238}\text{U}$ activity ratio of Krka River water. However, since the annual variability of the $^{234}\text{U}/^{238}\text{U}$ activity ratio of Zrmanja River water and the travel time of groundwater discharging into the Krka river are not known, the influence of Zrmanja River water on the $^{234}\text{U}/^{238}\text{U}$ activity ratios of Krka river at this stage remains a plausible explanation but cannot be quantified.

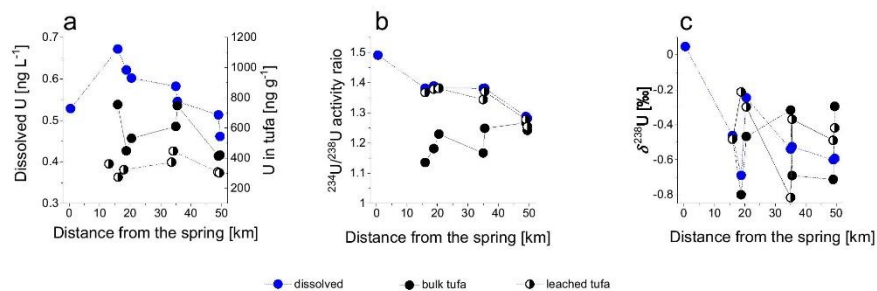


Fig. 3. Downstream variations of U concentrations (a); $^{234}\text{U}/^{238}\text{U}$ activity ratios (b); and $\delta^{238}\text{U}$ values (c) in dissolved U in water, bulk tufa and in the leachable fraction of tufa.

The flow section between sites K2-K5 is characterised by massive tufa precipitation at waterfalls and by intensive sedimentation in lentic sections of the river. Sedimentation of fine particles in lakes between sites K2 and K3, K4 and K5 and K5 and K6 is reflected by the decreased amount of particulate matter in the river between sites K2 and K5, from 2.0 mg L^{-1} to $<0.1 \text{ mg L}^{-1}$ (Table 1). Brennecke et al. (2011) and Jemison et al. (2016) analysed the ^{235}U - ^{238}U isotope fractionation induced by the adsorption of U species onto mineral surfaces and found that adsorption on common sedimentary minerals, such as quartz, illite, goethite or Mn oxides, produces a notable fractionation with adsorbed U(VI) enriched in a light (^{235}U) isotope. Assuming the same mechanism could operate in the ^{234}U - ^{238}U isotope pair as well and that at pH values around 8 in oxygenated water the dissolved U is present in U(VI) ionic complexes with carbonate, preferential adsorption on mineral particles followed by the sedimentation of lighter U(VI) would then push the $^{234}\text{U}/^{238}\text{U}$ activity ratio of water toward lower values. The same explanation applies to the Zrmanja River, which is also intersected with several barriers with lentic sections in-between.

The downstream behaviour of the $\delta^{238}\text{U}$ values of the Zrmanja River is similar to that of the $^{234}\text{U}/^{238}\text{U}$ activity ratios (a decrease with the distance from the spring, -0.02‰ to -0.60‰), while in the Krka River, a conspicuous anomaly occurs in the short river section K2-K4, where values first decreased from -0.46‰ to -0.69‰ and then increased to -0.25‰ (Fig. 3c).

In both rivers, a positive correlation between the $\delta^{238}\text{U}$ and $^{234}\text{U}/^{238}\text{U}$ activity ratios existed, although in the Zrmanja River, the correlation was rather weak ($r^2 = 0.89$ in Krka and 0.53 in Zrmanja). Apparently, this should be a contradiction, but all $\delta^{238}\text{U}$ values of river water were in the range of those of contributing bedrock and soil (Fig. 4d). The dissolved U could thus be derived from the weathering of leachable and residual fractions of any of them in different and seasonally changing and/or event-driven proportions. In particular, the residual U in bedrock had a large range of $\delta^{238}\text{U}$ values (-1.78 to $+1.53\text{‰}$). It was established that the $\delta^{238}\text{U}$ values of dissolved U in rivers resemble those of bedrock and that $\delta^{238}\text{U}$ values of river water largely reflect the U isotope variations between catchments, with no correlation to the $^{234}\text{U}/^{238}\text{U}$ activity ratios or hydrochemical parameters (Weyer et al., 2008; Andersen et al., 2016; Noordmann et al., 2016). While the analysed bedrock and soils show a rather narrow range of

$\delta^{238}\text{U}$ values for bulk samples, the U isotope composition of leachable and in particular the residual U fraction were much more variable (for leachable fraction -0.78 to -0.11‰ for bedrock, -0.56 to -0.03‰ for soil; residual -1.78 to $+1.53\text{‰}$ in bedrock, -0.56 to -0.03‰ in soil). Therefore, the variability of the $\delta^{238}\text{U}$ values of dissolved U in rivers could be to a greater extent governed by the isotopically more diverse residual U fractions of the bedrock and soil.

4.3. Uranium in tufa

The C and O isotope analyses of tufa in the Krka–Zrmanja aquifer showed that the bedrock and soil contributed not only non-carbonate detritus and organic matter, but also detrital carbonate that altered the isotopic composition of carbonate. It is therefore reasonable to assume, that the concentrations and isotope composition of U in carbonate fraction of tufa would be affected by the soil- and bedrock-derived carbonate, too.

The only previous data on U concentration in tufa from the Krka River (Francišković-Bilinski et al., 2004) was in the same range of values as in this study (Fig. 4a). Frank et al. (2006) analysed a drill core from a post-glacial tufa sequence in Thuringia (Germany), found that U concentrations and isotopic compositions varied according to accumulation rate and texture, and were more likely to reflect the changes of the U concentration and isotope composition of precipitating water than contamination with non-carbonate detritus. The tufa from the Krka and Zrmanja Rivers was formed in different sedimentary environments (cascades at sites K2, K4 and K6, paludal settings at K5 and Z3 and dam at K3). The bulk U concentrations showed no relation with the depositional setting, while the leachable (predominantly carbonate) U concentration was higher at paludal sites, while cascade and dam tufa were in approximately the same range of values.

The majority of U in recent tufa was bound to a leachable fraction (60–75%), which is less than in bedrock (70–88%) but much more than in the soil (14–33%) (Fig. 4a, Table S3, Supplementary materials). The exceptions were sites K2 (cascade) and Z3 (Zrmanja River, paludal tufa), where only 48% and 38% of U, respectively were leachable. Obviously, the governing factor for the incorporation of U into the leachable fraction of tufa is the concentration of dissolved U, which co-precipitates with the carbonate phase or is adsorbed to detrital minerals and

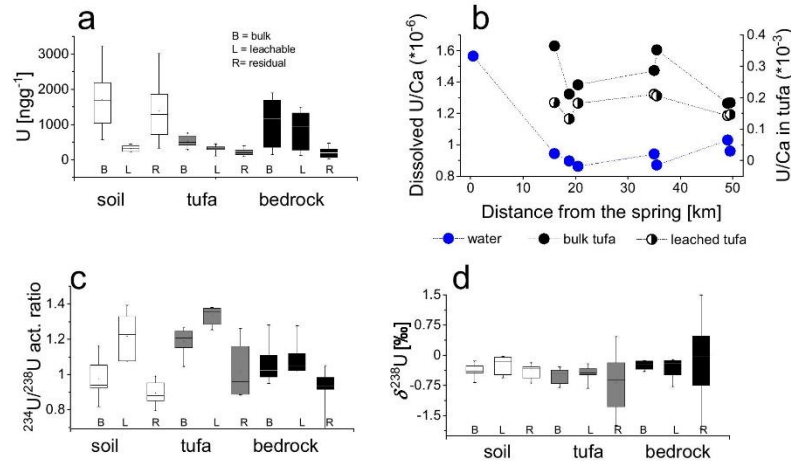


Fig. 4. Ranges of U concentrations in bulk, leachable and residual fractions of soil, tufa and bedrock (a); downstream variation of U/Ca ratio in water, bulk and the leachable fraction of tufa (b); ranges of $^{234}\text{U}/^{238}\text{U}$ activity ratios (c); and $\delta^{238}\text{U}$ values (d) in bulk, leachable and residual fractions of soil, tufa and bedrock.

deposited in tufa. The high affinity of $U(VI)O_2^{2+}$ to carbonate in an aerated environment results in the formation of $UO_2(CO_3)_2^{2-}$ complexes at pH < 6 and $UO_2(CO_3)_3^{4-}$ at a pH > 8. On one hand, this increases the solubility of U (for instance from soil) (Elless and Lee, 1998), while on the other hand, it facilitates the adsorption of U to carbonate surfaces (Krestou and Panias, 2004; Kelly et al., 2006) and its co-precipitation with calcite (Cumberland et al., 2016; Chen et al., 2016).

The composite processes of adsorption and co-precipitation of U in carbonate were suggested by Rihs et al. (2000), who found irregular U concentrations in a downstream profile of carbonate precipitated from a CO_2 -rich geothermal spring, where the apparent partitioning coefficients of U decreased with advanced precipitation. In the Krka River, the U/Ca ratio of water (Fig. 4b) decreased from sites K2 to K4 and then slightly increased toward K6. The $(U/Ca)_{carb}$ ratio of tufa scattered irregularly downstream, yielding downstream scattering of apparent distribution coefficients of U ($K_d = (U/Ca)_{carbonate} / (U/Ca)_{water}$) between 0.14 and 0.24 (0.06 in the Zrmanja River). These values are lower than those calculated by Rihs et al. (2000) for thermal water but close to values reported by Meece and Benninger (1993) for coral carbonate (0.05 to <0.2). No correlation between K_d and temperature, pH or precipitation rate was observed. Obviously, the U partitioning between water and leachable fraction of tufa in the Krka River is affected by several processes, which cannot be unambiguously disentangled and are further complicated by the diffuse groundwater recharge and consecutive interchange of the lentic and lotic sections of the river flow, which most likely plays a significant role in the U geochemistry.

The $^{234}U/^{238}U$ ratio of the leachable fraction in recent tufa resembles the $^{234}U/^{238}U$ activity ratio of water (1.25–1.37 in tufa and 1.28–1.49 in water) (Fig. 3b). No information on $^{234}U/^{238}U$ isotope fractionation during the precipitation of carbonate could be found in the literature. The obtained differences are small but larger than the uncertainty of the measurement at all sites except K4 and can be attributed to the presence of soil- and bedrock-derived detrital carbonate in tufa (Fig. 4c).

In contrast to $^{234}U/^{238}U$, the $^{238}U/^{235}U$ isotope fractionation during the precipitation of carbonate from aquatic solutions was studied in many laboratory experiments. At the pH range typical of karst water (7.5 and 8.5), no resolvable $^{238}U/^{235}U$ isotope fractionation could be observed (Chen et al., 2016), implying that the carbonate $\delta^{238}U$ value should be the same as that of the mother solution. Further experiments with seawater showed that the $^{238}U/^{235}U$ isotope fractionation could depend on the pH, ionic strength, pCO_2 and Mg^{2+} and Ca^{2+} concentrations (Chen et al., 2017). In natural terrestrial environments, highly variable U isotope fractionation was observed in speleothems, i.e. in authigenic carbonates precipitated in stable cave conditions from drip water (Stirling et al., 2007), while for river carbonate no data could be found. The $\delta^{238}U$ values of the leachable fraction of recent tufa analysed in this study were between -0.82 and -0.21% . The $\delta^{238}U$ values of the residual U fraction in tufa varied between -1.73 and $+0.46\%$ compared to -1.78 to $+1.53\%$ in the residual fraction of bedrock and -0.69 to -0.19% in the soil (Fig. 4d). Clearly, the residual fraction of tufa is a mixture of bedrock- and soil-derived detritus. The isotope separation between leachable U and river water was between -0.28 and $+0.48\%$ (Fig. 3c), although it is assumed that authigenic carbonates incorporate $\delta^{238}U$ values of the mother solution without significant isotope fractionation (Stirling et al., 2007; Andersen et al., 2014; Chen et al., 2016). For sample sites K2, K4, K5b and K6, this was indeed the case (most were within the standard uncertainty of the analysis of -0.1%). Small differences can be explained by the isotope fractionation during adsorption on mineral surfaces, which was found to be around 0.2% (Brennecke et al., 2011; Jemison et al., 2016). Similar isotope fractionation was reported to occur during the abiotic reductive precipitation of U (Brown et al., 2018), although this would be less likely in aerated river environment. At sites K3 and K5a, the differences in the $\delta^{238}U$ values between the leachable fraction of tufa and river water were too large to be attributed to adsorption-related fractionation. In the tufa from site K3, the leachable $\delta^{238}U$ values are 0.48% higher

than the $\delta^{238}U$ values of the water, while at site K5a, the leachable fraction of tufa is depleted in ^{238}U compared to the river water or any other leachable U source. Similar to $^{234}U/^{238}U$, a long-term observation of the isotopic composition of dissolved U and particulate U in water would be necessary to shed more light on U isotope fractionation in the tufa-precipitating stream.

4.3.1. Can U isotopes be the identifier of authigenic carbonate in tufa?

To roughly estimate the possible contributions of detrital leachable U from soil and bedrock to leachable U in tufa, the IsoSource mixing model (EPA) was used to calculate the mixing ratios of several contributing sources; however, the uncertainty of the results is highly dependent on the uncertainties of the end-members, which are in the case of tufa in the Krka River large. For calculation, the average $^{234}U/^{238}U$ activity ratios of soil and bedrock leachable fractions (1.22 and 1.08, respectively) and the $^{234}U/^{238}U$ activity ratio of water at each site were used (Figs. 3b and 4c). The calculation revealed that in the upper reaches of the Krka River (sites K2–K4), the most feasible combinations of sources were 80–84% of authigenic carbonate, 11–13% of soil carbonate and 5–7% of bedrock carbonate. In lower reaches, at cascades K6a and K6b, the distribution of sources was 41–61% of carbonate, 30–38% of soil and 9–13% of bedrock detrital carbonate. For paludal sites K5a,b and Z3, the most feasible distribution was 65–81% of authigenic carbonate, 13–26% of soil and 6–9% of bedrock detrital carbonate. The uncertainty for soil and bedrock contributions in some cases exceeded 100% because the $^{234}U/^{238}U$ activity ratios of soil and bedrock carbonate are highly variable. Interestingly, both potential sources had $^{234}U/^{238}U$ activity ratios higher than 1. The enrichment of soils in ^{234}U was explained by the addition of U to soils from ^{234}U -enriched soil solutions (Huckle et al., 2016), while the high $^{234}U/^{238}U$ activity ratio of the leachable fraction of bedrock was surprising because all analysed rock formations were of the Cretaceous to the Eocene age (Mamudžić, 1971); however, a bulk $^{234}U/^{238}U$ activity ratio up to 1.05 was previously reported by Deschamps et al. (2004) for limestone along stylolitic discontinuities in Mesozoic limestone. Although the mechanisms of the migration of ^{234}U were not fully explained, the same processes could alter the $^{234}U/^{238}U$ activity ratio of tectonically strongly disturbed carbonate rocks at Dinaric carbonate formations. The calculation for the estimation of contributing sources based on $\delta^{238}U$ values was not only speculative but, in some cases, not even possible because the tufa had lower or higher $\delta^{238}U$ values of leachable U than any of the potential contributing parameters. The best conclusion at this stage would be that the authigenic carbonate precipitated from a U-bearing river mostly resembles the $^{234}U/^{238}U$ activity ratio of dissolved U in water, but the presence of a detrital U-containing leachable phase can result in deviations from the $^{234}U/^{238}U$ activity ratio of dissolved U.

5. Conclusions

This study has demonstrated the use of U and its isotope ratios to better understand different possible environmental influences on tufa formation and to evaluate the contribution of the authigenic and detrital carbonate in tufa samples from the Krka and Zrmanja Rivers in Croatia, which could potentially be used to estimate the CO_2 storage in river carbonate. In the studied samples, the variability of classical geochemical parameters and traditional isotopes ($\delta^{18}O$, $\delta^{13}C$) showed that both detrital and authigenic carbonates are present in tufa and are affected by the suspended detrital carbonate in the river washed out from the bedrock and soil. The downstream profile of U concentration and the activity ratios of $^{234}U/^{238}U$ in the Krka River water showed effects of active self-purification processes of sedimentation, co-precipitation with carbonate, and adsorption of U species onto mineral surfaces followed by the preferential sedimentation of ^{234}U . The large scattering of $\delta^{238}U$ values in the Krka River showed that $\delta^{238}U$ is a much more sensitive tracer of bedrock composition than the $^{234}U/^{238}U$ activity ratios. The governing factor of the incorporation of U into tufa is the concentration

L. Rován, T. Zuliani, B. Horvat et al.

Science of the Total Environment 797 (2021) 149103

of dissolved U, which accumulates in the carbonate precipitate; however, the U partitioning between water and carbonate can be also affected by complicated hydrology, variable temperature, hydrological situation, and by detrital carbonates.

Overall, the U distribution and isotope composition in the carbonate fraction of tufa are controlled by many mechanisms and cannot be solely explained by any of them. In such a complex karst aquifer, geochemical parameters, traditional isotopes and U isotopic compositions are affected by the sources of materials for tufa precipitation and by environmental processes. Based on the present data and knowledge, some of the explanations are still speculative, so a long-term seasonal and event-based observation of the entire system, including water, suspended materials and precipitates, is needed to confirm the universality of conclusions.

CRediT authorship contribution statement

Leja Rován: Conceptualization, Data curation, Methodology, Visualization, Writing – original draft. **Tea Zuliani:** Methodology, Writing – review & editing. **Barbara Horvat:** Methodology, Writing – review & editing. **Tjaša Kanduč:** Methodology, Writing – review & editing. **Polona Vreča:** Methodology, Writing – review & editing. **Qasim Jamil:** Methodology. **Branko Čermelj:** Methodology, Writing – review & editing. **Elvira Bura-Nakić:** Funding acquisition, Data curation, Writing – review & editing. **Neven Čukrov:** Writing – review & editing. **Marko Štrok:** Supervision, Writing – review & editing. **Sonja Lojen:** Conceptualization, Data curation, Funding acquisition, Project administration, Visualization, Writing – original draft.

Declaration of competing interest

The authors declare that they have no known competing financial interests or personal relationships that could have appeared to influence the work reported in this paper.

Acknowledgement

This study was supported by the Slovenian Research Agency through the research project J1-9179, research programmes P1-0143 and P2-0075, the Young Researcher's programme and the Slovenian-Croatian bilateral collaboration project BI-HR-20-21-039. Research within this work was partially also funded by the Croatian Science Foundation, project IP-2018-01-7813, "REDOX". Special thanks to Mr. Tomislav Bulat (R. Bošković Institute), Mr. Stojan Žigon and Ms. Klara Nagode (J. Stefan Institute) for technical assistance and the National Park 'Krka' for the permission for sampling.

Appendix A. Supplementary data

Supplementary data to this article can be found online at <https://doi.org/10.1016/j.scitotenv.2021.149103>.

References

- Alshamsi, D.M., Murad, A.A., Aldaban, A., Hou, X., 2013. Uranium isotopes in carbonate aquifers of arid region setting. *J. Radioanal. Nucl. Chem.* 298, 1899–1905.
- Andersen, M.B., Romaniello, S., Vance, D., Little, S.H., Herdman, R., Lyons, T.W., 2014. A modern framework for the interpretation of $^{238}\text{U}/^{235}\text{U}$ in studies of ancient ocean redox. *Earth Planet. Sci. Lett.* 400, 184–194.
- Andersen, M.B., Stirling, C.H., Weyer, S., 2017. Uranium isotope fractionation. *Rev. Mineral. Geochem.* 82, 799–850.
- Andersen, M.B., Stirling, C.H., Zimmermann, B., Halliday, A.N., 2010. Precise determination of the open ocean $^{234}\text{U}/^{238}\text{U}$ composition. *Geochem. Geophys. Geosyst.* 11. <https://doi.org/10.1029/2010GC003318>.
- Andersen, M.B., Vance, D., Morford, J.L., Bura-Nakić, E., Breitenbach, S.F.M., Och, L., 2016. Closing in on the marine $^{238}\text{U}/^{235}\text{U}$ budget. *Chem. Geol.* 420, 11–22.
- Andrews, J.E., Brasier, A.T., 2005. Seasonal records of climatic change in annually laminated tufas: short review and future prospects. *J. Quat. Sci.* 20, 411–421.

- Avak, H., Brand, W.A., 1995. The fining MAT HDO-equilibration - a fully automated H₂O/gas phase equilibration system for hydrogen and oxygen isotope analyses. *Thermo Electron. Corp. Appl. News* 11, 1–13.
- Banks, V.J., Jones, P.F., 2012. Hydrogeological significance of secondary terrestrial carbonate deposition in karst environments. In: Kazemi, G.A. (Ed.), *Hydrogeology - A Global Perspective*. Intech, pp. 43–78.
- Bernasconi, S.M., Müller, I.A., Bergmann, K.D., Breitenbach, S.F.M., Fernandez, A., Hodell, D.A., Jaggi, M., Meckler, A.N., Millan, I., Ziegler, M., 2018. Reducing uncertainties in carbonate clumped isotope analysis through consistent carbonate-based standardization. *Geochem. Geophys. Geosyst.* 19, 2895–2914.
- Bonacci, O., 1999. Water circulation in karst and determination of catchment areas: example of the river zrnjanja. *Hydrol. Sci. J.* 44, 373–386.
- Bonacci, O., Andric, I., Roje-Bonacci, T., 2017. Hydrological analysis of skradinski Buk tufa waterfall (Krka River, dinaric karst, Croatia). *Environ. Earth Sci.* 76, 669.
- Bonacci, O., Jukić, D., Ljubenkov, I., 2006. Definition of catchment area in karst: case of the rivers Krčić and Krka, Croatia. *Hydrol. Sci. J.* 51, 682–699.
- Bourdon, B., Bureau, S., Andersen, M.B., Pili, E., Hubert, A., 2009. Weathering rates from top to bottom in a carbonate environment. *Chem. Geol.* 258, 275–287.
- Brennecke, G.A., Wasylenki, L.E., Bargar, J.R., Weyer, S., Anbar, A.D., 2011. Uranium isotope fractionation during adsorption to Mn-oxhydroxides. *Environ. Sci. Technol.* 45, 1370–1375.
- Brasier, A.T., Andrews, J.E., Marca-Bell, A.D., Dennis, P.F., 2010. Depositional continuity of seasonally laminated tufas: implications for $\delta^{18}\text{O}$ based palaeotemperatures. *Glob. Planet. Chang.* 71, 160–167.
- Brown, S.T., Basu, A., Ding, X., Christensen, J.N., DePaolo, D.J., 2018. Uranium isotope fractionation by abiotic reductive precipitation. *Proc. Natl. Acad. Sci.* 115, 8688–8693.
- Buhmann, D., Dreybrodt, W., 1985. The kinetics of calcite dissolution and precipitation in geologically relevant situations of karst areas: 1. Open system. *Chem. Geol.* 48, 189–211.
- Capuzzoli, E., Gandin, A., Pedley, M., 2014. Decoding tufa and travertine (fresh water carbonates) in the sedimentary record: the state of the art. *Sedimentology* 61, 1–21.
- Carter, J.F., Barwick, V.J., 2011. Good practice guide for isotope ratio mass spectrometry. *FIRMS* 1–41.
- Chabaux, F., Bourdon, B., Riotte, J., 2008. Chapter 3 U-series geochemistry in weathering profiles, river waters and lakes. *Radioact. Environ.* 13, 49–104.
- Chabaux, F., Riotte, J., Dequincey, O., 2003. U–th–ra fractionation during weathering and river transport. *Rev. Mineral. Geochem.* 52, 533–576.
- Chen, Q., Liu, S., He, H., Tang, J., Zhao, J., Feng, Y., Yang, X., Zhou, H., 2020. Seasonal variations of uranium in karst waters from northeastern Sichuan, Central China and controlling mechanisms. *Geochem. Int.* 58, 103–112.
- Chen, X., Romaniello, S.J., Anbar, A.D., 2017. Uranium isotope fractionation induced by aqueous speciation: implications for U isotopes in marine CaCO_3 as a paleoredox proxy. *Geochim. Cosmochim. Acta* 215, 162–172.
- Chen, X., Romaniello, S.J., Herrmann, A.D., Wasylenki, L.E., Anbar, A.D., 2016. Uranium isotope fractionation during coprecipitation with aragonite and calcite. *Geochim. Cosmochim. Acta* 188, 189–207.
- Cheng, H., Lawrence Edwards, R., Shen, C.-C., Polyak, V.J., Asmerom, Y., Woodhead, J., Hellstrom, J., Wang, Y., Kong, X., Spötl, C., Wang, X., Calvin Alexander, E., 2013. Improvements in ^{230}Th dating, ^{230}Th and ^{234}U half-life values, and U–Th isotopic measurements by multi-collector inductively coupled plasma mass spectrometry. *Earth Planet. Sci. Lett.* 371–372, 82–91.
- Čukrov, N., Čmuk, P., Mlakar, M., Omanovic, D., 2008. Spatial distribution of trace metals in the Krka River, Croatia: an example of the self-purification. *Chemosphere* 72, 1559–1566.
- Čukrov, N., Cuculić, V., Barišić, D., Lojen, S., Mikelić, I.L., Orešcanin, V., Vdovic, N., Fiket, Ž., Čermelj, B., Mlakar, M., 2013. Elemental and isotopic records in recent fluvio-lacustrine sediments in karstic river Krka, Croatia. *J. Geochem. Explor.* 134, 51–60.
- Čukrov, N., Tepić, N., Omanovic, D., Lojen, S., Bura-Nakić, E., Vojvodić, V., Pizeta, I., 2012. Qualitative interpretation of physico-chemical and isotopic parameters in the Krka River (Croatia) assessed by multivariate statistical analysis. *Int. J. Environ. Anal. Chem.* 92, 1187–1199.
- Cumberland, S.A., Douglas, G., Grice, K., Moreau, J.W., 2016. Uranium mobility in organic matter-rich sediments: a review of geological and geochemical processes. *Earth Sci. Rev.* 159, 160–185.
- De Boever, E., Brasier, A.T., Foubert, A., Kele, S., 2017. What do we really know about early diagenesis of non-marine carbonates? *Sediment. Geol.* 361, 25–51.
- Dedić, Ž., Ilijanić, N., Miko, S., 2018. A mineralogical and petrographic study of evaporites from Mali kukor, Vranjkovici and Slane stine deposits (Upper permian, Dalmatia, Croatia). *Geol. Croat.* 71, 19–28.
- Deschamps, P., Hillaire-Marcel, C., Michelot, J.-L., Doucelance, R., Ghaleb, B., Buschaert, S., 2004. $^{234}\text{U}/^{238}\text{U}$ disequilibrium along stylolitic discontinuities in deep mesozoic limestone formations of the eastern Paris basin: evidence for discrete uranium mobility over the last 1–2 million years. *Hydrol. Earth Syst. Sci.* 8, 35–46.
- Dietzel, M., Tang, J., Leis, A., Köhler, S.J., 2009. Oxygen isotopic fractionation during inorganic calcite precipitation - effects of temperature, precipitation rate and pH. *Chem. Geol.* 268, 107–115.
- Drysdale, R.N., Taylor, M.P., Ihlenfeld, C., 2002. Factors controlling the chemical evolution of travertine-depositing rivers of the barked karst, northern Australia. *Hydrol. Process.* 16, 2941–2962.
- Durand, S., Chabaux, F., Rihs, S., Düringer, P., Elsass, P., 2005. U isotope ratios as tracers of groundwater inputs into surface waters: example of the upper Rhine hydrosystem. *Chem. Geol.* 220, 1–19.
- Elless, M.P., Lee, S.V., 1998. Uranium solubility of carbonate-rich uranium-contaminated soils. *Water Air Soil Pollut.* 107, 147–162.
- EPA - United States Environmental Protection Agency, n., IsoSource: Stable Isotope Mixing Model for Partitioning an Excess Number of Sources, Version 1.3.1. accessible

- at. <https://www.epa.gov/eco-research/stable-isotope-mixing-models-estimating-source-proportions>.
- Epstein, S., Mayeda, T., 1953. Variation of O18 content of waters from natural sources. *Geochim. Cosmochim. Acta* 4, 213–224.
- Fleischer, R.L., 1982. Alpha-recoil damage and solution effects in minerals: uranium isotopic disequilibrium and radon release. *Geochim. Cosmochim. Acta* 46, 2191–2201.
- Ford, T.D., Pedley, H.M., 1996. A review of tufa and travertine deposits of the world. *Earth Sci. Rev.* 41, 117–175.
- Francišković-Bilinski, S., Barišić, D., Vertacnik, A., Bilinski, H., Prohic, E., 2004. Characterization of tufa from the dinaric karst of Croatia: mineralogy, geochemistry and discussion of climate conditions. *Facies* 50, 183–193.
- Frank, N., Kober, B., Mangini, A., 2006. Carbonate precipitation, U-series dating and U-isotopic variations in a holocene travertine platform at Bad Langensalza - Thuringia Basin, Germany. *Quaternaire* 17, 333–342.
- Gat, J.R., Gonfiantini, R., 1981. Stable Isotope Hydrology: Deuterium and Oxygen-18 in the Water Cycle. IAEA, Vienna, Austria.
- Gieskes, J.M., 1974. The alkalinity-total carbon dioxide system in seawater. In: Goldberg, E.D. (Ed.), *Marine Chemistry of the Sea*. John Wiley and Sons, New York, pp. 123–151.
- Golubić, S., Violante, C., Plenković-Moraj, A., Gragasović, T., 2008. Travertines and calcareous tufa deposits: an insight into diagenesis. *Geol. Croat.* 61, 363–378.
- González Martín, J.A., González Amuchastegui, M.J., 2014. Las Tobas en España. SEG, Badajoz.
- Guerrero, J.L., Vallejos, Á., Cerón, J.C., Sánchez-Martos, F., Pulido-Bosch, A., Bolívar, J.P., 2016. U-isotopes and ²²⁶Ra as tracers of hydrogeochemical processes in carbonated karst aquifers from arid areas. *J. Environ. Radioact.* 158–159, 9–20.
- Hatten, J.A., Goñi, M.A., Wheatcroft, R.A., 2012. Chemical characteristics of particulate organic matter from a small, mountainous river system in the Oregon coast range, USA. *Biogeochemistry* 107, 43–66.
- Herman, J.S., Lorah, M.M., 1988. Calcite precipitation rates in the field: measurement and prediction for a travertine-depositing stream. *Geochim. Cosmochim. Acta* 52, 2347–2355.
- Huang, Y., Fairchild, J.L., 2001. Partitioning of Sr2 and Mg2 into calcite under karst-analog experimental conditions. *Geochim. Cosmochim. Acta* 65, 47–62.
- Huckle, D., Ma, L., McIntosh, J., Vázquez-Ortega, A., Rasmussen, C., Chorover, J., 2016. U-series isotopic signatures of soils and headwater streams in a semi-arid complex volcanic terrain. *Chem. Geol.* 445, 68–83.
- Jemison, N.E., Johnson, T.M., Shiel, A.E., Lundstrom, C.C., 2016. Uranium isotopic fractionation induced by U(VI) adsorption onto common aquifer minerals. *Environ. Sci. Technol.* 50, 12232–12240.
- Jimenez-Lopez, C., Romanek, C.S., Caballero, E., 2006. Carbon isotope fractionation in synthetic magnesium calcite. *Geochim. Cosmochim. Acta* 70, 1163–1171.
- Kelly, S.D., Rasbury, E.T., Chattopadhyay, S., Kropf, A.J., Kemner, K.M., 2006. Evidence of a stable uranyl site in ancient organic-rich calcite. *Environ. Sci. Technol.* 40, 2262–2268.
- Kendall, C., Silva, S.R., Kelly, V.J., 2001. Carbon and nitrogen isotopic compositions of particulate organic matter in four large river systems across the United States. *Hydrol. Process.* 15, 1301–1346.
- Kraemer, T.F., Brabets, T.P., 2012. Uranium isotopes (²³⁴U/²³⁸U) in rivers of the Yukon Basin (Alaska and Canada) as an aid in identifying water sources, with implications for monitoring hydrologic change in arctic regions. *Hydrogeol. J.* 20, 469–481.
- Krestou, A., Panias, D., 2004. Uranium (VI) speciation diagrams in the UO22/CO32-/H2O system at 25°C. *Eur. J. Miner. Process. Environ. Prot.* 4, 113–129.
- Kulusić, A., Borojević Šostarić, S., 2014. Dinaric evaporite mélange: diagenesis of the Kozovo Polje evaporites. *Geol. Croat.* 67, 59–74.
- Leng, M.J., Lamb, A.L., Heaton, T.H.F., Marshall, J.D., Wolfe, B.B., Jones, M.D., Holmes, J.A., Arrowsmith, C., 2006. Isotopes in lake sediments. In: Leng, M.J. (Ed.), *Isotopes in Palaeoenvironmental Research*. Springer, Dordrecht, pp. 147–184.
- Li, L., Chen, J., Chen, T., Chen, Y., Hedding, D.W., Li, G., Li, L., Li, T., Robinson, L.F., West, A.J., Wu, W., You, C.-F., Zhao, L., Li, G., 2018. Weathering dynamics reflected by the response of riverine uranium isotope disequilibrium to changes in denudation rate. *Earth Planet. Sci. Lett.* 500, 136–144.
- Liu, J., Hrustić, E., Du, J., Gašparović, B., Canković, M., Cukrov, N., Zhu, Z., Zhang, R., 2019. Net submarine groundwater-derived dissolved inorganic nutrients and carbon input to the oligotrophic stratified karstic estuary of the Krka River (Adriatic Sea, Croatia). *J. Geophys. Res. Ocean.* 124, 4334–4349.
- Liu, Z., Dreybrodt, W., 1997. Dissolution kinetics of calcium carbonate minerals in H2O-CO2 solutions in turbulent flow: the role of the diffusion boundary layer and the slow reaction H2O + CO2 ↔ H+ + HCO3-. *Geochim. Cosmochim. Acta* 61, 2879–2889.
- Liu, Z., Svensson, U., Dreybrodt, W., Daoxian, Y., Buhmann, D., 1995. Hydrodynamic control of inorganic calcite precipitation in huanglong ravine, China: field measurements and theoretical prediction of deposition rates. *Geochim. Cosmochim. Acta* 59, 3087–3097.
- Lojén, S., Dolenc, T., Vokal, B., Cukrov, N., Mihelcic, G., Papesch, W., 2004. C and O stable isotope variability in recent freshwater carbonates (River krka, Croatia). *Sedimentology* 51, 361–375.
- Lojén, S., Trkov, A., Ščancar, J., Vázquez-Navarro, J.A., Cukrov, N., 2009. Continuous 60-year stable isotopic and earth-alkali element records in a modern laminated tufa (Jaruga, river krka, Croatia): implications for climate reconstruction. *Chem. Geol.* 258, 242–250.
- Malov, A.L., Zylkov, S.B., 2020. Study of the mobilization of uranium isotopes in a sandstone aquifer in combination with groundwater data. *Water* 12, 112.
- Mamudžić, P., 1971. Osnovna geološka karta SFRJ 1: 100 000, list Šibenik (Basic Geological Map of SFT Yugoslavia, page Šibenik). Geological Survey of Yugoslavia, Belgrade.
- Marcenko, E., Srdoc, D., Golubić, S., Pezdić, J., Head, M.J., 1989. Carbon uptake in aquatic plants deduced from their natural ¹³C and ¹⁴C content. *Radiocarbon* 31, 785–794.
- Maric, I., Šiljeg, A., Cukrov, N., Roland, V., Domazetović, F., 2020. How fast does tufa grow? Very high-resolution measurement of the tufa growth rate on artificial substrates by the development of a contactless image-based modelling device. *Earth Surf. Process. Landf.* 45, 2331–2349.
- Meece, D.E., Benninger, L.K., 1993. The coprecipitation of pu and other radionuclides with CaCO3. *Geochim. Cosmochim. Acta* 57, 1447–1458.
- Merz-Preiß, M., Riding, R., 1999. Cyanobacterial tufa calcification in two freshwater streams: ambient environment, chemical thresholds and biological processes. *Sediment. Geol.* 126, 103–124.
- Meyers, P.A., 1994. Preservation of elemental and isotopic source identification of sedimentary organic matter. *Chem. Geol.* 114, 289–302.
- Miyajima, T., Miyajima, Y., Hanba, Y.T., Yoshii, K., Koitabashi, T., Wada, E., 1995. Determining the stable isotope ratio of total dissolved inorganic carbon in lake water by GC/C/IRMS. *Limnol. Oceanogr.* 40, 994–1000.
- Navarro-Martínez, F., Sánchez-Martos, F., Salas, García A., Gisbert, Gallego J., 2020. The use of major, trace elements and uranium isotopic ratio (²³⁴U/²³⁸U) for tracing of hydrogeochemical evolution of surface waters in the Andarax River catchment (SE Spain). *J. Geochem. Explor.* 213, 106533.
- Noordmann, J., Weyer, S., Georg, R.B., Jöns, S., Sharma, M., 2016. ²³⁸U/²³⁵U isotope ratios of crustal material, rivers and products of hydrothermal alteration: new insights on the oceanic U isotope mass balance. *Isot. Environ. Health Stud.* 52, 141–163.
- Nyachoti, S., Jin, L., Tweedie, C.E., Ma, L., 2019. Insight into factors controlling formation rates of pedogenic carbonates: a combined geochemical and isotopic approach in dryland soils of the US southwest. *Chem. Geol.* 527, 118503.
- Parkhurst, D.L., Appelo, C.A.I., 1999. User's Guide to PHREEQC (Version 2) – A Computer Program for Speciation, Batch-reaction, One-dimensional Transport, and Inverse Geochemical Calculations (Denver, Colorado).
- Pedley, M., 1990. Classification and environmental models of cool freshwater tufas. *Sediment. Geol.* 68, 143–154.
- Pedley, M., 2009. Tufas and travertines of the Mediterranean region: a testing ground for freshwater carbonate concepts and developments. *Sedimentology* 56, 221–246.
- Rihs, S., Condomines, M., Sigmarsson, O., 2000. U, Ra and Ba incorporation during precipitation of hydrothermal carbonates: implications for ²²⁶Ra-Ba dating of impure travertines. *Geochim. Cosmochim. Acta* 64, 661–671.
- Riotte, J., Chabaux, F., 1999. (²³⁴U/²³⁸U) activity ratios in freshwaters as tracers of hydrological processes: the strengbach watershed (Vosges, France). *Geochim. Cosmochim. Acta* 63, 1263–1275.
- Riotte, J., Chabaux, F., Benedetti, M., Dia, A., Gérard, M., Boulgue, J., Etamé, J., 2003. Uranium colloidal transport and origin of the ²³⁴U-²³⁸U fractionation in surface waters: new insights from Mount Cameroon. *Chem. Geol.* 202, 365–381.
- Ritter, S.M., Isenbeck-Schröter, M., Schröder-Ritzrau, A., Scholz, C., Rheinberger, S., Höfle, B., Frank, N., 2018. Trace element partitioning in fluvial tufa reveals variable portions of biologically influenced calcite precipitation. *Geochim. Cosmochim. Acta* 225, 176–191.
- Rogerson, M., Pedley, H.M., Wadhawan, J.D., Middleton, R., 2008. New insights into biological influence on the geochemistry of freshwater carbonate deposits. *Geochim. Cosmochim. Acta* 72, 4976–4987.
- Romanek, C.S., Grossman, E.L., Morse, J.W., 1992. Carbon isotopic fractionation in synthetic aragonite and calcite: effects of temperature and precipitation rate. *Geochim. Cosmochim. Acta* 56, 419–430.
- Rován, L., Lojén, S., Zulfiani, T., Kanduč, T., Petric, M., Horvat, B., Rusjan, S., Štrok, M., 2020. Comparison of uranium isotopes and classical geochemical tracers in karst aquifer of Ljubljanka River catchment (Slovenia). *Water* 12, 2064.
- Rován, L., Štrok, M., 2019. Optimization of the sample preparation and measurement protocol for the analysis of uranium isotopes by MC-ICP-MS without spike addition. *J. Anal. At. Spectrom.* 34, 1882–1891.
- Saunders, P., Rogerson, M., Wadhawan, J.D., Greenway, G., Pedley, H.M., 2014. Mg/Ca ratios in freshwater microbial carbonates: thermodynamic, kinetic and vital effects. *Geochim. Cosmochim. Acta* 147, 107–118.
- Sharp, Z., 2017. *Principles of Stable Isotope Geochemistry*, 2nd edition. Pearson Education.
- Spötl, C., 2005. A robust and fast method of sampling and analysis of d13C of dissolved inorganic carbon in ground waters. *Isot. Environ. Health Stud.* 41, 217–221.
- Srdoc, D., Horvatincic, N., Obelic, B., Krajcar, I., Šliepevic, A., 1985. Procesi taloženja kalcita u krškim vodama s posebnim osvrtom na Plitvička jezera (Calcite deposition processes in karstwaters with special emphasis on the Plitvice Lakes, Yugoslavia). *KRS Jugosl.* 11, 1–104.
- Standards for Nuclear Safety Security and Safeguards Unit, 2019. Nuclear Certified Reference Materials 2019. Geel, Belgium.
- Stirling, C.H., Andersen, M.B., Potter, E.-K., Halliday, A.N., 2007. Low-temperature isotopic fractionation of uranium. *Earth Planet. Sci. Lett.* 264, 208–225.
- Suksi, J., Rasilainen, K., Pitkänen, P., 2006. Variations in ²³⁴U/²³⁸U activity ratios in groundwater—a key to flow system characterisation? *Phys. Chem. Earth, Parts A/B/C* 31, 556–571.
- Štrok, M., Smodiš, B., 2010. Fractionation of natural radionuclides in soils from the vicinity of a former uranium mine Žirovski vrh, Slovenia. *J. Environ. Radioact.* 101, 22–28.
- Tanweer, A., Gröning, M., Van Duren, M., Jaklitsch, M., Pöhltenstein, L., 2009. IAEA Technical Note No. 43 Stable Isotope Internal Laboratory Water Standards: Preparation, Calibration and Storage. International Atomic Energy Agency, Vienna.
- Teichert, B.M.A., Eisenhauer, A., Bohrmann, G., Haase-Schramm, A., Bock, B., Linke, P., 2003. U/Th systematics and ages of authigenic carbonates from hydrate ridge, Cascadia margin: recorders of fluid flow variations. *Geochim. Cosmochim. Acta* 67, 3845–3857.
- Thollon, M., Bayon, G., Toucanne, S., Trinquier, A., Germain, Y., Dosseto, A., 2020. The distribution of (²³⁴U/²³⁸U) activity ratios in river sediments. *Geochim. Cosmochim. Acta* 290, 216–234.

L. Rovati, T. Zulliani, B. Horvat et al.

Science of the Total Environment 797 (2021) 149103

- Trdin, M., Necemer, M., Benedik, L., 2017. Fast decomposition procedure of solid samples by lithium borates fusion employing salicylic acid. *Anal. Chem.* 89, 3169–3176.
- Wang, R.-M., You, C.-F., 2013. Precise determination of U isotopic compositions in low concentration carbonate samples by MC-ICP-MS. *Talanta* 107, 67–73.
- Weyer, S., Anbar, A.D., Gerdes, A., Gordon, G.W., Algeo, T.J., Boyle, E.A., 2008. Natural fractionation of $^{238}\text{U}/^{235}\text{U}$. *Geochim. Cosmochim. Acta* 72, 345–359.
- Yan, H., Liu, Z., Sun, H., 2020. Large degrees of carbon isotope disequilibrium during precipitation-associated degassing of CO_2 in a mountain stream. *Geochim. Cosmochim. Acta* 273, 244–256.
- Zavadlav, S., Rožic, B., Dolenc, M., Lojen, S., 2017. Stable isotopic and elemental characteristics of recent tufa from a karstic Krka River (south-East Slovenia): useful environmental proxies? *Sedimentology* 64, 808–831.
- Zebracki, M., Cagnat, X., Gairoard, S., Cariou, N., Eyrrolle-Boyer, F., Boulet, B., Antonelli, C., 2017. U isotopes distribution in the lower Rhone River and its implication on radionuclides disequilibrium within the decay series. *J. Environ. Radioact.* 178–179, 279–289.
- Zhao, M.Y., Zheng, Y.F., Zhao, Y.Y., 2016. Seeking a geochemical identifier for authigenic carbonate. *Nat. Commun.* 7, 10885.

Supplementary Material

Uranium isotopes as a possible tracer of terrestrial authigenic carbonate

Leja Rovan^{1,2}, Tea Zuliani^{1,2}, Barbara Horvat³, Tjaša Kanduč¹, Polona Vreča¹, Qasim Jamiš, Branko Čermelj⁴, Elvira Bura-Nakić⁵, Neven Cukrov⁵, Marko Štok^{1,2*}, Sonja Lojen^{1,6}

¹*Department of Environmental Sciences, Jožef Stefan Institute, Jamova cesta 39, 1000 Ljubljana, Slovenia*

²*Jožef Stefan International Postgraduate School, Jamova cesta 39, 1000 Ljubljana, Slovenia*

³*Slovenian National Building and civil Engineering Institute, Dimičeva ulica 12, 1000 Ljubljana, Slovenia*

⁴*Marine Biology Station, National Institute of Biology, Formače 40, 6330 Piran, Slovenia*

⁵*Division for Marine and Environmental Research, Rudfer Bošković Institute, Bijenička cesta 54, 10000 Zagreb, Croatia*

⁶*School of Environmental Sciences, University of Nova Gorica, Glavni trg 8, 5271 Vipava, Slovenia*

*corresponding author: marko.strok@ijs.si

Table S1: Results of chemical and isotopic analyses of Krka and Zrmanja river water.

Site	Distance from the spring [km]	$\delta^{18}\text{O}_{\text{VSMOW}}$ [‰]	$\delta^{13}\text{C}_{\text{V-PDB-DIC}}$ [‰]	DIC [mmol L ⁻¹]	log pCO ₂	S _{calc}	U [mg L ⁻¹]	²³⁴ U/ ²³⁸ U activity ratio	$\delta^{238}\text{U}$ [‰]	U/Ca -10 ⁻⁶
K1	0	-8.92	-11.40	4.86	-1.81	-0.40	0.53	1.491	0.05	1.56
K2	16	-8.52	-9.77	3.97	-2.92	1.03	0.67	1.381	-0.46	0.94
K3	18.8	-8.55	-9.23	3.93	-2.85	1.00	0.62	1.389	-0.69	0.90
K4	19.7	-8.54	-9.04	3.67	-2.83	0.92	0.60	1.382	-0.25	0.86
K5a	35	-8.29	-9.75	3.83	-2.82	0.94	0.58	1.381	-0.54	0.94
K5b	35.5	-8.29	-9.49	3.93	-2.79	0.94	0.55	1.381	-0.53	0.87
K6a	49	-7.48	-8.01	3.47	-2.78	0.83	0.51	1.288	-0.60	1.03
K6b	49.5	-7.51	-8.06	3.43	-3.02	1.05	0.46	1.282	-0.59	0.96
Z1	16	-8.29	-9.38	ND	ND	ND	0.38	1.510	-0.02	1.21
Z2	38	-7.89	-11.56	ND	ND	ND	0.28	1.374	-0.24	0.67
Z3	50	-7.53	-10.68	ND	ND	ND	0.26	1.309	-0.60	0.68

ND: not determined

Table S2. Isotopic and geochemical parameters analysed in bedrock, tufa and soil samples from the Krka and Zrmanja River.

Site	Type of rock	$\delta^{13}\text{C}_{\text{VPDB}}$ [‰]	$\delta^{18}\text{O}_{\text{VPDB}}$ [‰]	$\delta^{13}\text{C}$ of OC [‰]	C_{org} wt.%	"non-carbonate" wt.%	OC/N at.ratio	Ca^{2+} [mg g ⁻¹]	$\text{Ca}^{2+}_{\text{carb}}$ [mg g ⁻¹]	$\text{Ca}^{2+}_{\text{carb}}$ %	Mg^{2+} [mg g ⁻¹]	$\text{Mg}^{2+}_{\text{carb}}$ [mg g ⁻¹]	$\text{Mg}^{2+}_{\text{carb}}$ %	
Bedrock	K1	Sandstone	-2.26	-5.38	-26.08	ND	45.17	ND	194	129	67	14.10	2.47	17
	K2	Limestone	-0.84	-6.07	-26.40	ND	2.04	ND	398	353	89	2.58	1.40	54
	K3	Limestone	-2.06	-5.29	-24.85	ND	3.92	ND	378	341	90	3.14	1.73	55
	K4	Marl	-2.12	-5.02	-24.32	ND	3.98	ND	385	309	80	3.19	1.74	54
	K4	Breccia	0.76	-3.89	-24.11	ND	4.24	ND	377	349	92	4.23	2.79	66
	K5b	Conglomerate	-1.04	-5.16	-24.89	ND	1.97	ND	391	291	74	2.15	0.91	42
	Z1	Limestone	-0.92	-4.20	-26.33	ND	2.47	ND	376	352	94	4.16	2.54	61
	K2		-9.45	-7.91	-30.11	0.83	8.36	12.9	347	330	95	13.87	1.50	11
	K3		-9.36	-8.14	-28.63	0.65	5.91	15.7	356	347	98	12.25	1.64	13
	K4		-8.85	-8.28	-28.57	0.27	3.62	22.5	370	299	81	9.63	1.31	14
Tufa	K5a		-8.72	-7.72	-33.09	0.63	6.28	14.7	358	297	83	10.91	1.32	12
	K5b		-9.94	-8.63	-34.45	1.14	5.29	9.8	357	364	102	10.94	1.64	15
	K6a		-9.82	-8.02	-33.20	0.53	1.52	12.2	381	363	95	5.33	1.22	23
	K6b		-10.34	-8.47	-34.74	0.53	1.72	14.6	383	347	91	6.15	1.27	21
	Z3		-10.31	-7.47	-29.77	0.39	5.24	11.5	367	476	130	10.80	1.17	11
	K1		-2.18	-5.95	-30.21	4.03	9.21	13.9	260	132	51	74.2	3.33	4
	K2		-9.48	-9.09	-30.39	8.36	10.55	16.8	348	294	84	4.58	1.58	35
	K3		-6.47	-9.21	-29.31	9.19	51.98	13.7	166	150	90	18.3	1.94	11
	K4		-9.22	-8.77	-29.23	3.47	6.71	18.0	364	377	100	3.70	1.63	44
	K5a		-2.32	-5.95	-25.87	1.78	23.48	16.8	296	276	93	3.94	1.30	33
Soil	K5b		-5.69	-5.91	-28.90	1.93	36.10	11.9	238	193	81	10.9	1.21	11
	K6a		-9.08	-8.80	-30.71	12.8	38.63	24.4	235	152	65	8.62	1.09	13
	Z3		-3.34	-7.10	-27.13	4.14	75.58	13.3	84	67	80	6.03	0.36	6

*ND - not determined; "non-carbonate" = $\text{Al}_2\text{O}_3 + \text{SiO}_2 + \text{Fe}_2\text{O}_3 + \text{Na}_2\text{O} + \text{K}_2\text{O}$. Residual fraction is calculated as the difference between bulk and carbonate fraction.

Table S3: Uranium parameters analysed in bedrock, tufa and soil samples from the Krka and Zrmanja River.

Site	U [ng g ⁻¹]	U _{carb} [ng g ⁻¹]	U _{resid} [ng g ⁻¹]	U _{carb} %	²³⁴ U/ ²³⁸ U _{bulk}		²³⁴ U/ ²³⁸ U _{carb}		²³⁴ U/ ²³⁸ U _{resid}		$\delta^{238}\text{U}_{\text{carb}}$ [‰]	$\delta^{238}\text{U}_{\text{bulk}}$ [‰]	$\delta^{238}\text{U}_{\text{resid}}$ [‰]
					activity ratio	activity ratio	activity ratio	activity ratio					
Bedrock	K1	807	477	59	0.984	1.023	0.92	-0.14	-0.21	-0.02	-0.14	-0.21	-0.02
	K2	150	126	84	1.107	1.118	1.05	-0.23	-0.13	-0.75	-0.23	-0.13	-0.75
	K3	1694	1492	193	1.025	1.039	0.92	-0.13	-0.15	-0.01	-0.13	-0.15	-0.01
	K4	1891	1324	475	0.950	1.056	0.66	-0.17	-0.78	1.53	-0.17	-0.78	1.53
	K4	1445	1241	204	1.040	1.050	0.98	-0.35	-0.48	0.47	-0.35	-0.48	0.47
Tufa	K5b	1170	946	200	1.016	1.022	0.98	-0.40	-0.11	-1.78	-0.40	-0.11	-1.78
	Z1	1923	1682	176	1.001	1.007	0.94	-0.29	-0.41	0.90	-0.29	-0.41	0.90
	K2	755	362	396	1.136	1.367	0.924	-0.48	-0.48	-0.48	-0.48	-0.48	-0.48
	K3	448	273	173	1.182	1.379	0.869	-0.80	-0.21	-1.73	-0.80	-0.21	-1.73
	K4	531	324	204	1.229	1.381	1.064	-0.47	-0.30	-0.99	-0.47	-0.30	-0.99
	K5a	610	373	239	1.167	1.344	0.890	-0.32	-0.82	0.46	-0.32	-0.82	0.46
	K5b	748	447	303	1.249	1.371	1.069	-0.69	-0.37	-1.17	-0.69	-0.37	-1.17
	K6a	413	308	103	1.267	1.278	1.235	-0.71	-0.49	-1.38	-0.71	-0.49	-1.38
	K6b	420	303	113	1.242	1.254	1.210	-0.30	-0.42	0.03	-0.30	-0.42	0.03
	Z3	290	109	181	1.045	1.291	0.896	-0.41	-0.45	-0.39	-0.41	-0.45	-0.39
	Z3	1477	346	1142	0.946	1.077	0.906	-0.27	-0.19	-0.29	-0.27	-0.19	-0.29
Soil	K2	716	229	494	1.117	1.393	0.989	-0.15	-0.06	-0.19	-0.15	-0.06	-0.19
	K3	2362	320	2063	0.920	1.277	0.864	-0.26	-0.06	-0.30	-0.26	-0.06	-0.30
	K4	567	238	332	1.160	1.380	1.002	-0.39	-0.51	-0.30	-0.39	-0.51	-0.30
	K5a	1364	438	943	0.933	1.075	0.867	-0.45	-0.15	-0.59	-0.45	-0.15	-0.59
	K5b	2012	362	1649	0.928	1.221	0.864	-0.39	-0.56	-0.36	-0.39	-0.56	-0.36
	K6a	1892	424	1450	0.988	1.232	0.917	-0.43	-0.03	-0.54	-0.43	-0.03	-0.54
	Z3	3213	213	3017	0.818	1.079	0.799	-0.68	-0.46	-0.69	-0.68	-0.46	-0.69

"non-carbonate" = Al₂O₃ + SiO₂ + Fe₂O₃ + Na₂O + K₂O. Residual fraction is calculated as the difference between bulk and carbonate fraction.

Chapter 4

Conclusions

The focus of the PhD dissertation is on finding the most accurate and precise analytical method for the U and Th isotope ratios in samples with low-level U and Th concentrations using the instrument MC-ICP-MS and correctly interpret U and Th analytical data in the context of geochemical applications. Several protocols have been reported in the literature, but there is no consistency on the method with the minimum possible risk of contamination of our analyte during sample pre-treatment and separation protocol and with the quantification of possible biases of U or Th during sample preparation protocols. To accurately determine U and Th isotope ratios, it is obligatory to know and understand most of isotopic biases effects from the analytical procedure that contribute to the inaccurate result, either during sample preparation or measurement. Profound analytical work and careful method development with proper measurement protocol are very important in order to guarantee a validated measurement method.

This PhD dissertation evaluates and compares different analytical methods for the determination of U and Th isotope ratios in different sample materials using MC-ICP-MS. By reducing impurity effects and other potential contaminations, and by optimization of the mass-spectrometric measurement, the optimal procedure was applied to real samples where the influence of the matrix effect is significant and extremely small isotopic variations need to be detected with high accuracy and precision.

The optimal U and Th method can be used as an additional environmental tracer to gain more knowledge and understanding of complex systems with predominantly carbonate lithology. The developed methodology enables relatively easy measurement of isotope ratios at high levels of precision and accuracy, which is important for U and Th isotope measurements in environments where their concentrations in samples are low. The applied developed method was tested in two karstic geological settings, the Ljubljana River catchment and the Krka River in Croatia.

In summary, the main conclusions from the dissertation and hypothesis testing are specified below under each hypothesis of the dissertation:

1. Different sample pre-treatment and U separation protocols induce different levels of undesired biases between U and Th isotopes, which needs to be quantified in order to be able to select appropriate ones.

Prior to mass spectrometry analysis, a careful sample preparation procedure is needed to separate U isotopes from the sample matrix and other possible interferences and also to improve the detection limit, increase the sensitivity and enhance the accuracy of the result, especially for samples with low-level U concentrations. To identify the optimal analytical technique for determination of U isotope ratios using MC-ICP-MS, the most commonly

used sample preparation approaches for water samples were tested. Tested preconcentration techniques were coprecipitation with $\text{Fe}(\text{OH})_3$, $\text{Ca}_3(\text{PO}_4)_2$, MnO_2 , and evaporation. Tested separation techniques were extraction chromatography with UTEVA resin prepared in deionized water, extraction chromatography with UTEVA resin pre-cleaned in 6 M HNO_3 , a combination of ion exchange chromatography and extraction chromatography, ion exchange chromatography, and separation with solvent extraction (TBP). The experiment showed that the column chemistry indirectly leads to a matrix effect in the MC-ICP-MS. The most likely reason for this effect was organic material stripped from the resins during the collection of the U fraction. The presence of organics was especially observed in the case of U separation with solvent extraction (TBP), where results showed extensive deviations for U isotope ratios from the U isotopic standard. On the other hand, results from UTEVA resin, previously cleaned in 6 M HNO_3 , demonstrated significantly smaller deviations of $^{235}\text{U}/^{238}\text{U}$ and $^{234}\text{U}/^{238}\text{U}$ ratios from the U isotopic standard. Here we confirmed our first hypothesis that the presence of organic interference could extensively contribute to the mass bias effect in different levels for diverse sample pre-treatment and U separation protocols.

2. Optimization of U pre-treatment, separation and measurement protocols will result in methodology with lowest procedural blanks and undesired biases, which will be sufficiently good to be applicable in karst aquifer geochemistry.

The analytical method with the smallest procedural blanks and the most accurate purified U fraction results with the lowest amount of impurities and with the smallest bias from the standard reference value measured with MC-ICP-MS was selected as the optimal procedure for application to real samples. The study results indicated that the optimal analytical procedure was the combination of coprecipitation with $\text{Ca}_3(\text{PO}_4)_2$ as the preconcentration technique and extraction chromatography with UTEVA resin pre-cleaned in 6 M HNO_3 as the separation technique. In addition, the accurate and precise analysis of U isotope ratios was achieved with the optimization of MC-ICP-MS measurements by controlling and correcting the factors, which can occur during measurements as instrumental mass bias. With factors, such as the appropriate concentration of the aliquot of a purified natural U fraction, the appropriate cup configurations of U isotope measurements, and the long-term analytical performance of the MC-ICP-MS instrument, we achieved the most suitable performance for low-level U samples. U concentration of 5 ng/mL was selected as the lowest concentration with the smallest difference of $^{235}\text{U}/^{238}\text{U}$ and $^{234}\text{U}/^{238}\text{U}$ isotope ratios from the certified value. The analytical precision of the instrument at concentration 5 ng/mL showed that the instrument accuracy and precision for U isotope ratio measurement was in good agreement with the certified value of the U standard.

Developed methodology for the determination of U isotope ratios and consequently also of Th isotope ratios was afterwards applied to the samples from the environment where freshwater draining areas with a predominantly carbonate lithology were investigated. For these hydrogeological settings, not much is known compared to the presence and behavior of natural U and Th isotopes in ancient and recent marine environments, which were studied widely. In addition, U and Th isotopes in such karstic environment have much lower concentrations (mean: 0.3 $\mu\text{g}/\text{L}$), which become an analytical challenge and for that optimization of the method was necessary. The optimal method from our study was with the lowest procedural blanks and undesired biases sufficiently good to be applied in karst aquifer geochemistry. These findings thus confirm our second hypothesis.

3. U and Th isotopes will prove to be a useful tracer of geochemical processes in different studied karst aquifers.

U isotopes were used as a non-traditional isotope system to support traditional geochemical and isotopic tracers in an investigation of the origin and flow paths of groundwater in the first case study, the Ljubljana River catchment in Slovenia. The Krka River in Croatia was the second case study and it is presented as a unique groundwater-fed karstic river, characterized by complex hydrology, seasonally variable diffuse subsurface recharge and tufa precipitation in a turbulent stream at morphologic discontinuities and in lotic environments.

The use of U isotopes had several benefits over traditional geochemical techniques. U is an abundant trace element in natural waters in areas with a predominantly carbonate lithology; therefore it can be used as an additional tracer to gain more knowledge and understanding of complex karst hydrodynamics. Its isotopic composition varied in such an environment because of the U several processes that cause isotope fractionation effects (alpha recoil, redox chemistry, and adsorption). Additionally, isotope ratios were easily measured at high levels of precision and accuracy with optimized method, which is important for U isotope measurements in karstic waters where U concentrations are low.

The results at studied karstic locations brought a new perspective on the U and Th isotope disequilibrium to already known data from traditional geochemical tracers in river water, tufa, surrounding bedrock and soil samples. The differences in U isotope ratios and U concentrations within the watershed are partly due to the different lithology and mixing of waters from different sources. The variability of U concentrations and $^{234}\text{U}/^{238}\text{U}$ activity ratios in water was the largest in areas with less permeable and less soluble rocks, compared to areas where fractured carbonate rocks are in the abundance. Carbonate rocks weather more rapidly and the removal of ^{234}U from rock to water is much higher owing to the influence of the alpha recoil effect, therefore the $^{234}\text{U}/^{238}\text{U}$ activity ratios are higher. In the Ljubljana River system, results of the U isotopic disequilibrium were in the groundwater in crystalline aquifers around 1, whereas in more soluble parts of aquifers the values rose up to 1.8. The $^{234}\text{U}/^{238}\text{U}$ activity ratio also varies depending upon the mean transit time of groundwater recharging the karst stream. During storage, ^{234}U preferentially accumulates in groundwater, therefore, with prolonged storage the $^{234}\text{U}/^{238}\text{U}$ activity ratio slowly increases. Moreover, results from the Krka River study demonstrated that diffused groundwater discharge into the river could also contribute to the variability of the U isotopic composition in river water owing to water-rock interactions and the influence of the alpha recoil effect. Furthermore, the $^{234}\text{U}/^{238}\text{U}$ activity ratio of water in the Ljubljana River catchment was strongly negatively correlated with the discharge. U concentration and its isotopic composition deviated between high and low water discharge and the difference between U values at low and high flow conditions varied up to 20%. Tufa samples from the Krka River study displays $^{234}\text{U}/^{238}\text{U}$ activity ratios similar to those of the river water, which were higher and relatively constant compared to the bedrock, springs and tributaries. This indicates that the majority of U present in tufa samples is co-precipitated with the carbonate from the river water without fractionation and can demonstrate its authigenic origin. Additionally, U concentrations and its isotope ratios in carbonate materials from Krka study are shown to be reliable indicators of the storage of CO_2 as authigenic carbonate in tufa. They were also a useful indicator for the determination of tufa with U bond to detrital material and consequently relevant for both the construction of the CO_2 mass balance in a karst aquifer, as well as for dating. For $\delta^{238}\text{U}$ values, a large scattering appears to be in both karstic studies, because $\delta^{238}\text{U}$ is a much more sensitive tracer of bedrock composition than the $^{234}\text{U}/^{238}\text{U}$ activity ratio, therefore long-term

observation of $\delta^{238}\text{U}$ in river water with both seasonal and event-based sampling design would be necessary. The third hypothesis is thereby only partly confirmed. U and Th isotopes were proven to be a useful geochemical tracer of geochemical processes in two different studied karst aquifers and a valuable additional tool to the classical geochemical tracers. However, not many studies have been performed so far in such an environment and more detailed chemical and isotopic analyses over a longer period would increase future better understanding of U and Th isotopic compositions in the karst environment.

The findings of the dissertation represent a good foundation for future work in implementing U and Th isotopic analytical procedures for application in geochemistry or other possible use. U and Th isotopic composition have been proven to be a valuable tool in environmental science, oceanography, hydrology, geology, nuclear forensics, and science-based archaeology. In the context of application in geochemistry, U isotopes showed considerable potential as a geochemical tracer of groundwater and river water in karst aquifers. To identify and quantify the extent of authigenic carbonate formation for the C cycle, U and Th isotopes are still lagging behind the geochemical parameters and traditional stable isotopes. Thus, additional systematic samplings of river water, tufa, bedrock and soil, and other samples (lacustrine sediments and pore water) would upgrade the obtained information. In the context of dating applications, U and Th isotope ratios have a wide range of use, from establishing the proper age of different materials (stalagmites, corals, archeological samples, etc.), to understanding processes that happened a long time ago in terrestrial or marine environments. Therefore, the next big task for future research activities would be establishing a proper instrumental procedure for U-Th dating and applying it to a variety of samples. Optimal U methodology can also be used in nuclear safeguards. U isotope ratios could be employed to differentiate types of environmental nuclear contamination for monitoring applications or in the case of some possible accident at nuclear power plants. U isotope ratios could also be recognized as an important indicator in the environmental monitoring control of contaminated territories, such as in the vicinity of the uranium mining sites. There is also a possibility to use the $\delta^{238}\text{U}$ values of limestone or dolomite as an indicator of the redox state of the seawater in the geological past to differentiate U isotopic signature in abiotic and biotic systems.

Appendix A

Permissions for Reproduction of Included Publications

A.1 Permission for Reproduction of Publications 3.1

Text of the permission retrieved from <https://pubs.rsc.org/en/content/articlelanding/2019/ja/c9ja00144a#!divAbstract> on January 28, 2021.

“If you are the author of this article you do not need to formally request permission to reproduce figures, diagrams etc. contained in this article in third party publications or in a thesis or dissertation provided that the correct acknowledgement is given with the reproduced material”.

For more information on this and other retained rights, please visit: <https://www.rsc.org/journals-books-databases/journal-authors-reviewers/licences-copyright-permissions/#reuse-rsc-third-party>.

Acknowledgment:

Rovan, L., & Štok, M. (2019). Optimization of the sample preparation and measurement protocol for the analysis of uranium isotopes by MC-ICP-MS without spike addition. *Journal of Analytical Atomic Spectrometry*, 34(9), 1882–1891. <https://doi.org/10.1039/C9JA00144A> - Reproduced by permission of The Royal Society of Chemistry

A.2 Permission for Reproduction of Publications 3.2

Text of the permission for publication 3.2 retrieved from <https://www.mdpi.com/authors/rights> on January 28, 2021.

“For all articles published in MDPI journals, copyright is retained by the authors. Articles are licensed under an open access Creative Commons CC BY 4.0 license, meaning that anyone may download and read the paper for free. In addition, the article may be reused and quoted provided that the original published version is cited. These conditions allow for maximum use and exposure of the work, while ensuring that the authors receive proper credit”.

A.3 Permission for Reproduction of Publications 3.3

Text of the permission for publication 3.3 retrieved from <https://www.elsevier.com/about/policies/copyright> on July 18, 2021.

“Author rights

The below table explains the rights that authors have when they publish with Elsevier, for authors who choose to publish either open access or subscription. These apply to the corresponding author and all co-authors.

Author rights in Elsevier’s proprietary journals	Published open access	Published subscription
Retain patent and trademark rights	√	√
Retain the rights to use their research data freely without any restriction	√	√
Receive proper attribution and credit for their published work	√	√
Re-use their own material in new works without permission or payment (with full acknowledgement of the original article): 1. Extend an article to book length 2. Include an article in a subsequent compilation of their own work 3. Re-use portions, excerpts, and their own figures or tables in other works.	√	√
Use and share their works for scholarly purposes (with full acknowledgement of the original article): 1. In their own classroom teaching. Electronic and physical distribution of copies is permitted 2. If an author is speaking at a conference, they can present the article and distribute copies to the attendees 3. Distribute the article, including by email, to their students and to research colleagues who they know for their personal use 4. Share and publicize the article via Share Links, which offers 50 days’ free access for anyone, without signup or registration 5. Include in a thesis or dissertation (provided this is not published commercially) 6. Share copies of their article privately as part of an invitation-only work group on commercial sites with which the publisher has a hosting agreement	√	√
Publicly share the preprint on any website or repository at any time.	√	√
Publicly share the accepted manuscript on non-commercial sites	√	√
Publicly share the final published article	√	×
Retain copyright	√	×

”.

References

- Adriaens, A. G., Fassett, J. D., Kelly, W. R., Simons, D. S., & Adams, F. C. (1992). Determination of uranium and thorium concentrations in soils: a comparison of isotope dilution-secondary ion mass spectrometry and isotope dilution-thermal ionization mass spectrometry. *Analytical Chemistry*, *64*(23), 2945–2950. <https://doi.org/10.1021/ac00047a012>
- Albarède, F., Telouk, P., Blichert-Toft, J., Boyet, M., Agranier, A., & Nelson, B. (2004). Precise and accurate isotopic measurements using multiple-collector ICPMS. *Geochimica et Cosmochimica Acta*, *68*(12), 2725–2744. <https://doi.org/10.1016/j.gca.2003.11.024>
- Andersen, M. B., Elliott, T., Freymuth, H., Sims, K. W. W., Niu, Y., & Kelley, K. A. (2015). The terrestrial uranium isotope cycle. *Nature*, *517*(7534), 356–359. <https://doi.org/10.1038/nature14062>
- Andersen, M. B., Erel, Y., & Bourdon, B. (2009). Experimental evidence for ^{234}U – ^{238}U fractionation during granite weathering with implications for $^{234}\text{U}/^{238}\text{U}$ in natural waters. *Geochimica et Cosmochimica Acta*, *73*(14), 4124–4141. <https://doi.org/10.1016/j.gca.2009.04.020>
- Andersen, M. B., Romaniello, S., Vance, D., Little, S. H., Herdman, R., & Lyons, T. W. (2014). A modern framework for the interpretation of $^{238}\text{U}/^{235}\text{U}$ in studies of ancient ocean redox. *Earth and Planetary Science Letters*, *400*, 184–194. <https://doi.org/10.1016/j.epsl.2014.05.051>
- Andersen, M. B., Stirling, C. H., Porcelli, D., Halliday, A. N., Andersson, P. S., & Baskaran, M. (2007). The tracing of riverine U in Arctic seawater with very precise $^{234}\text{U}/^{238}\text{U}$ measurements. *Earth and Planetary Science Letters*, *259*(1–2), 171–185. <https://doi.org/10.1016/j.epsl.2007.04.051>
- Andersen, M. B., Stirling, C. H., Potter, E.-K., & Halliday, A. N. (2004). Toward epsilon levels of measurement precision on $^{234}\text{U}/^{238}\text{U}$ by using MC-ICPMS. *International Journal of Mass Spectrometry*, *237*(2–3), 107–118. <https://doi.org/10.1016/j.ijms.2004.07.004>
- Andersen, M. B., Stirling, C. H., & Weyer, S. (2017). Uranium Isotope Fractionation. *Reviews in Mineralogy and Geochemistry*, *82*(1), 799–850. <https://doi.org/10.2138/rmg.2017.82.19>
- Andersen, M. B., Stirling, C. H., Zimmermann, B., & Halliday, A. N. (2010). Precise determination of the open ocean $^{234}\text{U}/^{238}\text{U}$ composition. *Geochemistry, Geophysics, Geosystems*, *11*(12). <https://doi.org/10.1029/2010GC003318>
- Andersen, M. B., Vance, D., Keech, A. R., Rickli, J., & Hudson, G. (2013). Estimating U

- fluxes in a high-latitude, boreal post-glacial setting using U-series isotopes in soils and rivers. *Chemical Geology*, *354*, 22–32. <https://doi.org/10.1016/j.chemgeo.2013.06.021>
- Andersen, M. B., Vance, D., Morford, J. L., Bura-Nakić, E., Breitenbach, S. F. M., & Och, L. (2016). Closing in on the marine $^{238}\text{U}/^{235}\text{U}$ budget. *Chemical Geology*, *420*, 11–22. <https://doi.org/10.1016/j.chemgeo.2015.10.041>
- Andrews, J. E. (2006). Palaeoclimatic records from stable isotopes in riverine tufas: Synthesis and review. *Earth-Science Reviews*, *75*(1–4), 85–104. <https://doi.org/10.1016/j.earscirev.2005.08.002>
- Arenas, C., Vázquez-Urbez, M., Auqué, L., Sancho, C., Osácar, C., & Pardo, G. (2014). Intrinsic and extrinsic controls of spatial and temporal variations in modern fluvial tufa sedimentation: A thirteen-year record from a semi-arid environment. *Sedimentology*, *61*(1), 90–132. <https://doi.org/10.1111/sed.12045>
- Bacon, M. P., & Anderson, R. F. (1982). Distribution of thorium isotopes between dissolved and particulate forms in the deep sea. *Journal of Geophysical Research*, *87*(C3), 2045. <https://doi.org/10.1029/JC087iC03p02045>
- Ball, L., Sims, K. W. W., & Schwieters, J. (2008). Measurement of $^{234}\text{U}/^{238}\text{U}$ and $^{230}\text{Th}/^{232}\text{Th}$ in volcanic rocks using the Neptune MC-ICP-MS. *Journal of Analytical Atomic Spectrometry*, *23*(2), 173–180. <https://doi.org/10.1039/B703193A>
- Baskaran, M., Santschi, P. H., Benoit, G., & Honeyman, B. D. (1992). Scavenging of thorium isotopes by colloids in seawater of the Gulf of Mexico. *Geochimica et Cosmochimica Acta*, *56*(9), 3375–3388. [https://doi.org/10.1016/0016-7037\(92\)90385-V](https://doi.org/10.1016/0016-7037(92)90385-V)
- Baxter, D. C., Rodushkin, I., & Engström, E. (2012). Isotope abundance ratio measurements by inductively coupled plasma-sector field mass spectrometry. *Journal of Analytical Atomic Spectrometry*, *27*(9), 1355. <https://doi.org/10.1039/c2ja30153a>
- Becker, J. S. (2005). Recent developments in isotope analysis by advanced mass spectrometric techniques: Plenary lecture. *Journal of Analytical Atomic Spectrometry*, *20*(11), 1173. <https://doi.org/10.1039/b508895j>
- Benedik, L., Pintar, H., & Byrne, A. R. (1999). The leachability of some natural and man-made radionuclides from soil and sediments on acid attack. *Journal of Radioanalytical and Nuclear Chemistry*, *240*(3), 859–865. <https://doi.org/10.1007/BF02349863>
- Benedik, L., Rován, L., Klemenčič, H., Gantar, I., & Prosen, H. (2015). Natural radioactivity in tap waters from the private wells in the surroundings of the former Žirovski Vrh uranium mine and the age-dependent dose assessment. *Environmental Science and Pollution Research*, *22*(16), 12062–12072. <https://doi.org/10.1007/s11356-015-4481-z>
- Bigeleisen, J. (1996). Nuclear Size and Shape Effects in Chemical Reactions. Isotope Chemistry of the Heavy Elements. *Journal of the American Chemical Society*, *118*(15), 3676–3680. <https://doi.org/10.1021/ja954076k>
- Bischoff, J. L., & Fitzpatrick, J. A. (1991). U-series dating of impure carbonates: An isochron technique using total-sample dissolution. *Geochimica et Cosmochimica Acta*, *55*(2), 543–554. [https://doi.org/10.1016/0016-7037\(91\)90011-S](https://doi.org/10.1016/0016-7037(91)90011-S)
- Blake, J. B., & Schramm, D. N. (1973). ^{247}Cm as a Short-lived r-Process Chronometer. *Nature Physical Science*, *243*(130), 138–140. <https://doi.org/10.1038/physci243138a0>

- Blundy, J. (2003). Mineral-Melt Partitioning of Uranium, Thorium and Their Daughters. *Reviews in Mineralogy and Geochemistry*, 52(1), 59–123. <https://doi.org/10.2113/0520059>
- Bopp, C. J., Lundstrom, C. C., Johnson, T. M., & Glessner, J. J. G. (2009). Variations in $^{238}\text{U}/^{235}\text{U}$ in uranium ore deposits: Isotopic signatures of the U reduction process? *Geology*, 37(7), 611–614. <https://doi.org/10.1130/G25550A.1>
- Boulyga, S. F., Klötzli, U., & Prohaska, T. (2006). Improved abundance sensitivity in MC-ICP-MS for determination of $^{236}\text{U}/^{238}\text{U}$ isotope ratios in the 10^{-7} to 10^{-8} range. *Journal of Analytical Atomic Spectrometry*, 21(12), 1427–1430. <https://doi.org/10.1039/b608983f>
- Boulyga, S. F., Koepf, A., Konegger-Kappel, S., Macsik, Z., & Stadelmann, G. (2016). Uranium isotope analysis by MC-ICP-MS in sub-ng sized samples. *Journal of Analytical Atomic Spectrometry*, 31(11), 2272–2284. <https://doi.org/10.1039/C6JA00238B>
- Boulyga, S. F., Konegger-Kappel, S., Richter, S., & Sangély, L. (2015). Mass spectrometric analysis for nuclear safeguards. *Journal of Analytical Atomic Spectrometry*, 30(7), 1469–1489. <https://doi.org/10.1039/C4JA00491D>
- Boulyga, S. F., Matusевич, J. L., Mironov, V. P., Kudrjashov, V. P., Halicz, L., Segal, I., ... Sabine Becker, J. (2002). Determination of $^{236}\text{U}/^{238}\text{U}$ isotope ratio in contaminated environmental samples using different ICP-MS instruments. *Journal of Analytical Atomic Spectrometry*, 17(8), 958–964. <https://doi.org/10.1039/b201803a>
- Bourdon, B. (2003). Introduction to U-series Geochemistry. *Reviews in Mineralogy and Geochemistry*, 52(1), 1–21. <https://doi.org/10.2113/0520001>
- Bourdon, B., Bureau, S., Andersen, M. B., Pili, E., & Hubert, A. (2009). Weathering rates from top to bottom in a carbonate environment. *Chemical Geology*, 258(3–4), 275–287. <https://doi.org/10.1016/j.chemgeo.2008.10.026>
- Bourdon, B., Henderson, G. M., Lundstrom, C. C., & Turner, S. P. (2003). *Uranium-series geochemistry. (Reviews in Mineralogy and Geochemistry; Vol. 52)*. Washington, D.C., USA: Mineralogical Society of America.
- Brasier, A. T., Andrews, J. E., Marca-Bell, A. D., & Dennis, P. F. (2010). Depositional continuity of seasonally laminated tufas: Implications for $\delta^{18}\text{O}$ based palaeotemperatures. *Global and Planetary Change*, 71(3–4), 160–167. <https://doi.org/10.1016/j.gloplacha.2009.03.022>
- Brennecka, G. A., Borg, L. E., Hutcheon, I. D., Sharp, M. A., & Anbar, A. D. (2010). Natural variations in uranium isotope ratios of uranium ore concentrates: Understanding the $^{238}\text{U}/^{235}\text{U}$ fractionation mechanism. *Earth and Planetary Science Letters*, 291(1–4), 228–233. <https://doi.org/10.1016/j.epsl.2010.01.023>
- Brennecka, G. A., Wasylenki, L. E., Bargar, J. R., Weyer, S., & Anbar, A. D. (2011). Uranium Isotope Fractionation during Adsorption to Mn-Oxyhydroxides. *Environmental Science & Technology*, 45(4), 1370–1375. <https://doi.org/10.1021/es103061v>
- Brennecka, G. A., Weyer, S., Wadhwa, M., Janney, P. E., Zipfel, J., & Anbar, A. D. (2010). $^{238}\text{U}/^{235}\text{U}$ Variations in Meteorites: Extant ^{247}Cm and Implications for Pb-Pb Dating. *Science*, 327(5964), 449–451. <https://doi.org/10.1126/science.1180871>

- Bu, W., Zheng, J., Ketterer, M. E., Hu, S., Uchida, S., & Wang, X. (2017). Development and application of mass spectrometric techniques for ultra-trace determination of ^{236}U in environmental samples-A review. *Analytica Chimica Acta*, *995*, 1–20. <https://doi.org/10.1016/j.aca.2017.09.029>
- Bürger, S., Balsley, S. D., Baumann, S., Berger, J., Boulyga, S. F., Cunningham, J. A., ... Poths, J. (2012). Uranium and plutonium analysis of nuclear material samples by multi-collector thermal ionisation mass spectrometry: Quality control, measurement uncertainty, and metrological traceability. *International Journal of Mass Spectrometry*, *311*, 40–50. <https://doi.org/10.1016/j.ijms.2011.11.016>
- Bürger, S., Essex, R. M., Mathew, K. J., Richter, S., & Thomas, R. B. (2010). Implementation of Guide to the expression of Uncertainty in Measurement (GUM) to multi-collector TIMS uranium isotope ratio metrology. *International Journal of Mass Spectrometry*, *294*(2–3), 65–76. <https://doi.org/10.1016/j.ijms.2010.05.003>
- Capezzuoli, E., Gandin, A., & Pedley, M. (2014). Decoding tufa and travertine (fresh water carbonates) in the sedimentary record: The state of the art. *Sedimentology*, *61*(1), 1–21. <https://doi.org/10.1111/sed.12075>
- Carrasco Lourtau, A. M., & Rubio Montero, M. P. (2016). Evaluation of two radiochemical procedures for the determination of uranium and thorium isotopes in coal samples. *Journal of Radioanalytical and Nuclear Chemistry*, *307*(2), 1175–1181. <https://doi.org/10.1007/s10967-015-4296-x>
- Chabaux, F., Bourdon, B., & Riotte, J. (2008). Chapter 3 U-Series Geochemistry in Weathering Profiles, River Waters and Lakes. *Radioactivity in the Environment*, *13*(07), 49–104. [https://doi.org/10.1016/S1569-4860\(07\)00003-4](https://doi.org/10.1016/S1569-4860(07)00003-4)
- Chabaux, F., Riotte, J., & Dequincey, O. (2003). U-Th-Ra Fractionation During Weathering and River Transport. *Reviews in Mineralogy and Geochemistry*, *52*(1), 533–576. <https://doi.org/10.2113/0520533>
- Chen, J. H., & Wasserburg, G. J. (1981). Isotopic Determination of Uranium in Picomole and Subpicomole Quantities. *Analytical Chemistry*, *53*(13), 2060–2067. <https://doi.org/10.1021/ac00236a027>
- Chen, J., Zhang, D. D., Wang, S., Xiao, T., & Huang, R. (2004). Factors controlling tufa deposition in natural waters at waterfall sites. *Sedimentary Geology*, *166*(3–4), 353–366. <https://doi.org/10.1016/j.sedgeo.2004.02.003>
- Chen, Q., Liu, S., He, H., Tang, J., Zhao, J., Feng, Y., ... Zhou, H. (2020). Seasonal Variations of Uranium in Karst Waters from Northeastern Sichuan, Central China and Controlling Mechanisms. *Geochemistry International*, *58*(1), 103–112. <https://doi.org/10.1134/S0016702920010048>
- Chen, X., Romaniello, S. J., & Anbar, A. D. (2017). Uranium isotope fractionation induced by aqueous speciation: Implications for U isotopes in marine CaCO_3 as a paleoredox proxy. *Geochimica et Cosmochimica Acta*, *215*, 162–172. <https://doi.org/10.1016/j.gca.2017.08.006>
- Chen, X., Romaniello, S. J., Herrmann, A. D., Wasylenki, L. E., & Anbar, A. D. (2016). Uranium isotope fractionation during coprecipitation with aragonite and calcite. *Geochimica et Cosmochimica Acta*, *188*, 189–207. <https://doi.org/10.1016/j.gca.2016.05.022>

- Chen, Z., Auler, A. S., Bakalowicz, M., Drew, D., Griger, F., Hartmann, J., ... Goldscheider, N. (2017). The World Karst Aquifer Mapping project: concept, mapping procedure and map of Europe. *Hydrogeology Journal*, 25(3), 771–785. <https://doi.org/10.1007/s10040-016-1519-3>
- Cheng, H., Lawrence Edwards, R., Shen, C.-C., Polyak, V. J., Asmerom, Y., Woodhead, J., ... Calvin Alexander, E. (2013). Improvements in ^{230}Th dating, ^{230}Th and ^{234}U half-life values, and U–Th isotopic measurements by multi-collector inductively coupled plasma mass spectrometry. *Earth and Planetary Science Letters*, 371–372, 82–91. <https://doi.org/10.1016/j.epsl.2013.04.006>
- Cho, B. W., & Choo, C. O. (2019). Geochemical Behavior of Uranium and Radon in Groundwater of Jurassic Granite Area, Icheon, Middle Korea. *Water*, 11(6), 1278. <https://doi.org/10.3390/w11061278>
- Choppin, G. R., Liljezin, J., & Rydberg, J. (2002). Radionuclides in Nature. In *Radiochemistry and Nuclear Chemistry* (Vol. 136, pp. 94–122). Elsevier. <https://doi.org/10.1016/B978-075067463-8/50005-4>
- Church, T. M., & Sarin, M. M. (2008). Chapter 2 U- and Th-Series Nuclides in the Atmosphere: Supply, Exchange, Scavenging, and Applications to Aquatic Processes. *Radioactivity in the Environment*, 13(07), 11–47. [https://doi.org/10.1016/S1569-4860\(07\)00002-2](https://doi.org/10.1016/S1569-4860(07)00002-2)
- Colodner, D., Edmond, J., & Boyle, E. (1995). Rhenium in the Black Sea: comparison with molybdenum and uranium. *Earth and Planetary Science Letters*, 131(1–2), 1–15. [https://doi.org/10.1016/0012-821X\(95\)00010-A](https://doi.org/10.1016/0012-821X(95)00010-A)
- Condon, D. J., McLean, N., Noble, S. R., & Bowring, S. A. (2010). Isotopic composition ($^{238}\text{U}/^{235}\text{U}$) of some commonly used uranium reference materials. *Geochimica et Cosmochimica Acta*, 74(24), 7127–7143. <https://doi.org/10.1016/j.gca.2010.09.019>
- Condon, D. J., Schoene, B., McLean, N. M., Bowring, S. A., & Parrish, R. R. (2015). Metrology and traceability of U-Pb isotope dilution geochronology (EARTHTIME Tracer Calibration Part I). *Geochimica et Cosmochimica Acta*, 164, 464–480. <https://doi.org/10.1016/j.gca.2015.05.026>
- Connelly, J. N., Bizzarro, M., Krot, A. N., Nordlund, A., Wielandt, D., & Ivanova, M. A. (2012). The Absolute Chronology and Thermal Processing of Solids in the Solar Protoplanetary Disk. *Science*, 338(6107), 651–655. <https://doi.org/10.1126/science.1226919>
- Coplen, T. B. (2011). Guidelines and recommended terms for expression of stable-isotope-ratio and gas-ratio measurement results. *Rapid Communications in Mass Spectrometry*, 25(17), 2538–2560. <https://doi.org/10.1002/rcm.5129>
- Cuney, M. (2009). The extreme diversity of uranium deposits. *Mineralium Deposita*, 44(1), 3–9. <https://doi.org/10.1007/s00126-008-0223-1>
- Dabkowski, J., Limondin-Lozouet, N., Antoine, P., Andrews, J., Marca-Bell, A., & Robert, V. (2012). Climatic variations in MIS 11 recorded by stable isotopes and trace elements in a French tufa (La Celle, Seine Valley). *Journal of Quaternary Science*, 27(8), 790–799. <https://doi.org/10.1002/jqs.2567>
- Dahl, T. W., Boyle, R. A., Canfield, D. E., Connelly, J. N., Gill, B. C., Lenton, T. M., & Bizzarro, M. (2014). Uranium isotopes distinguish two geochemically distinct stages

- during the later Cambrian SPICE event. *Earth and Planetary Science Letters*, 401, 313–326. <https://doi.org/10.1016/j.epsl.2014.05.043>
- Dicke, R. H. (1969). The Age of the Galaxy from the Decay of Uranium. *The Astrophysical Journal*, 155, 123. <https://doi.org/10.1086/149854>
- Donohue, D. L. (1998). Strengthening IAEA safeguards through environmental sampling and analysis. *Journal of Alloys and Compounds*, 271–273, 11–18. [https://doi.org/10.1016/S0925-8388\(98\)00015-2](https://doi.org/10.1016/S0925-8388(98)00015-2)
- Dosseto, A., Bourdon, B., Gaillardet, J., Allègre, C. J., & Filizola, N. (2006). Time scale and conditions of weathering under tropical climate: Study of the Amazon basin with U-series. *Geochimica et Cosmochimica Acta*, 70(1), 71–89. <https://doi.org/10.1016/j.gca.2005.06.033>
- Dosseto, A., Bourdon, B., & Turner, S. P. (2008). Uranium-series isotopes in river materials: Insights into the timescales of erosion and sediment transport. *Earth and Planetary Science Letters*, 265(1–2), 1–17. <https://doi.org/10.1016/j.epsl.2007.10.023>
- Dosseto, A., Turner, S., & Douglas, G. (2006). Uranium-series isotopes in colloids and suspended sediments: Timescale for sediment production and transport in the Murray–Darling River system. *Earth and Planetary Science Letters*, 246(3–4), 418–431. <https://doi.org/10.1016/j.epsl.2006.04.019>
- Durand, S., Chabaux, F., Rihs, S., Düringer, P., & Elsass, P. (2005). U isotope ratios as tracers of groundwater inputs into surface waters: Example of the Upper Rhine hydrosystem. *Chemical Geology*, 220(1–2), 1–19. <https://doi.org/10.1016/j.chemgeo.2005.02.016>
- Eikenberg, J., Vezzu, G., Zumsteg, I., Bajo, S., Ruethi, M., & Wyssling, G. (2001). Precise two chronometer dating of Pleistocene travertine: The $^{230}\text{Th}/^{234}\text{U}$ and $^{226}\text{Ra}_{\text{ex}}/^{226}\text{Ra}(0)$ approach. *Quaternary Science Reviews*, 20(18), 1935–1953. [https://doi.org/10.1016/S0277-3791\(01\)00020-8](https://doi.org/10.1016/S0277-3791(01)00020-8)
- Ellison, S. L. R., & Williams, A. (2012). *Eurachem/CITAC guide: Quantifying Uncertainty in Analytical Measurement, Third edition*. Retrieved from www.eurachem.org.
- Faure, G. (1977). *Principles of isotope geology*. New York, United States: J. Wiley and Sons.
- Fleischer, R. L. (1982). Alpha-recoil damage and solution effects in minerals: uranium isotopic disequilibrium and radon release. *Geochimica et Cosmochimica Acta*, 46(11), 2191–2201. [https://doi.org/10.1016/0016-7037\(82\)90194-6](https://doi.org/10.1016/0016-7037(82)90194-6)
- Ford, D., & Williams, P. (2007). *Karst Hydrogeology and Geomorphology. Karst Hydrogeology and Geomorphology* (Vol. 31). West Sussex, England: John Wiley & Sons Ltd., <https://doi.org/10.1002/9781118684986>
- Frank, N., Kober, B., & Mangini, A. (2006). Carbonate precipitation, U-series dating and U-isotopic variations in a Holocene travertine platform at Bad Langensalza - Thuringia Basin, Germany. *Quaternaire*, 17(17/4), 333–342. <https://doi.org/10.4000/quaternaire.904>
- Fujii, Y., Higuchi, N., Haruno, Y., Nomura, M., & Suzuki, T. (2006). Temperature Dependence of Isotope Effects in Uranium Chemical Exchange Reactions. *Journal of Nuclear Science and Technology*, 43(4), 400–406. <https://doi.org/10.1080/18811248.2006.9711111>

- Garnett, E. R., Gilmour, M. A., Rowe, P. J., Andrews, J. E., & Preece, R. C. (2004). $^{230}\text{Th}/^{234}\text{U}$ dating of Holocene tufas: possibilities and problems. *Quaternary Science Reviews*, *23*(7–8), 947–958. <https://doi.org/10.1016/j.quascirev.2003.06.018>
- Ghiorso, A., Brittain, J. W., Manning, W. M., & Seaborg, G. T. (1951). The Uranium Isotope U^{236} . *Physical Review*, *82*(4), 558–558. <https://doi.org/10.1103/PhysRev.82.558.2>
- Gilmore, G. R. (2008). Radioactive Decay and the Origin of Gamma and X-Radiation. In *Practical Gamma-Ray Spectrometry* (pp. 1–24). Chichester, UK: John Wiley & Sons, Ltd. <https://doi.org/10.1002/9780470861981.ch1>
- Goldmann, A., Brenneka, G., Noordmann, J., Weyer, S., & Wadhwa, M. (2015). The uranium isotopic composition of the Earth and the Solar System. *Geochimica et Cosmochimica Acta*, *148*, 145–158. <https://doi.org/10.1016/j.gca.2014.09.008>
- Goldstein, S. J. (2003). Techniques for Measuring Uranium-series Nuclides: 1992–2002. *Reviews in Mineralogy and Geochemistry*, *52*(1), 23–57. <https://doi.org/10.2113/0520023>
- Goldstein, S. J., Rodriguez, J. M., & Lujan, N. (1997). Measurement and Application of Uranium Isotopes for Human and Environmental Monitoring. *Health Physics*, *72*(1), 10–18.
- Grenthe, I., Drożdżyński, J., Fujino, T., Buck, E. C., Albrecht-Schmitt, T. E., & Wolf, S. F. (2010). Uranium. In *The Chemistry of the Actinide and Transactinide Elements* (pp. 253–698). Dordrecht: Springer Netherlands. https://doi.org/10.1007/978-94-007-0211-0_5
- Grenthe, I., Fuger, J., Lemire, R. J., Muller, A. B., & Nguyen-Trung Cregu, C. Wanner, H. (1992). *Chemical thermodynamics of uranium*. Amsterdam (Netherlands): Elsevier Science Publishers.
- Grzymko, T. J., Marcantonio, F., McKee, B. A., & Mike Stewart, C. (2007). Temporal variability of uranium concentrations and $^{234}\text{U}/^{238}\text{U}$ activity ratios in the Mississippi river and its tributaries. *Chemical Geology*, *243*(3–4), 344–356. <https://doi.org/10.1016/j.chemgeo.2007.05.024>
- Günther-Leopold, I., Wernli, B., Kopajtic, Z., & Günther, D. (2004). Measurement of isotope ratios on transient signals by MC-ICP-MS. *Analytical and Bioanalytical Chemistry*, *378*(2), 241–249. <https://doi.org/10.1007/s00216-003-2226-1>
- Hain, K., Steier, P., Froehlich, M. B., Golser, R., Hou, X., Lachner, J., ... Sakaguchi, A. (2020). $^{233}\text{U}/^{236}\text{U}$ signature allows to distinguish environmental emissions of civil nuclear industry from weapons fallout. *Nature Communications*, *11*(1), 1275. <https://doi.org/10.1038/s41467-020-15008-2>
- Hartmann, A., Goldscheider, N., Wagener, T., Lange, J., & Weiler, M. (2014). Karst water resources in a changing world: Review of hydrological modeling approaches. *Reviews of Geophysics*, *52*(3), 218–242. <https://doi.org/10.1002/2013RG000443>
- Henderson, G. M. (2002). Seawater ($^{234}\text{U}/^{238}\text{U}$) during the last 800 thousand years. *Earth and Planetary Science Letters*, *199*(1–2), 97–110. [https://doi.org/10.1016/S0012-821X\(02\)00556-3](https://doi.org/10.1016/S0012-821X(02)00556-3)
- Henderson, G. M., Slowey, N. C., & Fleisher, M. Q. (2001). U-Th dating of carbonate platform and slope sediments. *Geochimica et Cosmochimica Acta*, *65*(16), 2757–2770.

- [https://doi.org/10.1016/S0016-7037\(01\)00621-4](https://doi.org/10.1016/S0016-7037(01)00621-4)
- Hiess, J., Condon, D. J., McLean, N., & Noble, S. R. (2012). $^{238}\text{U}/^{235}\text{U}$ Systematics in Terrestrial Uranium-Bearing Minerals. *Science*, *335*(6076), 1610–1614. <https://doi.org/10.1126/science.1215507>
- Hoffmann, D. L., Prytulak, J., Richards, D. A., Elliott, T., Coath, C. D., Smart, P. L., & Scholz, D. (2007). Procedures for accurate U and Th isotope measurements by high precision MC-ICPMS. *International Journal of Mass Spectrometry*, *264*(2–3), 97–109. <https://doi.org/10.1016/j.ijms.2007.03.020>
- Hoffmann, P. (2008). General Aspects of Environmental Sampling. In *Environmental Sampling for Trace Analysis* (pp. 10–71). Weinheim, Germany: Wiley-VCH Verlag GmbH. <https://doi.org/10.1002/9783527615872.ch2>
- Horsky, M., Irrgeher, J., & Prohaska, T. (2016). Evaluation strategies and uncertainty calculation of isotope amount ratios measured by MC ICP-MS on the example of Sr. *Analytical and Bioanalytical Chemistry*, *408*(2), 351–367. <https://doi.org/10.1007/s00216-015-9003-9>
- Horwitz, E. P., Dietz, M. L., Chiarizia, R., Diamond, H., Essling, A. M., & Graczyk, D. (1992). Separation and preconcentration of uranium from acidic media by extraction chromatography. *Analytica Chimica Acta*, *266*(1), 25–37. [https://doi.org/10.1016/0003-2670\(92\)85276-C](https://doi.org/10.1016/0003-2670(92)85276-C)
- Horwitz, E. P., Dietz, M. L., Nelson, D. M., LaRosa, J. J., & Fairman, W. D. (1990). Concentration and separation of actinides from urine using a supported bifunctional organophosphorus extractant. *Analytica Chimica Acta*, *238*, 263–271. [https://doi.org/10.1016/S0003-2670\(00\)80546-2](https://doi.org/10.1016/S0003-2670(00)80546-2)
- Hou, X., & Roos, P. (2008). Critical comparison of radiometric and mass spectrometric methods for the determination of radionuclides in environmental, biological and nuclear waste samples. *Analytica Chimica Acta*, *608*(2), 105–139. <https://doi.org/10.1016/j.aca.2007.12.012>
- Hu, Z., & Gao, S. (2008). Upper crustal abundances of trace elements: A revision and update. *Chemical Geology*, *253*(3–4), 205–221. <https://doi.org/10.1016/j.chemgeo.2008.05.010>
- Huckle, D., Ma, L., McIntosh, J., Vázquez-Ortega, A., Rasmussen, C., & Chorover, J. (2016). U-series isotopic signatures of soils and headwater streams in a semi-arid complex volcanic terrain. *Chemical Geology*, *445*, 68–83. <https://doi.org/10.1016/j.chemgeo.2016.04.003>
- Inn, K. G. W., Robin Hutchinson, J. M., Kelly, W. R., Greenberg, R., Norris, A., Krey, P., ... Percival, D. R. (2016). Analysis of U and Th in soils and sediments B—Why do we sometimes get the WRONG RESULT? *Journal of Radioanalytical and Nuclear Chemistry*, *307*(3), 2513–2520. <https://doi.org/10.1007/s10967-015-4566-7>
- International Atomic Energy Agency. (1991). *Guidelines for Leaching Studies on Coal Fly Ash and Other Solid Wastes With Special Reference to the Use of Radioanalytical Techniques*, IAEA-TECDOC-616. Vienna. Retrieved from <https://www.iaea.org/publications/872/guidelines-for-leaching-studies-on-coal-fly-ash-and-other-solid-wastes-with-special-reference-to-the-use-of-radioanalytical-techniques>

- International Atomic Energy Agency. (2019). *World Thorium Occurrences, Deposits and Resources*, IAEA-TECDOC-1877. IAEA. Vienna. Retrieved from <https://www.iaea.org/publications/13550/world-thorium-occurrences-deposits-and-resources>
- Irrgeher, J., & Prohaska, T. (2014). Metrology. In T. Prohaska, J. Irrgeher, A. Zitek, & N. Jakubowski (Eds.), *Sector Field Mass Spectrometry for Elemental and Isotopic Analysis* (pp. 183–196). Cambridge: Royal Society of Chemistry. <https://doi.org/10.1039/9781849735407-00183>
- Irrgeher, J., & Prohaska, T. (2016). Application of non-traditional stable isotopes in analytical ecogeochemistry assessed by MC ICP-MS - A critical review. *Analytical and Bioanalytical Chemistry*, 408(2), 369–385. <https://doi.org/10.1007/s00216-015-9025-3>
- Irrgeher, J., Vogl, J., Santner, J., & Prohaska, T. (2014). Measurement Strategies. In T. Prohaska, J. Irrgeher, A. Zitek, & N. Jakubowski (Eds.), *Sector Field Mass Spectrometry for Elemental and Isotopic Analysis* (pp. 126–151). Cambridge: Royal Society of Chemistry. <https://doi.org/10.1039/9781849735407-00126>
- ISO. (2006a). *Standard ISO 11464: Soil quality — Pretreatment of samples for physico-chemical analysis*. Geneva. Retrieved from <https://www.iso.org/standard/37718.html>
- ISO. (2006b). *Standard ISO 5667-5: Water quality—sampling—part 5: guidance on sampling of drinking water from treatment works and piped distribution systems*. Geneva. Retrieved from <https://www.iso.org/standard/36694.html>
- ISO. (2008). *Standard ISO/IEC GUIDE 98-3:2008: Uncertainty of measurement — Part 3: Guide to the expression of uncertainty in measurement (GUM:1995)*. Geneva. Retrieved from <https://www.iso.org/standard/50461.html>
- Ivanovich, M., & Harmon, R. S. (1992). *Uranium-series disequilibrium: applications to earth, marine, and environmental sciences*. Oxford, UK: Oxford Science Publications.
- Ivanovich, M., Tellam, J. H., Longworth, G., & Monaghan, J. J. (1992). Rock/Water Interaction Timescales Involving U and Th Isotopes in a Permo-Triassic Sandstone. *Radiochimica Acta*, 58–59(2), 423–432. <https://doi.org/10.1524/ract.1992.5859.2.423>
- Jakubowski, N., Horsky, M., Roos, P. H., Vanhaecke, F., & Prohaska, T. (2014). Inductively Coupled Plasma Mass Spectrometry. In T. Prohaska, J. Irrgeher, A. Zitek, & N. Jakubowski (Eds.), *Sector Field Mass Spectrometry for Elemental and Isotopic Analysis* (pp. 208–318). Cambridge: Royal Society of Chemistry. <https://doi.org/10.1039/9781849735407-00208>
- Jeřkovský, M., Kaizer, J., Kontul, I., Lujaniené, G., Müllerová, M., & Povinec, P. P. (2019). Analysis of environmental radionuclides. In *Handbook of Radioactivity Analysis: Volume 2* (Vol. 2, pp. 137–261). Elsevier. <https://doi.org/10.1016/B978-0-12-814395-7.00003-9>
- Jia, G., Torri, G., Ocone, R., Di Lullo, A., De Angelis, A., & Boschetto, R. (2008). Determination of thorium isotopes in mineral and environmental water and soil samples by α -spectrometry and the fate of thorium in water. *Applied Radiation and Isotopes*, 66(10), 1478–1487. <https://doi.org/10.1016/j.apradiso.2008.03.015>
- Jurečič, S., Benedik, L., Planinšek, P., Nečemer, M., Kump, P., & Pihlar, B. (2014). Analysis of uranium in the insoluble residues after decomposition of soil samples by

- various techniques. *Applied Radiation and Isotopes*, 87, 61–65. <https://doi.org/10.1016/j.apradiso.2013.11.077>
- Kappel, S., Boulyga, S. F., & Prohaska, T. (2012). Direct uranium isotope ratio analysis of single micrometer-sized glass particles. *Journal of Environmental Radioactivity*, 113, 8–15. <https://doi.org/10.1016/j.jenvrad.2012.03.017>
- Kaufman, A. (1993). An evaluation of several methods for determining ages in impure carbonates. *Geochimica et Cosmochimica Acta*, 57(10), 2303–2317. [https://doi.org/10.1016/0016-7037\(93\)90571-D](https://doi.org/10.1016/0016-7037(93)90571-D)
- Kelly, S. D., Rasbury, E. T., Chattopadhyay, S., Kropf, A. J., & Kemner, K. M. (2006). Evidence of a stable uranyl site in ancient organic-rich calcite. *Environmental Science and Technology*, 40(7), 2262–2268. <https://doi.org/10.1021/es051970v>
- Kendall, B., Brennecke, G. A., Weyer, S., & Anbar, A. D. (2013). Uranium isotope fractionation suggests oxidative uranium mobilization at 2.50Ga. *Chemical Geology*, 362, 105–114. <https://doi.org/10.1016/j.chemgeo.2013.08.010>
- Kigoshi, K. (1971). Alpha-Recoil Thorium-234: Dissolution into Water and the Uranium-234/Uranium-238 Disequilibrium in Nature. *Science*, 173(3991), 47–48. <https://doi.org/10.1126/science.173.3991.47>
- Kolodny, Y., Torfstein, A., Weiss-Sarusi, K., Zakon, Y., & Halicz, L. (2017). ²³⁸U-²³⁵U-²³⁴U fractionation between tetravalent and hexavalent uranium in seafloor phosphorites. *Chemical Geology*, 451, 1–8. <https://doi.org/10.1016/j.chemgeo.2016.12.032>
- Kónya, J., & Nagy, N. M. (2018a). Environmental Radioactivity. In *Nuclear and Radiochemistry* (pp. 399–419). Elsevier. <https://doi.org/10.1016/B978-0-12-813643-0.00013-5>
- Kónya, J., & Nagy, N. M. (2018b). Radioactive Decay. In *Nuclear and Radiochemistry* (pp. 49–84). Elsevier. <https://doi.org/10.1016/B978-0-12-813643-0.00004-4>
- Kopylova, Y., Guseva, N., Shestakova, A., Khvashevskaya, A., & Arakchaa, K. (2015). Uranium and thorium behavior in groundwater of the natural spa area “Choygan mineral water” (East Tuva). *IOP Conference Series: Earth and Environmental Science*, 27, 012034. <https://doi.org/10.1088/1755-1315/27/1/012034>
- Kraemer, T. F., & Brabets, T. P. (2012). Uranium isotopes (²³⁴U/²³⁸U) in rivers of the Yukon Basin (Alaska and Canada) as an aid in identifying water sources, with implications for monitoring hydrologic change in arctic regions. *Hydrogeology Journal*, 20(3), 469–481. <https://doi.org/10.1007/s10040-012-0829-3>
- Kristo, M. J., Gaffney, A. M., Marks, N., Knight, K., Cassata, W. S., & Hutcheon, I. D. (2016). Nuclear Forensic Science: Analysis of Nuclear Material Out of Regulatory Control. *Annual Review of Earth and Planetary Sciences*, 44(1), 555–579. <https://doi.org/10.1146/annurev-earth-060115-012309>
- Krupp, E. M., & Donard, O. F. X. (2005). Isotope ratios on transient signals with GC–MC–ICP–MS. *International Journal of Mass Spectrometry*, 242(2–3), 233–242. <https://doi.org/10.1016/j.ijms.2004.11.026>
- Ku, T.-L., Mathieu, G. G., & Knauss, K. G. (1977). Uranium in open ocean: concentration and isotopic composition. *Deep Sea Research*, 24(11), 1005–1017. [https://doi.org/10.1016/0146-6291\(77\)90571-9](https://doi.org/10.1016/0146-6291(77)90571-9)
- L’Annunziata, M. F. (2012). Radiation Physics and Radionuclide Decay. In *Handbook of*

- Radioactivity Analysis* (pp. 1–162). Elsevier. <https://doi.org/10.1016/B978-0-12-384873-4.00001-3>
- Langmuir, D. (1978). Uranium solution-mineral equilibria at low temperatures with applications to sedimentary ore deposits. *Geochimica et Cosmochimica Acta*, *42*(6), 547–569. [https://doi.org/10.1016/0016-7037\(78\)90001-7](https://doi.org/10.1016/0016-7037(78)90001-7)
- Langmuir, D., & Herman, J. S. (1980). The mobility of thorium in natural waters at low temperatures. *Geochimica et Cosmochimica Acta*, *44*(11), 1753–1766. [https://doi.org/10.1016/0016-7037\(80\)90226-4](https://doi.org/10.1016/0016-7037(80)90226-4)
- Lawrence Edwards, R., Chen, J. H., & Wasserburg, G. J. (1987). ^{238}U - ^{234}U - ^{230}Th - ^{232}Th systematics and the precise measurement of time over the past 500,000 years. *Earth and Planetary Science Letters*, *81*(2–3), 175–192. [https://doi.org/10.1016/0012-821X\(87\)90154-3](https://doi.org/10.1016/0012-821X(87)90154-3)
- Layne, G. D., & Sim, K. W. (2000). Secondary ion mass spectrometry for the measurement of $^{232}\text{Th}/^{230}\text{Th}$ in volcanic rocks. *International Journal of Mass Spectrometry*, *203*(1–3), 187–198. [https://doi.org/10.1016/S1387-3806\(00\)00312-2](https://doi.org/10.1016/S1387-3806(00)00312-2)
- Lidman, F., Peralta-Tapia, A., Vesterlund, A., & Laudon, H. (2016). $^{234}\text{U}/^{238}\text{U}$ in a boreal stream network — Relationship to hydrological events, groundwater and scale. *Chemical Geology*, *420*, 240–250. <https://doi.org/10.1016/j.chemgeo.2015.11.014>
- Liesch, T., Hinrichsen, S., & Goldscheider, N. (2015). Uranium in groundwater — Fertilizers versus geogenic sources. *Science of The Total Environment*, *536*, 981–995. <https://doi.org/10.1016/j.scitotenv.2015.05.133>
- Liu, C., Shi, Z., & Zachara, J. M. (2009). Kinetics of Uranium(VI) Desorption from Contaminated Sediments: Effect of Geochemical Conditions and Model Evaluation. *Environmental Science & Technology*, *43*(17), 6560–6566. <https://doi.org/10.1021/es900666m>
- Lloyd, N. S., Chenery, S. R. N., & Parrish, R. R. (2009). The distribution of depleted uranium contamination in Colonie, NY, USA. *Science of The Total Environment*, *408*(2), 397–407. <https://doi.org/10.1016/j.scitotenv.2009.09.024>
- Lojen, S., Dolenc, T., Vokal, B., Cukrov, N., Mihelčić, G., & Papesch, W. (2004). C and O stable isotope variability in recent freshwater carbonates (River Krka, Croatia). *Sedimentology*, *51*(2), 361–375. <https://doi.org/10.1111/j.1365-3091.2004.00630.x>
- Loveland, W. D., Morrissey, D. J., & Seaborg, G. T. (2017). Radioactive Decay Kinetics. In *Modern Nuclear Chemistry* (Vol. 39, pp. 57–92). Hoboken, NJ, USA: John Wiley & Sons, Inc. <https://doi.org/10.1002/9781119348450.ch3>
- Ludwig, K. R. (2003). Mathematical-Statistical Treatment of Data and Errors for $^{230}\text{Th}/\text{U}$ Geochronology. *Reviews in Mineralogy and Geochemistry*, *52*(1), 631–656. <https://doi.org/10.2113/0520631>
- Ludwig, K. R., & Paces, J. B. (2002). Uranium-series dating of pedogenic silica and carbonate, Crater Flat, Nevada. *Geochimica et Cosmochimica Acta*, *66*(3), 487–506. [https://doi.org/10.1016/S0016-7037\(01\)00786-4](https://doi.org/10.1016/S0016-7037(01)00786-4)
- Ludwig, K. R., Simmons, K. R., Szabo, B. J., Winograd, I. J., Landwehr, J. M., Riggs, A. C., & Hoffman, R. J. (1992). Mass-Spectrometric ^{230}Th - ^{234}U - ^{238}U Dating of the Devils Hole Calcite Vein. *Science*, *258*(5080), 284–287. <https://doi.org/10.1126/science.258.5080.284>

- Luo, S., Ku, T.-L., Roback, R., Murrell, M., & McLing, T. L. (2000). In-situ radionuclide transport and preferential groundwater flows at INEEL (Idaho): decay-series disequilibrium studies. *Geochimica et Cosmochimica Acta*, *64*(5), 867–881. [https://doi.org/10.1016/S0016-7037\(99\)00373-7](https://doi.org/10.1016/S0016-7037(99)00373-7)
- Luo, X., Rehkämper, M., Lee, D.-C., & Halliday, A. N. (1997). High precision $^{230}\text{Th}/^{232}\text{Th}$ and $^{234}\text{U}/^{238}\text{U}$ measurements using energy-filtered ICP magnetic sector multiple collector mass spectrometry. *International Journal of Mass Spectrometry and Ion Processes*, *171*(1–3), 105–117. [https://doi.org/10.1016/S0168-1176\(97\)00136-5](https://doi.org/10.1016/S0168-1176(97)00136-5)
- Malov, A. I., & Zykov, S. B. (2020). Study of the mobilization of Uranium isotopes in a sandstone aquifer in combination with groundwater data. *Water*, *12*(1). <https://doi.org/10.3390/w12010112>
- Mason, A. J., & Henderson, G. M. (2010). Correction of multi-collector-ICP-MS instrumental biases in high-precision uranium–thorium chronology. *International Journal of Mass Spectrometry*, *295*(1–2), 26–35. <https://doi.org/10.1016/j.ijms.2010.06.016>
- Murphy, M. J., Froehlich, M. B., Fifield, L. K., Turner, S. P., & Schaefer, B. F. (2015). In-situ production of natural ^{236}U in groundwaters and ores in high-grade uranium deposits. *Chemical Geology*, *410*, 213–222. <https://doi.org/10.1016/j.chemgeo.2015.06.024>
- Nakai, S., Fukuda, S., & Nakada, S. (2001). Thorium isotopic measurements on silicate rock samples with a multi-collector inductively coupled plasma mass spectrometer. *The Analyst*, *126*(10), 1707–1710. <https://doi.org/10.1039/b101593l>
- Nomura, M., Higuchi, N., & Fujii, Y. (1996). Mass dependence of uranium isotope effects in the U(IV)-U(VI) exchange reaction. *Journal of the American Chemical Society*, *118*(38), 9127–9130. <https://doi.org/10.1021/ja954075s>
- Noordmann, J., Weyer, S., Georg, R. B., Jöns, S., & Sharma, M. (2016). $^{238}\text{U}/^{235}\text{U}$ isotope ratios of crustal material, rivers and products of hydrothermal alteration: new insights on the oceanic U isotope mass balance. *Isotopes in Environmental and Health Studies*, *52*(1–2), 141–163. <https://doi.org/10.1080/10256016.2015.1047449>
- Nu Instruments Ltd. (2014). *Nu Plasma II multi-collector ICP-MS*. North Wales (UK): Nu Instruments Ltd. Retrieved from www.nu-ins.com
- Nyachoti, S., Jin, L., Tweedie, C. E., & Ma, L. (2019). Insight into factors controlling formation rates of pedogenic carbonates: A combined geochemical and isotopic approach in dryland soils of the US Southwest. *Chemical Geology*, *527*, 118503. <https://doi.org/10.1016/j.chemgeo.2017.10.014>
- Oi, T., Kawada, K., Hosoe, M., & Kakihana, H. (1991). Fractionation of Lithium Isotopes in Cation-Exchange Chromatography. *Separation Science and Technology*, *26*(10–11), 1353–1375. <https://doi.org/10.1080/01496399108050537>
- Oliver, I. W., Graham, M. C., MacKenzie, A. B., Ellam, R. M., & Farmer, J. G. (2007). Assessing depleted uranium (DU) contamination of soil, plants and earthworms at UK weapons testing sites. *Journal of Environmental Monitoring*, *9*(7), 740. <https://doi.org/10.1039/b700719a>
- Ordóñez-Regil, E., Schleiffer, J. J., Adloff, J. P., & Roessler, K. (1989). Chemical Effects of α -Decay in Uranium Minerals. *Radiochimica Acta*, *47*(4).

- <https://doi.org/10.1524/ract.1989.47.4.177>
- Paces, J. B., Nichols, P. J., Neymark, L. A., & Rajaram, H. (2013). Evaluation of Pleistocene groundwater flow through fractured tuffs using a U-series disequilibrium approach, Pahute Mesa, Nevada, USA. *Chemical Geology*, *358*, 101–118. <https://doi.org/10.1016/j.chemgeo.2013.08.043>
- Palme, H., & O'Neill, H. S. C. (2007). Cosmochemical Estimates of Mantle Composition. In *Treatise on Geochemistry* (pp. 1–38). Elsevier. <https://doi.org/10.1016/B0-08-043751-6/02177-0>
- Palmer, M. R., & Edmond, J. M. (1993). Uranium in river water. *Geochimica et Cosmochimica Acta*, *57*(20), 4947–4955. [https://doi.org/10.1016/0016-7037\(93\)90131-F](https://doi.org/10.1016/0016-7037(93)90131-F)
- Park, J.-H., & Jeong, K. (2018). Experimental evaluation of the detection methods of thermal ionization mass spectrometry for isotopic analysis of ultra-trace level uranium. *Microchemical Journal*, *137*, 334–341. <https://doi.org/10.1016/j.microc.2017.11.013>
- Pedley, M. (1990). Classification and environmental models of cool freshwater tufas. *Sedimentary Geology*, *68*(1–2), 143–154. [https://doi.org/10.1016/0037-0738\(90\)90124-C](https://doi.org/10.1016/0037-0738(90)90124-C)
- Pereira de Oliveira, O., De Bolle, W., Alonso, A., Richter, S., Wellum, R., Ponzevera, E., ... Kessel, R. (2010). Demonstrating the metrological compatibility of uranium isotope amount ratio measurement results obtained by GSMS, TIMS and MC-ICPMS techniques. *International Journal of Mass Spectrometry*, *291*(1–2), 48–54. <https://doi.org/10.1016/j.ijms.2010.01.005>
- Pietruszka, A. J., Carlson, R. W., & Hauri, E. H. (2002). Precise and accurate measurement of ^{226}Ra – ^{230}Th – ^{238}U disequilibria in volcanic rocks using plasma ionization multicollector mass spectrometry. *Chemical Geology*, *188*(3–4), 171–191. [https://doi.org/10.1016/S0009-2541\(02\)00106-7](https://doi.org/10.1016/S0009-2541(02)00106-7)
- Pietruszka, A. J., & Reznik, A. D. (2008). Identification of a matrix effect in the MC-ICP-MS due to sample purification using ion exchange resin: An isotopic case study of molybdenum. *International Journal of Mass Spectrometry*, *270*(1–2), 23–30. <https://doi.org/10.1016/j.ijms.2007.11.001>
- Plater, A. J., Ivanovich, M., & Dugdale, R. E. (1992). Uranium series disequilibrium in river sediments and waters: the significance of anomalous activity ratios. *Applied Geochemistry*, *7*(2), 101–110. [https://doi.org/10.1016/0883-2927\(92\)90029-3](https://doi.org/10.1016/0883-2927(92)90029-3)
- Platzner, I. T. (1997). *Modern Isotope Ratio Mass Spectrometry*. Chichester, UK: Wiley.
- Pollington, A. D., Kinman, W. S., Hanson, S. K., & Steiner, R. E. (2016). Polyatomic interferences on high precision uranium isotope ratio measurements by MC-ICP-MS: applications to environmental sampling for nuclear safeguards. *Journal of Radioanalytical and Nuclear Chemistry*, *307*(3), 2109–2115. <https://doi.org/10.1007/s10967-015-4419-4>
- Porcelli, D. (2003). The Behavior of U- and Th-series Nuclides in Groundwater. *Reviews in Mineralogy and Geochemistry*, *52*(1), 317–361. <https://doi.org/10.2113/0520317>
- Porcelli, D. (2008). Chapter 4 Investigating Groundwater Processes Using U- and Th-Series Nuclides. *Radioactivity in the Environment*, *13*(07), 105–153.

- [https://doi.org/10.1016/S1569-4860\(07\)00004-6](https://doi.org/10.1016/S1569-4860(07)00004-6)
- Prohaska, T. (2014). Interferences. In T. Prohaska, J. Irrgeher, A. Zitek, & N. Jakubowski (Eds.), *Sector Field Mass Spectrometry for Elemental and Isotopic Analysis* (pp. 121–125). Cambridge: Royal Society of Chemistry. <https://doi.org/10.1039/9781849735407-00121>
- Prohaska, T., Irrgeher, J., Zitek, A., & Jakubowski, N. (2014). *Sector Field Mass Spectrometry for Elemental and Isotopic Analysis*. Cambridge: Royal Society of Chemistry. <https://doi.org/10.1039/9781849735407>
- Ravbar, N., Petrič, M., & Kogovšek, J. (2010). The Characteristics of Groundwater Flow in Karst Aquifers During Long Lasting Low Flow Conditions, Example from SW Slovenia. In B. Andreo, F. Carrasco, J. Durán, & J. LaMoreaux (Eds.), *Advances in Research in Karst Media. Environmental Earth Sciences* (pp. 131–136). Berlin, Heidelberg: Springer. https://doi.org/10.1007/978-3-642-12486-0_20
- Richter, S., Alonso-Munoz, A., Eykens, R., Jacobsson, U., Kuehn, H., Verbruggen, A., ... Keegan, E. (2008). The isotopic composition of natural uranium samples—Measurements using the new $n(^{233}\text{U})/n(^{236}\text{U})$ double spike IRMM-3636. *International Journal of Mass Spectrometry*, 269(1–2), 145–148. <https://doi.org/10.1016/j.ijms.2007.09.012>
- Richter, S., Eykens, R., Kühn, H., Aregbe, Y., Verbruggen, A., & Weyer, S. (2010). New average values for the $n(^{238}\text{U})/n(^{235}\text{U})$ isotope ratios of natural uranium standards. *International Journal of Mass Spectrometry*, 295(1–2), 94–97. <https://doi.org/10.1016/j.ijms.2010.06.004>
- Richter, S., & Goldberg, S. A. (2003). Improved techniques for high accuracy isotope ratio measurements of nuclear materials using thermal ionization mass spectrometry. *International Journal of Mass Spectrometry*, 229(3), 181–197. [https://doi.org/10.1016/S1387-3806\(03\)00338-5](https://doi.org/10.1016/S1387-3806(03)00338-5)
- Riotte, J., & Chabaux, F. (1999). ($^{234}\text{U}/^{238}\text{U}$) activity ratios in freshwaters as tracers of hydrological processes: the Strengbach watershed (Vosges, France). *Geochimica et Cosmochimica Acta*, 63(9), 1263–1275. [https://doi.org/10.1016/S0016-7037\(99\)00009-5](https://doi.org/10.1016/S0016-7037(99)00009-5)
- Riotte, J., Chabaux, F., Benedetti, M., Dia, A., Gérard, M., Boulègue, J., & Etamé, J. (2003). Uranium colloidal transport and origin of the ^{234}U – ^{238}U fractionation in surface waters: new insights from Mount Cameroon. *Chemical Geology*, 202(3–4), 365–381. <https://doi.org/10.1016/j.chemgeo.2002.10.002>
- Robinson, L. F., Belshaw, N. S., & Henderson, G. M. (2004). U and Th concentrations and isotope ratios in modern carbonates and waters from the Bahamas. *Geochimica et Cosmochimica Acta*, 68(8), 1777–1789. <https://doi.org/10.1016/j.gca.2003.10.005>
- Rodríguez, P. B., Tomé, F. V., & Lozano, J. C. (2001). Concerning the low uranium and thorium yields in the electrodeposition process of soil and sediment analyses. *Applied Radiation and Isotopes*, 54(1), 29–33. [https://doi.org/10.1016/S0969-8043\(00\)00192-5](https://doi.org/10.1016/S0969-8043(00)00192-5)
- Romaniello, S. J., Field, M. P., Smith, H. B., Gordon, G. W., Kim, M. H., & Anbar, A. D. (2015). Fully automated chromatographic purification of Sr and Ca for isotopic analysis. *Journal of Analytical Atomic Spectrometry*, 30(9), 1906–1912.

- <https://doi.org/10.1039/C5JA00205B>
- Rovan, L., Lojen, S., Zuliani, T., Kanduč, T., Petrič, M., Horvat, B., ... Štrok, M. (2020). Comparison of Uranium Isotopes and Classical Geochemical Tracers in Karst Aquifer of Ljubljana River catchment (Slovenia). *Water*, *12*(7), 2064. <https://doi.org/10.3390/w12072064>
- Rovan, L., & Štrok, M. (2019). Optimization of the sample preparation and measurement protocol for the analysis of uranium isotopes by MC-ICP-MS without spike addition. *Journal of Analytical Atomic Spectrometry*, *34*(9), 1882–1891. <https://doi.org/10.1039/C9JA00144A>
- Rovan, L., Zuliani, T., Horvat, B., Kanduč, T., Vreča, P., Jamil, Q., ... Lojen, S. (2021). Uranium isotopes as a possible tracer of terrestrial authigenic carbonate. *Science of The Total Environment*, *797*, 149103. <https://doi.org/10.1016/j.scitotenv.2021.149103>
- Rubin, K. (2001). Analysis of $^{232}\text{Th}/^{230}\text{Th}$ in volcanic rocks: a comparison of thermal ionization mass spectrometry and other methodologies. *Chemical Geology*, *175*(3–4), 723–750. [https://doi.org/10.1016/S0009-2541\(00\)00340-5](https://doi.org/10.1016/S0009-2541(00)00340-5)
- Rutgers van der Loeff, M. M., & Geibert, W. (2008). Chapter 7 U- and Th-Series Nuclides as Tracers of Particle Dynamics, Scavenging and Biogeochemical Cycles in the Oceans. *Radioactivity in the Environment*, *13*(07), 227–268. [https://doi.org/10.1016/S1569-4860\(07\)00007-1](https://doi.org/10.1016/S1569-4860(07)00007-1)
- Saari, H.-K., Schmidt, S., Huguet, S., & Lanoux, A. (2008). Spatiotemporal variation of dissolved ^{238}U in the Gironde fluvial–estuarine system (France). *Journal of Environmental Radioactivity*, *99*(2), 426–435. <https://doi.org/10.1016/j.jenvrad.2007.11.016>
- Sakaguchi, A., Kawai, K., Steier, P., Quinto, F., Mino, K., Tomita, J., ... Yamamoto, M. (2009). First results on ^{236}U levels in global fallout. *Science of The Total Environment*, *407*(14), 4238–4242. <https://doi.org/10.1016/j.scitotenv.2009.01.058>
- Sappa, G., Vitale, S., & Ferranti, F. (2018). Identifying Karst Aquifer Recharge Areas using Environmental Isotopes: A Case Study in Central Italy. *Geosciences*, *8*(9), 351. <https://doi.org/10.3390/geosciences8090351>
- Schaffhauser, T., Chabaux, F., Ambroise, B., Lucas, Y., Stille, P., Reuschlé, T., ... Fritz, B. (2014). Geochemical and isotopic (U, Sr) tracing of water pathways in the granitic Ringelbach catchment (Vosges Mountains, France). *Chemical Geology*, *374–375*, 117–127. <https://doi.org/10.1016/j.chemgeo.2014.02.028>
- Schauble, E. A. (2007). Role of nuclear volume in driving equilibrium stable isotope fractionation of mercury, thallium, and other very heavy elements. *Geochimica et Cosmochimica Acta*, *71*(9), 2170–2189. <https://doi.org/10.1016/j.gca.2007.02.004>
- Selvig, L. K., Inn, K. G. W., Outola, I. M. J., Kurosaki, H., & Lee, K. A. (2005). Dissolution of resistate minerals containing uranium and thorium: Environmental implications. *Journal of Radioanalytical and Nuclear Chemistry*, *263*(2), 341–348. <https://doi.org/10.1007/s10967-005-0060-y>
- Sen, I. S., & Peucker-Ehrenbrink, B. (2012). Anthropogenic Disturbance of Element Cycles at the Earth's Surface. *Environmental Science & Technology*, *46*(16), 8601–8609. <https://doi.org/10.1021/es301261x>
- Seth, B., Thirlwall, M. F., Houghton, S. L., & Craig, C.-A. (2003). Accurate measurements

- of Th–U isotope ratios for carbonate geochronology using MC-ICP-MS. *Journal of Analytical Atomic Spectrometry*, *18*(11), 1323–1330. <https://doi.org/10.1039/B308908H>
- Shen, C.-C., Lawrence Edwards, R., Cheng, H., Dorale, J. A., Thomas, R. B., Bradley Moran, S., ... Edmonds, H. N. (2002). Uranium and thorium isotopic and concentration measurements by magnetic sector inductively coupled plasma mass spectrometry. *Chemical Geology*, *185*(3–4), 165–178. [https://doi.org/10.1016/S0009-2541\(01\)00404-1](https://doi.org/10.1016/S0009-2541(01)00404-1)
- Siebert, C., Möller, P., Magri, F., Shalev, E., Rosenthal, E., Al-Raggad, M., & Rödiger, T. (2019). Applying Rare Earth Elements, Uranium, and $^{87}\text{Sr}/^{86}\text{Sr}$ to Disentangle Structurally Forced Confluence of Regional Groundwater Resources: The Case of the Lower Yarmouk Gorge. *Geofluids*, *2019*, 1–21. <https://doi.org/10.1155/2019/6727681>
- Skwarzec, B., Strumińska, D. I., & Borylo, A. (2001). The Radionuclides ^{234}U , ^{238}U and ^{210}Po in Drinking Water in Gdańsk Agglomeration (Poland). *Journal of Radioanalytical and Nuclear Chemistry*, *250*(2), 315–318. <https://doi.org/10.1023/A:1017903814852>
- Somayajulu, B. L. K., & Goldberg, E. D. (1966). Thorium and uranium isotopes in seawater and sediments. *Earth and Planetary Science Letters*, *1*(3), 102–106. [https://doi.org/10.1016/0012-821X\(66\)90084-7](https://doi.org/10.1016/0012-821X(66)90084-7)
- Spooner, P. T., Chen, T., Robinson, L. F., & Coath, C. D. (2016). Rapid uranium-series age screening of carbonates by laser ablation mass spectrometry. *Quaternary Geochronology*, *31*, 28–39. <https://doi.org/10.1016/j.quageo.2015.10.004>
- Steier, P., Bichler, M., Keith Fifield, L., Golser, R., Kutschera, W., Priller, A., ... Maria Wild, E. (2008). Natural and anthropogenic ^{236}U in environmental samples. *Nuclear Instruments and Methods in Physics Research B*, *266*(10), 2246–2250. <https://doi.org/10.1016/j.nimb.2008.03.002>
- Steiger, R. H., & Jäger, E. (1977). Subcommittee on geochronology: Convention on the use of decay constants in geo- and cosmochronology. *Earth and Planetary Science Letters*, *36*(3), 359–362. [https://doi.org/10.1016/0012-821X\(77\)90060-7](https://doi.org/10.1016/0012-821X(77)90060-7)
- Stirling, C. H., Andersen, M. B., Potter, E.-K., & Halliday, A. N. (2007). Low-temperature isotopic fractionation of uranium. *Earth and Planetary Science Letters*, *264*(1–2), 208–225. <https://doi.org/10.1016/j.epsl.2007.09.019>
- Stirling, C. H., Halliday, A. N., & Porcelli, D. (2005). In search of live ^{247}Cm in the early solar system. *Geochimica et Cosmochimica Acta*, *69*(4), 1059–1071. <https://doi.org/10.1016/j.gca.2004.06.034>
- Stirling, C. H., Lee, D. C., Christensen, J. N., & Halliday, A. N. (2000). High-precision in situ ^{238}U - ^{234}U - ^{230}Th isotopic analysis using laser ablation multiple-collector ICPMS. *Geochimica et Cosmochimica Acta*, *64*(21), 3737–3750. [https://doi.org/10.1016/S0016-7037\(00\)00457-9](https://doi.org/10.1016/S0016-7037(00)00457-9)
- Štrok, M., & Smodiš, B. (2010). Fractionation of natural radionuclides in soils from the vicinity of a former uranium mine Žirovski vrh, Slovenia. *Journal of Environmental Radioactivity*, *101*(1), 22–28. <https://doi.org/10.1016/j.jenvrad.2009.08.006>
- Stylo, M., Neubert, N., Wang, Y., Monga, N., Romaniello, S. J., Weyer, S., & Bernier-Latmani, R. (2015). Uranium isotopes fingerprint biotic reduction. *Proceedings of the*

- National Academy of Sciences*, 112(18), 5619–5624.
<https://doi.org/10.1073/pnas.1421841112>
- Suksi, J., Rasilainen, K., & Pitkänen, P. (2006). Variations in $^{234}\text{U}/^{238}\text{U}$ activity ratios in groundwater—A key to flow system characterisation? *Physics and Chemistry of the Earth, Parts A/B/C*, 31(10–14), 556–571. <https://doi.org/10.1016/j.pce.2006.04.007>
- Swarzenski, P. W. (2003). The Behavior of U- and Th-series Nuclides in the Estuarine Environment. *Reviews in Mineralogy and Geochemistry*, 52(1), 577–606. <https://doi.org/10.2113/0520577>
- Teichert, B. M. A., Eisenhauer, A., Bohrmann, G., Haase-Schramm, A., Bock, B., & Linke, P. (2003). U/Th systematics and ages of authigenic carbonates from Hydrate Ridge, Cascadia Margin: recorders of fluid flow variations. *Geochimica et Cosmochimica Acta*, 67(20), 3845–3857. [https://doi.org/10.1016/S0016-7037\(03\)00128-5](https://doi.org/10.1016/S0016-7037(03)00128-5)
- Thakkar, A. H. (2001). Rapid sequential separation of actinides using Eichrom's extraction chromatographic material. *Journal of Radioanalytical and Nuclear Chemistry*, 248(2), 453–456. <https://doi.org/10.1023/A:1010660915984>
- Thirlwall, M. F. (2001). Inappropriate tail corrections can cause large inaccuracy in isotope ratio determination by MC-ICP-MS. *Journal of Analytical Atomic Spectrometry*, 16(10), 1121–1125. <https://doi.org/10.1039/b103828c>
- Thirlwall, M. F. (2002). Multicollector ICP-MS analysis of Pb isotopes using a ^{207}Pb - ^{204}Pb double spike demonstrates up to 400 ppm/amu systematic errors in Tl-normalization. *Chemical Geology*, 184(3–4), 255–279. [https://doi.org/10.1016/S0009-2541\(01\)00365-5](https://doi.org/10.1016/S0009-2541(01)00365-5)
- Tissot, F. L. H., & Dauphas, N. (2015). Uranium isotopic compositions of the crust and ocean: Age corrections, U budget and global extent of modern anoxia. *Geochimica et Cosmochimica Acta*, 167, 113–143. <https://doi.org/10.1016/j.gca.2015.06.034>
- Trdin, M., Nečemer, M., & Benedik, L. (2017). Fast Decomposition Procedure of Solid Samples by Lithium Borates Fusion Employing Salicylic Acid. *Analytical Chemistry*, 89(5), 3169–3176. <https://doi.org/10.1021/acs.analchem.6b04980>
- Turner, S., van Calsteren, P., Vigier, N., & Thomas, L. (2001). Determination of thorium and uranium isotope ratios in low-concentration geological materials using a fixed multi-collector-ICP-MS. *Journal of Analytical Atomic Spectrometry*, 16(6), 612–615. <https://doi.org/10.1039/B008351H>
- Uvarova, Y. A., Kyser, T. K., Geagea, M. L., & Chipley, D. (2014). Variations in the uranium isotopic compositions of uranium ores from different types of uranium deposits. *Geochimica et Cosmochimica Acta*, 146, 1–17. <https://doi.org/10.1016/j.gca.2014.09.034>
- Vajda, N., Martin, P., & Kim, C.-K. (2012). Alpha Spectrometry. In *Handbook of Radioactivity Analysis* (pp. 363–422). Elsevier. <https://doi.org/10.1016/B978-0-12-384873-4.00006-2>
- van Calsteren, P., & Thomas, L. (2006). Uranium-series dating applications in natural environmental science. *Earth-Science Reviews*, 75(1–4), 155–175. <https://doi.org/10.1016/j.earscirev.2005.09.001>
- Van Orman, J. A., Grove, T. L., & Shimizu, N. (1998). Uranium and thorium diffusion in diopside. *Earth and Planetary Science Letters*, 160(3–4), 505–519.

- [https://doi.org/10.1016/S0012-821X\(98\)00107-1](https://doi.org/10.1016/S0012-821X(98)00107-1)
- Vanhaecke, F., & Kyser, K. (2012). The Isotopic Composition of the Elements. In F. Vanhaecke & P. Degryse (Eds.), *Isotopic Analysis* (pp. 1–29). Weinheim, Germany: Wiley-VCH Verlag GmbH & Co. KGaA. <https://doi.org/10.1002/9783527650484.ch1>
- Vanhaecke, F., van Holderbeke, M., Moens, L., & Dams, R. (1996). Evaluation of a commercially available microconcentric nebulizer for inductively coupled plasma mass spectrometry. *Journal of Analytical Atomic Spectrometry*, *11*(8), 543. <https://doi.org/10.1039/ja9961100543>
- Varga, Z., Krachler, M., Nicholl, A., Ernstberger, M., Wiss, T., Wallenius, M., & Mayer, K. (2018). Accurate measurement of uranium isotope ratios in solid samples by laser ablation multi-collector inductively coupled plasma mass spectrometry. *Journal of Analytical Atomic Spectrometry*, *33*(6), 1076–1080. <https://doi.org/10.1039/C8JA00006A>
- Vera Tomé, F., Jurado Vargas, M., & Martín Sánchez, A. (1994). Yields and losses at each step in preparing uranium and thorium samples for alpha spectrometry. *Applied Radiation and Isotopes*, *45*(4), 449–452. [https://doi.org/10.1016/0969-8043\(94\)90110-4](https://doi.org/10.1016/0969-8043(94)90110-4)
- Wall, J. D., & Krumholz, L. R. (2006). Uranium Reduction. *Annual Review of Microbiology*, *60*(1), 149–166. <https://doi.org/10.1146/annurev.micro.59.030804.121357>
- Wang, R.-M., & You, C.-F. (2013). Precise determination of U isotopic compositions in low concentration carbonate samples by MC-ICP-MS. *Talanta*, *107*, 67–73. <https://doi.org/10.1016/j.talanta.2012.12.044>
- Watanabe, Y., & Nakai, S. (2006). Accurate U-Th radioactive disequilibrium analyses of carbonate rock samples using commercially available U and Th reagents and multi-collector ICP-MS. *Microchimica Acta*, *156*(3–4), 289–295. <https://doi.org/10.1007/s00604-006-0579-9>
- Wefing, A.-M., Arps, J., Blaser, P., Wienberg, C., Hebbeln, D., & Frank, N. (2017). High precision U-series dating of scleractinian cold-water corals using an automated chromatographic U and Th extraction. *Chemical Geology*, *475*, 140–148. <https://doi.org/10.1016/j.chemgeo.2017.10.036>
- Weyer, S., Anbar, A. D., Gerdes, A., Gordon, G. W., Algeo, T. J., & Boyle, E. A. (2008). Natural fractionation of $^{238}\text{U}/^{235}\text{U}$. *Geochimica et Cosmochimica Acta*, *72*(2), 345–359. <https://doi.org/10.1016/j.gca.2007.11.012>
- White, W. B. (2002). Karst hydrology: recent developments and open questions. *Engineering Geology*, *65*(2–3), 85–105. [https://doi.org/10.1016/S0013-7952\(01\)00116-8](https://doi.org/10.1016/S0013-7952(01)00116-8)
- Wickleder, M. S., Fourest, B., & Dorhout, P. K. (2008). Thorium. In *The Chemistry of the Actinide and Transactinide Elements* (pp. 52–160). Dordrecht: Springer Netherlands. https://doi.org/10.1007/1-4020-3598-5_3
- Wieser, M. E., Buhl, D., Bouman, C., & Schwieters, J. (2004). High precision calcium isotope ratio measurements using a magnetic sector multiple collector inductively coupled plasma mass spectrometer. *Journal of Analytical Atomic Spectrometry*, *19*(7), 844. <https://doi.org/10.1039/b403339f>

- Wieser, M. E., & Schwieters, J. B. (2005). The development of multiple collector mass spectrometry for isotope ratio measurements. *International Journal of Mass Spectrometry*, *242*(2–3), 97–115. <https://doi.org/10.1016/j.ijms.2004.11.029>
- Williams, R. W. (2010). *Uncertainty in Measurement of Isotope Ratios by Multi-Collector Mass Spectrometry*. Livermore, California.
- Yang, L. (2009). Accurate and precise determination of isotopic ratios by MC-ICP-MS: A review. *Mass Spectrometry Reviews*, *28*(6), 990–1011. <https://doi.org/10.1002/mas.20251>
- Yang, L., Tong, S., Zhou, L., Hu, Z., Mester, Z., & Meija, J. (2018). A critical review on isotopic fractionation correction methods for accurate isotope amount ratio measurements by MC-ICP-MS. *Journal of Analytical Atomic Spectrometry*, *33*(11), 1849–1861. <https://doi.org/10.1039/C8JA00210J>
- Yokoyama, T., Makishima, A., & Nakamura, E. (1999). Separation of Thorium and Uranium from Silicate Rock Samples Using Two Commercial Extraction Chromatographic Resins. *Analytical Chemistry*, *71*(1), 135–141. <https://doi.org/10.1021/ac9805807>
- Zebracki, M., Cagnat, X., Gairoard, S., Cariou, N., Eyrolle-Boyer, F., Boulet, B., & Antonelli, C. (2017). U isotopes distribution in the Lower Rhone River and its implication on radionuclides disequilibrium within the decay series. *Journal of Environmental Radioactivity*, *178–179*, 279–289. <https://doi.org/10.1016/j.jenvrad.2017.09.004>
- Zhang, W., Guan, P., Jian, X., Feng, F., & Zou, C. (2014). In situ geochemistry of Lower Paleozoic dolomites in the northwestern Tarim basin: Implications for the nature, origin, and evolution of diagenetic fluids. *Geochemistry, Geophysics, Geosystems*, *15*(7), 2744–2764. <https://doi.org/10.1002/2013GC005194>
- Zhao, M.-Y., & Zheng, Y.-F. (2014). Marine carbonate records of terrigenous input into Paleotethyan seawater: Geochemical constraints from Carboniferous limestones. *Geochimica et Cosmochimica Acta*, *141*, 508–531. <https://doi.org/10.1016/j.gca.2014.07.001>
- Zhao, M.-Y., Zheng, Y.-F., & Zhao, Y.-Y. (2016). Seeking a geochemical identifier for authigenic carbonate. *Nature Communications*, *7*(1), 10885. <https://doi.org/10.1038/ncomms10885>

Bibliography

Publications Related to the Thesis

Journal Articles

- Rovan, L., Zuliani, T., Horvat, B., Kanduč, T., Vreča, P., Jamil, Q., ... Lojen, S. (2021). Uranium isotopes as a possible tracer of terrestrial authigenic carbonate. *Science of The Total Environment*, 797, 49103. <https://doi.org/10.1016/j.scitotenv.2021.149103>.
- Rovan, L., Lojen, S., Zuliani, T., Kanduč, T., Petrič, M., Horvat, B., ... Štrok, M. (2020). Comparison of Uranium Isotopes and Classical Geochemical Tracers in Karst Aquifer of Ljubljana River catchment (Slovenia). *Water*, 12(7), 2064. <https://doi.org/10.3390/w12072064>
- Rovan, L., & Štrok, M. (2019). Optimization of the sample preparation and measurement protocol for the analysis of uranium isotopes by MC-ICP-MS without spike addition. *Journal of Analytical Atomic Spectrometry*, 34(9), 1882–1891. <https://doi.org/10.1039/C9JA00144A>
- Benedik, L., Rován, L., Klemenčič, H., Gantar, I., & Prosen, H. (2015). Natural radioactivity in tap waters from the private wells in the surroundings of the former Žirovski Vrh uranium mine and the age-dependent dose assessment. *Environmental Science and Pollution Research*, 22(16), 12062–12072. <https://doi.org/10.1007/s11356-015-4481-z>

Conference Paper

- Rovan, L., Lojen, S., Zuliani, T., Horvat, B., Štrok, M. (2021). Hydrogeochemical impact on the karst watershed of the Krka River in Slovenia interpreted by U and Th isotopic composition. In: *Goldschmidt virtual 2021*, Online.
- Lojen, S., Zuliani, T., Rován, L., Horvat, B., Kanduč, T., Vreča, P., Jamil, Q., Štrok, M.. (2021) Uranium and strontium isotopes in recent and interglacial tufa in Krka National Park (Croatia). In: *Goldschmidt virtual 2021*, Online.
- Rovan, L., Lojen, S., Zuliani, T., Kanduč, T., Vreča, P., Horvat, B., Štrok, M. (2021). Novel U and Th isotopic tracers for characterization of karstic freshwater and recent tufa from the Krka River (Croatia). In: *EGU General Assembly 2021*, Online.
- Lojen, S., Jamil, Q., Zuliani, T., Rován, L., Kanduč, T., Vreča, P., Štrok, M., Bura-Nakić, E., Cukrov, N. (2021). Sr isotope fractionation in a karst river: case study of Krka, Croatia. In: *EGU General Assembly 2021*, Online.
- Rovan, L., Lojen, S., Zuliani, T., Horvat, B., Štrok, M. (2021). What can U and Th isotopic

- composition tell us about environmental processes in karstic settings? In: *13th Jožef Stefan International Postgraduate School Students' Conference and 15th Young Researchers' Day*, Online.
- Rovan, L., Štok, M. (2020). Behaviour of U isotopes in two different karst aquifers, Ljubljana River and Krka River (Slovenia). In: *12th Jožef Stefan International Postgraduate School Students' Conference and 14th Young Researchers' Day*, Online.
- Rovan, L., Štok, M. (2019). Water-rock interactions of uranium and thorium isotopes in a Ljubljana River catchment. In: *The 24th International Symposium on Environmental Biogeochemistry, Potsdam*, Potsdam: Helmholtz Centre, Germany.
- Lojen, S., Rován, L., Zuliani, T., Kanduč, T., Štok, M., Petrič, M., Rusjan, S. (2019). Non-traditional isotopes as tracers of water-rock interactions in a complex karst aquifer: case study of Ljubljana, Slovenia. In: *Goldschmidt 2019*, Barcelona, Spain.
- Rovan, L., Benedik, L., Štok, M. (2019). Tracing of uranium isotopes in Ljubljana River catchment. In: *11th Jožef Stefan International Postgraduate School Students' Conference and 13th Young Researchers' Day*, Planica, Slovenia.
- Rovan, L., Benedik, L., Štok, M. (2018). Method development for the determination of uranium isotope ratios by MC-ICP-MS. In: *18th Radiochemical Conference*, Mariánské Lázně, Czech Republic.
- Rovan, L., Benedik, L., Štok, M. (2018). Uranium isotopic composition in karstic aquifer of Ljubljana River. In: *Uranium-biogeno: International Conference Uranium Biogeochemistry*, Monte Verità, Ascona, Switzerland.
- Rovan, L., Benedik, L., Štok, M. (2018). Determination of uranium isotope ratios by MC-ICP-MS. In: *10th Jožef Stefan International Postgraduate School Students' Conference and 12th Young Researchers' Day*, Piran, Slovenia.
- Benedik, L., Rován, L., Klemenčič, H., Smrke, J., Gantar, I., Prosen, H. (2014). Natural radionuclides in drinking water from the surroundings of the former Žirovski vrh uranium mine. In: *17th Radiochemical Conference*, Mariánské Lázně, Czech Republic.

Biography

The author of this thesis Leja Rován was born on January 29, 1992, in Celje, Slovenia. She finished primary school in Vransko, Slovenia, and high school at First High School in Celje (I. gimnazija v Celju), Slovenia. In 2010, she enrolled in the first-cycle academic bachelor study programme in chemistry at the Faculty of Chemistry and Chemical Technology at the University of Ljubljana and received her degree in chemistry with the defense entitled “Natural radionuclides in drinking water from the surroundings of the former Žirovski Vrh uranium mine” in 2014. In the same year, she entered the second-cycle master’s programme in chemistry at the same faculty. Following the defense in 2017, she obtained her master’s degree in chemistry with the defense entitled “Distribution of ^{210}Po in the fish tissues from the Gulf of Trieste (Northern Adriatic Sea)”. Both bachelor and master degree’s laboratory works were performed at the Department of Environmental Sciences at the Jožef Stefan Institute. During her master studies, she did 3 months of Erasmus+ exchange traineeship at the Department of Environmental Chemistry and Radiochemistry at the University of Gdansk, Poland, where she broadened her practical and theoretical knowledge on radiochemistry. In 2017, she started her PhD studies at the Jožef Stefan International Postgraduate School, Ljubljana, Slovenia, under the supervision of Assist. Prof. Dr. Marko Štok.

The majority of experimental work related to her PhD was conducted at the Department of Environmental Sciences, Jožef Stefan Institute. The focus of her PhD research was to accurately determine uranium and thorium isotope ratios with multicollector inductively coupled plasma mass spectrometry (MC-ICP-MS) for low-level sample concentrations and to correctly interpret analytical data in the context of application in geochemistry. The results of both optimization of mass-spectrometric measurement methods and isotope behavior during sample preparation provide means for establishing the methodology, which enables accurate determination of uranium and thorium isotope ratios in real samples, mostly from the environment with predominantly carbonate lithology. During her PhD studies, she attended numerous workshops and various national and international conferences related to her work. In addition, she was also trained to work in the ISO 17025 accredited laboratory, to perform radiochemical analysis in various samples, which will contribute to her gained knowledge in her future research.